

**Department of Electrical and Computer Engineering
Centre for Smart Grid and Sustainable Power Systems**

**Application of SMES Unit to Improve the Performance of
Doubly Fed Induction Generator Based WECS**

A. M. Shiddiq Yunus

**This thesis is presented for the Degree of
Doctor of Philosophy
of
Curtin University**

June 2012

Declaration

“To the best of my knowledge and belief this thesis contains no material previously published by any other person except due acknowledgement has been made. This thesis contains no material which has been accepted for the award of any other degree or diploma in any university”

Signature :
Date : 1/10/2012

In the Name of Allah,
The Entirely Merciful, the Especially Merciful

Dedicated to:

My respected parents:

A. Muhammad Yunus Baso (Rahimahullah) and Hj. A. St. Mangindara Husain

My beloved wife:

A. Sutriani Mappasulle

My beloved daughters:

A. Watsiqah A. Shiddiq and A. Zahrah A. Shiddiq

ABSTRACT

Due to the rising demand of energy over several decades, conventional energy resources have been continuously and drastically explored all around the world. As a result, global warming is inevitable due to the massive exhaust of CO₂ into the atmosphere from the conventional energy sources. This global issue has become a high concern of industrial countries who are trying to reduce their emission production by increasing the utilization of renewable energies such as wind energy. Wind energy has become very attractive since the revolution of power electronics technology, which can be equipped with wind turbines. Wind energy can be optimally captured with wind turbine converters. However, these converters are very sensitive if connected with the grid as grid disturbances may have a catastrophic impact on the overall performance of the wind turbines.

In this thesis, superconducting magnetic energy storage (SMES) is applied on wind energy conversion systems (WECSs) that are equipped with doubly fed induction generators (DFIGs) during the presence of voltage sags and swells in the grid side. Without SMES, certain levels of voltage sags and swells in the grid side may cause a critical operating condition that may require disconnection of WECS to the grid. This condition is mainly determined by the voltage profile at the point of common coupling (PCC), which is set up differently by concerned countries all over the world. This requirement is determined by the transmission system operator (TSO) in conjunction with the concerned government. The determined requirement is known as grid codes or fault ride through (FRT) capability.

The selection of a SMES unit in this thesis is based on its advantages over other energy storage technologies. Compared to other energy storage options, the SMES unit is ranked first in terms of highest efficiency, which is 90-99%. The high efficiency of the SMES unit is achieved by its low power loss because electric currents in the coil encounter almost no resistance and there are no moving parts, which means no friction losses. Meanwhile, DFIG is selected because it is the most popular installed WECS over the world. In 2004 about 55% of the total installed WECS worldwide were equipped with DFIG. There are two main strategies that can be applied to meet the grid requirements of a particular TSO. The first strategy is

development of new control techniques to fulfil the criterion of the TSOs. This strategy, however, is applicable only to the new WECS that have not been connected to the power grid. If new control techniques are applied to the existing grid-connected WECSs, they will not be cost effective because the obsolete design must be dismantled and re-installed to comply with current grid code requirements. The second strategy is the utilization of flexible AC transmission system (FACTS) devices or storage energy devices to meet the grid code requirements. This strategy seems more appropriate for implementation in the existing WECS-grid connection in order to comply with the current grid code requirements. By appropriate design, the devices might be more cost effective compared to the first strategy, particularly for the large wind farms that are already connected to the grid.

A new control algorithm of a SMES unit, which is simple but still involves all the important parameters, is employed in this study. Using the hysteresis current control approach in conjunction with a fuzzy logic controller, the SMES unit successfully and effectively improves the performance of the DFIG during voltage sag and swell events in the grid side; thus, this will prevent the WECS equipped with DFIG from being disconnected from the grid according to the selected fault ride through used in this study. The dynamic study of DFIG with SMES during short load variation is carried out as an additional advantage of SMES application on a DFIG system. In this study, the proposed SMES unit is controlled to compensate the reduced transfer power of DFIG during the short load variation event. Moreover, the SMES unit is also engaged in absorbing/storing some amount of excessive power that might be transferred to the grid when the local loads are suddenly decreased. Finally, the studies of intermittent misfires and fire-through that take place within the converters of DFIG are carried out in order to investigate the impact of these converter faults on the performance of DFIG. In this part, the proposed SMES unit is controlled to effectively improve the DFIG's performance in order to prevent it from being disconnected or shut down from the power grid during the occurrence of these intermittent switching faults.

ACKNOWLEDGMENTS

I praise and glorify the name of Allah the Almighty who always protected, sustained and helped me and my family and created pleasant opportunities for me to capitalize on.

I would like to express my deepest gratitude to my supervisor Associate Professor Dr. Mohammad A. S. Masoum and my co-supervisor Dr. Ahmed Abu Siada for their invaluable support and excellent supervision during my PhD study at Curtin University. I would also like to sincerely gratitude to Professor Syed Islam and all staff of Electrical and Computer Engineering department for their supports.

I would like to acknowledge the support of Dr. Mansour Mohseni, Dr. Dedet Chandra Riawan and all my PhD's colleagues for fruitful discussion and friendship which made the academic life easy and enjoyable. Special thanks to my relatives Muhammad Suradi and Muhammad Suardi and their families, who made my stay in Perth stress free as I was far away from my family.

Many thanks to my Indonesian friends who made my life easier with their sincere advices and their presence around me whenever I needed them most.

Last but not the least, I would like to thank my respected and beloved mother for her unconditional love and prayers for me. Heartfelt grateful to my beloved wife for her encouragement, invaluable support, love and her patience while looking after our daughters alone in my absence. I would like to apologize especially during the period she was critically ill. I would also like to apologize to my elder daughter who spent most of her childhood without the love and care of her father. My daughter, I wish you never say again "*Abi! cepat pulang!*" ("Daddy! Come back soon, please!") after the completion of my study.

Perth, Western Australia, May 2012

Andi Muhammad Shiddiq Yunus

LIST OF PUBLICATIONS

Most of the research results presented in this thesis have been published (or are presently under review) in the journals and conference papers listed below.

International Journals:

- [1] **A. M. Shiddiq Yunus**, M. A. S. Masoum, A. Abu Siada, “*Application of SMES to Enhance the Dynamic Performance of DFIG during Voltage Sag and Swell*”, **IEEE Transactions on Applied Superconductivity**, 2012 (Accepted and In Press).
- [2] **A. M. Shiddiq Yunus**, A. Abu Siada, M. A. S. Masoum, “*Application of SMES Unit to Improve the Voltage Profile of The Power System with DFIG during Grid Dip and Swell*”, *International Journal of Advances in Engineering and Technology (IJAET)*, Vol.1, No.5, Nov. 2011.
- [3] **A. M. Shiddiq Yunus**, A. Abu Siada, M. A. S. Masoum, “*Application of SMES Unit to Improve the Performance of Wind Turbine Conversion System*”, **Elixir**, *Electrical Engineering Online Journal*, Vol.38, pp. 4315-4319, 2011.
- [4] **A. M. Shiddiq Yunus**, M. A. S. Masoum, A. Abu Siada, “*Improving Dynamic Performance of Wind Energy Conversion System using Fuzzy-Based Hysteresis Current Controlled SMES*”, **IET Proceedings on Power Electronics**, (Accepted in 2012 and in press)
- [5] **A. M. Shiddiq Yunus**, A. Abu Siada, M. A. S. Masoum, “*Impact of SMES on DFIG Power Dispatch during Intermittent Misfire and Fire-through Faults*”, **IEEE Transactions on Applied Superconductivity**, Paper Number: TAS-2012-0045 (Submitted on May 2012 and under second review).
- [6] **A. M. Shiddiq Yunus**, M. A. S. Masoum, A. Abu Siada, “*Impact of Converter Station Faults on Dynamic Performance of DFIG*”, **IET Proceedings on Renewable Power Generation**, Paper Number: RPG-2011-0339 (Submitted on December 2011 and under review).

International Conferences:

- [1] **A. M. Shiddiq Yunus**, “*The Wide Application of Superconducting Magnetic Energy Storage (SMES) in Power System*”, The 10th Postgraduate Electrical Engineering and Computing Symposium 2009, Perth, Australia. 2009.

- [2] **A. M. Shiddiq Yunus**, Ahmed Abu Siada, M. A. S. Masoum, “*Application of Unequal Firing Angle Control Algorithm of the SMES Unit in Damping Sub-Synchronous Resonance*”, International Conference of Electrical Energy and Industrial Electronics System (EEIES) 2009. Parkroyal, Penang, Malaysia 7-8 December 2009.
- [3] **A. M. Shiddiq Yunus**, Ahmed Abu Siada, M. A. S. Masoum, “*Effects of SMES on Dynamic Behaviours’ of Type D-Wind Turbine Generator-Grid Connected during Short Circuit*”, IEEE Power Engineering Society General Meeting PES GM, Detroit, Michigan, USA, pp. 1-7, July 26-29, 2011.
- [4] **A. M. Shiddiq Yunus**, Ahmed Abu Siada, M. A. S. Masoum, “*Effects of SMES Unit on the Performance of Type-4 Wind Turbine Generator during Voltage Sag*”, IET Renewable Power Generation Conference, Edinburgh, UK, September 2011.
- [5] **A. M. Shiddiq Yunus**, M. A. S. Masoum, Ahmed Abu Siada, “*Application of Statcom to Improve the Low-Voltage-Ride-Through Capability of Type-D Wind Turbine Generator*”, IEEE Power and Energy Society Innovative Smart Grid Technologies Conference, ISGT Asia 2011, Perth, Australia. November 2011.
- [6] **A. M. Shiddiq Yunus**, Ahmed Abu Siada, M. A. S. Masoum, “*Application of SMES Unit to Improve the High-Voltage-Ride-Through Capability of DFIG-Grid Connected during Voltage Swell*”, IEEE Power and Energy Society Innovative Smart Grid Technologies Conference, ISGT Asia 2011, Perth, Australia. November 2011.
- [7] **A. M. Shiddiq Yunus**, Ahmed Abu Siada, M. A. S. Masoum, “*Improvement of LVRT Capability of Variable Speed Wind Turbine Generator using SMES Unit*”, IEEE Power and Energy Society Innovative Smart Grid Technologies Conference, ISGT Asia 2011, Perth, Australia, November 2011.
- [8] Y. M. Alharbi, **A. M. Shiddiq Yunus**, Ahmed Abu Siada, “*Application of Statcom to Improve the High-Voltage-Ride-Through Capability of Wind Turbine Generator*”, IEEE Power and Energy Society Innovative Smart Grid Technologies Conference, ISGT Asia 2011, Perth, Australia, November 2011.
- [9] **A. M. Shiddiq Yunus**, Ahmed Abu Siada, M. A. S. Masoum, “*Impact of DC-Link Fault on the Dynamic Performance of DFIG*”, (Has been accepted and will be published in the proceedings and scheduled for presentation at the 2012 IEEE PES General Meeting, 22-26 July 2012, San Diego, CA, USA.
- [10] **A. M. Shiddiq Yunus**, M. A. S. Masoum, Ahmed Abu Siada, “*Impact of Intermittent Misfire and Fire-Through on the Performance of Full Converter Based WECS*” Australasian Universities Power Engineering Conference (AUPEC) 2012, Bali, Indonesia, 26-29 September 2012.

- [11] Y. M. Alharbi, **A. M. Shiddiq Yunus**, Ahmed Abu Siada, “*Application of UPFC to Improve the LVRT Capability of Wind Turbine Generator*” Australasian Universities Power Engineering Conference (AUPEC) 2012, Bali, Indonesia, 26-29 September 2012.
- [12] **A. M. Shiddiq Yunus**, Ahmed Abu Siada, M. A. S. Masoum, Syed Islam, “*Impact of DC-Link Faults on the Performance of Full Converter Based WECS*” (Submitted on June 2012 to the Middle East Power Systems Conference (MEPCON) 2012 that will be held at Alexandria, Egypt, 23-25 December 2012).

TABLE OF CONTENTS

DECLARATION	i
DEDICATION	ii
ABSTRACT	iii
ACKNOWLEDGMENT	v
LIST OF PUBLICATIONS	vi
TABLE OF CONTENTS	ix
LIST OF FIGURES	xii
LIST OF TABLES	xvi
CHAPTER 1 INTRODUCTION	1
1.1. BACKGROUND	1
1.2. INTEGRATING RENEWABLE ENERGIES INTO THE POWER SYSTEM	3
1.3. CONTRIBUTION AND SIGNIFICANCE OF RESEARCH	5
1.4. THESIS OUTLINE	6
1.5. REFERENCES	7
CHAPTER 2 RENEWABLE WIND ENERGY SYSTEM	10
2.1. INTRODUCTION	10
2.2. BASIC WIND THEORY	13
2.3. TECHNOLOGY DEVELOPMENT OF WIND ENERGY CONVERSION SYSTEM (WECS)	17
2.3.1. POWER LIMITATION SCHEME OF WECS	17
2.3.2. FIXED SPEED WECS (TYPE A)	18
2.3.3. LIMITED VARIABLE SPEED WECS (TYPE B)	20
2.3.4. VARIABLE SPEED WECS	21
2.3.4.1. DOUBLY FED INDUCTION GENERATOR (DFIG OR TYPE C)	21
2.3.4.2. FULL CONVERTER WECS (TYPE D)	23
2.4. MARKET SHARE	25
2.5. SUMMARY	26
2.6. REFERENCES	27
CHAPTER 3 MODELLING OF DOUBLY FED INDUCTION GENERATOR (DFIG)	29
3.1. MODEL STRUCTURE OF DFIG	29
3.2. TURBINE ROTOR MODEL	30
3.3. GENERATOR MODEL	31
3.4. CONVERTER MODEL	33
3.5. MODEL OF ROTOR SPEED CONTROLLER	34
3.6. MODEL OF PITCH ANGLE CONTROLLER	35
3.7. MODEL OF TERMINAL VOLTAGE CONTROLLER	36
3.8. THE T-FORM EQUIVALENT CIRCUIT OF DFIG MACHINE	38
3.9. CONTROL SCHEME OF DFIG'S CONVERTERS	39
3.9.1. CONTROL SCHEME OF GRID SIDE CONVERTERS (GSC)	39
3.9.2. CONTROL SCHEME OF ROTOR SIDE CONVERTERS (RSC)	43
3.10. SUMMARY	44
3.11. REFERENCES	44

CHAPTER 4 ENERGY STORAGE TECHNOLOGIES FOR RENEWABLE ENERGY RESOURCES	47
4.1. INTRODUCTION	47
4.2. BATTERY ENERGY STORAGE SYSTEM (BESS)	48
4.3. ULTRACAPACITOR (UC)	51
4.4. SUPERCONDUCTING MAGNETIC ENERGY STORAGE (SMES)	53
4.5. FLYWHEEL ENERGY STORAGE SYSTEM (FESS)	60
4.6. COMPRESSED AIR ENERGY STORAGE (CAES)	62
4.7. PUMPED HYDRO SYSTEM (PHS)	64
4.8. COMPARISON OF STORAGE ENERGY TECHNOLOGIES	67
4.9. SUMMARY	71
4.10. REFERENCES	72
CHAPTER 5 SMES UNIT CONFIGURATION AND CONTROL SCHEME	78
5.1. INTRODUCTION	78
5.2. HYSTERESIS CURRENT CONTROL (HCC)	81
5.3. FUZZY LOGIC CONTROL (FLC)	89
5.4. SUMMARY	95
5.5. REFERENCES	96
CHAPTER 6 APPLICATION OF SMES UNIT ON THE POWER SYSTEM WITH DOUBLY FED INDUCTION GENERATOR (DFIG)	99
6.1. INTRODUCTION	99
6.2. FAULT RIDE THROUGH OF SPANISH'S GRID CODE	103
6.3. APPLICATION OF SMES UNIT ON DFIG DURING GRID DISTURBANCES	105
6.3.1. SYSTEM UNDER STUDY	105
6.3.2. VOLTAGE SAG	108
6.3.3. VOLTAGE SWELL	111
6.3.4. SMES RESPONSES DURING VOLTAGE SAG AND SWELL	113
6.3.5. SMES CAPACITY	117
6.3.6. VOLTAGE SAG COMPLIANCE WITH FRT OF SPAIN	117
6.3.7. VOLTAGE SWELL COMPLIANCE WITH FRT OF SPAIN	118
6.4. APPLICATION OF SMES UNIT TO IMPROVE THE DYNAMIC PERFORMANCE OF DFIG	119
6.4.1. SMALL DISTURBANCE	119
6.4.2. LARGE DISTURBANCE	124
6.5. IMPACT OF SMES ON DFIG POWER DISPATCH DURING INTERMITTENT MISFIRE AND FIRE-THROUGH FAULTS	130
6.5.1. MISFIRE AND FIRE-THROUGH	130
6.5.2. MISFIRE ON GSC AND RSC	133
6.5.3. FIRE-THROUGH ON GSC AND RSC	136
6.5.2. SMES BEHAVIORS	139
6.6. SUMMARY	142
6.7. REFERENCES	143
CHAPTER 7 LIST OF CONTRIBUTIONS OF THESIS AND FUTURE WORKS	150
7.1. SUMMARY OF THE WORK	150
7.2. LIST OF CONTRIBUTIONS	151
7.3. FUTURE WORKS	152
7.4. REFERENCES	154

APPENDIX	155
APPENDIX A-1	156
APPENDIX B-1	157
APPENDIX B-2	158
APPENDIX B-3	159
APPENDIX B-4	160
APPENDIX B-5	161
APPENDIX B-6	162
APPENDIX B-7	163
APPENDIX C-1	164
BIOGRAPHY OF THE AUTHOR	165

LIST OF FIGURES

Figure 2.1.	The peak capacity of solar PV generation installed	10
Figure 2.2.	The peak capacity of wind power generation installed in 2010	11
Figure 2.3.	The progress of wind power generation installed peak capacity in Australia	12
Figure 2.4.	The 2010-installed capacity of wind power generation in Australia by state	12
Figure 2.5.	Wind spectrum based on work by Van Der Hoven	14
Figure 2.6.	Typical power curve of a 1500-kW wind turbine generator	15
Figure 2.7.	Typical c_p - λ curve for a three-bladed rotor	16
Figure 2.8.	Power vs. wind speed of WECS with different type of power control schemes: Stall control (passive control), (b) Pitch Control and (c) Active-stall control	18
Figure 2.9.	Typical configuration of fixed-speed WECS (Type A)	19
Figure 2.10.	Typical configuration of Type B WECS	20
Figure 2.11.	Example illustrative of mechanical power vs. turbine speed showing fixed speed WECS and variable speed WECS for various wind speed (5-12 m/s)	22
Figure 2.12.	Typical configuration of DFIG (Type C)	23
Figure 2.13.	Typical configuration of Type D WECS	24
Figure 2.14.	Typical configuration of Type D WECS with back-to-back converter	24
Figure 2.15.	Typical configuration of Type D WECS based on a boost converter	25
Figure 2.16	World market share of yearly installed power for different wind turbine generator types	26
Figure 3.1.	General structure of the model for DFIG based variable speed wind turbine	30
Figure 3.2.	Optimal rotor speed-power characteristic of typical variable speed WECS	35
Figure 3.3.	Pitch angle controller model.	36
Figure 3.4.	Voltage controller model for a wind turbine with DFIG	37
Figure 3.5.	Equivalent circuit of DFIG in T- form	38
Figure 3.6.	Control system of the GSC	40
Figure 3.7.	Park's transformation from 3-phase reference frame to $dq0$ reference frame; (a) 3-phase voltage and (b) 3-phase current	41
Figure 3.8.	Park transformation from $dq0$ reference frame to 3-phase reference frame; (a) 3-phase voltage and (b) 3-phase current	42
Figure 3.9.	Control system of the RSC	43
Figure 4.1.	Typical classic lead acid battery system	49
Figure 4.2.	Typical configuration of a WECS-grid connected with BESS	50
Figure 4.3.	Typical diagram of simple UC	52
Figure 4.4.	Comparison of energy and power density of UC, BESS, and conventional capacitor	52
Figure 4.5.	Typical schematic diagram of a SMES unit	56
Figure 4.6.	New type dispersed power system that uses SMES unit	59
Figure 4.7.	12-pulse SMES unit configuration with GTO	59

Figure 4.8.	Application of SMES unit on variable speed WECS during grid disturbances	60
Figure 4.9.	Typical model of a FESS	61
Figure 4.10.	Typical model for a CAES	63
Figure 4.11.	Pumped hydroelectric storage system	66
Figure 4.12.	Bar chart of storage energy technologies' efficiency	68
Figure 4.13.	Life time bar chart of storage energy technologies	68
Figure 4.14.	Colum chart of maximum energy capacity of EST	69
Figure 4.15.	Power rating vs. discharge time for various ESTs	70
Figure 4.16.	Estimated cost in US\$/kW of EST	70
Figure 5.1.	Typical configuration of CSC based SMES with 12-pulse converter	79
Figure 5.2.	Typical configuration of VSC based SMES with a DC-DC Chopper	79
Figure 5.3.	SMES unit configuration and the proposed HCC-FLC control scheme	80
Figure 5.4.	Typical of an IGBT based VSC with a series active load	81
Figure 5.5.	Equivalent schematic diagram of a VSC with a series active load	82
Figure 5.6.	3-phase HCC method	84
Figure 5.7.	Typical hysteresis current	85
Figure 5.8.	Typical switching signal	85
Figure 5.9.	Basic Phase-Locked Loop (PLL)	86
Figure 5.10.	Control algorithm of VSC	86
Figure 5.11.	Single line equivalent circuit of VSC	87
Figure 5.12.	Membership function type of fuzzy logic; (a) Zigmoidal (b) Gaussian, and (c) Trapezoidal (continued on next page)	90
Figure 5.12.	Membership function type of Fuzzy logic; (d) Triangular	91
Figure 5.13.	Typical structure of a FLC	92
Figure 5.14.	Control algorithm of DC-DC chopper	93
Figure 5.15.	(a) Class D DC-DC chopper topology with a SMES coil (continued on next page)	93
Figure 5.15.	(b) Operation range of SMES coil	94
Figure 6.1.	Fault ride through of Spain's grid codes	104
Figure 6.2.	System under study	105
Figure 6.3.	Memberships function for the input variable P_G (pu)	106
Figure 6.4.	Memberships function for the input variable I_{SMES} (pu)	107
Figure 6.5.	Memberships function for the output variable D (duty cycle)	107
Figure 6.6.	Surface graph-duty cycle	108
Figure 6.7.	DFIG responses during voltage sag without/with a SMES unit; (a) active power and (b) reactive power (continued on next page)	109
Figure 6.7.	DFIG responses during voltage sag without/with a SMES unit; (c) PCC voltage, (d) Shaft speed, and (e) Voltage at DC link of DFIG	110
Figure 6.8.	DFIG responses during voltage swell without/with a SMES unit; (a) active power and (b) reactive power (continued on next page)	111

Figure 6.8.	DFIG responses during voltage swell without/with a SMES unit; (c) PCC voltage, (d) Shaft speed, and (e) Voltage at DC link of DFIG	112
Figure 6.9.	SMES transient responses during voltage sag and swell including; (a) Current, (b) Voltage, and (c) Duty cycle (continued on next page)	114
Figure 6.9.	SMES transient responses during voltage sag and swell including; (d) Stored energy and (e) Voltage at DC link of SMES	115
Figure 6.10.	Voltage profile at PCC where the DFIG based WECS is connected	118
Figure 6.11.	Voltage response at PCC during swell event: (a) Voltage response at the PCC and (b) Zoomed area of voltage response at the PCC	119
Figure 6.12.	System under study	120
Figure 6.13.	Load profile under study	121
Figure 6.14.	Memberships function for the input variable P_G (pu)	121
Figure 6.15.	Memberships function for the input variable I_{SMES} (pu)	122
Figure 6.16.	Memberships function for the output variable D (duty cycle)	122
Figure 6.17.	Surface graph- Duty cycle	123
Figure 6.18.	(a) Power transfer to the grid and (b) Duty cycle response during dynamic event (continued on next page)	123
Figure 6.18.	(c) Stored energy of SMES during dynamic event	124
Figure 6.19.	Response of the DFIG during 3-phase short circuit fault at point A; (a) Generated power of DFIG, (b) Rotor shaft speed and (c) Voltage across DFIG DC-link (continued on next page)	126
Figure 6.19.	Response of the DFIG during 3-phase short circuit fault at point A; (d) Voltage profile at PCC, (e) Duty cycle response of the SMES unit, and (f) Stored energy response of the SMES unit	127
Figure 6.20.	Response of the DFIG during 3-phase short circuit fault at point B; (a) Generated power of DFIG and (b) Rotor shaft speed (continued on next page)	128
Figure 6.20.	Response of the DFIG during 3-phase short circuit fault at point B; (c) Voltage across DFIG DC-link, (d) Voltage profile at PCC, and (e) Duty cycle response of the SMES unit (continued to next page)	129
Figure 6.20.	Response of the DFIG during 3-phase short circuit fault at point B; (f) Stored energy response of the SMES unit	130
Figure 6.21.	System under study for DFIG-SMES with misfire and fire-through	131
Figure 6.22.	Converters configuration of the DFIG	131
Figure 6.23.	Simulation of misfire fault in IGBT-1; (a) GSC signal and (b) RSC signal	132
Figure 6.24.	Simulation of fire-through fault in IGBT-1; (a) GSC signal, (b) RSC signal	133
Figure 6.25.	Effect of GSC misfire on DFIG dynamic responses with and without SMES coils; (a) power and (b) shaft speed, and (c) Voltage at PCC	134

Figure 6.26.	Effect of RSC misfire on DFIG dynamic responses with and without SMES unit; (a) Power, (b) Shaft speed, and (c) Voltage at PCC	135
Figure 6.27.	Effect of RSC misfire on DFIG dynamic responses with and without SMES unit; (a) Power (continued on next page)	136
Figure 6.27.	Effect of fire-through at GSC on DFIG's responses with and without SMES unit; (b) shaft speed, (c) Electromagnetic torque and (d) Voltage at PCC	137
Figure 6.28.	Effect of fire-through at RSC on DFIG's responses with and without SMES coil; (a) Power (continued on next page)	137
Figure 6.28.	Effect of fire-through at RSC on DFIG's responses with and without SMES coil; (b) Shaft speed and (c) Voltage at PCC	138
Figure 6.29.	SMES behaviours during misfire fault; (a) Energy, (b) Duty cycle, and (c) Voltage across the SMES coil	140
Figure 6.30.	SMES behaviours during fire-through fault; (a) Energy, (b) Duty cycle, and (c) Voltage across the SMES coil	141
Figure B-4.	Typical $C_p-\lambda$ (<i>lambda</i>) characteristic of simulated wind turbine	160
Figure B-5.	Turbine characteristic of simulated DFIG; (a) Power vs. wind speed, (b) λ (<i>lambda</i>) vs. wind speed and (c) C_p vs. wind speed	161
Figure C-1.	(a) Block Diagram of simulated SMES configuration, (b) Hysteresis current controller, and (c) Fuzzy logic controller	164

LIST OF TABLES

Table 2.1.	Applicability of power control system on various type of WECS	27
Table 4.1.	Comparison of ESTs in term of advantages-disadvantages and their applications in power system	71
Table 5.1.	Rules of duty cycle	93
Table A-1.	Approximation of power curves	156
Table B-1.	Drive train parameters of the simulated DFIG	157
Table B-2.	Converter parameters of the simulated DFIG	158
Table B-3.	Generator parameters of the simulated DFIG	159
Table B-6a.	Parameters of the DFIG	162
Table B-6b.	Parameters of the transmission line	162
Table B-6c.	Parameters of the proposed SMES unit	162
Table B-7a.	Parameters of the DFIG	163
Table B-7b.	Parameters of the transmission line	163
Table B-7c.	Parameters of the proposed SMES unit	163

Chapter 1

Introduction

1.1. Background

It is well known that conventional resources of energy such as oil, coal, and gas are used predominantly worldwide today. The massive utilization of these energy resources, particularly in meeting the demands of the world's population for electric power, resulted in adverse effects on the environment for example, air pollution that contributes to global warming and causes human health problems, and acid rain that can cause skin disease, kill living creatures and decrease the lifespan of buildings. Moreover, the demand for energy is increasing because of rapid industrial and technological developments, particularly in developed nations. Industrial development plays a significant role in energy demand because large amounts of energy are required to support industrial systems operations.

Consequently, it is not unlikely that one day the resources for these conventional forms of energy will be exhausted because of the ever-growing demand and because reproducing them will take hundreds to thousands of years. Most of the energy used today is derived from conventional resources such as oil, gas, and coal. These produce CO_2 when burned, and when CO_2 is released into the atmosphere, it will harm the ozone layer, and global warming will increase. The other pollutant that may be produced along with CO_2 is nitrogen oxide such as NO , NO_2 , and N_2O which are collectively known as NO_x and any sulphur content of the fuel results in SO_x emissions. NO_x and SO_x together contribute to acid rain that harms living creatures and shortens the lifespan of buildings, bridges, and other structures [1]. Thus, clean and renewable forms of energy need to be explored in order to reduce the detrimental

effects of conventional sources and to have alternatives to replace the finite capacities of conventional energy resources.

Non-conventional energy or so-called renewable energy is the type of energy that continuously replenishes itself and exists abundantly in nature, such as solar power, wind, biomass, and tides. The only limitation on renewable energy besides their low efficiency is that geographical and climatic conditions dictate its availability. Therefore, not all regions in the world have the same renewable energy capacity; moreover, the amount of renewable energy in one region varies over time. This variation challenges developers to maximize the exploration. Although they may be difficult to control, renewable energy resources are worthy of exploration because they cannot run out, and they cause marginal damage to the environment. Furthermore, their use does not fall under stringent requirements [2].

Not surprisingly, consumers and developers all around the world worry about the emissions from conventional energy, because the environment is unable to absorb and purify the current level of emissions. This situation of increasing emissions had brought together all the concerned nations at the international climate convention in Kyoto in 1997. This event resulted in an agreement called the Kyoto Protocol in which the developed nations of the world agreed to reduce their emissions [2]. According to the agreement, the USA has to reduce carbon dioxide (CO₂) emissions by 6% (where this agreement was not ratified by US congress) while Japan must reduce them by 7%. The European Union (EU) committed to reducing its CO₂ emissions by 8%. All nations under the agreement had to reach these reduction targets between 1998 and 2010. In effect, policies like the Kyoto Protocol force the participating countries to resort to renewable energy resources, because they almost certainly cannot reduce their industrial production.

What these policies mean for developers is that they must aggressively explore how to make renewable energy feasible as quickly as possible. The application of renewable energy resources is not as easy as imagined. The energy's intermittent characteristic, its fluctuation and the inconsistencies in the amount of produced energy are the most difficult problems that the concerned countries must address. Moreover, renewable energy's interconnection with the existing grid must comply

with all the standard requirements of transmission line operators (TSOs) in order to maintain the quality, reliability and stability of the whole, interconnected system.

1.2. Integrating Renewable Energies into the Power System

Renewable energy resources have been in operation for several decades, such as the power plants on remote islands that are powered by wind, solar energy, and diesel engines. These energy resources are highly beneficial to isolated islands compared to the established conventional power plant systems. For example, these islands would pay a high price for relying on diesel generators to power them, since they would need to transport the fuel. Moreover, oil prices fluctuate significantly over the course of a decade. A conventional power plant is also unsustainable for remote islands, because it would deteriorate the islands' environment sooner or later. The renewable energy resources can be designed to stand alone or to be hybridized with the conventional ones already on the island. Interestingly, most of the conventional power plants that currently exist on these islands function merely as a backup for the power plants running on renewable energy resources. Fortunately, recent advancements in energy storage technologies (ESTs) can replace the conventional power plants as a back-up system. Integrating a renewable energy resource power plant with the existing power grid is not as easy as building a stand-alone renewable energy-based power plant. To implement the former, designers must consider issues related to stability, power quality and reliability.

Solar and wind energy resources are two popular types of renewable energies that have attracted numerous manufactures in the last decades. The power plan that runs on the solar energy system is still an expensive technology, so most of this technology is presently used for small to medium-scale energy demands at private residences or at the small industry levels, even though 50 MW scales have been installed in some places but they still remains small in the total percentages if compared with the small scales which are still popular in private residences. Although it is intermittent, solar energy is more stable than wind energy, because the latter might vary from minute to minute or even second to second. This advantage of solar power, therefore, makes it much easier to implement, particularly with an appropriate energy storage selection.

The first generation of wind energy conversion systems (WECS) was the direct connected WECS type. This technology uses a fixed speed turbine to generate power. It dominated renewable energy installations worldwide, comprising up to 70% of all installations in 1995 [3]. This technology remained popular until the electronic power revolution that updated the WECS so that they could maximize wind energy capture. This technology is called variable speed WECS, and it can optimally capture wind energy 5% more than the fixed speed WECS option. Furthermore, the variable speed WECS can reduce the impact of transient wind gusts and subsequent fatigue unlike the fixed speed turbines [4, 5]. Due to the extensive penetration of WECS into the existing power network, the TSOs have developed new requirements for integrating WECS to the grid, which are called grid codes [6]. One of the important parts of the grid code is the voltage profile at the point of common coupling (PCC), which determines the connection or disconnection status of WECS from the grid. Two strategies can improve the performance or the fault ride through (FRT) capability of the WECS. Most literatures have studied the path of developing new control techniques to fulfil the criterion of TSOs [7-11]. However, this strategy is effective only for new installations and new connections of WECS to the grid. Alternatively, designers can apply a flexible AC transmission system (FACTS) device or storage energy system [12], and this technique is more cost effective for large existing WECS.

Variable speed WECS, such as doubly fed induction generator (DFIG) and Type D WECS (or so called full converter WECS), were introduced to overcome the weakness of the fixed speed type in capturing maximum wind energy and to contribute reactive power to the grid when required [13]. Compared to full scale variable speed WECS, DFIG is very sensitive to grid faults [8]; although the DFIGs are usually connected far away from the grid, the grid faults will affect the voltage profile at PCC. The significant voltage drop/rise at PCC will cause high currents in the stator windings and may induce over-current in the rotor windings. Moreover, during a grid fault, voltage drops at the DFIG terminal, high current flows at both grid and rotor side converters and high voltage at the DC link may lead to converter station blocking. This condition will force the DFIG to be disconnected from the system. If the DFIG contributes to a large portion of power to the grid, then the financial loss of a disconnection would be uncountable. Most of the studies on DFIG

address the improvement of its FRT capability during voltage sag [7-11]. No attention, however, has been given to improving the DFIG performance under voltage sag and voltage swell conditions using the same controller. Both sag and swell can lead to the disconnection of WECS when the voltage profile during these disturbances that occur at the grid side violates the minimum and maximum voltage levels set by the grid code.

Numerous studies have explored the ability of the superconducting magnetic energy storage (SMES) to smooth out WECS's power output. Most of these studies have connected SMES to the fixed speed WECS [14-20]. These studies, however, could not claim that SMES are more effective than BESS or hybrid energy storages in term of cost and capability. The only situations that would make better use of SMES than other storage options are the multi-purpose conditions, such as improving the FRT capability of WECS during sag and swell events in the grid side.

As a part of this thesis, a short load variation on a power system with DFIG is also studied. During this load variation, the SMES unit is able to compensate the variation close to the predetermined power that DFIG must transfer. Moreover, a new study of misfire and fire-through that takes place within both the grid-side converter (GSC) and the rotor-side converter (RSC) of the DFIG is also included in this study. The impact of these switching faults on the performance of DFIG with and without SMES will be investigated and discussed.

1.3. Contribution and Significance of Research

The main purpose of this research is to develop a new control algorithm for a SMES unit, which should be simple, efficient, and easy to implement with an existing connected WECS-grid. The contributions and significance of this study can be highlighted as follows:

1. Develop and design a hysteresis current control (HCC) along with a fuzzy logic control (FLC) scheme on a SMES unit that will be applied to DFIGs.
2. Study the effect of grid voltage sag and swell on the DFIG's performance with and without the SMES unit considering the FRT of Spain's grid code.

3. Study the application of the SMES on dynamic stability of the power system with DFIG connected during short term load variation.
4. Evaluate the capability of the SMES on DFIG's performance during misfire and fire-through faults in the GSC and the RSC of the DFIG.

1.4. Thesis Outline

This thesis is divided into six chapters:

- **Chapter 1. Introduction**

This chapter describes the background, motivations, contributions, significance and the outlines of the research.

- **Chapter 2. Renewable Wind Energy System**

Wind basic theory is the preamble of this chapter, followed by the history and basic technical concepts of most well-known WECS of the past few decades, such as fixed speed WECS and variable speed WECS. The market share of these WECSs is also included to highlight the progress of each WECS technology that is installed annually worldwide.

- **Chapter 3. Doubly Fed Induction Generator (DFIG)**

The technical aspects of variable speed WECS based on a DFIG is given more attention since it is the main player of the WECS studied with SMES in this thesis. The overall modeling system of several important parts of DFIG will be described in this chapter, including the control system of both mechanical and electrical parts of the DFIG systems.

- **Chapter 4. Storage Energy Technologies for Renewable Energy Resources**

The characteristics of common EST that are applicable for power systems are discussed. A brief technical and economic aspect of each EST is described and both advantages and disadvantages are presented. Discussion of the SMES unit system is given more space in this chapter. Finally, the summary is provided in the last section for easy comparison.

- **Chapter 5. SMES Unit Configuration and Control Scheme**

A brief configuration that is commonly used in the SMES power system unit is introduced in the first part of this chapter, followed by the advantages of voltage-source converter (VSC) over current-source converter (CSC) configuration. The eminence of an insulated gate bipolar transistor (IGBT) over gate turn off thyristor (GTO) switching device is also briefly discussed. The overall configuration of the SMES unit, including the new proposed control system of the hysteresis current controller and the fuzzy logic controller is comprehensively discussed in this chapter.

- **Chapter 6. Application of SMES in the Power System with Doubly Fed Induction Generator**

In this chapter, the advantages of DFIG over other WECS types are briefly discussed. The new application of the SMES unit in improving the DFIG's performance and compliance with the FRT of Spain's grid code during voltage sag and swell is introduced. The detail membership functions of fuzzy logic inputs and output of all studied cases are demonstrated. The simulation results comparing the dynamic responses with and without being connected to the SMES unit are analyzed for the case of voltage sag, voltage swell, and short term load variation. A section about converter faults, such as misfire and fire-through, is also included. SMES impacts on the system under these faults are investigated and discussed. Many publications related to the research are set forth in this chapter.

- **Chapter 7. List of Contribution of Thesis and Future Work**

An incorporation of a summary of each chapter is provided followed by the final list of contributions for overall studies in this thesis. Future works are addressed for potential improvement and further SMES unit applications.

1.5. References

- [1] L. Freris and D. Infield, "Renewable Energy in Power System", Wiltshire: A John Wiley & Sons. 2008
- [2] F. A. Farret and M. G. Simoes, "Integration of Alternative Sources of Energy", New Jersey: A John Wiley & Son. Inc. 2006

- [3] H. Polinder, D.-J. Bang, H. Li, and Z. Cheng, "Concept Report on Generator Topologies, Mechanical and Electromagnetic Optimization," Project UpWind. 2007
- [4] J. M. Carrasco, L. G. Franquelo, J. T. Bialasiewicz, E. Galvan, R. C. P. Guisado, M. A. M. Prats, J. I. Leon, and N. Moreno-Alfonso, "Power-Electronic Systems for the Grid Integration of Renewable Energy Sources: A Survey", *IEEE Transactions on Industrial Electronics*, vol. 53, pp. 1002-1016. 2006
- [5] P. W. Carlin, A. S. Laxson, and E. B. Muljadi, "The History and State of the Art of Variable-Speed Wind Turbine Technology", NREL, Colorado. 2001
- [6] M. Altin, O. Goksu, R. Teodorescu, P. Rodriguez, B. B. Jensen, and L. Helle, "Overview of Recent Grid Codes for Wind Power Integration", in *12th International Conference on Optimization of Electrical and Electronic Equipment (OPTIM) 2010*, pp. 1152-1160. 2010
- [7] S. Seman, J. Niiranen, and A. Arkkio, "Ride-Through Analysis of Doubly Fed Induction Wind-Power Generator under Unsymmetrical Network Disturbance", *IEEE Transactions on Power Systems*, vol. 21, pp. 1782-1789. 2006
- [8] J. Lopez, E. Gubia, E. Olea, J. Ruiz, and L. Marroyo, "Ride Through of Wind Turbines with Doubly Fed Induction Generator under Symmetrical Voltage Dips", *IEEE Transactions on Industrial Electronics*, vol. 56, pp. 4246-4254. 2009
- [9] M. Mohseni, S. M. Islam, and M. A. S. Masoum, "Impacts of Symmetrical and Asymmetrical Voltage Sags on DFIG-Based Wind Turbines Considering Phase-Angle Jump, Voltage Recovery, and Sag Parameters", *IEEE Transactions on Power Electronics*, vol. 26, pp. 1587-1598. 2011
- [10] Y. Xiangwu, G. Venkataramanan, P. S. Flannery, W. Yang, D. Qing, and Z. Bo, "Voltage-Sag Tolerance of DFIG Wind Turbine with a Series Grid Side Passive-Impedance Network", *IEEE Transactions on Energy Conversion*, vol. 25, pp. 1048-1056. 2010
- [11] S. Hu, X. Lin, Y. Kang, and X. Zou, "An Improved Low-Voltage Ride-Through Control Strategy of Doubly Fed Induction Generator During Grid Faults", *IEEE Transactions on Power Electronics*, vol. 26, pp. 3653-3665. 2011
- [12] J. G. Slootweg, S. W. H. de Haan, H. Polinder, and W. L. Kling, "General Model for Representing Variable Speed Wind Turbines in Power System Dynamics Simulations", *IEEE Transactions on Power Systems*, vol. 18, pp. 144-151. 2003
- [13] F. Blaabjerg and Z. Chen, "Power Electronics for Modern Wind Turbines", Aalborg: Morgan & Claypool Publishers. 2006
- [14] J. Hee-Yeol, A. R. Kim, K. Jae-Ho, P. Minwon, Y. In-Keun, K. Seok-Ho, S. Kideok, K. Hae-Jong, S. Ki-Chul, T. Asao, and J. Tamura, "A Study on the Operating Characteristics of SMES for the Dispersed Power Generation System", *IEEE Transactions on Applied Superconductivity*, vol. 19, pp. 2028-2031. 2009
- [15] S. S. Chen, L. Wang, W. J. Lee, and Z. Chen, "Power Flow Control and Damping Enhancement of A Large Wind Farm Using A Superconducting Magnetic Energy Storage Unit", *Renewable Power Generation, IET*, vol. 3, pp. 23-38. 2009

- [16] M. H. Ali, P. Minwon, Y. In-Keun, T. Murata, and J. Tamura, "Improvement of Wind-Generator Stability by Fuzzy-Logic-Controlled SMES", *IEEE Transactions on Industry Applications*, vol. 45, pp. 1045-1051. 2009
- [17] F. Zhou, G. Joos, C. Abbey, L. Jiao, and B. T. Ooi, "Use of Large Capacity SMES to Improve the Power Quality and Stability of Wind Farms", in *Power Engineering Society General Meeting, 2004. IEEE*, vol.2, pp. 2025-2030. 2004
- [18] M. R. I. Sheikh, S. M. Muyeen, R. Takahashi, T. Murata, and J. Tamura, "Minimization of Fluctuations of Output Power and Terminal Voltage of Wind Generator by Using STATCOM/SMES", in *PowerTech, 2009 IEEE Bucharest*, pp. 1-6. 2009
- [19] T. Asao, R. Takahashi, T. Murata, J. Tamura, M. Kubo, A. Kuwayama, and T. Matsumoto, "Smoothing Control of Wind Power Generator Output by Superconducting Magnetic Energy Storage System", in *International Conference on Electrical Machines and Systems, 2007, ICEMS*, pp. 302-307. 2007
- [20] J. Hee-yeol, P. Dae-Jin, S. Hyo-Ryong, P. Minwon, and Y. In-Keun, "Power Quality Enhancement of Grid-Connected Wind Power Generation System by SMES", in *Power Systems Conference and Exposition, 2009. PSCE '09. IEEE/PES*, pp. 1-6. 2009

“Every reasonable effort has been made to acknowledge the owners of copyright material. I would be pleased to hear from any copyright owner who has been omitted or incorrectly acknowledged.”

Chapter 2

Renewable Wind Energy System

2.1. Introduction

Solar and wind energy resources are today's two most popular renewable energy resources. They are both environment-friendly and sufficiently available naturally, so their utilization continues to show a significant growth worldwide. As can be seen in Fig. 2.1, all countries that predominantly install solar (photovoltaic) PV show considerable installation growth in 2010. The steepest growth occurred in Germany, aided by the fact that its government has accelerated the tariff reduction to promote the solar installation. Germany accounted for 44.3% of global capacity growth in 2010. Germany currently has 43.5% of the world's solar peak capacity, with an installed capacity of 17.3 GW by the end of 2010. This is four times more than that of its nearest rivals, Spain and Japan. Despite overall rapid capacity growth around the globe, the PV's power generation share globally is still low, contributing only 0.1% of the world's total power generation [1].

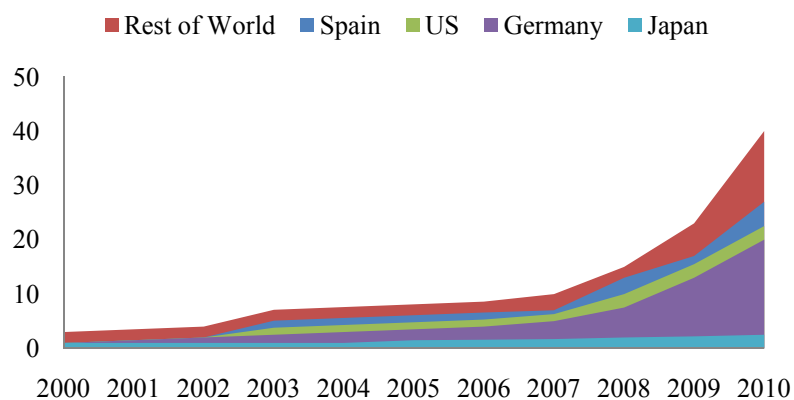


Fig. 2.1. The peak capacity of solar PV generation installed [1]

The total installed peak capacity of wind power generation, on the other hand, has shown immense growth by a record 39.4 GW, reaching 200 GW by the end of 2010. Wind power's total installed capacity in 2010 was estimated at around 340 TWh. This indicates that about 1.6% of the total electricity generation worldwide is supplied by wind power generation. The wind power generation's installed peak capacity in 2010 is illustrated in Fig. 2.2. Note that wind power plants are designed for peak capacity as wind power plant rarely outputs full capacity compared with a conventional power plant e.g. coal.

■ Rest of World ■ Germany ■ Spain ■ US ■ India ■ China

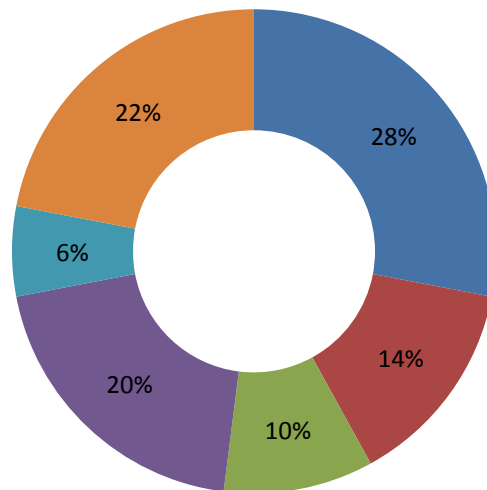


Fig. 2.2. The peak capacity of wind power generation installed in 2010 [1]

In total, Europe remains the largest regional market for wind power generation. Namely, Germany and Italy together dominate the globe's installed wind power generation capacity by about 87.7 GW or 44% of the total installed capacity throughout the world [1]. In 2010, China showed an interest in wind power generation by installing 22% of 199.5 GW, which surpassed the US, followed by Germany, Spain, and then India. This indicates that China and India dominate the Asia-Pacific region's wind power generation installed capacity.

Australia is a developed country that is very concerned about its carbon economy issues. The Australian government has set a 20% renewable energy target for 2020, and today about 5100 GWh of its power is annually supplied by wind

power. This represents approximately 2% of the total national electricity consumption.

At the end of 2010, there were 1880 MW of wind peak capacity that had been installed in Australia, which was spread over 52 wind farms. Over the past decade, the amount of wind capacity has increased 30% per year on average. The progress of total installed wind capacity since 2000 and the 2010-installed wind capacity in Australia, by state, are shown in Figs. 2.3 and 2.4, respectively [2].

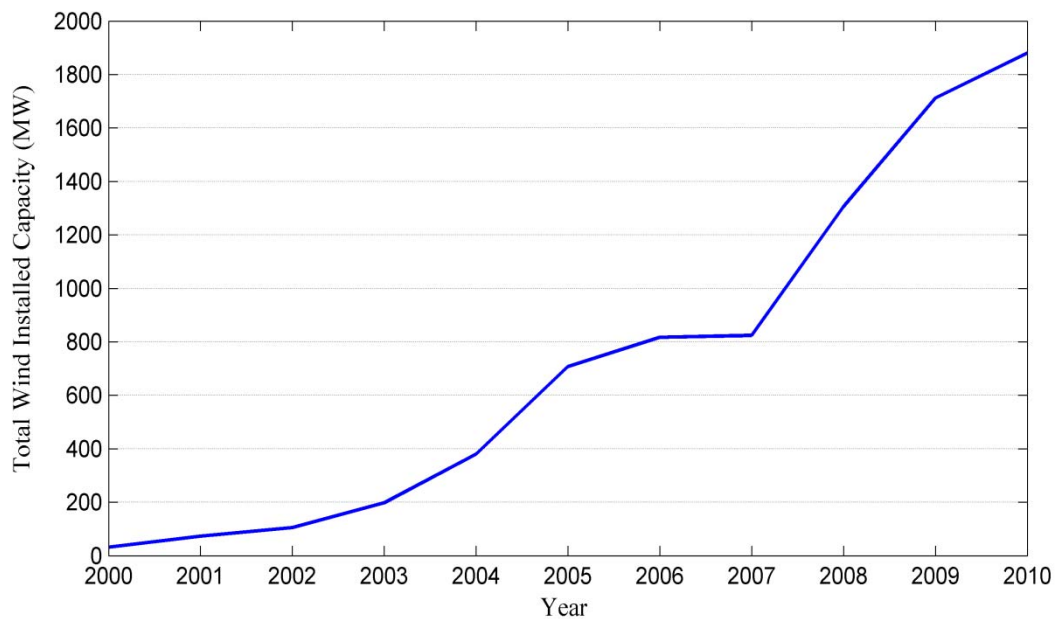


Fig. 2.3. The progress of wind power generation installed peak capacity in Australia [2]



Fig. 2.4. The 2010-installed capacity of wind power generation in Australia by state [2]

This chapter will now briefly present information about the total installed capacity, progress, recent technological development and total electricity generation of wind power throughout the world. It should be noted that total wind power generation was 16 times larger than total solar PV generation in 2010. This implies that wind power generation is more popular and may continue to dominate the solar PV module system in terms of new installations.

2.2. Basic Wind Theory

Wind can be defined as the movement of air masses in the atmosphere. The movement is caused by the different temperatures on the earth's surface. The sun irradiates unevenly on the earth's surface, and the different heat regions have different pressures, because hot air rises more than cold air. The different pressures will attempt to even out, causing the movement of air masses from the higher pressure region to the lower one [3]. In addition, the direction of wind is also influenced by the earth's rotation. Meanwhile, obstacles on the earth's surface such as buildings, hills, and trees will influence the speed of the wind to some extent. The flatter an area is, the faster the wind speed will be.

The wind speed at any given location is continuously varying. There are changes in a location's mean wind speed from year to year (annual), changes across seasons (seasonal), with passing weather (synoptic), on a daily basis (diurnal), and from second to second (turbulence), as illustrated in Fig. 2.5. All these changes on their different timescales make predicting the overall energy capture (annual and seasonal) from a site a difficult task, so ensuring that the variability of energy production does not adversely affect the local electricity network to which the wind turbine is connected is a challenge [4].

Industries began to use wind energy several decades ago. It was firstly utilized for mechanical purposes such as pumping water and milling grain. During the earliest stages of wind power, industries still relied on conventional fossil fuel machines as their main source of electricity generation due to their consistent power source output. However, since the oil-price shock in the 1970s, the majority of concerned parties directed their attention to alternative energy resources, such as wind. The first wind turbine for generating electricity was developed as early as the beginning of the 1970s, and during the 1990s, wind energy became one of the most

popular sustainable energy resources. In addition, worldwide wind capacity doubled approximately every three years in the 1990s [5].

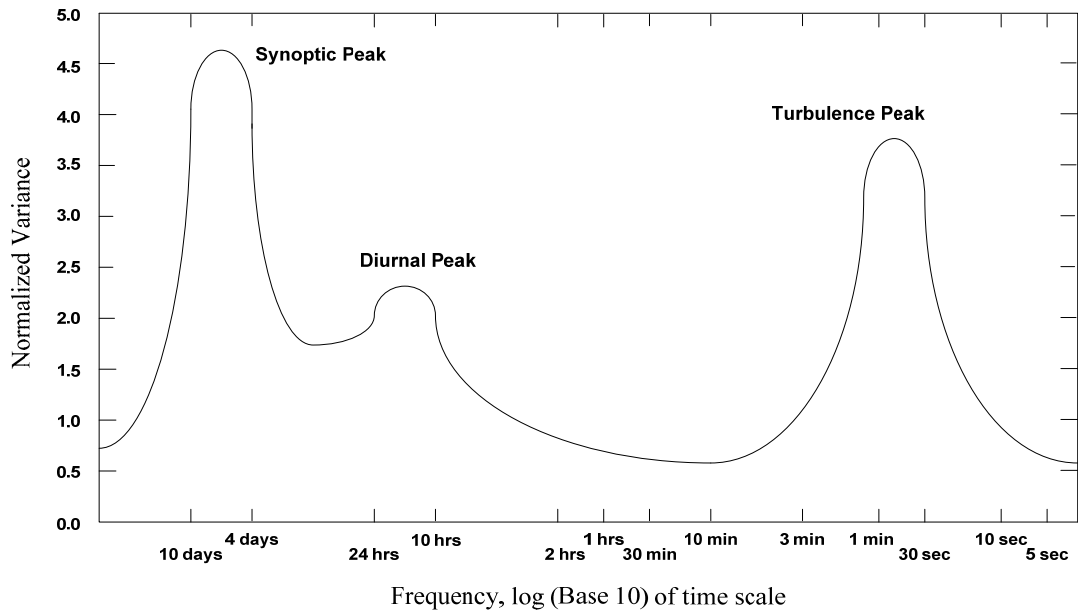


Fig. 2.5. Wind spectrum based on work by Van Der Hoven [6]

The global installed peak capacity increased from less than 2000 MW at the end of 1990 to 94000 MW by the end of 2007. In 2008, wind power already provided a little over 1% of the world’s electricity generation. It is projected that wind power will be providing about 10% of the globe’s electricity by about 2020 [7].

Usually, wind turbines are classified according to their power curves. The fundamental formula for wind energy is stated in Eq. 2.1.

$$P_W = \frac{1}{2} \rho A v^3 c_p \quad (2.1)$$

where:

ρ = air density (kg/m³),

v = wind speed (m/s),

A = swept area (m²), and

c_p = power coefficient.

In Eq. 2.1, the generated power is proportional to the cube of the wind speed that hits the blades. If such wind speed increases about 5%, then the generated power will increase by roughly 15%. An example of a power curve for a 1500 kW-rated wind turbine generator can be seen in Fig. 2.6.

By using Eq. 2.1, one can obtain the power-curve of a 1500-kW generator. In Fig. 2.4, point A is called the cut-in velocity, which is typically 5 m/s. At this point, the turbine starts to generate power. Points B to C shows the rated power of the wind turbine: within these wind speeds, the turbine will generate power at the designated rated level of the turbine. In the example of Fig. 2.6, the turbine would start its rated power from 15 m/s to 25 m/s.

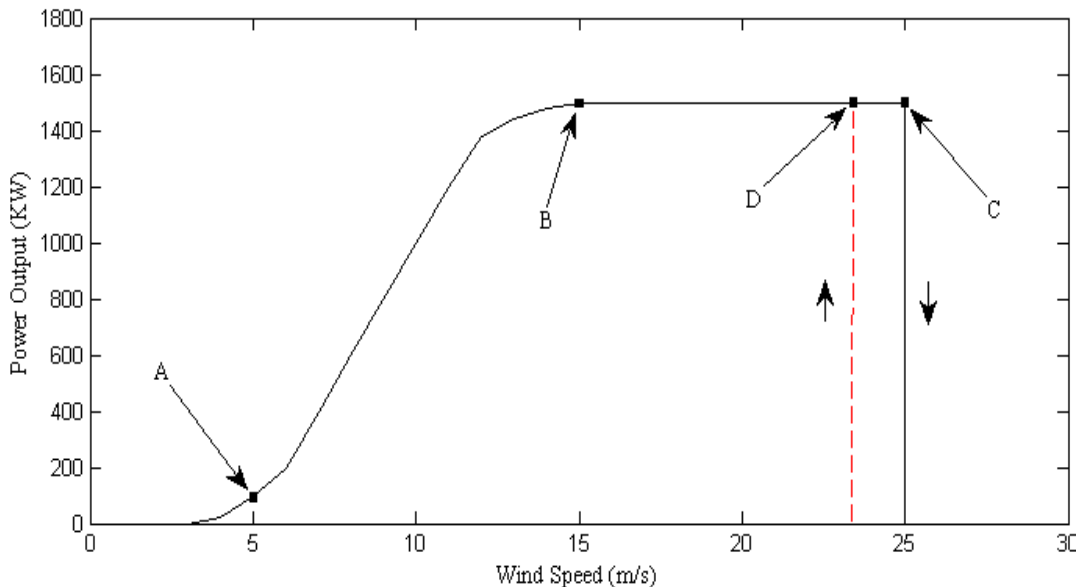


Fig. 2.6. Typical power curve of a 1500 kW wind turbine generator

When wind velocity reaches 25 m/s, the wind turbine will be shut down to avoid overloading and damaging the generator. Alternatively, it could be controlled in such a way to keep its speed within the safe speed margin. This safeguard is shown at point C, and it is called the cut-out point [8]. When the wind velocity returns to a safe speed (the turbine's rated speed), the turbine will then restart, but there may be a delay before it returns to full operation. This delay is represented at point D, and it is called a hysteresis loop [5]. Notice that the power curves may differ among turbines, because the curve depends on the manufacturer's design of the wind turbines technologies (e.g., pitch, stall, and variable speed).

Traditionally, the power coefficient, c_p is plotted as a function of the tip-speed ratio (λ), given Eq. 2.2:

$$\lambda = \frac{v_t}{v_w} \quad (2.2)$$

where:

$$v_t = \Omega R \quad (2.3)$$

and:

λ is the tip speed ratio,

v_t is the blade tip speed (m/s),

v_w is the wind speed (m/s),

Ω is the angular velocity of the rotor (rad/s), and

R is the radius (m).

The typical c_p - λ characteristic is illustrated in Fig. 2.7.

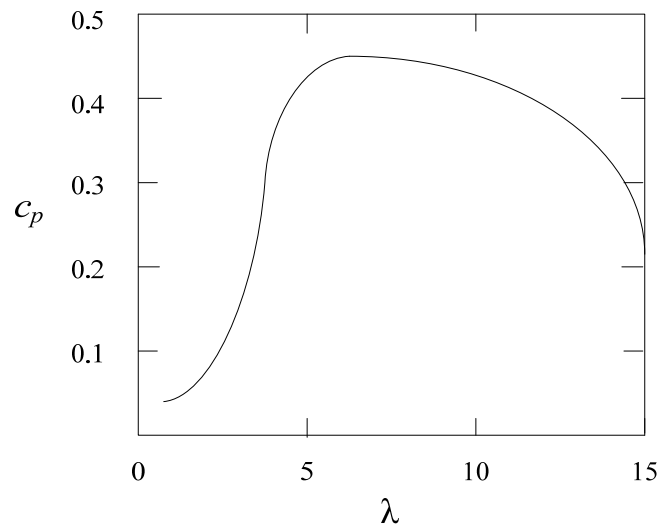


Fig. 2.7. Typical c_p - λ curve for a three-bladed rotor [6]
(Note: for large modern turbines, c_p is normally in the range of 0.4-0.5)

Fig. 2.7 shows that to operate at high efficiency, the tip speed ratio must be maintained constant for maximum output, and this requires the rotor speed to be controlled so that it changes proportionally with the wind speed. Most large modern WECS are designed as variable speed WECS so that they can control the rotor speed.

This concept is very attractive, because the rotor's inertia can absorb or release energy when it accelerates or decelerates, respectively. Thus, smooth power output can be achieved easily [6].

Two turbine technologies currently exist; the fixed-speed turbine and the variable-speed turbine. The first category is also commonly recognized as the Danish concept of the wind turbine. Fixed speed has only a very narrow range of rotational speed that, in turn, limits the range of power that the turbine can produce during wind speed variations. The second technology, a variable speed wind turbine, can potentially capture more energy than a fixed speed wind turbine of the same construction [9]. Moreover, according to Ref [10], it is possible for a variable-speed wind turbine to increase the power plant's annual energy production by approximately 5%.

2.3. Technology Development of Wind Energy Conversion System (WECS)

2.3.1. Power Limitation Scheme of WECS

There are three possible aerodynamics power limitation schemes for a WECS. The first is called stall control (passive control), which is the simplest, most robust, and cheapest control scheme. In this scheme, the blades are bolted onto the hub with a fixed angle which in turn will limit the aerodynamic power on the blades. The disadvantages, however, include the low efficiency during low wind speeds, no assisted start up and variations in the maximum steady-state power due to variations in air density and grid frequency [5]. This type of control system is effective only for the fixed speed WECS.

The second scheme is introduced as pitch control or so called active control. This type of control operates by turned out and turned the blades into the wind as the power output becomes too high or too low respectively, normally by employing a hydraulic or electric drive [4]. Therefore, pitch control system can maintain the output power close to the rated power of the generator. It also assists start up and emergency stop. Thus it becomes more popular compare with the first one. Some drawbacks are the complexity of the control mechanism and higher power fluctuation during wind gust event. The utilization of pitch control system has been adopted in both fixed speed WECS and variable speed WECS.

Active stall control is the third type of power limitation scheme. This scheme is combining the stall and pitching controls. The stall of the blade is actively controlled by pitching the blades. At the low wind speeds, the blades will operate similar to the second scheme (pitch control). However, at high wind speeds, the blade is directed into the deeper stall by being pitched slightly into the direction opposite to that of a pitch controlled scheme (the second scheme). This control yields smoother power output during the high wind speeds compared with the second scheme. The comparison is illustrated in Fig. 2.8.

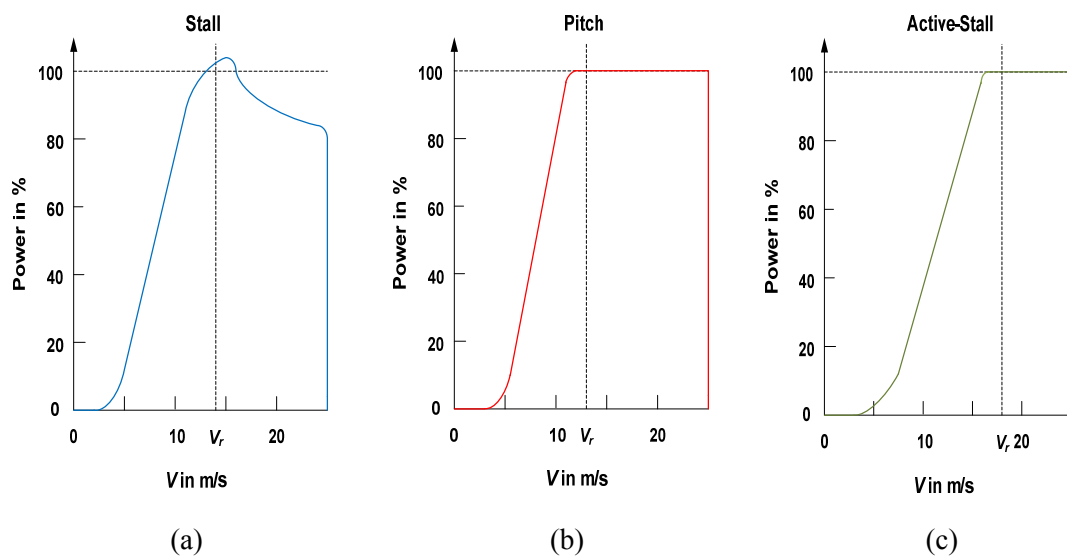


Fig. 2.8. Power vs. wind speed of WECS with different type of power control schemes; (a) Stall control (passive control), (b) Pitch Control, and (c) Active-stall control [11]

The explanation of WECS type will be presented in the following sections and the utilization of this power limitation schemes in conjunction with all types of WECS will be carried out in the summary.

2.3.2. Fixed Speed WECS (Type A)

The first type of wind turbine is fixed (or constant) speed WECS. It is also called the Danish Concept wind turbine. To simplify the classification due to the fast development of wind turbine types, the fixed speed wind turbine is classified as Type A WECS. Type A uses asynchronous squirrel cage-induction generator to convert the mechanical energy into electricity. A gearbox is used to match up the difference in the operating speeds of wind turbine rotor and the generator. The generator's slip slightly varies with the amount of generated power and is therefore not entirely

constant. However, because these speed variations are in the order of 1%, this wind turbine type is normally referred to as constant-speed or fixed-speed WECS [5].

In fixed speed WECS, the generator is directly connected to the mains supply grid. Thus, the generator speed is not only determined by its poles number but also by the grid frequency. The “Danish Concept” of directly connecting a wind turbine to the grid is commonly used for power ratings up to 2.3 MW. Typically, its configuration consists of a squirrel-cage induction generator (SCIG) that is connected via a transformer to the grid. The WECS equipped with SCIG mainly operates at a fixed slip which varies between 1 to 2%. To limit the power aerodynamically, different power limitation control such as stall control, active stall control, or pitch control can be employed. When connecting the induction generator directly to the grid, the short duration of inrush current which may be 5 to 7 times higher than the rated current of the generator will occur. This will disturb the grid causing high torque spikes in the drive train of the wind turbines. Thus, to avoid such disturbance, this type must be equipped with a current limiter such as a soft starter as shown in the typical fixed speed WECS in Fig. 2.9.

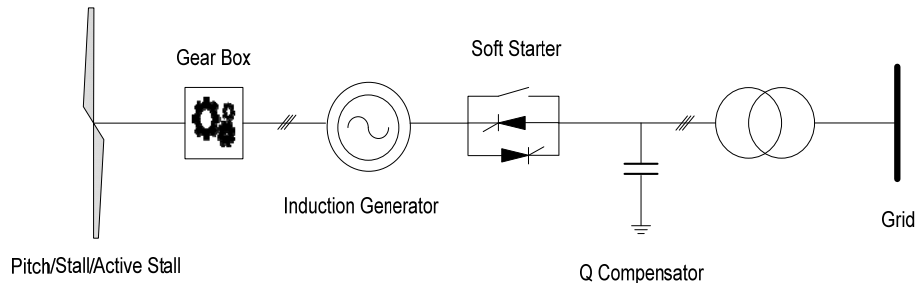


Fig. 2.9. Typical configuration of fixed speed WECS (Type A)

Some advantages of wind turbines with direct connected induction generator include simple, robust, and inexpensive construction. In addition, they don't require any synchronization devices. This results in lower cost and higher reliability which make them more attractive in most applications. However, wind turbines with direct connected induction generator also have a few drawbacks including slow active power control and requiring a stiff power grid to enable their stable operation as these machines naturally operate at about constant speed. When wind gust occur, the fixed speed WECSs may experiencing high mechanical stress due to the torque pulsation in the drive train and gearbox. Consequently, the fixed speed technology

will require expensive mechanical construction to absorb this high mechanical stress. Other disadvantages with induction generator are high starting currents as mentioned earlier and their demand for reactive power. To mitigate the power reactive absorption from the grid, a reactive power compensator must be applied to the system. It is usually done by switching of capacitor banks [12].

2.3.3. Limited Variable Speed WECS (Type B)

The limited variable-speed WECS (Type B) configuration is also known as the variable-speed WECS with OptiSlip® [5]. It corresponds to a WECS with the inclusion of a resistance bank at the rotor for limited control of the speed. Since mid 1990s, this relatively simple technology has been adopted by the Danish Manufacture Vestas. The wound rotor induction generator (WRIG) is directly connected to the grid. Similar to the fixed-speed WECS type, a capacitor bank is connected close to the generator to perform the reactive power compensation. A soft-starter is used to damping the high inrush current to achieve a smoother grid connection. The unique feature of this scheme is the additional variable rotor resistance, which can be changed by an optical controlled converter mounted on the rotor shaft. This makes the total rotor resistance controllable. By employing an optical coupling, the cost associated with the slip rings, brushes, and maintenance can be considerably reduced. The variable rotor resistance allows controlling the slip; therefore, the power output is controlled in this way. The range of dynamic speed control depends on the size of the variable rotor resistance, which is typically 0-10% above the synchronous speed [5]. The typical configuration of type B WECS is shown in Fig. 2.10.

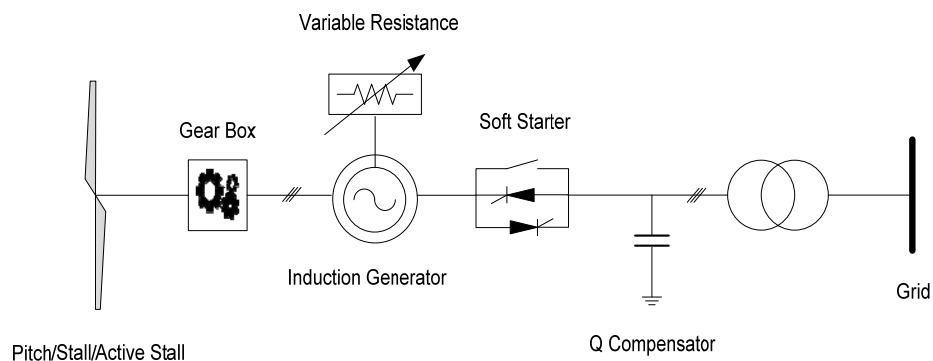


Fig. 2.10. Typical configuration of Type B WECS

2.3.4. Variable Speed WECS

As mentioned earlier, the variable-speed WECS is able to capture more energy compared to the fixed speed type. Moreover, with proper control of the power electronics devices, variable-speed WECS could also contribute to the stability of the grid by absorbing or injecting limited amount of reactive power. Compared to fixed-speed type, variable-speed WECS has less mechanical stress with rare rapid power fluctuations, because the rotor acts as a flywheel. However, with the addition of power electronic devices, the control system becomes more complex and an additional cost of 7% must be allocated [10].

The basic difference of fixed-speed WECS with the variable types in terms of the captured active power can be evaluated in Fig. 2.11. As can be seen in the illustrative power curve versus turbine speed, the mechanical output power at variable speed is higher than that of the fixed speed for various wind speed. For example, when wind speed is 11 m/s, fixed speed type can only produce about 0.82 pu power whilst the variable speed type produced is around 0.9 pu power. This indicates the superiority of variable-speed WECS in capturing power over various range of wind speed.

2.3.4.1. Doubly Fed Induction Generator (DFIG or Type C)

Instead of using a squirrel-cage induction generator, a Type C WECS uses a doubly fed induction generator. Similar to the previous type, it requires a gearbox. The stator winding of the generator is directly connected to the grid, and the rotor winding is connected to a power electronic converter which is usually with a back-to-back IGBT based converter with current control loops. The variable-speed operation becomes possible due to the task of the power electronic converter to compensate the difference between mechanical and electrical frequency by injecting a rotor current with variable frequency, thus, the electrical and mechanical rotor frequencies are decoupled [5].

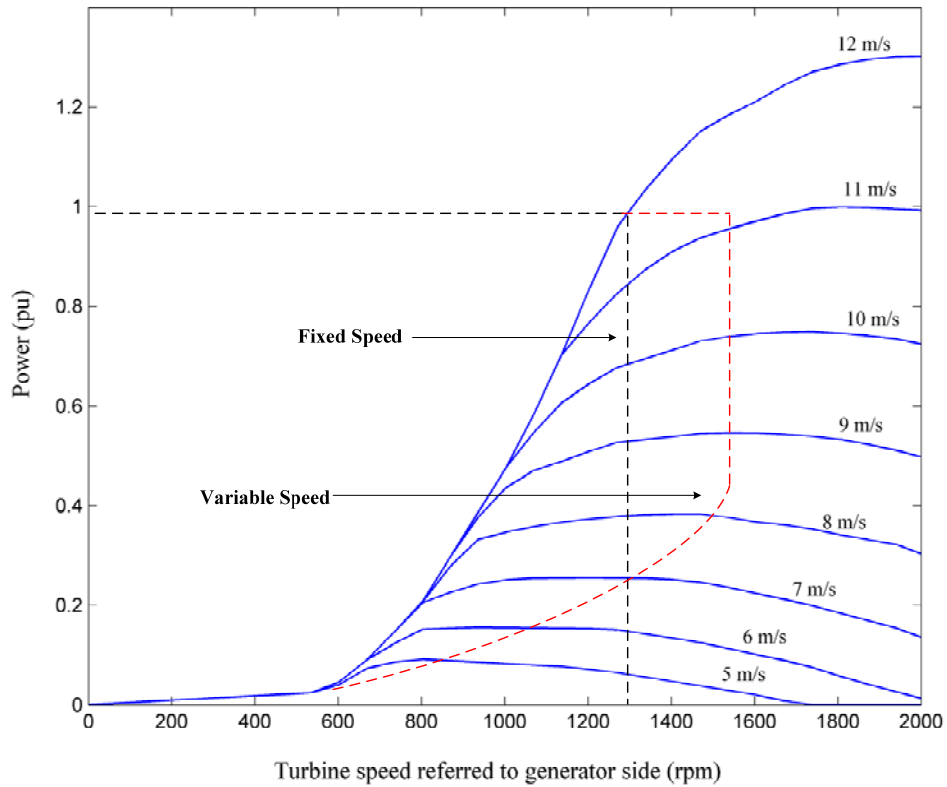


Fig. 2.11. Example illustrative of mechanical power vs. turbine speed showing fixed-speed WECS and variable-speed WECS for various wind speed (5-12 m/s)

A DFIG uses a medium scale power converter which is rated approximately about 30% of its rated power [5]. In this type, a slip ring is used to make the electrical connection to the rotor possible. The electrical power is delivered to the grid through both the rotor and the stator if the generator is running super-synchronously. If the generator is running sub-synchronously, electrical power is delivered into the rotor from the grid. With 30% scale of converters rating, a speed variation of $\pm 30\%$ around synchronous speed can be obtained [12]. Furthermore, with appropriate control design of the converters, controlling both active (P_{ref}) and reactive power (Q_{ref}) for better grid performance can be achieved.

Compared to the both Type A and B, the DFIG does neither require a soft starter nor a reactive power compensator. The system is slightly more expensive than the classical system explained before. However, it is still possible to reduce the total cost on the gearbox and the absence of employing a reactive power compensation units and it is also possible to gain the benefit from capturing more energy from the wind [12]. The typical configuration of a DFIG is depicted in Fig. 2.12.

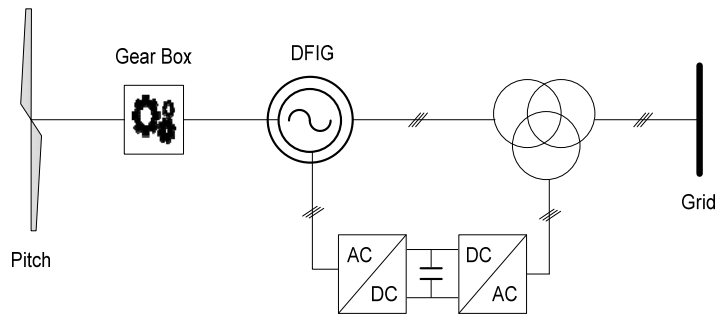


Fig. 2.12. Typical configuration of DFIG (Type C)

The detailed explanation of DFIG type, including modeling of DFIG structure such as generator model, converter model and control system, is discussed in Chapter 3.

2.3.4.2. Full Converter WECS (Type D)

Another variable-speed WECS available on the market niche is called full converter WECS or so called Type D WECS. This type typically does not require a gearbox if the generator used is of the multi-poles type (dashed line in Fig. 2.13 indicates that this type is possible with and without gearbox depending on its generator type). Since its configuration involving the full-scale power converters, the cost of the total construction might be quite expensive. In this scheme, the mechanical energy from the wind is converted to electricity by the low speed multi-poles synchronous generator [5] that has the same rotational speed as the wind turbine rotor which allows the elimination of the gearbox. By appropriate poles number design of the generator (such as low speed wound rotor synchronous generator), the rotational speeds between generator rotor and wind turbine rotor can be made equal. This will considerably reduce the overall construction cost of the system. The generator can have a wound rotor or a rotor with permanent magnets. The stator is not coupled directly to the grid but interfaced through a power converter or a diode rectifier with a single voltage-source converter. The electronic converter makes it possible to operate the wind turbine at variable speed [5]. The typical configuration of Type D WECS is shown in Fig. 2.13. The dashed box indicates that this configuration can be with and without gear box depend on the design of poles number.

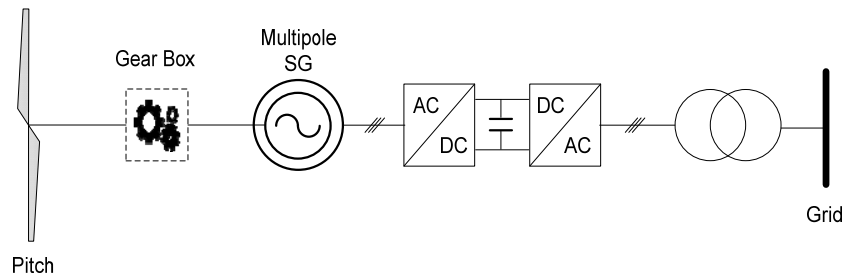


Fig. 2.13. Typical configuration of Type D WECS

The system shown in Fig. 2.14 can be with a permanent-magnet synchronous generator (PMSG) or wound rotor synchronous generator (WRSG) however, PMSG is quite cheaper and thereby quite attractive. Generator is decoupled from the grid by a DC link. With a proper control scheme, the power converter that is connected between the generator and the grid enables the system to control active and reactive power very fast. However, besides the high cost that may be tripled compared to the DFIG's, the disadvantage is that it is a more complex system with more sensitive power electronic components [12]. There are two common configurations of Type D WECS as shown in Figs. 2.14 and 2.15.

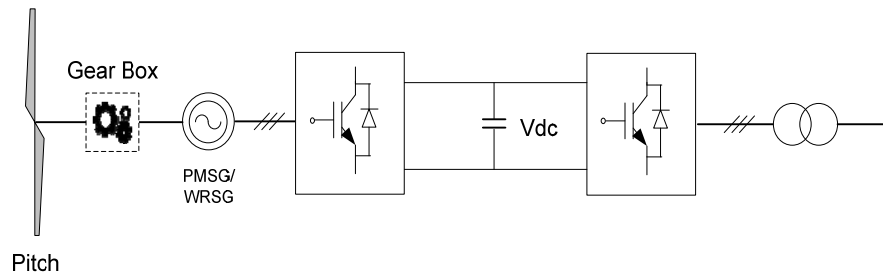


Fig. 2.14. Typical configuration of Type D WECS with back-to-back converter

The majority of Type D is equipped with multi-poles synchronous generator which will avoid the use of gearbox that normally is available with induction generator. The removal of a gearbox in WECS will significantly reduce losses, cost, and improve the reliability of the WECS. The Type D configuration shown in Fig. 2.14 consists of two converters; machine side converter (MSC) and GSC. MSC operates as a driver that is controlling the generator torque, whilst GSC will control the amount of active and reactive power to be transferred to the grid. The capacitor is used as a storage device to store the captured wind energy that can be instantaneously transferred to the grid. In this configuration, the voltage across the capacitor (called

DC link voltage) will be maintained constant at a designed level normally through the GSC's controller.

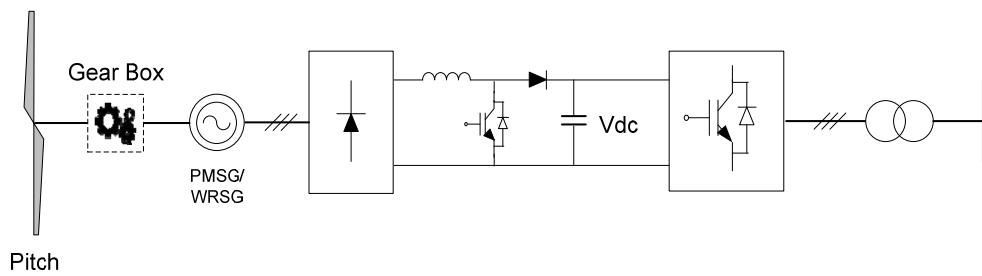


Fig. 2.15. Typical configuration of Type D WECS based on a boost converter

The other common configuration of Type D is shown in Fig. 2.15. Instead of using MSC, a conventional 3-phase passive rectifier is employed along with a chopper (a boost converter). This alternative technology is less expensive than the previous configuration. When the speed of synchronous generator varies, the voltage at the DC side of the rectifier will change accordingly, the chopper will adapt this change to the voltage at the DC link [10].

2.4. Market Share

The massive injection of WECS into the grid during the last few decades cannot be separated from the high achievement of the wind turbine generator system equipped with power electronics, which has been discussed in detail in the three sections above. The predictions of wind power installation are also astonishing. One prediction holds that almost 2400 GW will be installed worldwide in 2030, including new turbines in Europe, North America, China, India, Asia, Latin America, Africa and the Middle East [2]. To the best of the author's knowledge, the only source of online public information regarding the market share of WECS technology is in Ref [13]. Fig. 2.16 depicts the market share of yearly installed power for various wind turbine generator technologies.

As this figure indicates, Type A, or the fixed speed squirrel cage induction generator type, dominated the market share of WECS installation in 1995. However, the trend shows that this type no longer dominated the market after 2001. Up to 1997, Type B, or the limited variable speed WECS, was the second most commonly installed WECS type worldwide. Since 1998, it has suffered a decrease in the number

of its installed capacity. Although Type B decreased insignificantly from 1998 to 2001, this trend hinted at the lower attraction that this type would soon encounter. In 2004, its market niche fell significantly to only about 2% installed.

On the other hand, the advantages of the WECS equipped with a DFIG have compelled most power industries to apply this type confidently since 1998. DFIG has remained on top of the market in the installations, achieving 60% of its total installed capacity in 2003 and reducing only slightly in 2004. Meanwhile, Type D, or the so called full converter WECS, was designed with full cover of active and reactive power to the grid. However, Type D is still a costly technology compared to the DFIG due to Type D's 100%-rated converter. Since 1995, the Type D WECS remained below 25% installation worldwide until 2004.

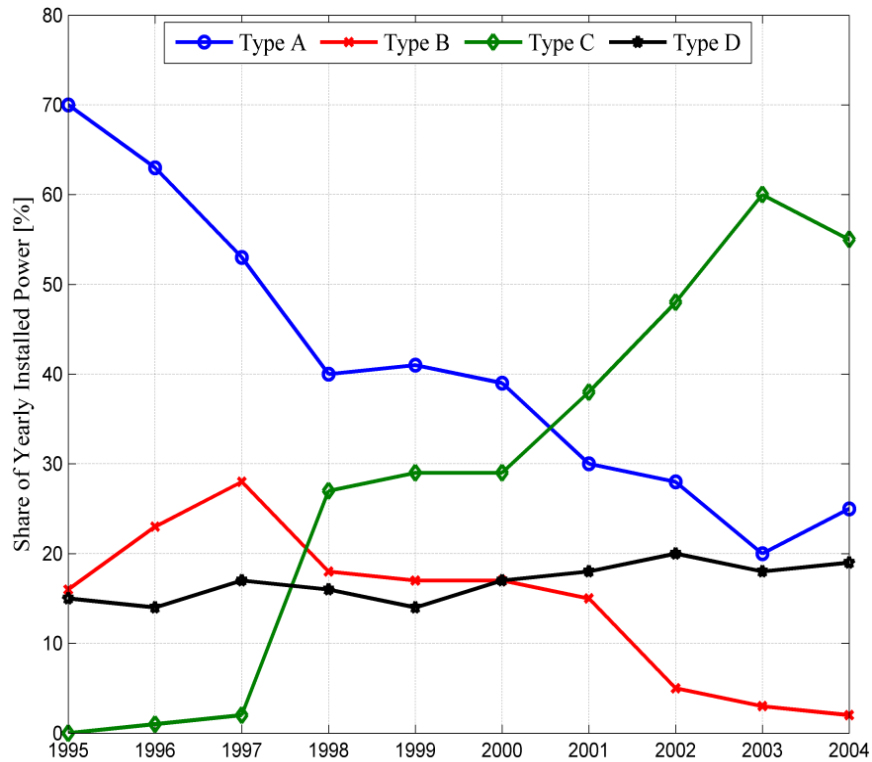


Fig. 2.16. World market share of yearly installed power for different wind turbine generator types [13]

2.5. Summary

Overall, recent market trends reveal that the solar PV module and wind power have been the two dominating installed renewable energy resources worldwide. Yet a

comparison between these two types of energy involving both real total installed capacity and projection suggests that wind power is more promising today and will continue to be in the near future. The development of wind power technology has achieved a convincing stage due to the revolutionary WECS equipped converter. The first wind turbines were the large fixed speed WECSs that dominated global renewable energy installations from 1995 to 2000. However, this fixed speed technology had limited capacity to capture wind energy, so it suffered from wind gusts and was unable to make any contributions to voltage stability during grid disturbances. Gradually, the variable speed types surpassed the first model in popularity, particularly the DFIG type. The modeling of the DFIG is far more complex than the fixed-speed type. A DFIG model basically consists of a rotor, a generator, a converter and some parts associated with the controllers such as the pitch angle controller, the rotor-speed controller and the terminal-voltage controller. These parts are discussed in the previous section.

The aerodynamics system has three types of power control: stall control (passive control), pitch control (active control), and active stall control. The adoption of these control schemes on WECS types is summarized in Table. 2.1.

Table 2.1. Applicability of power control system on various type of WECS [5]

Speed Control of WECS		Power Limitation		
		Stall	Pitch	Active Stall
Fixed Speed	Type A	Yes	Yes	Yes
Variable Speed	Type B	No	Yes	No
	Type C	No	Yes	No
	Type D	No	Yes	No

All three power control schemes can be equipped with Type A or fixed speed WECS. Type A with an active stall has just recently become popular and is now available in the market niche. Of all variable-speed WECS, only the fast pitch mechanism system is effective enough to be adopted. Stall and active stall are not suitable because they are incapable of quickly reducing power. If a wind gust comes along while a stall or active stall wind turbine is operating at its maximum speed, the aerodynamic torque will get high with the consequence of runaway conditions [5]. Therefore, as listed in Table 2.1, neither stall nor active stall is preferable for variable-speed WECS types.

2.6. References

- [1] www.bp.com, accessed: 22 February, 2012
- [2] "Global Wind Report: Annual Market Update 2010", Global Wind Energy Council. 2011
- [3] W. Tong, "Wind Power Generation and Wind Turbine Design", Southampton: WIT Press.2010
- [4] M. Stiebler, "Wind Energy Systems for Electric Power Generation", Berlin: Springer.2008
- [5] T. Ackerman, "Wind Power in Power System", West Sussex: John Wiley and Sons, Ltd.2005
- [6] L. Freris, "Renewable energy in power system", Chichester: John Wiley & Sons, Ltd.2008
- [7] P. Musgrove, "Wind Power", New York: Cambridge University Press.2010
- [8] J. F. Manwell, J. G. McGowan, and A. L. Rogers, "Wind Energy Explained: Theory, Design and Application", Chichester: John Wiley & Sons, Ltd.2002
- [9] V. Ahkmatov. "Analysis of Dynamic Behaviour of Power Systems with Large Amount of Wind Power",<http://www.dtu.dk/upload/centre/cet/projekter/99-05/05-va-thesis.pdf>, accessed: 25 February, 2011
- [10] J. M. Carrasco, L. G. Franquelo, J. T. Bialasiewicz, E. Galvan, R. C. P. Guisado, M. A. M. Prats, J. I. Leon, and N. Moreno-Alfonso, "Power-Electronic Systems for the Grid Integration of Renewable Energy Sources: A Survey", *IEEE Transactions on Industrial Electronics*, vol. 53, pp. 1002-1016.2006
- [11] R. Strzelecki and G. Benyek, "Power Electronics in Smart Electrical Energy Network", London: Springer.2008
- [12] F. Blaabjerg and Z. Chen, "Power Electronics for Modern Wind Turbines", Aalborg: Morgan & Claypool Publishers.2006
- [13] H. Polinder, D.-J. Bang, H. Li, and Z. Cheng, "Concept Report on Generator Topologies, Mechanical and Electromagnetic Optimization", Project UpWind. 2007

“Every reasonable effort has been made to acknowledge the owners of copyright material. I would be pleased to hear from any copyright owner who has been omitted or incorrectly acknowledged.”

Chapter 3 | **Modelling of Doubly Fed Induction Generator (DFIG)**

In this chapter, the modelling of DFIG will be explained in detail as the focus of this thesis is laid on this type of WECS. Compared with a fixed-speed wind turbine generator, DFIG is more complex because it requires more control functions to control the rotor speed, pitch angle, and terminal voltage, as well as GSC and RSC.

3.1. Model Structure of DFIG

The overall general model of DFIG is shown in Fig 3.1. It mainly consists of the models for rotor, generator and converter, as well as controllers for rotor speed, pitch angle and terminal voltage. In this section, the wind speed model will not be discussed as it can be simplified with the use of a constant or variable value block according to the user preference. This block can be a constant or signal source that is available in the Simulink/MATLAB software package. The wind speed used in this study, however, is assumed to remain constant, which is reasonable for simulations that involve grid disturbance as stated in Ref [1].

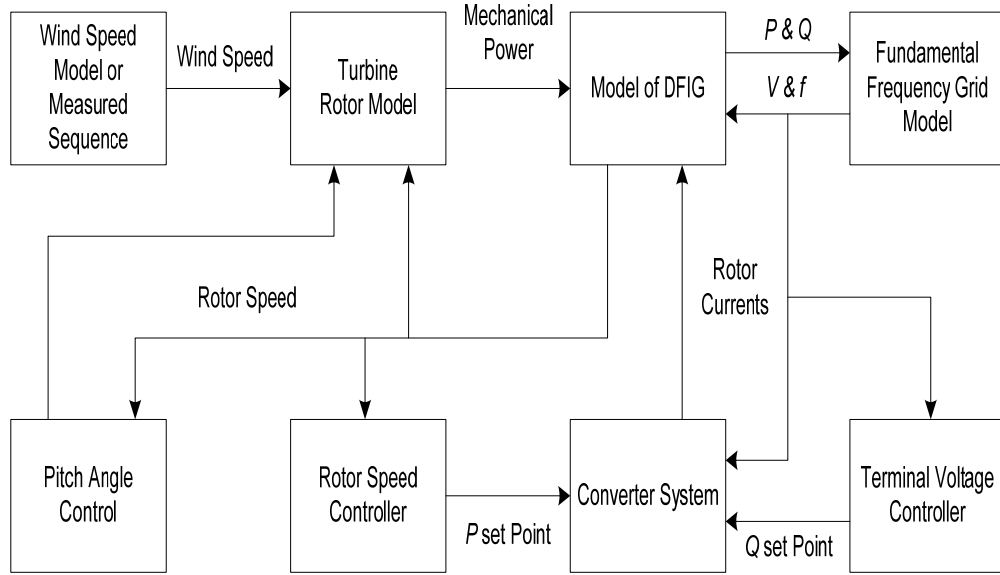


Fig. 3.1. General structure of the model for DFIG based variable-speed wind turbine [2]

3.2. Turbine Rotor Model

The well-known equation that shows the relationship of wind speed and the extracted mechanical power from the wind is:

$$P_{wt} = \frac{\rho}{2} A_{wt} c_p(\lambda, \theta) v_w^3 \quad (3.1)$$

where:

P_{wt} is the extracted mechanical power from the wind (watt),

ρ is air density (kg/m^3),

c_p is power coefficient,

λ is tip speed ratio ($=v_t/v_w$), where v_t is blade tip speed (m/s) and v_w wind speed at hub height upstream of the rotor (m/s),

θ is the pitch angle (degree), and

A_{wt} is the area covered by wind turbine rotor (m^2).

The difference between the fixed speed and variable speed WECS in terms of their capabilities in extracting mechanical power is determined by the value of constants c_1 to c_9 [3] of Eq. 3.2 and Eq. 3.3 which are derived in Appendix A.

$$c_p(\lambda, \theta) = c_1 \left(\frac{c_2}{\lambda_i} - c_3 \theta - c_4 \theta^{c_5} - c_6 \right) \exp \left(\frac{-c_7}{\lambda_i} \right) \quad (3.2)$$

where:

$$\lambda_i = \left[\left(\frac{1}{\lambda + c_8 \theta} \right) - \left(\frac{c_9}{\theta^3 + 1} \right) \right]^{-1} \quad (3.3)$$

3.3. Generator Model

The generator model is built up by the well-known related equations that are provided for wound rotor induction generator as below. The voltage equations are based on the d - q (direct-quadrature) reference frame which can be found in detail in Ref [4], however, in this reference the equations are for squirrel cage induction generator where u_{dr} and u_{qr} are equal to zero. All quantities are in per unit (pu).

$$u_{ds} = -R_s i_{ds} - \omega_s \psi_{qs} + \frac{d\psi_{ds}}{dt} \quad (3.4)$$

$$u_{dr} = -R_r i_{dr} - s \omega_s \psi_{qr} + \frac{d\psi_{dr}}{dt} \quad (3.5)$$

$$u_{qs} = -R_s i_{qs} + \omega_s \psi_{ds} + \frac{d\psi_{qs}}{dt} \quad (3.6)$$

$$u_{qr} = -R_r i_{qr} + s \omega_s \psi_{dr} + \frac{d\psi_{qr}}{dt} \quad (3.7)$$

where:

u is the voltage (V in pu),

i is the current (A in pu),

R is the resistance (ohm in pu),

Ψ is the flux (wb in pu), and

s is the slip.

The subscripts d and q stand for direct and quadrature component respectively, while subscripts s and r correspond to rotor and stator, respectively.

The slip s can be defined as:

$$s = 1 - \frac{p \omega_m}{2 \omega_s} \quad (3.8)$$

where:

p is pole number,

ω_m is the angular mechanical frequency of wind turbine rotor and generator rotor (rad/s in pu), and

ω_s is the angular electrical frequency of generator stator (rad/s in pu).

The flux linkage in Eqs. 3.4 to 3.7 can be calculated using the following equations:

$$\psi_{ds} = -(L_{s\sigma} + L_m)i_{ds} - L_m i_{dr} \quad (3.9)$$

$$\psi_{qs} = -(L_{s\sigma} + L_m)i_{qs} - L_m i_{qr} \quad (3.10)$$

$$\psi_{dr} = -(L_{r\sigma} + L_m)i_{dr} - L_m i_{ds} \quad (3.11)$$

$$\psi_{qr} = -(L_{r\sigma} + L_m)i_{qr} - L_m i_{qs} \quad (3.12)$$

where:

L is the inductance (H in pu) and subscripts m and σ stand for mutual and leakage, respectively.

The voltage-current relationship result in per unit quantities can be expressed as follows:

$$u_{ds} = -R_s i_{ds} + \omega_s [(L_{s\sigma} + L_m)i_{qs} + L_m i_{qr}] \quad (3.13)$$

$$u_{qs} = -R_s i_{qs} - \omega_s [(L_{s\sigma} + L_m)i_{ds} + L_m i_{dr}] \quad (3.14)$$

$$u_{dr} = -R_r i_{dr} + s\omega_s [(L_{r\sigma} + L_m)i_{qr} + L_m i_{qs}] + \frac{d\psi_{dr}}{dt} \quad (3.15)$$

$$u_{qr} = -R_r i_{qr} - s\omega_s [(L_{r\sigma} + L_m)i_{dr} + L_m i_{ds}] + \frac{d\psi_{qr}}{dt} \quad (3.16)$$

The electrical torque, T_e can be calculated as:

$$T_e = \psi_{qr} i_{dr} - \psi_{dr} i_{qr} \quad (3.17)$$

And the generator speed is given by:

$$\frac{d\omega_m}{dt} = \frac{1}{2H_m}(T_m - T_e) \quad (3.18)$$

where:

H_m is mechanical inertia constant of generator rotor (s)

Finally, we can calculate the generated active P and reactive Q power from the generator that both come from stator and rotor. The reactive power, however, is generated depending on the control strategy of the RSC that feeds the rotor winding [2].

$$P = P_s + P_r = u_{ds}i_{ds} + u_{qs}i_{qs} + u_{dr}i_{dr} + u_{qr}i_{qr} \quad (3.19)$$

$$Q = Q_s + Q_r = u_{qs}i_{ds} - u_{ds}i_{qs} + u_{qr}i_{dr} - u_{dr}i_{qr} \quad (3.20)$$

3.4. Converter Model

For the simulation of WECS with the grid disturbances, the converter model used in this thesis is incorporated with a low frequency representation of the behaviors of the converter during fault [2]. From Fig. 3.1, the rotor currents are derived from both active and reactive power set points, generated by rotor speed controller and terminal voltage controller, respectively. By neglecting the resistance of the stator and assuming that d-axis coincides with the maximum of the stator flux, the electrical torque will only depend on the quadrature component of the rotor current [5]. With the assumptions that u_{qr} equals u_t , the d-axis coincides with the maximum of the stator flux, and from Eqs. 3.13 to 3.17 the following relation between i_{qr} and T_e can be obtained:

$$T_e = \frac{L_m u_t i_{qr}}{\omega_s (L_{s\sigma} + L_m)} \quad (3.21)$$

where:

u_t is the terminal voltage (V in pu).

It is shown in Fig. 3.1 that the reactive power exchange between grid and the stator terminal is dependent on the direct component of rotor current. Therefore, by neglecting the stator resistance in Eqs. 3.13 to 3.16 and 3.19 to 3.20, it can be expressed that:

$$Q_s = -\frac{L_m u_t i_{dr}}{L_{s\sigma} + L_m} - \frac{u_t^2}{\omega_s (L_{s\sigma} + L_m)} \quad (3.22)$$

However, the total reactive power exchange with the grid is not only depending on control of the generator but also relies on the control of GSC which feeds the rotor winding. Therefore, the following equations are applied to the converter:

$$P_c = u_{dc} i_{dc} + u_{qc} i_{qc} \quad (3.23)$$

$$Q_c = u_{qc} i_{dc} - u_{dc} i_{qc} \quad (3.24)$$

where:

Subscript c refers to the converter.

3.5. Model of Rotor Speed Controller

The rotor speed controller is aimed to achieve the optimal energy capture. The relationship of power for the optimal energy capture with the rotor speed is depicted in Fig. 3.2. At low wind speed, the rotor speed is maintained at its minimum value by adjusting the generator torque. At medium wind speed, rotor speed varies proportionally according to the wind speed in order to maintain the tip speed ratio, λ , at its optimum value. After the rotor speed reaches the nominal value, the generated power will be maintained in its nominal value at the same time as well [2].

The speed controller of the variable speed WECS operates based on the actual rotor speed with a sample frequency f_{ss} (Hz) that is on the order of 20 Hz. A set point for the generated power is derived by using the power curve that shows the relationship between rotor speed and the power. Taking into account the actual generator speed, a torque set point is derived from the power set point. From this torque set point, a current set point can be derived using Eq. 3.21.

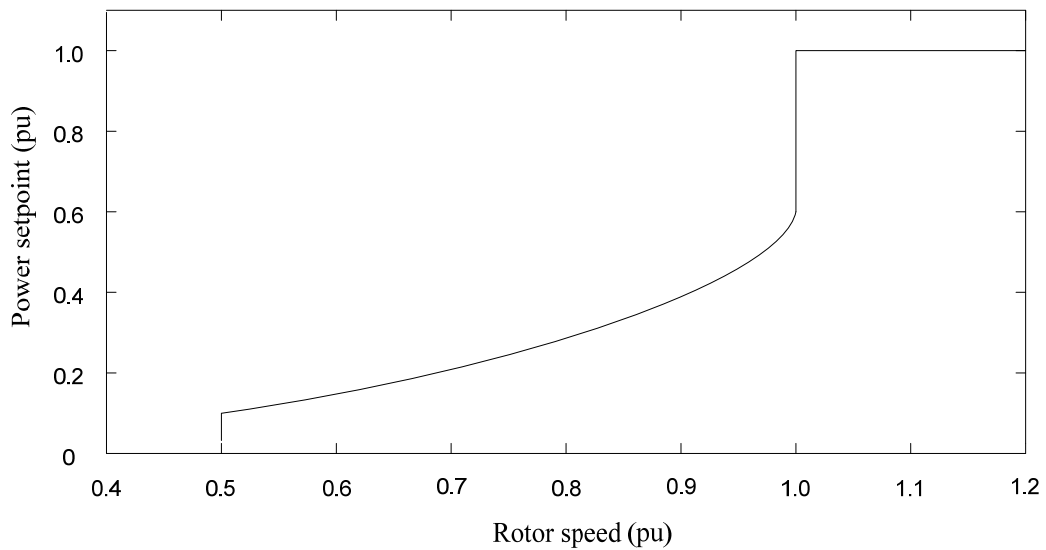


Fig. 3.2. Optimal rotor speed-power characteristic of typical variable speed WECS [2]

3.6. Model of Pitch Angle Controller

Pitch angle control is aimed to control the rotor speed when the wind speed is high. In this circumstance, rotor speed will not be allowed to rotate very fast which could damage the mechanical system. Therefore, the pitch blade mechanism is designed to limit the speed of the rotor when the wind speed is high to avoid the problems [2]. Besides, the pitch control system apparently is useful not only when the wind speed is high but also when a grid disturbance occurs. Therefore, it can be said that pitch control mechanism is also acting as an over-speed protection [6]. When voltage sag for instance occurs on the grid side, power will tend to drop according to the level of sag and followed by the drop of voltage at the PCC. Therefore, the rotor speed will accelerate in such a way to respond to the power drop during this event. With the pitch control mechanism, such damages of the generator caused by high rotor speed during the voltage sag can be avoided.

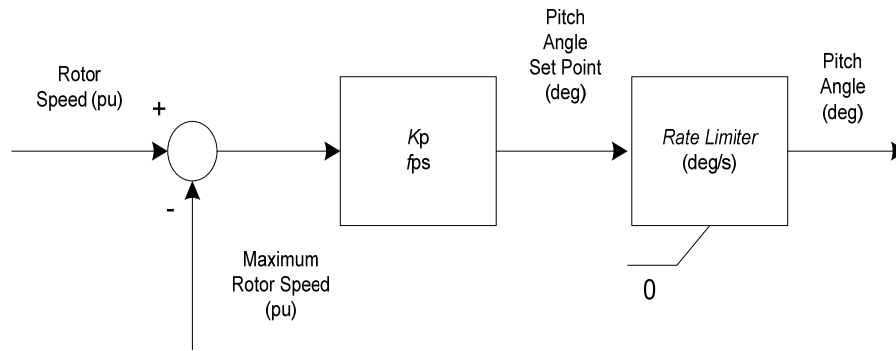


Fig. 3.3. Pitch angle controller model [2]

(Note: K_p is a constant and f_{ps} is the sample frequency of the pitch angle controller)

Eqs. 3.2 and 3.3 can be used to calculate the impact of θ on the performance coefficient. By inserting the results into Eq. 3.1, the mechanical power extracted from the wind can be obtained.

It should be noted that the pitch angle cannot change immediately but only with finite rate which depends on the selected blade size. Usually, the maximum rate change of the pitch angle is laid within 3-10 Hz. Because the change of pitch angle is slow, therefore, it works with a sample frequency f_{ps} on the order of 1-3 Hz [2].

Fig. 3.3 shows the typical concept of pitch controller. It uses a proportional (P) controller. In this controller, a slight over speeding above the nominal limit of the rotor can be tolerated (depending on the selected value of K_p) without posing any problems for the wind turbine.

3.7. Model of Terminal Voltage Controller

Theoretically, a DFIG is able to contribute to terminal voltage control particularly when it is connected to a weak grid. However, if a DFIG is connected to a strong grid, the design control is not necessary to participate in the terminal voltage control [7]. The typical control scheme of terminal voltage is shown in Fig. 3.4.

The Eq. 3.22 shows that the reactive power exchange with the grid can be controlled, thus the terminal voltage is also controllable. The first term on the right-hand side of Eq. 3.22 determines the amount of reactive power exchange with the grid by simply controlling the direct component of the rotor, i_{dr} .

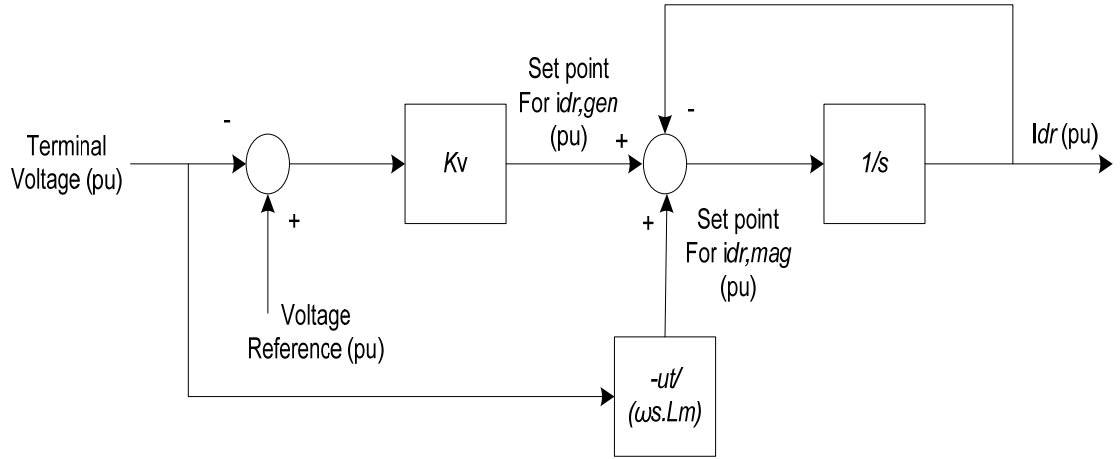


Fig. 3.4. Voltage controller model for a wind turbine with DFIG [2]

(Note: K_V is the voltage controller constant; u_t is the terminal voltage; ω_s is the angular frequency of the stator; L_m is the mutual inductance; i_{dr} is the direct component of the rotor current; $i_{dr,mag}$ and $i_{dr,gen}$ are the currents to magnetize the generator and a part generating reactive power respectively)

The second term represents the magnetization of the stator; therefore, Eq. 3.22 can be rewritten as:

$$Q_s = \frac{L_m u_t (i_{dr,mag} + i_{dr,gen})}{L_{s\sigma} + L_m} - \frac{u_t^2}{\omega_s (L_{s\sigma} + L_m)} \quad (3.25)$$

In which i_{dr} is split into two parts: magnetizing the generator ($i_{dr,mag}$) and generating reactive power ($i_{dr,gen}$). The generator self-magnetization is given as:

$$i_{dr,mag} = -\frac{u_t}{\omega_s L_m} \quad (3.26)$$

And the amount of reactive power exchange between the stator and the grid is given below:

$$Q_s = -\frac{L_m u_t i_{dr,gen}}{L_{s\sigma} + L_m} \quad (3.27)$$

3.8. The T-Form Equivalent Circuit of DFIG Machine

Some other references also conveniently adopted the transient model of DFIG using the T-form equivalent circuit as depicted in Fig. 3.5 [8].

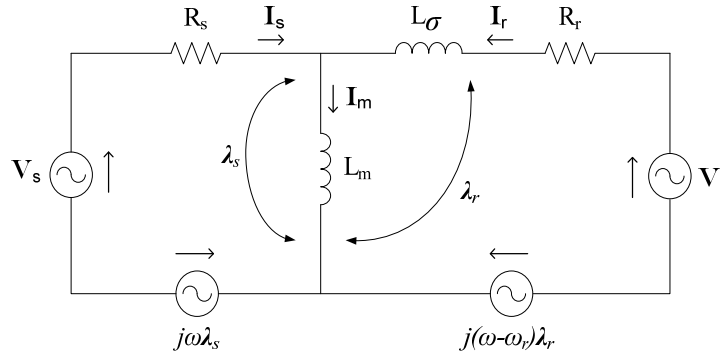


Fig. 3.5. Equivalent circuit of DFIG in T-form [8]

The stator winding is directly connected to a transformer low voltage side while the rotor winding is connected to a bidirectional back-to-back IGBT based VSC. The converter helps in decoupling the mechanical and electrical frequencies and facilitates variable-speed operation. As the DFIG is equipped with partial scale converter, the turbine cannot operate in the full range from zero to the rated speed; however, the speed range is proven to be quite sufficient [9]. Simplifying the model of DFIG without losing the model accuracy is possible with the “T- form” equivalent circuit of Fig. 3.5 [10]. This simplification facilitates the analysis of DFIG circuit. As the detailed analysis of DFIG in “T- form” is available and discussed in Refs [11-13], a quick review and presentation of the key equations are provided here. The stator and rotor voltage vectors in the arbitrary reference frame are given as:

$$V_s = R_s I_s + \frac{d\lambda_s}{dt} + j\omega\lambda_s \quad (3.28)$$

$$V_r = R_r I_r + \frac{d\lambda_r}{dt} + j(\omega - \omega_r)\lambda_r \quad (3.29)$$

where:

ω is the angular speed (rad/s), while subscripts, s and r indicate stator and rotor parameters/quantities, respectively.

From Fig. 3.5, the flux space vectors of stator and rotor can be expressed as:

$$\lambda_s = L_m I_m \quad (3.30)$$

$$\lambda_r = L_\sigma I_r + L_m I_m \quad (3.31)$$

where:

L_m is the magnetizing inductance (H in pu) and

L_σ is the leakage inductance (H in pu).

Since $I_m = I_s + I_r$, the stator current can be calculated as:

$$I_s = \frac{\lambda_s}{L_m} - I_r \quad (3.32)$$

3.9. Control Scheme of DFIG's Converters

3.9.1. Control Scheme of Grid Side Converter (GSC)

In generic models, the main task of GSC controller is to maintain the fixed set value of DC link voltage. Failure to regulate the DC link voltage in the safety margin will lead to damage of the power electronic device. If such voltage is increased above the safety margin, the DC link capacitor will be damaged and, consequently, the system will lose its grid control capabilities. The generic control scheme of DC link voltage (V_{DC}) is shown in Fig. 3.6. To simplify the calculation, most control concepts currently use the direct-quadrature ($d-q$) form. The benefit of using this method is that all 3-phase quantities are expressed as DC components, which make them easy to control. Moreover, both active and reactive power can be controlled independently (decoupled) to achieve the most optimal responses to the system [14].

The control system for GSC is much simpler compared to the control system for RSC, as will be explained later. The control system for GSC in this study is mainly determined by the value of the DC link voltage (V_{DC}). Through a conventional PI (proportional-integral) controller, a direct quantity current reference

(I_d^*) is generated by the difference value of reference DC link voltage (V_{DC}^*) and its measured value (V_{DC}).

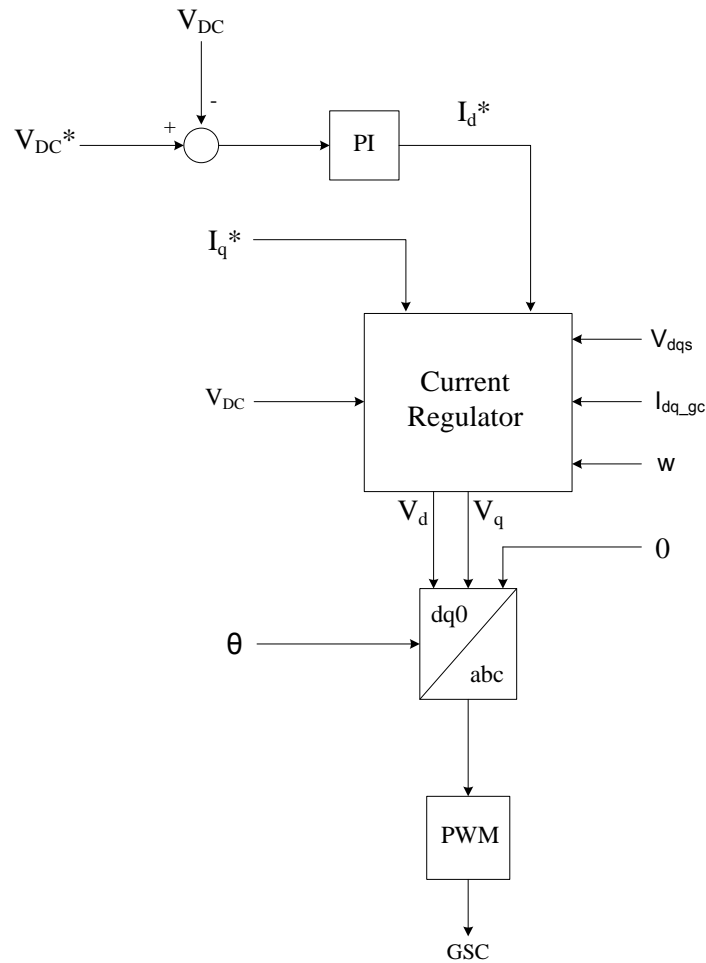


Fig. 3.6. Control system of the GSC

The value of quadrature quantity current reference (I_q^*) is set up to zero in this study. Along with both I_{dq}^* values, direct-quadratic quantities of stator voltage (V_{dqs}), direct-quadrature quantities of the grid converter current (I_{dq_gc}) and the turbine speed (w) are calculated to obtain the V_d and V_q in the current regulator. By using Clarke's transformation ($dq0-abc$), the pulsation signal for the GSC switching device can be generated through a PWM (pulse width modulation). The use of Park's transformation (shown in Fig. 3.7 and 3.8) is very famous in converting the 3-phase signal into a represented stationary frame to eliminate inter-phases dependency [15-19]. The basic principle of Park's transformation can be explained as follows [20, 21]:

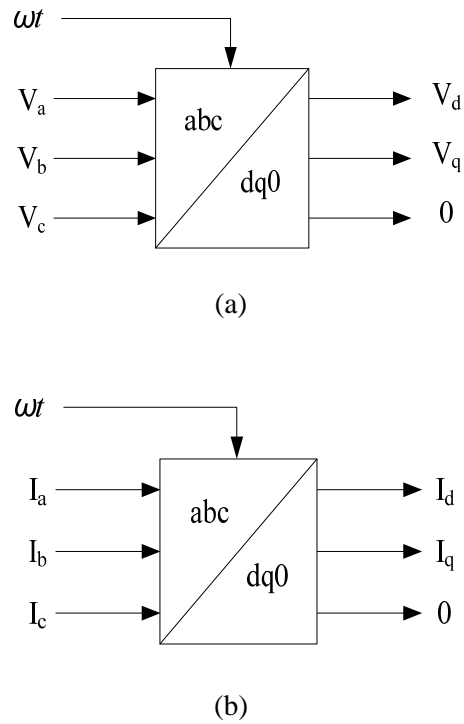


Fig. 3.7. Park's transformation from 3-phase reference frame to $dq0$ reference frame;
 (a) 3-phase voltage and (b) 3-phase current

In Matlab, this transformation block is available, where it is flexible to be used for both voltage and current sinusoidal signals. The abc - $dq0$ transformation computes the direct axis, quadratic axis and zero sequence quantities in a two-axis rotating reference frame for a 3-phase sinusoidal signal [21]. The transformation's equations are stated in Eqs. 3.33 to 3.35:

$$V_d = \frac{2}{3} \left(V_a \sin(\omega t) + V_b \sin\left(\omega t - \frac{2\pi}{3}\right) + V_c \sin\left(\omega t + \frac{2\pi}{3}\right) \right) \quad (3.33)$$

$$V_q = \frac{2}{3} \left(V_a \cos(\omega t) + V_b \cos\left(\omega t - \frac{2\pi}{3}\right) + V_c \cos\left(\omega t + \frac{2\pi}{3}\right) \right) \quad (3.34)$$

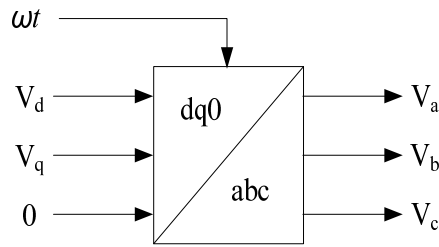
$$V_0 = \frac{1}{3} (V_a + V_b + V_c) \quad (3.35)$$

where :

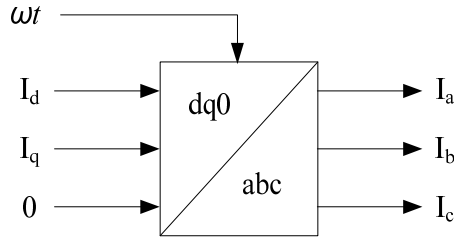
ω is angular velocity (rad/s) of the rotating frame.

In the case of a 3-phase current, the same equations can be used.

The reverse of $abc-dq0$ transformation is shown in Fig. 3.8. This $dq0-abc$ transformation is used to transform three quantities (direct axis, quadratic axis and zero-sequence components) expressed in a two-axis reference frame returns to 3-phase quantities [21].



(a)



(b)

Fig. 3.8. Park transformation from $dq0$ reference frame to 3-phase reference frame; (a) 3-phase voltage and (b) 3-phase current

The transformation can be obtained through Eqs. 3.36 to 3.38:

$$V_a = V_d \sin(\omega t) + V_q \cos(\omega t) + V_0 \quad (3.36)$$

$$V_b = V_d \sin\left(\omega t - \frac{2\pi}{3}\right) + V_q \cos\left(\omega t - \frac{2\pi}{3}\right) + V_0 \quad (3.37)$$

$$V_c = V_d \sin\left(\omega t + \frac{2\pi}{3}\right) + V_q \cos\left(\omega t + \frac{2\pi}{3}\right) + V_0 \quad (3.38)$$

For the use of 3-phase current, the 3-phase voltage quantity (V_{abc}) is simply replaced with the 3-phase current (I_{abc}).

3.9.2. Control Scheme of Rotor Side Converter (RSC)

Mostly, the generated electrical power is controlled through RSC as explained below.

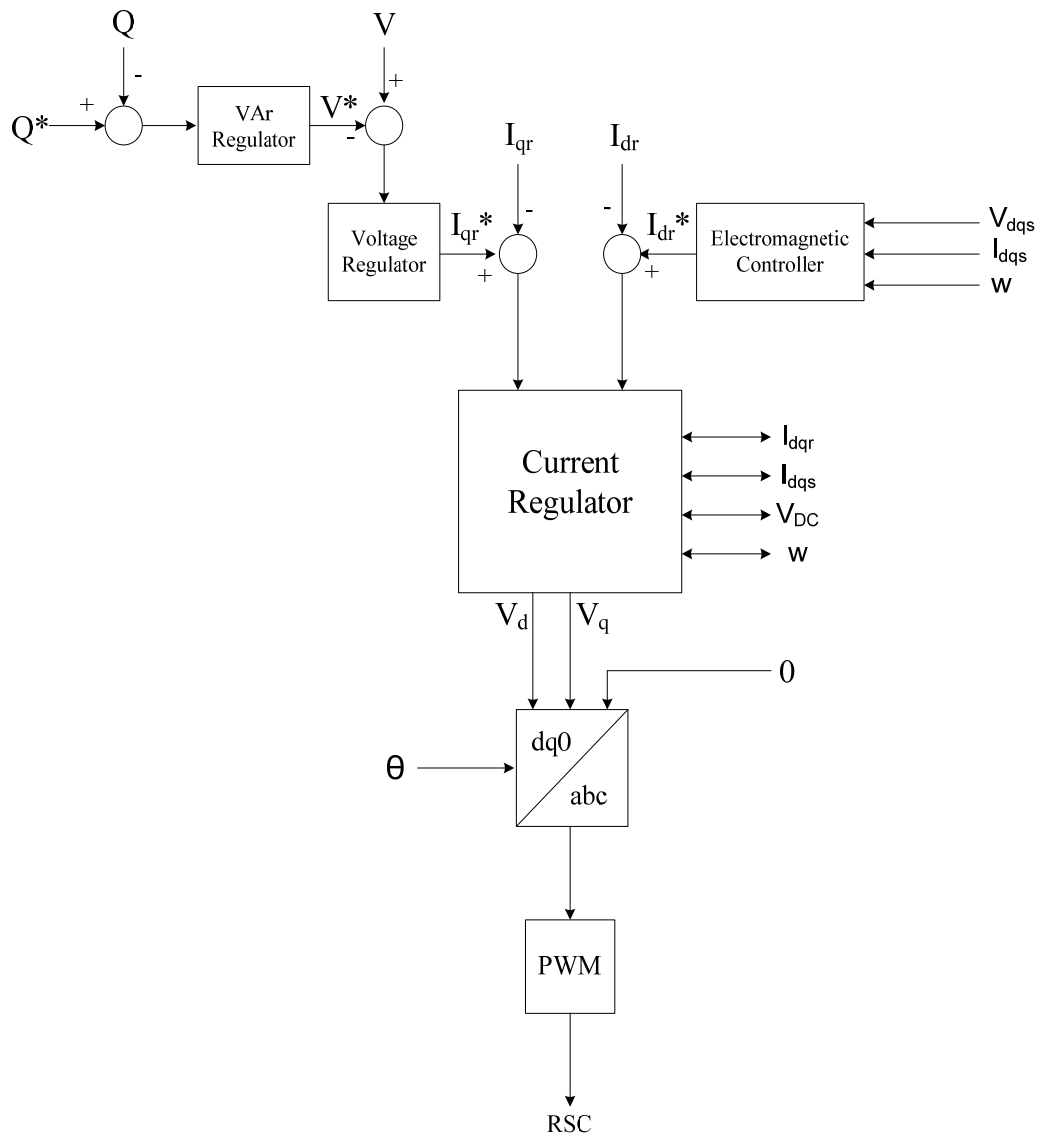


Fig. 3.9. Control system of the RSC

The main controller for RSC is a current regulator. This is based on the PI controller, which will generate a direct-quadrature voltage (V_{dq}) as a reference signal of PWM that determines the switching signal of the RSC's switches. This signal is

generated after transforming it into a V_{abc} form, as shown in Fig. 3.9. The inputs of the current regulator are acquired from both direct-quadrature currents of the DFIG's rotor (I_{dqr}) and stator (I_{dqs}).

The V_{DC} and the rotor speed (w) are used to calculate the modulation and the phase angle. The electromagnetic controller, which is determined by calculating the stator direct-quadrature value of both voltage (V_{dqs}) and current (I_{dqs}), collectively with the rotor speed (w), is used to obtain the reference value of the rotor direct current (I_{dr}^*). Meanwhile, to obtain the reference value of a rotor quadrature current (I_{qr}^*), a voltage regulator is applied where its input depends on the difference value between the measured voltage (V) and the reference voltage (V^*). To attain the voltage reference (V^*), a VAr regulator is applied where its value is dictated from the difference value between measured reactive power (Q) and the determined reactive power reference (Q^*).

3.10. Summary

In this chapter, the general equations used for simulating the DFIG WECS are presented. The overall generic model of the rotor, generator, and converter are comprehensively explained. The control systems of rotor speed, pitch angle, and terminal voltage are also provided. Additionally, the detail structure of a current regulator-based controller for both the GSC and RSC is briefly discussed. To facilitate the simulation without reducing the accurateness of the model, the $d-q$ frame form representative was applied. The Park's transformation, which is widely used in the $d-q$ frame representation of DFIG and its control models, are also comprehensively discussed in this chapter.

3.11. References

- [1] J. M. Miller, J. C. K. Yeung, Y. Q. Ma, and G. Sartorelli, "Ultracapacitors Improve SWECS Low Wind Speed Energy Recovery. Ultracapacitor and Battery For Low Wind Energy Harvesting", in *Power Electronics and Machines in Wind Applications, 2009. PEMWA 2009. IEEE*, pp. 1-6. 2009
- [2] T. Ackerman, "Wind Power in Power System", West Sussex: John Wiley and Sons, Ltd. 2005
- [3] S. Heier, "Grid Integration of Wind Energy Conversion Systems", Chichester: John Wiley & Sons Ltd, UK. 1998.

- [4] P. Kundur, "Power System Stability and Control", Toronto: McGraw-Hill, Inc. 1994
- [5] H. Siegfried, "Grid Integration of Wind Energy Conversion Systems", Chichester and New York: Wiley. 1998
- [6] A. D. Hansen, N. A. Cutululis, H. Markou, P. Sorensen, and F. Iov, "Grid Fault and Design-Basis for Wind Turbines-Final Report", National Laboratory for Sustainable Energy (Riso DTU). 2010
- [7] V. Ahkmatov. "Analysis of Dynamic Behaviour of Power Systems With Large Amount of Wind Power", <http://www.dtu.dk/upload/centre/cet/projekter/99-05/05-va-thesis.pdf>, accessed: 25 February, 2011
- [8] M. Mohseni and S. M. Islam, "Stabilization of Fixed-Speed Wind Generators Using Adjacent Doubly Fed Induction Generator". *IEEE PES Innovative Smart Grid Technologies, ISGT Asia 2011*, Perth, Australia, 13-16 November. 2011
- [9] J. M. Carrasco, L. G. Franquelo, J. T. Bialasiewicz, E. Galvan, R. C. P. Guisado, M. A. M. Prats, J. I. Leon, and N. Moreno-Alfonso, "Power-Electronic Systems for the Grid Integration of Renewable Energy Sources: A Survey", *IEEE Transactions on Industrial Electronics*, vol. 53, pp. 1002-1016. 2006
- [10] G. R. Slemon, "Modelling of Induction Machines for Electric Drives", *IEEE Transactions on Industry Applications*, vol. 25, pp. 1126-1131. 1989
- [11] M. Mohseni, S. M. Islam, and M. A. Masoum, "Enhanced Hysteresis-Based Current Regulators in Vector Control of DFIG Wind Turbines", *IEEE Transactions on Power Electronics*, vol. 26, pp. 223-234. 2011
- [12] M. Mohseni, S. M. Islam, and M. A. S. Masoum, "Impacts of Symmetrical and Asymmetrical Voltage Sags on DFIG-Based Wind Turbines Considering Phase-Angle Jump, Voltage Recovery, and Sag Parameters", *IEEE Transactions on Power Electronics*, vol. 26, pp. 1587-1598. 2011
- [13] M. Mohseni, M. A. S. Masoum, and S. Islam, "Emergency Control of DFIG-Based Wind Turbines to Meet New European Grid Code Requirements", in *Innovative Smart Grid Technologies (ISGT), 2011 IEEE PES*, pp. 1-6. 2011
- [14] S. M. Bolik, "Modelling and Analysis of Variable Speed Wind Turbines with Induction Generator during Grid Fault", Institute of Energy Technology Aalborg University. 2004
- [15] M. P. Kazmierkowski, M. A. Dzieniakowski, and W. Sulkowski, "Novel Space Vector Based Current Controllers for PWM-Inverters", *IEEE Transactions on Power Electronics*, vol. 6, pp. 158-166. 1991
- [16] P. Ching-Tsai and C. Ting-Yu, "An Improved Hysteresis Current Controller for Reducing Switching Frequency", *IEEE Transactions on Power Electronics*, vol. 9, pp. 97-104. 1994
- [17] A. Tilli and A. Tonielli, "Sequential Design of Hysteresis Current Controller for Three-Phase Inverter", *IEEE Transactions on Industrial Electronics*, vol. 45, pp. 771-781. 1998
- [18] J. F. A. Martins, A. J. Pires, and J. F. Silva, "A Novel and Simple Current Controller for Three-Phase PWM Power Inverters", *IEEE Transactions on Industrial Electronics*, vol. 45, pp. 802-804. 1998
- [19] E. Aldabas, L. Romeral, A. Arias, and M. G. Jayne, "Software-Based Digital Hysteresis-Band Current Controller", *Electric Power Applications, IEE Proceedings*, vol. 153, pp. 184-190. 2006

- [20] http://en.wikipedia.org/wiki/Dqo_transformation, accessed: 6 May, 2012
- [21] http://www.mathworks.com.au/help/toolbox/physmod/powersys/ref/dq0_to_ab-c_transformation.html, accessed: 6 May, 2012

“Every reasonable effort has been made to acknowledge the owners of copyright material. I would be pleased to hear from any copyright owner who has been omitted or incorrectly acknowledged.”

Chapter 4 | **Energy Storage Technologies for Renewable Energy Resources**

4.1. Introduction

The inherent intermittent behavior of renewable energy sources will result in inconsistent power output. Meanwhile, the customer needs the voltage output to be stable, at least within the range of the equipment's safety margin, and the customer must be able to access power immediately. These needs have made diesel and other conventional constant power output generators the dominant supplies ever since the power generator was introduced in the nineteenth century. After the Kyoto Protocol in 1997 [1], the demand for flexible renewable energy sources has skyrocketed as countries wish to mitigate the adverse environmental effects of conventional energy sources. In response to this demand, all sustainable energy systems must limit their reliance upon conventional resources and increase the engagements of renewable energy resources over the next 20-30 years [2]. Overcoming the uncertain behavior of the renewable energy resources would make this goal feasible. Developers have been revising EST for a few decades, and the technology has become so mature that its storage capacity worldwide is currently the equivalent of about 125 GW [3].

Energy storage in a power system can be defined as any installation or method, usually subject to independent control, which is capable of storing energy and using it in the power system when required [4]. Energy storage devices are intended to supply energy when the system is under high demand; they are also designated to save energy during low energy demand. These devices are very important to maintaining the continuity of power supply when the main source of power cannot meet all the power demands. On account of this role, energy storage devices are also

considered as back-up power systems. Therefore, devices such as solar panels and wind turbine generators not only run on renewable resources, but also increase the value of electricity generated by backing it up during peak demand periods or during the fluctuations of energy resources. With the proper controller, the natural intermittent characteristic of renewable resources can be smoothed out through energy storage devices [5]. In this chapter, some well-known storage systems that are pervasive in current power systems will be presented. The chapter will also explain their advantages and limitations as well as their applications to renewable energy resources such as PV and wind. Finally, a short summary and comparison will appear in the last section.

4.2. Battery Energy Storage System (BESS)

The BESS stores energy in a chemical form. When BESS is connected to the power system, it releases energy back into the network whenever there is a demand. Then, BESS recharges when the grid returns to its normal operation [6]. Batteries are considered as very old storage technologies as they were invented roughly one hundred years ago. Therefore, they are well utilized, explored, and tested and have been a highly popular form of energy storage solution since the early twentieth century. Many types of batteries are available in the market, but this chapter focuses on the batteries that store energy in electric power utility applications, and it pays particular attention to their application in renewable energy sources. Unlike other storage systems, BESS has no significant effect on the environment [7]. The efficiency of this storage system is around 60% to 80% [2, 8, 9] depending on how often the batteries cycle and how often the electrolytes are used. The lead-acid battery is still the most commonly used battery because of its relatively economic power density, especially in the automotive industry. However, it is not designed for deep discharge applications and its charging state should always be kept at the maximum charge level through constant voltage. Thus, the common lead-acid battery is not suitable as a storage device for distributed generations (DG), such as small PVs and wind distributed generators that must repeatedly discharge as much as 80% of their capacity [1]. Flow battery currently attracts engineers because it can store energy in the 5-500 MW range and operates in time fractions from 1 second to 12 hours [10]. Although BESS possesses great energy storage potential, it cannot endure high cycling rates, nor can it store large amounts of energy in a small volume.

Instead, they have a short life cycle and a limited discharge capability [2, 11]. Therefore, high-capacity power systems need large battery banks that may be less effective than other storage devices. BESS requires routine monthly inspections to ensure adequate water levels and no corrosion on the battery's terminals. Additionally, the battery state of charge should also be evaluated two to three times per year [1]. These frequent check-up routines will increase the maintenance cost of the battery banks. In addition, the battery contains toxic materials, so inappropriate disposal of used-batteries will harm the ecological system. Accordingly, operators who choose to use BESS must follow the strict regulations of used-battery disposal. A typical common battery and then the BESS connected with WECS are depicted in Figs. 4.1 and 4.2, respectively.

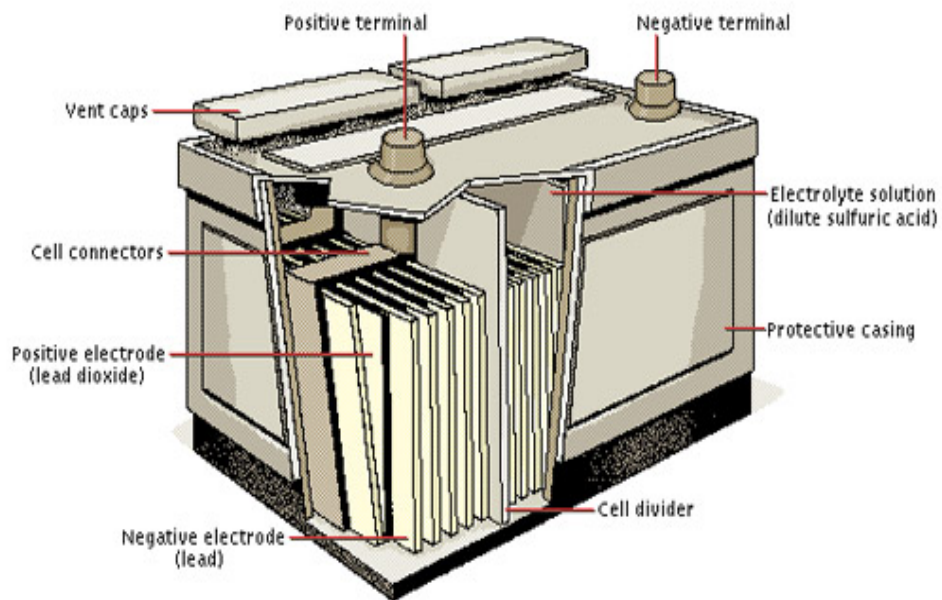


Fig. 4.1. Typical classic lead acid battery system [12]

Many studies have presented the application of BESS in conjunction with wind power generation. Some studies have simulated, analyzed, and discussed the hybrid system of energy storages between battery and capacitor [13-16], with flywheel [17] and thermal energy storage [18]. A dual battery scheme is introduced in Ref [19]. This method utilizes two BESSs where the power generated by the wind turbine charges one BESS while concurrently, the second BESS discharges power into the grid. In addition, there are some publications presenting introductory information on the types of batteries that may be directly connected to the DC-link of the variable speed WECS such as the PMSG [20, 21].

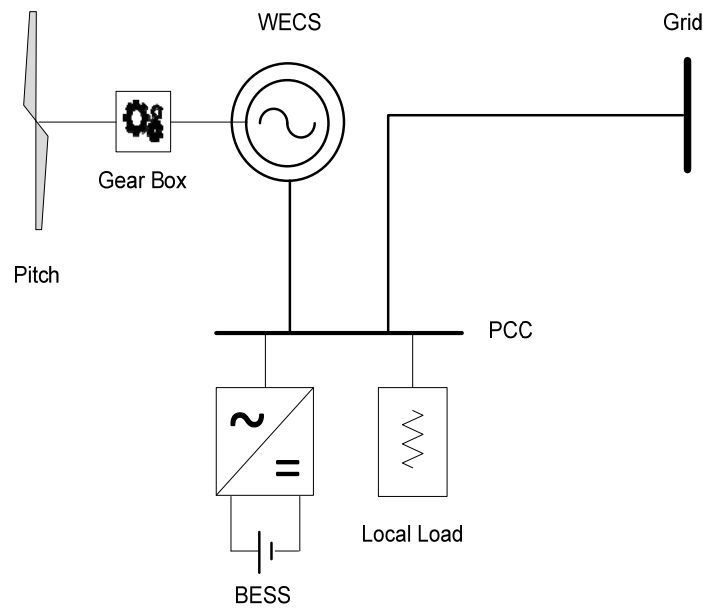


Fig. 4.2. Typical configuration of a WECS-grid connected with BESS

Refs [22, 23] have successfully simulated the small capacity of a wind-diesel hybrid system (WDHS) that is backed up by a 240 V Ni-Cd battery during load and wind variations. Refs [22, 23] provide discussions on batteries that work in conjunction with the static synchronous compensator (STATCOM) to achieve better charging/discharging process with the grid. Finally, the application of a battery as a mature storage technology in a hybrid renewable system of wind and PV panels connected to the grid is studied in Refs [24-26]. The combination of two or more types of EST might result in a system that performs better. However, one must note that any addition or combination of an EST will increase the cost of the system and make the control system more complex. Therefore, reliable control algorithms must be applied to the combined systems.

BESS is the most common and most suitable storage system for photovoltaic (PV) solar panels, because there are enough BESS in the market niche to match the size of most PV systems. There are many reports on various applications of BESS with PV systems. For example, Ref [27] demonstrates BESS supplying a standalone PV system with a rather simple controller. Ref [28] provides details of a multi-objective capacity hybrid power system with PV-wind-diesel-battery. Ref [29] presents a model to assess the economic and environmental impact of PV with diesel-BESS for remote villages.

Although the battery has proven to be proficient at smoothing and backing up the wind and PV output power, the main drawbacks of batteries are their maintenance costs and relatively short life cycles. Manufacturers consider these drawbacks carefully, and they often choose alternative energy storage systems. Moreover, for large wind farm systems, relatively large battery banks must be connected, which consequently increases the maintenance costs and replacement costs as mentioned above.

4.3. Ultracapacitor (UC)

UC has the characteristics of both a capacitor and a battery. However, UC undergoes no chemical reaction as does a battery, so the UC's cycling capacity is significantly higher [2]. UC is also referred to as supercapacitor or electrochemical capacitor, but the term ultracapacitor seems to be more familiar in the power industry [1]. The basic concept of UC is laid out in Eq. 4.1 and can be better understood using Fig. 4.3.

$$C = \epsilon \frac{A}{d} \quad (4.1)$$

where:

ϵ is dielectric constant,

d is thickness (mm), and

A is the geometric area (mm²).

UC has several advantages over BESS, including higher cycle capacity (more than 100,000 cycles) with efficiency greater than 90%. UC has been used for peak shaving purposes with a power range of hundreds of kilowatts in just one second (faster than battery) [1]. UC has often been characterized as being somewhere between a battery and a conventional capacitor. As can be seen in Fig. 4.4, the energy density of UC is lower than the energy density of BESS, but UC's energy density is higher than that of a conventional capacitor. Inversely, in terms of power density, UC has less power density than a conventional capacitor has but more power density than BESS.

A presentation has been included in [30] of an application of UC with a battery to improve the power dispatch of WECS during low wind speed. Installing UC instead of a conventional capacitor on PMSG based WECS is discussed in [31] and UC's combination with fuel cells is introduced in Ref [32].

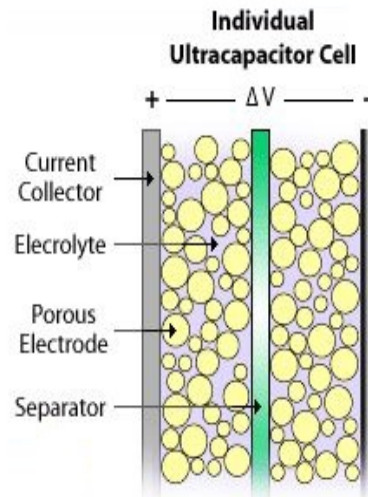


Fig. 4.3. Typical diagram of simple UC [33]

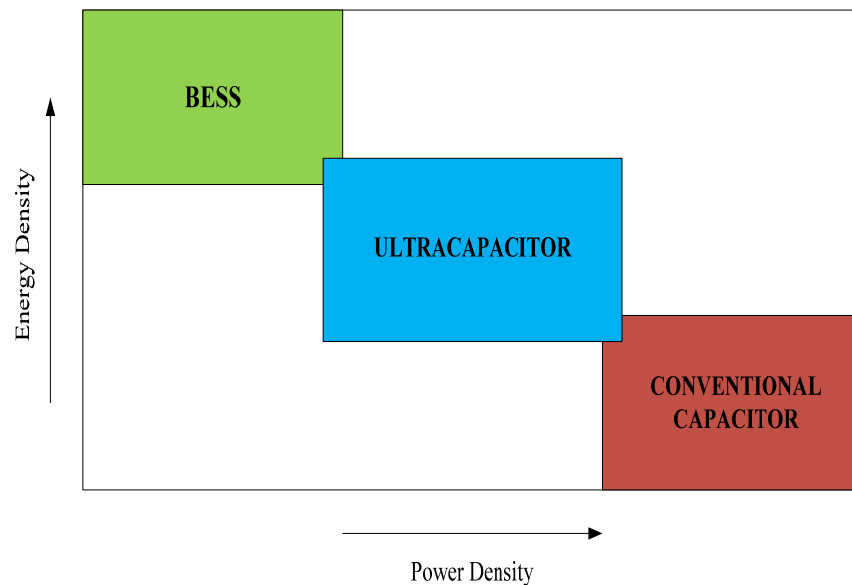


Fig. 4.4. Comparison of energy and power density of UC, BESS, and conventional capacitor [1]

The advantages of connecting UC with a large PV system over connecting a battery or a shunt capacitor to stabilize the large PV systems is presented in Ref [34], along with comparisons of connecting UC with hydro and thermal power systems. Study that tested UC's ability to meet load demands when connected to a standalone

PV system is in Ref [35] and the studies that examined UC's ability to match the power demand of a micro-grid when connected to an integrated PV are listed in Refs [36, 37]. The new, composite energy storages of UC and BESS, which are designed to manage dynamic energy on a micro-grid, are discussed in Ref [38] and a composite of UC, BESS, and PV for electric vehicles is designed and modeled in Ref [39]. Unlike BESS, UC has sufficient efficiency for grid application and achieves about 90%. UC's estimated cost/kW is also more competitive than BESS's, as indicated in Fig. 4.16. However, UC has low power density, so the size of UC remains in the wattage scale. Recent prototypes have increase UC's kW range, but its scalability is still incompatible for large-scale WECS and for PV system applications.

4.4. Superconducting Magnetic Energy Storage (SMES)

Superconducting coil stores energy within a magnetic field created by the flow of direct current in a coil that should be maintained within a superconductive state through immersion in liquid Helium at 4.2 K in a vacuum-insulated cryostat. SMES is the only storage system known to store electrical energy directly based on electric current [40]. The energy content in an electromagnetic field is determined by the flow of current through the N turns of the magnet coil. The product, NI , is called the magnetomotive force. The electromotive force in the coil can be calculated with Eq. 4.2, and the energy produced is given by Eq. 4.3. The stored energy can be calculated by integrating the magnetic field strength, H , over the entire volume in which the induction, B , is significant. By assuming the H - B characteristic is linear, the volume energy density can be obtained from Eqs. 4.2 and 4.3, as shown in Eq. 4.4. The energy density that a magnetic field achieves can then be calculated according to Eqs. 4.3 and 4.4.

$$e = -N \frac{d\phi}{dt} \quad (4.2)$$

$$E = \int_0^{\phi} Ni(t) d\phi = \int_0^B lHA dB = \int_{Volume} \int_0^B H dB \quad (4.3)$$

$$E_{Volume} = \frac{B^2}{2\mu} \quad (4.4)$$

where:

e is electromotive force (V),

E is stored energy (J),

N is number of turns,

i is current (A),

θ is flux (Wb),

l is length (m),

H is magnetic field strength (A.turns/m),

A is geometric area (m²),

B is magnetic induction (Wb/m²), and

μ is permeability (Wb/Am).

Simplifying Eq. 4.4, the energy stored in an inductor is proportional to the inductance value and square of the current as indicated by Eq. 4.5.

$$E = \frac{1}{2} Li^2 \quad (4.5)$$

where:

E is the stored energy (J),

L is the inductance value of the coil (H), and

i is the current flow in the coil (A).

Therefore, it seems reasonable to assume that high values of energy density are possible only with such media as air or a vacuum with very high current values. However, regardless of the media, the electrical resistance of the coil is always a limiting factor [1]. The critical temperature is the point at which the electrical resistance drops drastically. By using liquid helium, one can bring all superconductors' states close to 4 K. Generally, a superconducting coil can be made of Niobium-Titane (NbTi) filaments that operates at extremely low temperatures [2]. After the 1980s, new superconductors made of copper oxide ceramic became available. By using liquid nitrogen, this material can be chilled to around 100 K. This new material is known as high-temperature superconductors (HTS) [1].

To allow power exchange between the SMES coil and the system, a power electronic converter is interfaced with the SMES coil and the grid to control the energy exchange between them. Given the rapid development of materials that exhibit superconductivity closer to room temperature, this technology will become economically viable in the next few years [41]. The overall efficiency of SMES depends on the coil material and the configuration used, which typically exhibits a range of 90-98% [2, 7, 40, 42]. The SMES unit is highly efficient due to its lower power loss. Electric currents in the coil encounter almost no resistance, and the unit has no moving parts. The other advantages of SMES over other storage systems include the SMES's short and quick time delay during the charge and discharge process [43]. The SMES can make power available almost immediately, and it can provide very high power output for a short period. Thus, if a customer's demand is immediate, then SMES is a viable option [44]. Moreover, compared to the capacity of a large pumped hydro, the proposed large capacity of SMES is arguably the only device that can accommodate large bulk power load leveling applications with high efficiency [7]. Although the SMES's cost per unit of energy stored is high compared to that of other storage technologies, it is cost competitive with other FACTS and transmission upgrade solutions. At present, these facilities are generally applied to provide power-grid stability in a distribution system as well as to provide good power quality at manufacturing facilities with critical loads that are highly susceptible to voltage instabilities [6].

Many sources of information on storage mention the SMES's capability of storing high Wh. As an example, Ref [1] mentions that SMES is able to store up to about 10 MW. Better yet, its capacity is even higher over a shorter time span, because a coil of a 150 to 500-m radius would be able to support a load of 5000 MWh. Ref [45] claims that SMES is even capable of storing energy in the range of 1000 to 10,000 MWh. As for the total SMES currently installed throughout the world, they may offer as much as 100 MW capacity [40]. Micro-SMES devices in the range of 1 to 10 MW are available in the market niche, and more than 30 micro-SMES with a total approximate capacity of 50 MW have been installed in different parts of the US for good power quality or an uninterruptible power supply [46]. The Engineering Test Model is a large SMES with a capacity of about 20 MWh, and it is

capable of providing 400 MW of power for 100 seconds or 10 MW of power for 2 hours [44].

A SMES system includes a superconductor coil, a power condition system, a cryogenic refrigerator and a cryostat or vacuum vessel to maintain the coil at a low temperature-required to maintain it in the superconducting state. The typical SMES configuration is shown in Fig. 4.5.

The ACCEL Instruments GmbH team in Germany has designed a 2-MJ SMES system to ensure the power quality of a laboratory plant at DortmunderElektrizitäts und Wasserwerke [45]. American Superconductor has a commercial device called D-SMES, which is a shunt-connected flexible AC transmission device that was designed to augment grid stability, improve power transfer and increase reliability [1]. The major drawback of SMES is its high cost of implementation as well as the environmental issues associated with strong magnetic fields [11].

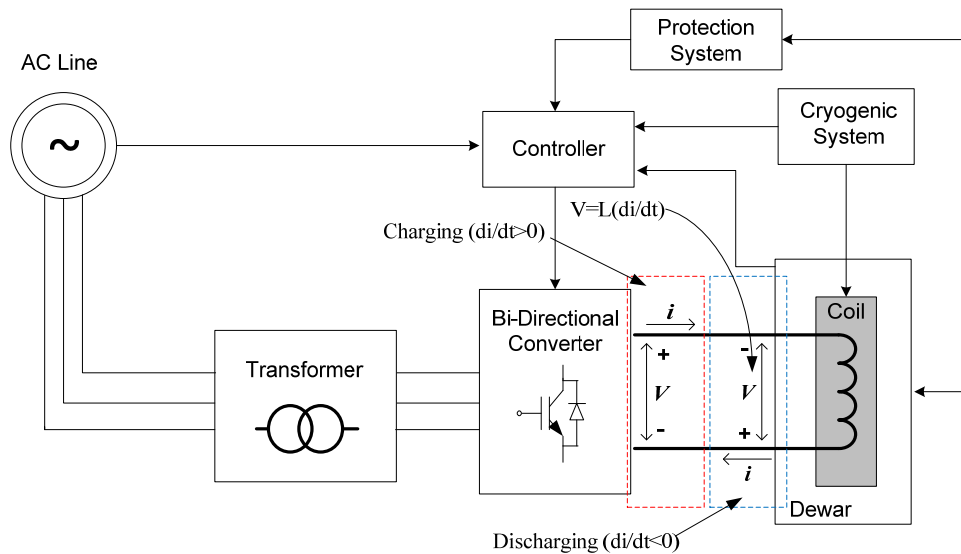


Fig. 4.5. Typical schematic diagram of a SMES unit [48]

However, with the use of appropriate HTS materials, designers may overcome these drawbacks and thus encourage a market niche for SMES in the near future [3]. Other disadvantages of SMES are noted in [49], such as the coil's sensitivity to temperature. Small changes in temperature can cause the coil to become unstable and lose energy in heat form since the superconductor state value depends on the cryogenic temperature. In addition, refrigeration can cause parasitic losses within the

system. The disadvantages mentioned above mostly pertain to possible technical problems, so designers should be able to mitigate them with accurate designs.

The suitability of the SMES unit for renewable energy-based power systems has been demonstrated in many studies, however no article (to the best of author knowledge) available for the test and experiment information of SMES on wind turbine system. SMES can regulate the natural intermittence of most renewable energy resources with its high efficiency, quick response, and long life duration. While it is true that the solar power system provides a fairly constant energy resource with relative ease compared to wind energy systems, it simply cannot provide enough power for large-scale operations without being enormous and expensive. Thus, the SMES unit may be a competitive choice as a ETS candidate compared to other ETS. An early SMES's application to renewable energy is presented in Ref [50], In this study, SMES is used to steady the output power of PV arrays. Ref [51], then describes an advanced system design of PV/SMES. This reference includes three main objectives for applying SMES to PVs connected to a distribution system. The first objective is to smooth the output power of the PV due to the insulation fluctuation. In addition, the SMES system can also support an active and reactive power demand fluctuation in a power distribution system. This hybrid system is also designed to reduce the transient influence caused by a sudden change in the effective and reactive load demand. Ref [51] also introduces the concept of the I/V (current/voltage) converter that uses IGBT, and allows energy to transfer from the SMES coil to the utility system and vice-versa. A new type of dispersed system is introduced in [52]. In this reference, the system consists of a PV, Fuel Cell (FC), and SMES. Both the PV and FC use a boost chopper to transfer power. Meanwhile, the SMES is connected to an I/V converter that uses GTO to allow the charging and discharging process with the grid, as illustrated in Fig. 4.6.

The main purpose of applying SMES to wind WECS is to stabilize the system in order to compensate for the WECS's fluctuating output power. Some papers have been published regarding this objective, and a few are listed in Refs [53-58]. In Ref [53], the study tests a squirrel cage induction generator and then presents a comparison of the results of the STATCOM and SMES connected to the system. However, this study does not work out the detailed model control of the SMES unit.

The application of SMES that is controlled by fuzzy logic and connected to a wind farm is presented in Ref [54]. In this reference, the study uses a 6-pulse CSC. The CSC consists of 6-GTO to allow the transfer and absorption of energy from the SMES coil to the power system and vice-versa, which is depicted in Fig. 4.7. However, the fuzzy logic, only consists of one input to control the level degree of CSC's firing angles in order to allow transfer or absorb energy which is unrealistic to apply because the capacity of the SMES coil, on the other hand, has to be taken into consideration to make it closer in a realistic application as described in Chapter 5 of this thesis. In addition, using 6-GTO in SMES application might cause harmonic distortion. Therefore, the 6-GTO should be more robust when it is applied to a 12-pulse CSC with the appropriate transformer connection in order to eliminate the 5th, 7th, 17th, and 19th harmonics in the system [59].

The focus of Ref [55] is to enhance the transient stability of the system by using SMES under various wind fluctuations. This SMES unit consists of an AC/DC converter that is controlled by regulating the modulation index and the phase angle. However, the result for the transient response of active power output (P_{IG}) with or without SMES does not seem very significant, whereas the transient response of active power in a tie line is quite significant.

The enhancement of the transient stability of a wind-SMES connected to the grid is also studied in [56]. The system studied in Ref [56] is similar to the one studied in Ref [54]. However, the SMES configuration used in [56] consists of a VSC and a DC-DC chopper, which both use IGBTs. The controller of VSC is using PWM while conventional PI controller is used to control the DC-DC chopper. The same system as well as a SMES configuration are also presented in [57], and the only difference in this study is its application of fuzzy logic to determine the duty cycle of the DC-DC chopper. Refs [54], [56], and [57] all ignore the capacity of the SMES coil while determining the optimal energy transfer/absorbance of the SMES coil, even though this capacity must be taken into consideration in real applications.

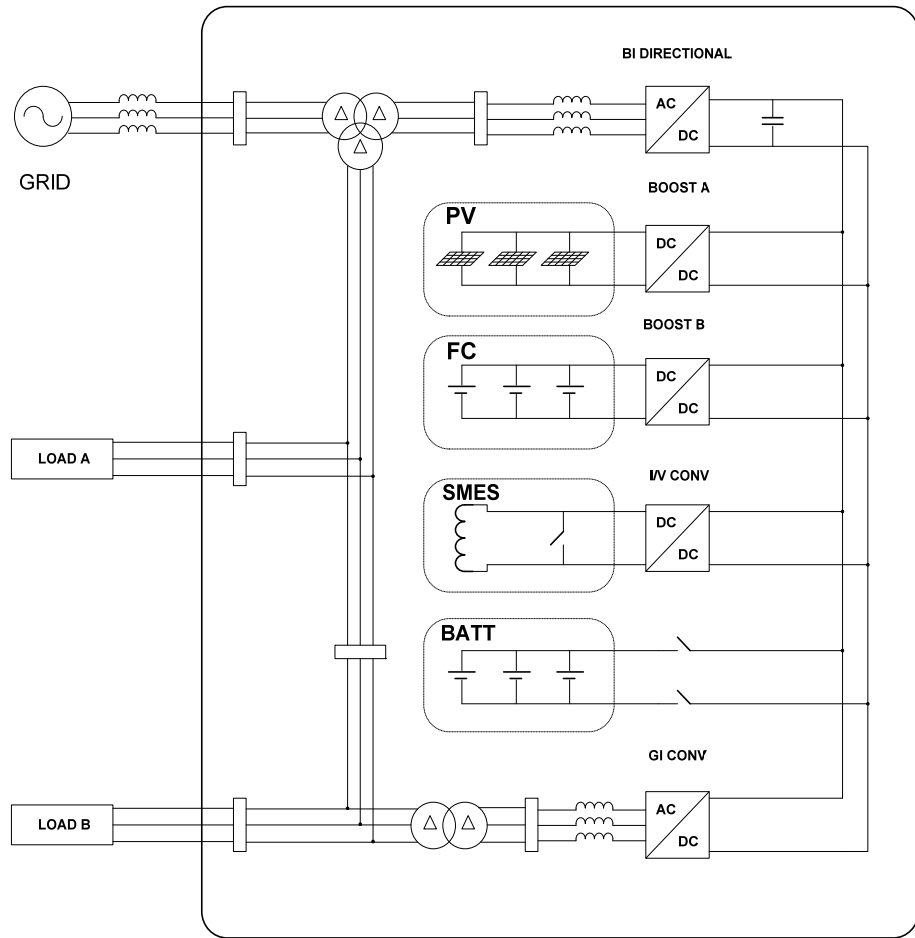


Fig. 4.6. New type dispersed power system that uses SMES unit [52]

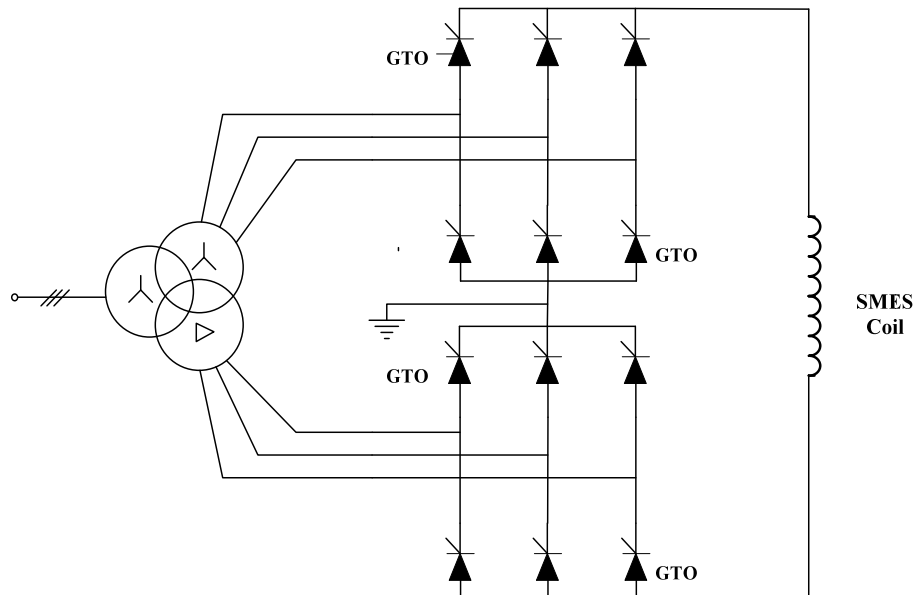


Fig. 4.7. 12-pulse SMES unit configuration with GTO

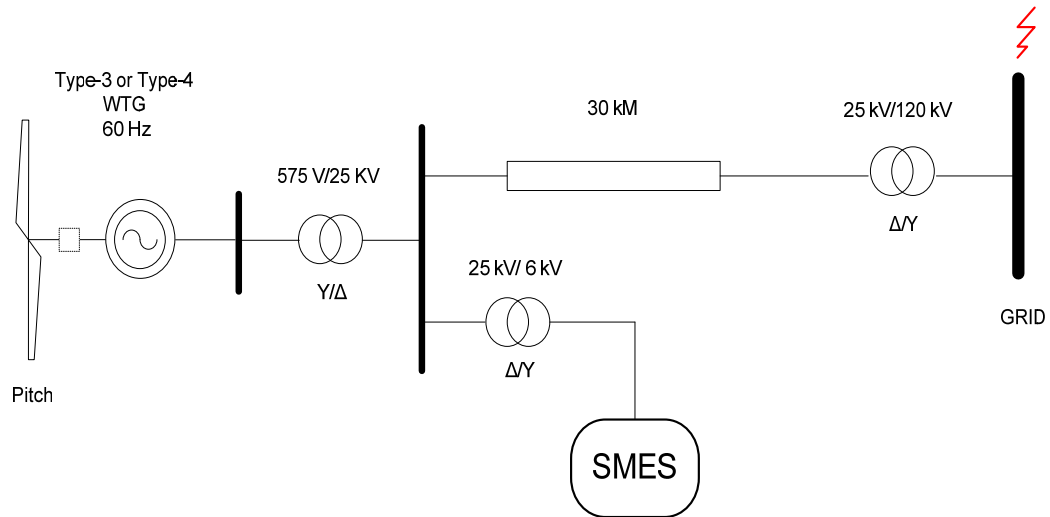


Fig. 4.8. Application of SMES unit on variable speed WECS during grid disturbances [60]

The application of SMES on DFIG WECS is discussed in [58]. This study aims to improve the voltage stability of the wind turbine generator system during any short circuit in the transmission line, while Ref [61] discusses the SMES unit's proficiency at reducing the high voltage profile at the PCC during a swell event on the grid side. The application of SMES on WECS equipped with Type D system is firstly discussed in Refs [62] and [63], SMES is employed on a variable speed WECS, after which the authors compare the transient responses during a voltage sag event on the grid side, as depicted in Fig. 4.8. A review of the control algorithm and the objectives of some SMES applications on WECS are also discussed briefly in Chapter 5.

4.5. Flywheel Energy Storage System (FESS)

A flywheel operates by storing energy in a spinning mass. Through a coupled electric machine, the system can store power by accelerating the shaft and then retrieve the power by slowing the shaft. The amount of stored energy depends on the moment inertia of the rotor, I , which itself depends on the distribution of mass density around the rotating axis, $\rho(x)$, and the geometrical radius of the rotor, r . From Eq. (4.6) energy will not depend on the moment inertia only but also on square of the angular speed, ω of the flywheel shaft, as formulated below [1]:

$$E = \frac{1}{2} I \omega^2 \quad (4.6)$$

$$I = \int \rho(x) r^2 dx \quad (4.7)$$

where:

E is stored energy (J),

I is the moment inertia (kg/m^2),

ω is angular speed (rad/s),

ρ is mass density (kg/m^3), and

r is rotor radius (m).

x is rotating axis position

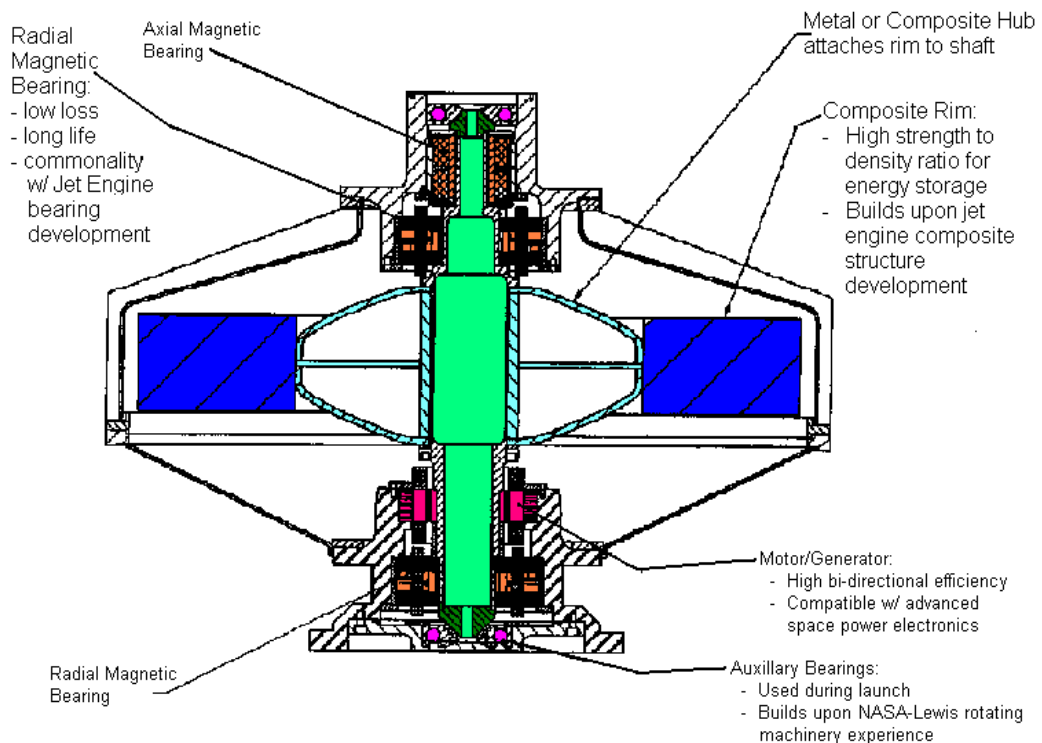


Fig. 4.9. Typical model of a FESS [64]

Normally, high-capacity flywheels are required to store energy in an electrical power system. A 200-ton flywheel is estimated to lose about 200 kW in friction. The flywheel's overall efficiency will drop to 78% after 5 hours and then to 45% after one day; therefore, long term storage is not foreseeable for this device [2]. Numerous studies have discussed the feasibility of flywheels for renewable energy systems, particularly the WECS system. In Refs [64-66], the FESS is connected directly to the DC-link of the Type D WECS (the full converter WECS). It is proven that this setup can improve the quality of power delivered by a wind generator. However, since the

FESS is applied inside the converter station of the WECS, this concept is only applicable to the new design and can be included only in new connections to the grid. A combination of STATCOM with FESS is introduced in [68]. This concept's objective is to improve the quality of the power output of a fixed speed WECS. The combination of the two devices requires high-performance power electronics, therefore, its installation and operating costs might become high and its proposed control algorithm is very complicated due to the multiple levels of control used in this study.

4.6. Compressed Air Energy Storage (CAES)

Compressed air energy storage (CAES) works based on conventional gas turbine generation concept. CAES decouples the compression and expansion cycles of a conventional gas turbine into two separate processes and stores energy in the form of compressed air, which is elastic potential energy. During low demand, CAES stores energy by compressing air into an airtight space. To extract the stored energy, CAES draws the compressed air from the storage vessel, heats the air and then expands it through a high-pressure turbine, which captures some of the energy in the compressed air. The air then is mixed with fuel and combusted with the exhaust that is expanded through a low-pressure turbine. Both the high and low-pressure turbines are connected to an electrical generator [40]. This storage technology burns about one-third of the premium fuel that a conventional, simple-cycle combustion engine burns and produces one-third of the pollutants that the conventional engine produces per kWh generated [8]. A typical configuration of a CAES appears in Fig 4.10.

Compressed air is the medium that allows elastic energy to be embedded in the gas. The ideal gas law relates the pressure P , the volume V , and temperature T of a gas, as indicated by [1]:

$$PV = nRT \quad (4.8)$$

where:

P is the pressure (N/m^2)

V is the volume (m^3),

T is temperature of a gas (K),

n is the number of moles, and

R is the universal gas constant (8.31 J/mol. K).

What is important to remember is that it is very difficult to accelerate the energy density for any unusually shape volume. Therefore, if a piston without friction is assumed under an isobaric process, a simplified volumetric energy density can be calculated by [1]:

$$E_{volume} = \frac{1}{V_0} \eta RT \int_{V_0}^V \frac{dV}{V} = \frac{1}{V_0} P_0 V_0 \ln \frac{V_0}{V} = P_0 \ln \frac{V_0}{V} \quad (4.9)$$

where:

P_0 is the initial pressure (N/m²),

V_0 and V are the initial and final volumes in m³, respectively.

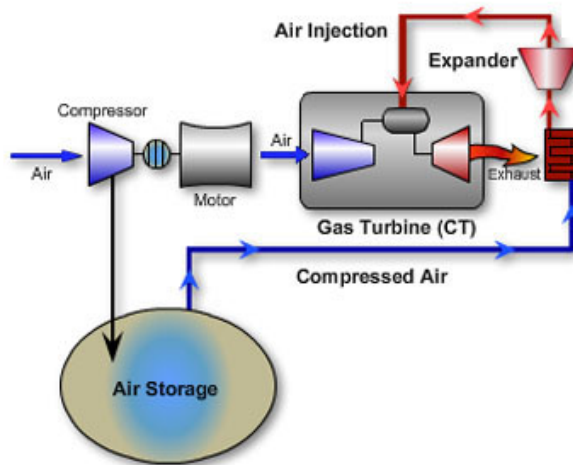


Fig. 4.10. Typical model for a CAES [69]

CAES units have already been implemented in Germany and the U.S. (Alabama) with capacities of 290 MW and 110 MW, respectively [70]. The ratings of CAES had reached MW scales, because the smaller units that use storage tanks aboveground usually have only a few hours of energy storage [8].

The literature has also extensively studied CAES in collaboration with WECS. In Ref [71], the researchers have utilized a stochastic electricity market model to

estimate the impact of significant wind power generation on system operation and on the economic value of investment in CAES. Given the results of this study, one can conclude that decentralized CAES installation at or close to a large wind generation site may underestimate the economic value of the CAES investment option. The security constraints for CAES along with its connection to WECS and the optimum schedule of generating units for minimizing the cost of supplying energy are studied in Ref [72]. Then, Ref [73], further studies the ancillary services that are constrained by CAES's security requirements. The study and comparison of different types of wind-diesel and CAES (WDCAS) configurations are described in [74]. This WDCAS arrangement not only increases the penetration rate of wind energy but also improves the start up speed of the diesel engine.

Although CAES is technically approved to be effective with renewable energy systems, it must still be combined with other functions before one can economically justify its operation [3]. In order to improve its efficiency or to remove the need for an additional conventional fuel generation, CAES must be combined with other EST which, in turn, increases the cost and makes the control system more complicated. Generally speaking, the main disadvantages of CAES [9] include its need for high energy input during the power production process and the greenhouse gases emissions that result from CAES's reliance on natural gas. However, this shortage will be overcome in the future with the advent of a third generation of CAES that does not use natural gas in the generation process. The new system will store heat during compression, which it can be reused during generation to warm the compressed air [75]. These ambitions, however, are still under research, and the new system might need considerable time before it is ready for implementation. The other drawback that researchers may need to take into account is CAES's location limitation. This system requires a location with a suitable underground reservoir where a power plant can be constructed [49].

4.7. Pumped Hydro System (PHS)

The pumped hydro system is one of the most mature storage energy systems in existence. This large-scale energy system is the most widespread storage technology used today [8] with approximately 280 installations worldwide [7] and the total capacity of around 3900 MW [3]. Its principle of operation is based on the condition

of power demand. When power demand is low, the power station system will pump water from the lower level reservoir to fill the upper level one. When the demand is high, water from the upper level reservoir will flow to the lower level reservoir through a turbine coupled with a generator, as illustrated in Fig 4.11. The efficiency of the pumped hydro storage system is between 65%-80% depending on the characteristic of the equipment [2, 8, 76]. The efficiency of the pumped hydro storage system is somewhat compromised from frictional losses, turbulence and viscous drag. The turbine has intrinsic efficiency as well, and the final conversion of hydro power to electricity is also accumulated in the total efficiency calculation. Therefore, any calculations of the overall efficiency of the PHS must consider the ratio of the energy supplied to the consumer and the energy consumed while pumping. The energy used for pumping a volume, V of water up to a height, h with a pumping efficiency of η_p is given by Eq. 4.10, and the energy supplied to the grid while the pump generates at an efficiency of η_g is given by Eq. 4.11 [1].

$$E_{pumping} = \frac{\rho ghV}{\eta_p} \quad (4.10)$$

$$E_{generator} = \rho ghV\eta_g \quad (4.11)$$

where:

ρ is mass density (kg/m^3),

g is gravity (9.8 m/s^2),

h is the reservoir height (m),

V is the water volume (m^3),

η_p is the machine efficiency during pumping, and

η_g is the machine efficiency during generating power.

Because the power output is determined by the height of the reservoir, civil construction might be very expensive, especially if the reservoir's location is far from the existing power line. Landscapes with enough height are usually located in the mountains and far from the cities in the valley. Moreover, the reservoir requires immense square footage, which will drastically transform the surrounding environment, and during periods of high rainfall, the pumping hydro's capacity of

may reduce [77]. Therefore, the restrictions of this storage system are geographical constraints and weather conditions. To reduce environmental degradation, the large reservoir can be placed underground. This placement has been proven technically feasible, but the cost associated with this scheme is very high, so no such construction exists yet [8]. Another drawback of this storage system is its construction and establishment. A pumped hydro storage system requires a long time to plan. One recently constructed PHS in the Alps took about 30 years to plan and 7 years to construct. This type of storage system is rated for 8.5 GWh [76].

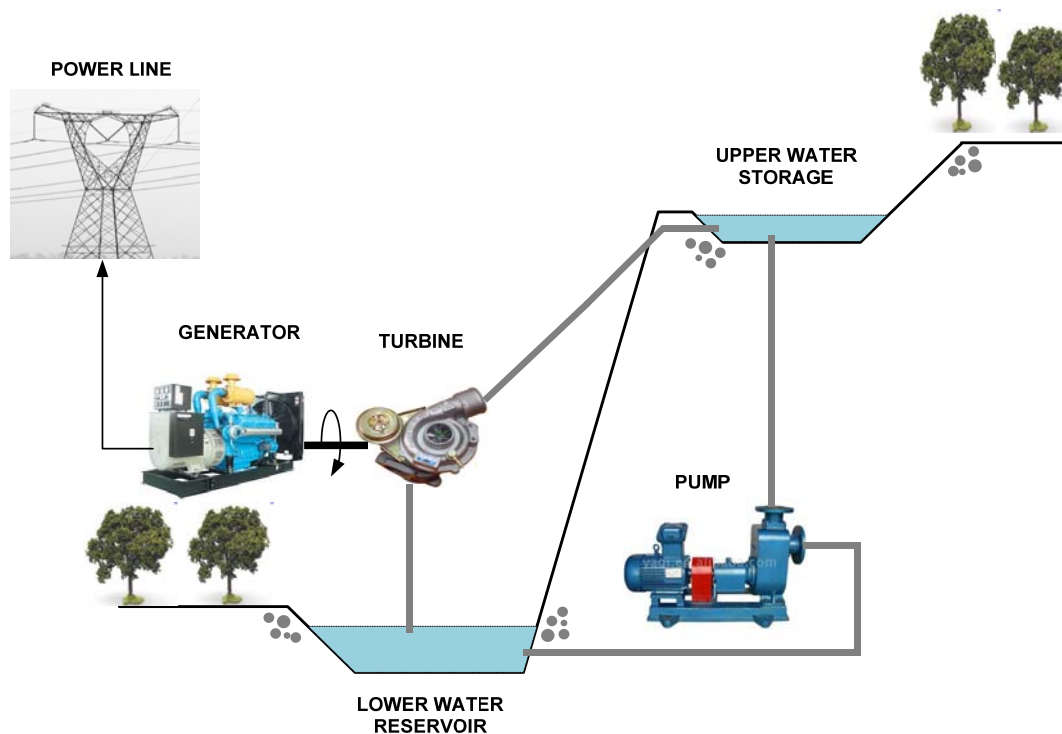


Fig. 4.11. Pumped hydroelectric storage system

A PHS is generally limited to high power applications for several reasons including high cost ranging from USD 100 million to USD 3 billion (\$600-2000/kW), environmental damage due to the reservoir establishment (approximately 10-20 km²) and the long project lead time (typically 7-10 years) [3], [40]. Therefore, a PHS is not suitable for small to medium-scale demands (within the kW to MW range). If a wind farm were not sufficiently large enough, it would be necessary to use PHS. Even then, the PHS should be for multiple purposes, such as peak shaving and grid stability, in order to justify the high investments, because it is not effective to have two reservoirs dedicated for mitigating the wind fluctuations in small wind production [3].

4.8. Comparison of Storage Energy Technologies

In general, EST can be applied for one or more of the following purposes [4]: to improve the efficiency of a system's operation, to reduce primary fuel use via energy conservation, to serve an area where no alternative energy source is available, and to secure an existing energy supply. When planning renewable energy resources, developers must consider some technical logistics and regulations to achieve higher efficiency and cost effectiveness for the overall system. One of the most influential parameters in selecting storage energy technologies is their round-trip efficiency. Compared to other storage technologies, SMES is still the leader in overall system efficiency (98%) followed by UC¹ at 90% and FESS at 85%. BESS and PHS achieve the same efficiency at 80%, whilst CAES remains at 70%. A summary of the round trip efficiency of the EST as individual devices and as overall systems is depicted in the bar chart diagram of Fig. 4.12.

At the present time, developers must urgently consider the lifetime of the ESTs if they want their performance to match the life prediction of the currently installed renewable energy systems. Only by improving the lifetime of the ESTs can developers connect these devices to existing systems and achieve optimal economic goals. The ESTs life time determination will come, of course, after calculating the normal schedules of the maintenance of the plants. Fig. 4.13 is a comparison of the life times of EST devices, summarized from Refs [3, 40].

As can be seen in Fig. 4.14, currently, PHS is the only EST that could store up power up to GW scale, followed by CAES which capable of store up to 350 MW of power. According to Refs [7], [78], SMES capacity is currently in 1.0 GW scale. Meanwhile, BESS, although quite popular in power system applications, is to be sized at a maximum of 10 MW for common electrochemical batteries; however, flow batteries currently are available in the range of 5-500 MW [10]. The latest design for FESS is capable of 100 KW, and a concept for a larger FESS with 10s of MW is

¹Detailed information for individual efficiency is unavailable in references [7] and [78]

currently under development. UC power size is still in the range of 7-10 W that available commercially. The size of 10-20 KW however, is under prototype development [78].

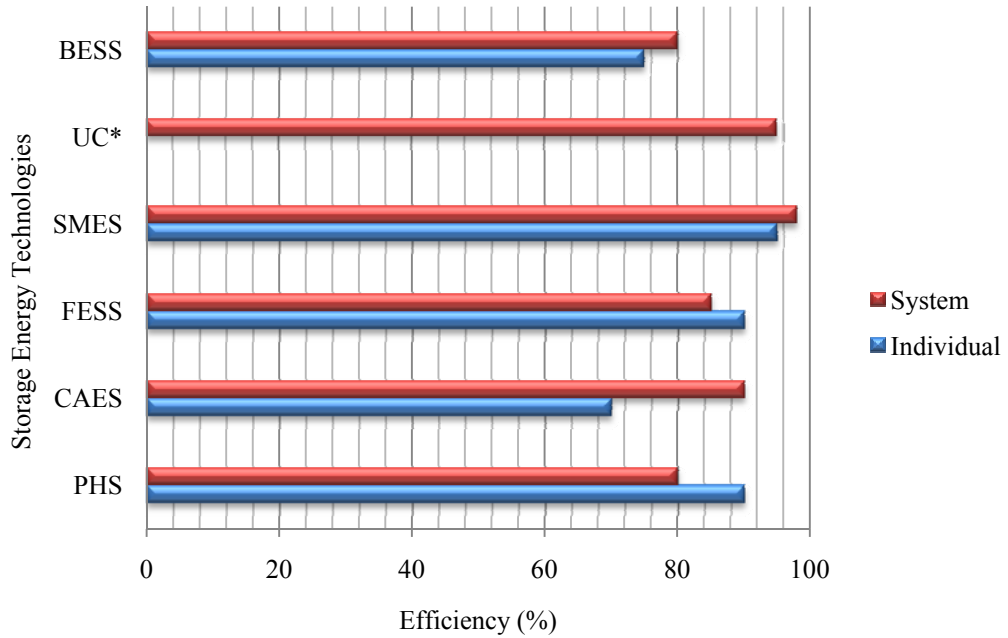


Fig. 4.12. Bar chart of storage energy technologies' efficiency [7, 78]
 (Note: * Detailed information for individual efficiency is unavailable in Refs [7] and [78])

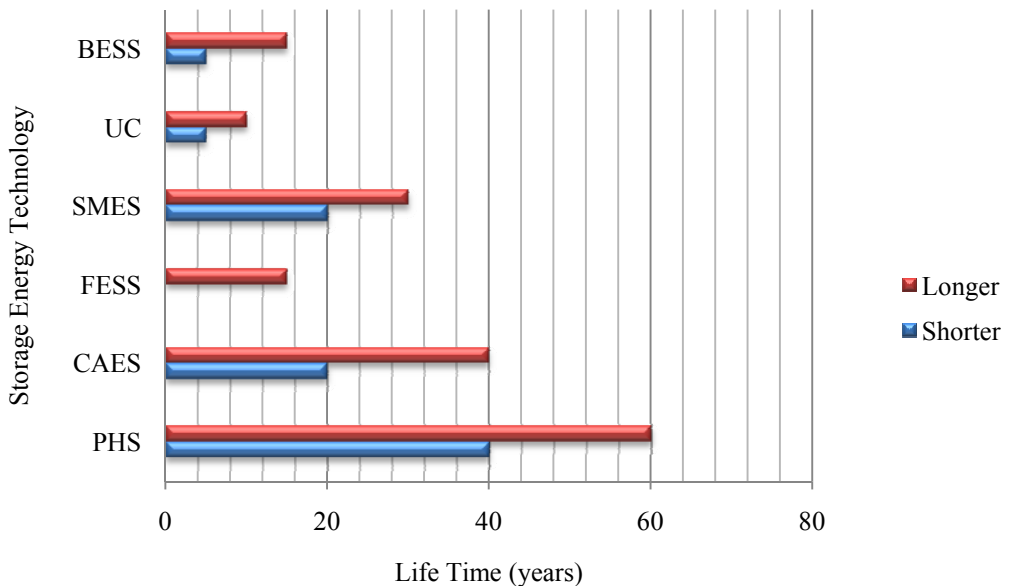


Fig. 4.13. Life time bar chart of storage energy technologies [3, 40]

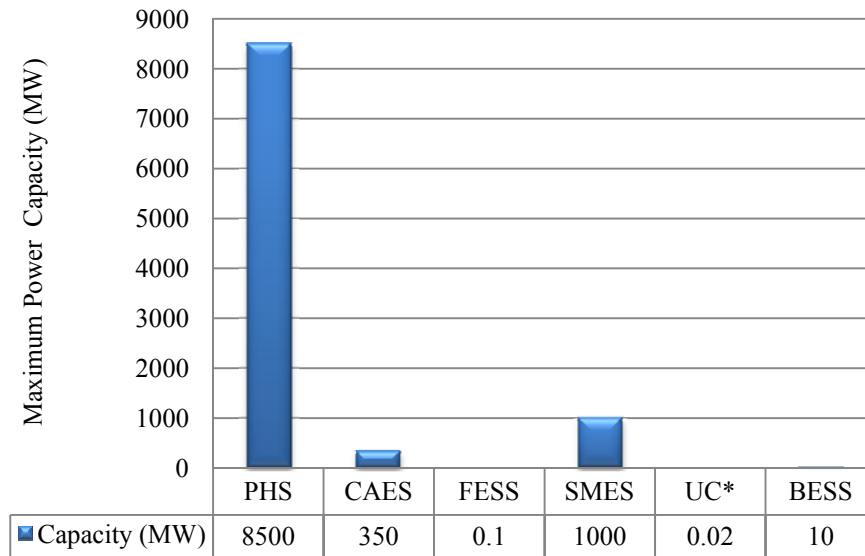


Fig. 4.14. Colum chart of maximum energy capacity of EST [7],[78]

At its full size of 10 MW, BESS can discharge fully within minutes to a maximum of 4 hours. Meanwhile, large-capacity SMES (1000 MW) can discharge from within minutes to a maximum of 5 hours, whereas small-scale SMES can discharge within seconds to minutes. FESS has only a 3-hour discharge time. CAES has a long discharge time, with its longest time running about 26 hours for a full rating CAES. Finally, PHS has the largest energy storage in the world. It can be discharge over a course of days at its GW size. Fig. 4.15 demonstrates the discharge time of each EST at their maximum power ratings.

In addition to technical consideration, the economics of ESTs are also essential to consider. The overall benefits of the system must be calculated accurately if the authorities are to know whether installing and running the system is feasible. Therefore, the selection of EST should be cost effective in all aspects. Fig. 4.16 shows the estimated cost in US\$ per kW for each EST. FESS has the highest cost per kW, ranging from 500 to \$6,000/kW followed by PHS at a maximum cost of 1,600\$/kW. SMES has a medium cost per KW that lies at \$1,000/kW. The UC's cost per kW is relatively cheap, which may make UC a suitable connection to small-to-medium-scale kW systems. BESS also has competitive cost per kW, as it lies in the range of \$350-\$1,000/kW. In fact, it is already used widely in the UPS system.

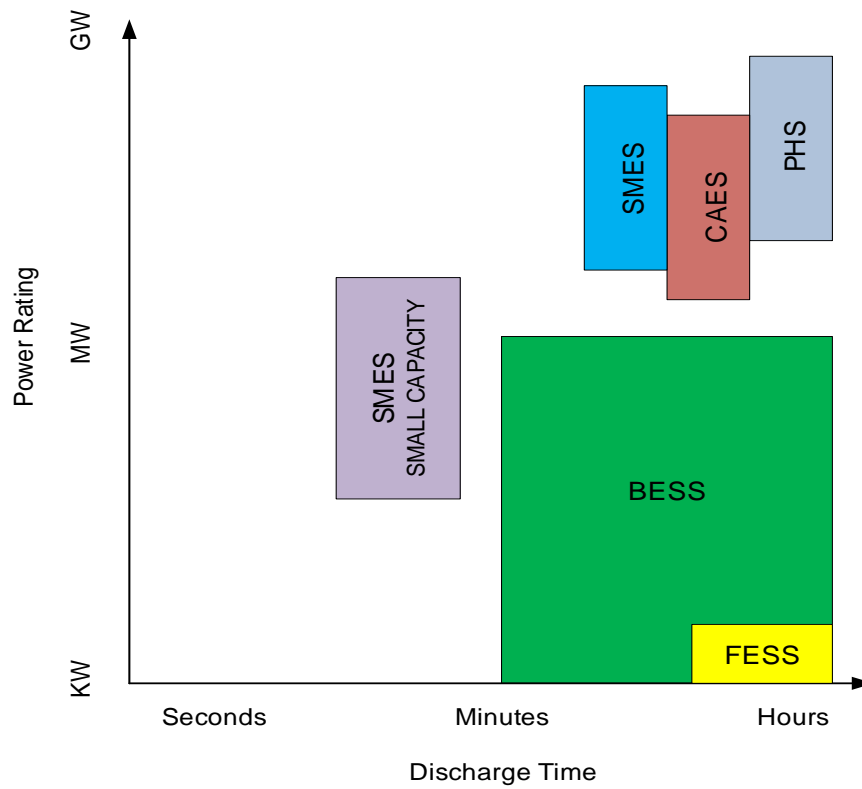


Fig. 4.15. Power rating vs. discharge time for various ESTs [7]

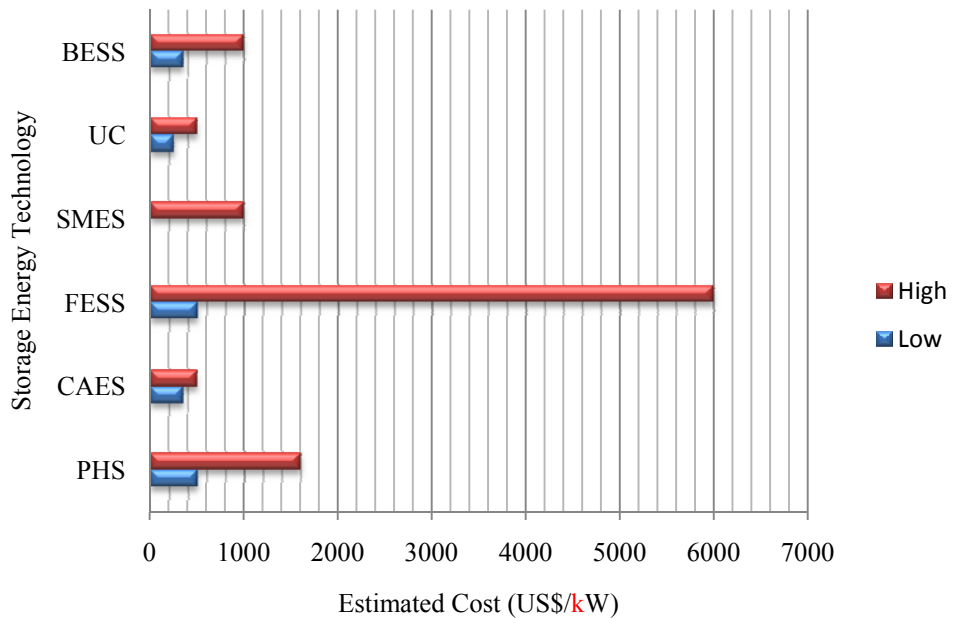


Fig. 4.16. Estimated cost in US\$/kW of EST [78]

(Note: SMES low estimated cost is not available in this Ref. [78] as it is available only in its maximum estimated cost)

The economic consideration of connecting an EST to the power system must include close estimates of all economic aspects in order to achieve the most cost-effective combinations. For example, developers may discover that using a hybrid of two or more ESTs might be better for certain power system after they conduct all calculations for the related generating and load systems.

4.9. Summary

Table 4.1 provides a summary of the advantages and disadvantages of the available ESTs, including their common applications [7],[78-80].

Table 4.1. Comparison of ESTs in term of advantages-disadvantages and their applications in power system

Energy Storage Technology (EST)	Advantages	Disadvantages	Applications
BESS and Flow Battery	<ul style="list-style-type: none"> - Mostly available in the market niche - High power and energy capacity 	<ul style="list-style-type: none"> - Short life time - Cannot endure high cycling rates - Temperature 	<ul style="list-style-type: none"> - Uninterruptable power supply (UPS) - Power quality variability reduction - Integrating with renewable energies (PV and Wind) - Peak shaving - Voltage and current limitation
UC	<ul style="list-style-type: none"> - High efficiency - Quick recharge 	<ul style="list-style-type: none"> - Low energy density - Limited power system applications 	<ul style="list-style-type: none"> - Power quality - Transportation defence - Emergency power bridging - Consumer electronics - Some applications for wind power have been done
SMES	<ul style="list-style-type: none"> - Very long life time - Very high efficiency - Quick recharge - High power capacity 	<ul style="list-style-type: none"> - Low energy density - High production cost 	<ul style="list-style-type: none"> - Power quality - T&D application - System stability
FESS	<ul style="list-style-type: none"> - Adequate long life time - Insignificant environment impact - Low maintenance efforts - Quick recharge 	<ul style="list-style-type: none"> - Low energy density - Low energy capacity - Large standby losses 	<ul style="list-style-type: none"> - Power quality - Transportation defense

(Continued from previous page)

<p style="text-align: center;">CAES</p>	<ul style="list-style-type: none"> - Adequate high energy and power capacity - Adequate long life time 	<ul style="list-style-type: none"> - Geographical constraint - Require conventional fuel gas 	<ul style="list-style-type: none"> - Spinning/standing reserve energy - Arbitrage - Frequency Regulation - Peak shaving - Currently only two operation sites
<p style="text-align: center;">PHS</p>	<ul style="list-style-type: none"> - High power and energy density - Very long life time 	<ul style="list-style-type: none"> - Special site requirements - Ecological adverse for site establishment - Expensive site construction - Long planning and construction project time - Have a substantial time delay associated with the energy conversion of stored mechanical energy back into electricity 	<ul style="list-style-type: none"> - Spinning/standing reserve energy - Arbitrage - Load levelling - 150 operation sites in the USA

4.10. References

- [1] F. A. Farret and M. G. Simoes, "Integration of Alternative Sources of Energy", New Jersey: Wiley-Interscience. 2006
- [2] H. Ibrahim, A. Ilinca, and J. Perron, "Energy Storage Systems-Characteristics and Comparisons", *Renewable and Sustainable Energy Reviews*, vol. 12, pp. 1221-1250. 2008
- [3] M. Beaudin, H. Zareipour, A. Schellenberglabe, and W. Rosehart, "Energy Storage for Mitigating the Variability of Renewable Electricity Sources: An Updated Review", *Energy for Sustainable Development*, vol. 14, pp. 302-314. 2010
- [4] A. Ter-Gazari, "Energy Storage for Power Systems", Stevenage: P. Peregrinus on behalf of the Institution of Electrical Engineers. 1994
- [5] E. A. DeMeo and J. F. Galdo, "Renewable Energy Technology Characterizations," EPRI and U.S. Department of Energy, Wahington DC. 1997
- [6] R. Baxter, "Energy Storage: A Nano Technical Guide", Oklahoma: PenWell Corporation. 2006
- [7] S. C. Smith, P. K. Sen, and B. Kroposki, "Advancement of Energy Storage Devices and Applications in Electrical Power System", in *Power and Energy Society General Meeting - Conversion and Delivery of Electrical Energy in the 21st Century, 2008 IEEE*, pp. 1-8. 2008

- [8] R. B. Schainker, "Executive Overview: Energy Storage Options for A Sustainable Energy Future", in *Power Engineering Society General Meeting, 2004. IEEE*, vol.2, pp. 2309-2314. 2004
- [9] B. R. Alamri and A. R. Alamri, "Technical Review of Energy Storage Technologies when Integrated with Intermittent Renewable Energy", in *International Conference on Sustainable Power Generation and Supply, 2009. SUPERGEN '09*, pp. 1-5. 2009
- [10] <http://www.icrepq.com/icrepq-08/327-faias.pdf>
- [11] N. Koshizuka, F. Ishikawa, H. Nasu, M. Murakami, K. Matsunaga, S. Saito, O. Saito, Y. Nakamura, H. Yamamoto, R. Takahata, Y. Itoh, H. Ikezawa, and M. Tomita, "Progress of Superconducting Bearing Technologies for Flywheel Energy Storage Systems", *Physica C: Superconductivity*, vol. 386, pp. 444-450. 2003
- [12] <http://www.alternative-energy-news.info/images/technical/lead-acid-battery.jpg>, accessed: 25 January, 2012
- [13] L. Wei, G. Joos, and J. Belanger, "Real-Time Simulation of a Wind Turbine Generator Coupled with a Battery Supercapacitor Energy Storage System", *IEEE Transactions on Industrial Electronics*, vol. 57, pp. 1137-1145. 2010
- [14] Y. Yoshida, W. Guohong, and T. Minakawa, "Mitigating Fluctuation of Wind Turbine Power Generation System by Introduction of Electrical Energy Storage with Combined Use of EDLC and Lead Acid Storage Battery", in *International Conference on Power System Technology (POWERCON), 2010*, pp. 1-7. 2010
- [15] A. M. Gee and R. W. Dunn, "Novel Battery / Supercapacitor Hybrid Energy Storage Control Strategy for Battery Life Extension in Isolated Wind Energy Conversion Systems", in *Universities Power Engineering Conference (UPEC), 2010*, pp. 1-6. 2010
- [16] H. Jia, Y. Fu, Y. Zhang, and W. He, "Design of Hybrid Energy Storage Control System for Wind Farms Based on Flow Battery and Electric Double-Layer Capacitor", in *Power and Energy Engineering Conference (APPEEC), 2010 Asia-Pacific*, pp. 1-6. 2010
- [17] L. Barote, M. Georgescu, and C. Marinescu, "Smart Storage Solution for Wind Systems", in *PowerTech, 2009 IEEE Bucharest*, pp. 1-6. 2009
- [18] M. Zamani, G. H. Riahy, N. Abdolghani, M. H. Zamani, and G. Shahgholian, "Utilization of Thermal Energy Storage for Reducing Battery Bank Size of Hybrid (Wind-PV) Systems", in *International Conference on Clean Electrical Power (ICCEP), 2011*, pp. 709-714. 2011
- [19] D. L. Yao, S. S. Choi, K. J. Tseng, and T. T. Lie, "Determination of Short-Term Power Dispatch Schedule for a Wind Farm Incorporated With Dual-Battery Energy Storage Scheme", *IEEE Transactions on Sustainable Energy*, vol. 3, pp. 74-84. 2012
- [20] X. Y. Wang, D. Mahinda Vilathgamuwa, and S. S. Choi, "Determination of Battery Storage Capacity in Energy Buffer for Wind Farm", *IEEE Transactions on Energy Conversion*, vol. 23, pp. 868-878. 2008
- [21] L. Barote, R. Weissbach, R. Teodorescu, C. Marinescu, and M. Cirstea, "Stand-Alone Wind System with Vanadium Redox Battery Energy Storage", in *International Conference on Optimization of Electrical and Electronic Equipment, 2008*, pp. 407-412. 2008
- [22] S. Teleke, M. E. Baran, A. Q. Huang, S. Bhattacharya, and L. Anderson, "Control Strategies for Battery Energy Storage for Wind Farm Dispatching", *IEEE Transactions on Energy Conversion*, vol. 24, pp. 725-732. 2009

- [23] A. Arulampalam, M. Barnes, N. Jenkins, and J. B. Ekanayake, "Power Quality and Stability Improvement of a Wind Farm Using STATCOM Supported with Hybrid Battery Energy Storage", *Generation, Transmission and Distribution, IEE Proceedings*, vol. 153, pp. 701-710. 2006
- [24] F. Giraud and Z. M. Salameh, "Steady-State Performance of A Grid-Connected Rooftop Hybrid Wind-Photovoltaic Power System with Battery Storage", *IEEE Transactions on Energy Conversion*, vol. 16, pp. 1-7. 2001
- [25] Q. Xianyi, "Application Research of Flywheel Battery in the Wind and Solar Complementary Power Generation", in *International Conference on Computer Application and System Modeling (ICCSM), 2010*, pp. v.13, pp. 546-550.2010
- [26] V. Khadkikar, R. K. Varma, and R. Seethapathy, "Grid Voltage Regulation Utilizing Storage Batteries In PV Solar System; Wind Plant Based Distributed Generation System", in *Electrical Power & Energy Conference (EPEC), 2009 IEEE*, pp. 1-6. 2009
- [27] S. G. Tesfahunegn, O. Ulleberg, T. M. Undeland, and P. J. S. Vie, "A Simplified Battery Charge Controller for Safety and Increased Utilization in Standalone PV Applications", in *International Conference on Clean Electrical Power (ICCEP), 2011*, pp. 137-144. 2011
- [28] A. Saif, K. G. Elrab, H. H. Zeineldin, S. Kennedy, and J. L. Kirtley, "Multi-Objective Capacity Planning of a PV-Wind-Diesel-Battery Hybrid Power System", in *IEEE International Energy Conference and Exhibition*, pp. 217-222. 2010
- [29] R. W. Wies, R. A. Johnson, A. N. Agrawal, and T. J. Chubb, "Simulink Model for Economic Analysis and Environmental Impacts of A PV With Diesel-Battery System for Remote Villages", *IEEE Transactions on Power Systems*, vol. 20, pp. 692-700. 2005
- [30] J. M. Miller, J. C. K. Yeung, Y. Q. Ma, and G. Sartorelli, "Ultracapacitors Improve SWECS Low Wind Speed Energy Recovery. Ultracapacitor and Battery for Low Wind Energy Harvesting", in *Power Electronics and Machines in Wind Applications, 2009. IEEE*, pp. 1-6. 2009
- [31] G. Mandic and A. Nasiri, "Modeling and simulation of A Wind Turbine System with Ultracapacitors for Short-Term Power Smoothing", in *IEEE International Symposium on Industrial Electronics*, pp. 2431-2436. 2010
- [32] N. Gyawali and Y. Ohsawa, "Effective Voltage and Frequency Control Strategy for A Stand-Alone System with Induction Generator/Fuel Cell/Ultracapacitor", in *Integration of Wide-Scale Renewable Resources Into the Power Delivery System, 2009 CIGRE/IEEE PES Joint Symposium*, pp. 1-11. 2009
- [33] J. Kho. <http://venturebeat.com/2008/11/18/energ2-aims-to-improve-ultracapacitors-for-electric-cars-industry/>, accessed: 25 January, 2012
- [34] R. Shah and N. Mithulananthan, "A Comparison of Ultracapacitor, BESS and Shunt Capacitor on Oscillation Damping of Power System with Large-Scale PV Plants", in *Universities Power Engineering Conference (AUPEC)*, pp. 1-6. 2011
- [35] C. Jae Hoon and H. Won-Pyo, "Power Control and Modeling of A Solar-Ultra Capacitor Hybrid Energy System for Stand-Alone Applications", in *International Conference on Control Automation and Systems*, pp. 811-814. 2010

- [36] S. Manfredi and M. Pagano, "On the Use of Ultracapacitor to Support Microgrid Photovoltaic Power System", in *International Conference on Clean Electrical Power*, pp. 491-497. 2011
- [37] P. J. Binduhewa, A. C. Renfrew, and M. Barnes, "Ultracapacitor Energy Storage for Microgrid Micro-Generation", in *4th IET Conference on Power Electronics, Machines and Drives, 2008*, pp. 270-274. 2008
- [38] Z. Haihua, T. Bhattacharya, T. Duong, T. S. T. Siew, and A. M. Khambadkone, "Composite Energy Storage System Involving Battery and Ultracapacitor With Dynamic Energy Management in Microgrid Applications", *IEEE Transactions on Power Electronics*, vol. 26, pp. 923-930. 2011
- [39] X. Jianming, K. Longyun, and Z. Yanning, "Design of a Hybrid PV/UC/Batteries System", in *IEEE International Conference on Cyber Technology in Automation, Control, and Intelligent Systems*, pp. 57-61. 2011
- [40] H. Chen, T. N. Cong, W. Yang, C. Tan, Y. Li, and Y. Ding, "Progress in Electrical Energy Storage System: A Critical Review", *Progress in Natural Science*, vol. 19, pp. 291-312. 2009
- [41] L. Freris and D. Infield, "Renewable Energy in Power System", Wiltshire: A John Wiley & Sons. 2008
- [42] P. F. Ribeiro, B. K. Johnson, M. L. Crow, A. Arsoy, and Y. Liu, "Energy Storage Systems for Advanced Power Applications", *Proceedings of the IEEE*, vol. 89, pp. 1744-1756. 2001
- [43] E. Ancha, V. G. Agelidis, O. Anaya-Lara, and T. J. E. Miller, "Power electronic control in electrical systems", Oxford: Newnes. 2002
- [44] www.wikipedia.org, accessed: 12 January, 2012
- [45] R. Loyd, S. Schoenung, T. Nakamura, W. Hassenzahl, J. Rogers, J. Purcell, D. Lieurance, and M. Hilal, "Design Advances in Superconducting Magnetic Energy Storage for Electric Utility Load Leveling", *IEEE Transactions on Magnetics*, vol. 23, pp. 1323-1330. 1987
- [46] P. J. Hall and E. J. Bain. "Energy-Storage Technologies and Electricity Generation", <http://www.bis.gov.uk/assets/bispartners/foresight/docs/energy/energy-storage-technologies-and-electricity-generation.pdf>, accessed: 13 January, 2012
- [47] D. C. Naish, D. I. McCubbin, M. O. Edberg, and M. M. Harfoot, "Outlook of Energy Storage Technologies". 2008
- [48] A. M. Shiddiq-Yunus, M. A. S. Masoum, and A. A. Siada, "Application of SMES to Enhance the Dynamic Performance of DFIG During Voltage Sag and Swell", *IEEE Transactions on Applied Superconductivity*. 2012 (In Press)
- [49] W. Tong, "Wind Power Generation and Wind Turbine Design", Southampton, UK: WIT Press. 2010
- [50] K. S. Tam, P. Kumar, and M. Foreman, "Enhancing the Utilization of Photovoltaic Power Generation by Superconductive Magnetic Energy Storage", *IEEE Transactions on Energy Conversion*, vol. 4, pp. 314-321. 1989
- [51] I. Tsukagoshi, I. Takano, and Y. Sawada, "Transient Performance of PV/SMES Hybrid Dispersed Power Source", in *Power Engineering Society Summer Meeting, 2001*, vol.3, pp. 1579-1584. 2001
- [52] T. Monai, I. Takano, H. Nishikawa, and Y. Sawada, "Response Characteristics and Operating Methods of New Type Dispersed Power Supply System Using Photovoltaic Fuel Cell and SMES", in *Power Engineering Society Summer Meeting, 2002*, vol.2, pp. 874-879. 2002

- [53] F. Zhou, G. Joos, C. Abbey, L. Jiao, and B. T. Ooi, "Use of Large Capacity SMES to Improve the Power Quality and Stability of Wind Farms", in *Power Engineering Society General Meeting*, vol.2, pp. 2025-2030. 2004
- [54] M. Hasan Ali, T. Murata, and J. Tamura, "Stabilization of Power System Including Wind Generator by Fuzzy Logic-Controlled Superconducting Magnetic Energy Storage", in *International Conference on Power Electronics and Drives Systems, 2005*, pp. 1611-1616. 2005
- [55] C. Shiang-Shong, W. Li, C. Zhe, and L. Wei-Jen, "Power-Flow Control and Transient-Stability Enhancement Of A Large-Scale Wind Power Generation System Using A Superconducting Magnetic Energy Storage (SMES) Unit", in *Power and Energy Society General Meeting - Conversion and Delivery of Electrical Energy in the 21st Century*, pp. 1-6. 2008
- [56] M. R. I. Sheikh, S. M. Muyeen, R. Takahashi, T. Murata, and J. Tamura, "Transient Stability Enhancement of Wind Generator Using Superconducting Magnetic Energy Storage Unit", in *18th International Conference on Electrical Machines*, pp. 1-6. 2008
- [57] M. H. Ali, P. Minwon, Y. In-Keun, T. Murata, and J. Tamura, "Improvement of Wind-Generator Stability by Fuzzy-Logic-Controlled SMES", *IEEE Transactions on Industry Applications*, vol. 45, pp. 1045-1051. 2009
- [58] J. Shi, Y. J. Tang, L. Ren, J. D. Li, and S. J. Chen, "Application of SMES in Wind Farm to Improve Voltage Stability", *Physica C: Superconductivity*, vol. 468, pp. 2100-2103. 2008
- [59] J. C. Das, "Power System Analysis: Short-Circuit Load Flow and Harmonics", New York: Marcel Dekker. 2002
- [60] A. M. S. Yunus, A. A. Siadah, and M. A. S. Masoum, "Improvement of LVRT Capability of Variable Speed Wind Turbine Generator Using SMES Unit", in *IEEE Power and Energy Society Innovative Smart Grid Technologies Conference (ISGT 2011)*, Perth, Australia. 2011
- [61] A. M. S. Yunus, A. A. Siada, and M. A. S. Masoum, "Application of SMES Unit to Improve the High Voltage Ride through Capability of DFIG-Grid Connected during Voltage Swell", in *IEEE Power and Energy Society Innovative Smart Grid Technologies Conference (ISGT 2011)*, Perth, Australia. 2011
- [62] A. M. S. Yunus, A. Abu-Siada, and M. A. S. Masoum, "Effects of SMES on Dynamic Behaviors of Type D-Wind Turbine Generator-Grid Connected During Short Circuit", in *Power and Energy Society General Meeting, 2011 IEEE*, pp. 1-6. 2011
- [63] A. M. S. Yunus, A. Abu-Siada, and M. A. S. Masoum, "Effect of SMES Unit on the Performance of Type-4 Wind Turbine Generator During Voltage Sag", in *IET Conference on Renewable Power Generation (RPG 2011)*, pp. 1-4. 2011
- [64] <http://physics.oregonstate.edu/~hetheriw/projects/energy/topics/doc/storage/flywheel/flyparts.gif>, accessed: 20 January, 2012
- [65] G. Cimuca, S. Breban, M. M. Radulescu, C. Saudemont, and B. Robyns, "Design and Control Strategies of an Induction-Machine-Based Flywheel Energy Storage System Associated to a Variable-Speed Wind Generator", *IEEE Transactions on Energy Conversion*, vol. 25, pp. 526-534. 2010
- [66] K. Idjdarene, D. Rekioua, T. Rekioua, and A. Tounzi, "Direct Torque Control Strategy for a Variable Speed Wind Energy Conversion System Associated to a Flywheel Energy Storage System", in *Second International Conference on Developments in Systems Engineering (DESE), 2009*, pp. 17-22. 2009

- [67] M. Khaterchi, J. Belhadj, and M. Elleuch, "Participation of Direct Drive Wind Turbine to the Grid Ancillary Services Using a Flywheel Energy Storage System", in *7th International Multi-Conference on Systems Signals and Devices (SSD), 2010*, pp. 1-6. 2010
- [68] G. O. Suvire and P. E. Mercado, "Improvement of Power Quality in Wind Energy Applications Using A DSTATCOM Coupled with a Flywheel Energy Storage System", in *Power Electronics Conference, 2009. COBEP '09. Brazilian*, pp. 58-64. 2009
- [69] <http://www.matternetwork.com/2010/8/2010-year-compressed-air-energy.cfm>, accessed: 10 January, 2012
- [70] T. M. Masaud, L. Keun, and P. K. Sen, "An Overview of Energy Storage Technologies in Electric Power Systems: What Is the Future?", in *North American Power Symposium (NAPS), 2010*, pp. 1-6. 2010
- [71] J. S. Derk, "Compressed Air Energy Storage in an Electricity System with Significant Wind Power Generation", *IEEE Transactions on Energy Conversion*, vol. 22, pp. 95-102. 2007
- [72] H. Daneshi, A. Daneshi, N. M. Tabari, and A. N. Jahromi, "Security-Constrained Unit Commitment in A System With Wind Generation and Compressed Air Energy Storage", in *6th International Conference on the European Energy Market, 2009*. pp. 1-6. 2009
- [73] H. Daneshi, A. K. Srivastava, and A. Daneshi, "Generation Scheduling with Integration of Wind Power and Compressed Air Energy Storage", in *Transmission and Distribution Conference and Exposition, 2010 IEEE PES*, pp. 1-6. 2010
- [74] H. Ibrahim, A. Ilinca, R. Younes, J. Perron, and T. Basbous, "Study of a Hybrid Wind-Diesel System with Compressed Air Energy Storage", in *Electrical Power Conference, 2007. IEEE Canada*, pp. 320-325. 2007
- [75] J. Taylor and A. Halnes, "Analysis of Compressed Air Energy Storage," in *PCIC Europe 2010 Conference Record*, pp. 1-5. 2010
- [76] W. Leonhard and E. M. Grobe, "Sustainable Electrical Energy Supply with Wind and Pumped Storage - A Realistic Long-Term Strategy or Utopia?", in *Power Engineering Society General Meeting, 2004. IEEE*, vol.2, pp. 1221-1225. 2004
- [77] S. Faias, P. Santos, J. Sousa, and R. Castro, "An Overview on Short and Long-Term Response Energy Storage Devices for Power System Applications". 2012
- [78] A. Daneshi, N. Sadrmomtazi, H. Daneshi, and M. Khederzadeh, "Wind Power Integrated with Compressed Air Energy Storage", in *IEEE International Conference on Power and Energy (PECon), 2010*, pp. 634-639. 2010
- [79] Office of Utility Technologies, U.S. Department of Energy and EPRI, "Renewable Energy Technology Characterizations", Office of Utility Technologies, Energy Efficiency and Renewable Energy, U.S. Department of Energy, Washington, D.C. 1997
- [80] M. H. Ali, W. Bin, and R. A. Dougal, "An Overview of SMES Applications in Power and Energy Systems", *IEEE Transactions on Sustainable Energy*, vol. 1, pp. 38-47. 2010

“Every reasonable effort has been made to acknowledge the owners of copyright material. I would be pleased to hear from any copyright owner who has been omitted or incorrectly acknowledged.”

Chapter 5

SMES Unit Configuration and Control Scheme

5.1. Introduction

Generally, there are two major configuration of SMES; CSC and VSC as discussed in Chapter 3. Traditionally, CSC is connected through a 12-pulse converter configuration to eliminate the AC side fifth and seventh harmonic currents and DC side sixth harmonic voltage, thus resulting in a significant saving in harmonic filters [1] as shown in Fig. 5.1. However, because the 12-pulse converter configuration uses two 6-pulse CSCs that are connected in parallel, it results in increased cost. VSC on the other hand, must be connected with a DC-DC chopper through a DC link which facilitates energy exchange between the SMES coil and the AC grid as illustrated in Fig. 5.2. Ref [2] estimates the total cost of switching devices of CSC to be 173% of the switching devices and power diodes required for equivalent capacity of VSC and the chopper. Moreover, a VSC has a better self-commutating capability and it injects less harmonic currents into the AC grid than a comparable CSC. Since the switching frequency of an IGBT lies on the range of 2-20 KHz as opposed to a maximum of 1.0 kHz in GTO switching frequency, the use of IGBT is more beneficial in this configuration compared to GTO [3]. The SMES unit configuration used in this PhD research consists of a VSC and a DC-DC chopper which are connected through a DC shunt capacitor. The VSC is controlled by a HCC while the DC-DC chopper is controlled by a FLC (Fig. 5.3).

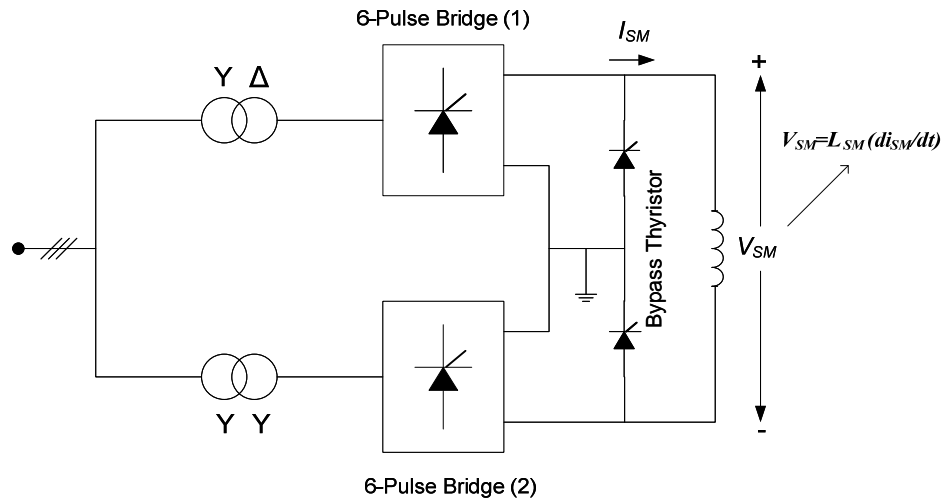


Fig. 5.1. Typical configuration of CSC based SMES with 12-pulse converter

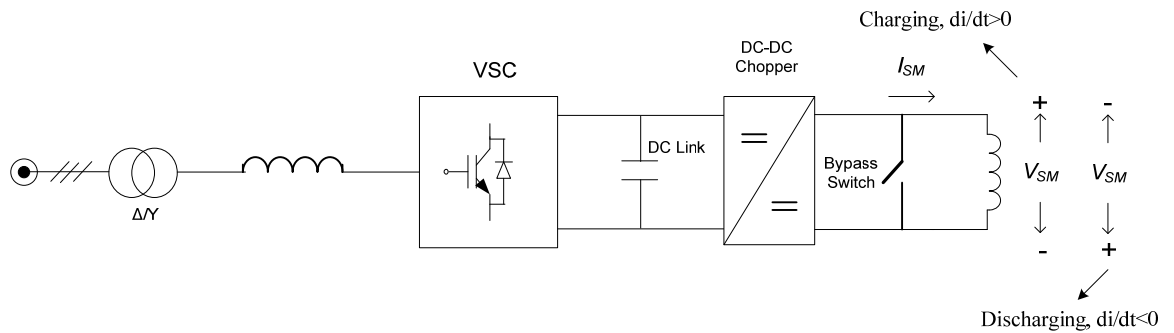


Fig. 5.2. Typical configuration of VSC based SMES with a DC-DC chopper

While the control system of the DC-DC chopper is presented in [4], the control approach for the VSC as a part of the SMES configuration is not presented. In contrast with Ref [4], the DC-DC chopper control system is not presented in [5]. The configuration of SMES in [6] is new but its application is limited to low WECS capacity and since the SMES coil is proposed to be connected to the individual DFIG's converters, this topology will be only be appropriated for new WECS installations. Application of SMES system to micro-grids is presented in [7] where the SMES is used to stabilize the entire micro-grid system. The control scheme presented in this work is very complex because it is working for three different levels of controls; this will lead to high implementation and maintenance cost, and requires robust computational system.

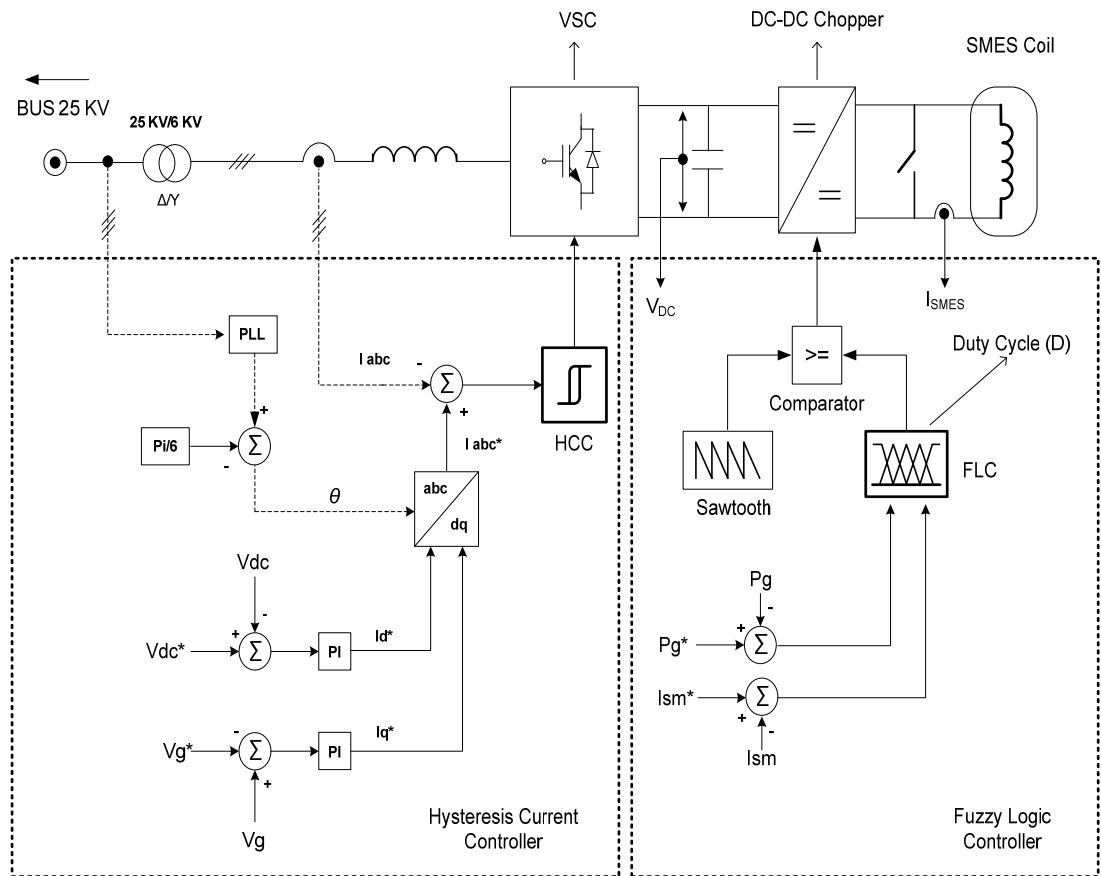


Fig. 5.3. SMES unit configuration and the proposed HCC-FLC control scheme [8]

The proposed control algorithm in this thesis is much simpler and closer to realistic applications compared with the similar controller proposed in Refs [9, 10]. In the aforementioned papers, the four proposed PI controllers require more computational time to optimally tune their parameters to maintain the overall system stability and to achieve satisfactory dynamic response during transient events. Moreover, the control system for the DC-DC chopper in these studies has only considered the generated active power (P_G) as a control parameter but fails to account the energy capacity of the SMES unit. The control scheme in this paper comprises solely of two PI controllers and considers the SMES coil current to take the SMES stored energy capacity into account along with the DFIG generated power as control parameters to determine the direction and level of power exchange between the SMES coil and the ac system. This control system is efficient, simple and is easy to implement as elaborated in the next section.

5.2. Hysteresis Current Control (HCC)

A current controller is basically applied to follow the current command of an apparatus such as a motor drive, UPS, active filter, etc [11-14]. Due to the advanced technology improvement of power electronics, current controller techniques have become popular over last decades as proposed in [15-26]. However, due to simplicity, insensitivity to load parameters variations, fast dynamic response and inherent maximum current limiting characteristic [27], HCC is a rather popular one. The basic implementation of HCC is based on deriving the switching signals from the comparison of the actual phase current with a fixed tolerance band around the reference current associated with that phase. However, not only is this type of band control dependent on the corresponding phase voltage, but is also affected by the voltage of the other two phases [28].

The circuit diagram of a 3-phase VSC connected to series load is shown in Fig. 5.4. Three phase output voltage of the inverter (V_{abc}) can be transformed to a vector represented in the stationary frame, where $x(t) = x_\alpha(t) + jx_\beta(t)$ is defined by [29]:

$$\begin{bmatrix} x_\alpha \\ x_\beta \end{bmatrix} = \frac{2}{3} \begin{bmatrix} 1 & -\frac{1}{2} & -\frac{1}{2} \\ 0 & \frac{\sqrt{3}}{2} & -\frac{\sqrt{3}}{2} \end{bmatrix} \begin{bmatrix} x_a \\ x_b \\ x_c \end{bmatrix} \quad (5.1)$$

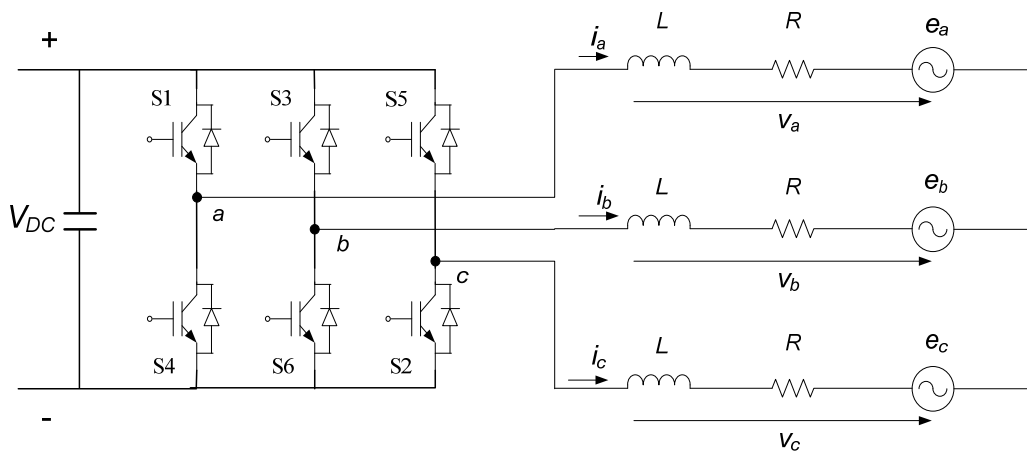


Fig.5.4. Typical of an IGBT based VSC with a series active load

The fundamental operation of a HCC can be explained through its application on voltage source inverters (VSI) for the ease of understanding. Consider the circuit

diagram of a 3-phase VSI connected to the load as shown in Fig. 5.4. In Fig. 5.4, the load currents i_a , i_b and i_c are to be controlled by a current controller. This assumes that the neutral point of the load circuit is isolated and the line current can be controlled to follow the current command by switching the IGBTs' device to the positive or negative dc voltage source terminal ($\pm V_{DC}$). For simplification, the IGBT based VSI can be re-depicted as in Fig. 5.5.

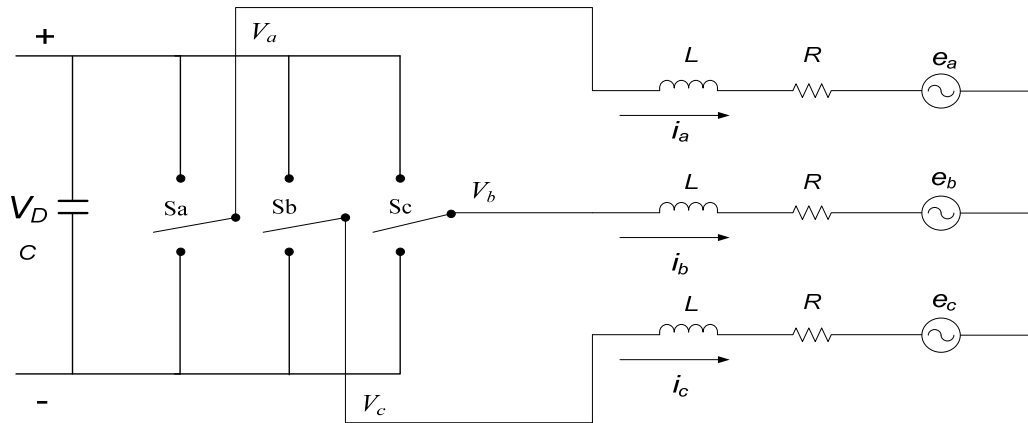


Fig.5.5. Equivalent schematic diagram of a VSC with a series active load

From Fig. 5.5, the terminal voltage of the VSI can be obtained mathematically as given by power system (active load) [11]:

$$\left. \begin{aligned} V_a &= S_a * V_{DC} \\ V_b &= S_b * V_{DC} \\ V_c &= S_c * V_{DC} \end{aligned} \right\} \quad (5.2)$$

Where S_a , S_b , and S_c are the switching function of each phase.

The value of these switching functions is determined by the controller where when S_a , S_b or S_c is connected to $+V_{DC}$, each of S_a , S_b or S_c is equal to 1 and each of them is equal to 0 when connected to $-V_{DC}$.

Refers to Fig. 5.2, by implementing the Kirchoff's second law, it can be obtained:

$$\left. \begin{aligned} \frac{di_a}{dt} &= \frac{1}{3L} [2(v_a - e_a) - (v_b - e_b) - (v_c - e_c)] - \frac{R}{L} i_a \\ \frac{di_b}{dt} &= \frac{1}{3L} [2(v_b - e_b) - (v_a - e_a) - (v_c - e_c)] - \frac{R}{L} i_b \\ \frac{di_c}{dt} &= \frac{1}{3L} [2(v_c - e_c) - (v_a - e_a) - (v_b - e_b)] - \frac{R}{L} i_c \end{aligned} \right\} \quad (5.3)$$

Using (5.1), the vector representation of (5.3) is

$$\frac{dI_0}{dt} = \frac{1}{L} (V_n - e_0) - \frac{R}{L} I_0 \quad (5.4)$$

where:

I_0 is the output current (A) and

e_0 is the counter-emf voltage space vector (V).

If I^* is the current reference or the current command space vector and I_e is the current error space vector, therefore:

$$I_e = I^* - I_0 \quad (5.5)$$

The differential equation of current error vector can be derived from Eqs. 5.4 and 5.5 as:

$$L \frac{dI_e}{dt} + RI_e = L \frac{dI^*}{dt} + RI^* - (V_n - e_0) \quad (5.6)$$

Therefore, the current error vector, I_e changes with L/R time constant. It is also depending on others variable such as current command space vector, I^* , and its derivative, dI^*/dt . Moreover, I_e is also influenced by VSI output voltage, V_n and counter-emf, e_0 . If R is neglected, the desired output voltage, V_n^* to achieve the zero current error can be calculated by [29]:

$$V_n^* = e_0 + L \frac{dI^*}{dt} \quad (5.7)$$

By substituting Eqs. 5.7 to 5.6, it can be obtained:

$$L \frac{dI_e}{dt} = V_n^* - V_n \quad (5.8)$$

From Eqs. 5.6 and 5.7, we can obtain the information that zero current error is determined by the decisive value of both counter-emf voltage space vector and the command current vector.

In this study a 3-phase hysteresis method is used to control the switching operations VSC of the SMES as illustrated in Fig. 5.6. In this method, three hysteresis bands of width h are defined around the reference value of the 3-phase currents. Each phase current is controlled with the two-level hysteresis comparator shown in Fig. 5.4, when the line current is lesser or greater than the reference current by the hysteresis band h , the respective inverter leg is switched to positive or negative direction.

The example of typical hysteresis current and switching signal can be obtained in Figs. 5.7 and 5.8 respectively.

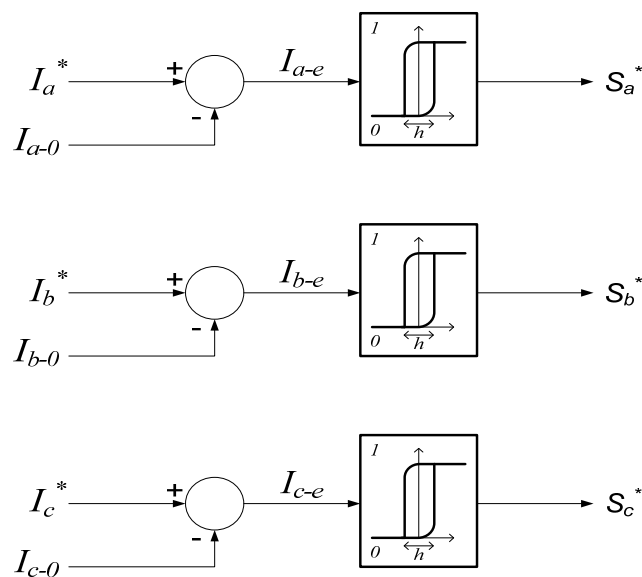


Fig. 5.6. 3-phase HCC method

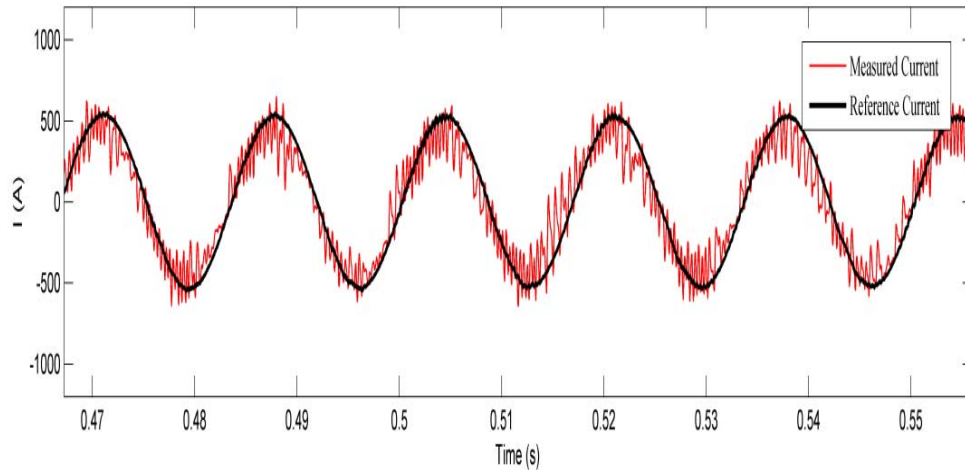


Fig.5.7. Typical hysteresis current [33]

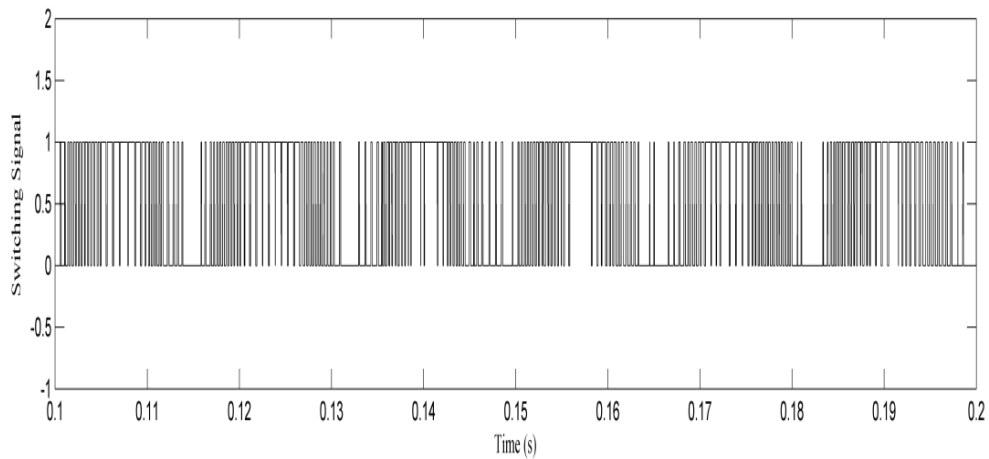


Fig.5.8. Typical switching signal

The effect of interference between phases (referred as inter-phases dependency) can lead to high switching frequencies. To maintain the advantages of the hysteresis methods, this phase dependency can be minimized by using phase-locked loop (PLL) technique to maintain the converter switching at a fixed predetermined frequency level [30].

PLL is a feedback loop that locks two different waveforms that have same frequency but different in phase shift. Fundamentally, a PLL works by comparing frequency of two waveforms and then adjusting the frequency of the waveform in the loop to exactly match with frequency of the input waveform. A block diagram of PLL shown in Fig. 5.9 will easily describe the principle concept of a PLL.

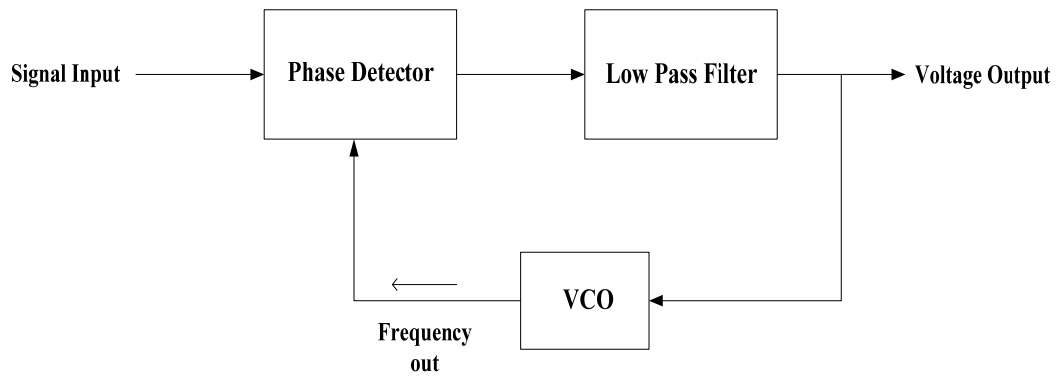


Fig.5.9. Basic phase-locked loop (PLL) [31]

As can be seen in Fig. 5.9, the heart of a PLL is a phase detector along with a voltage controlled oscillator (VCO). If the two frequencies are different, the output of the phase detector varies and changes the input to the VCO to dictate its output frequency equal to the input waveform frequency. The low pass filter here is aimed to generate correction voltage from the phase detector output.

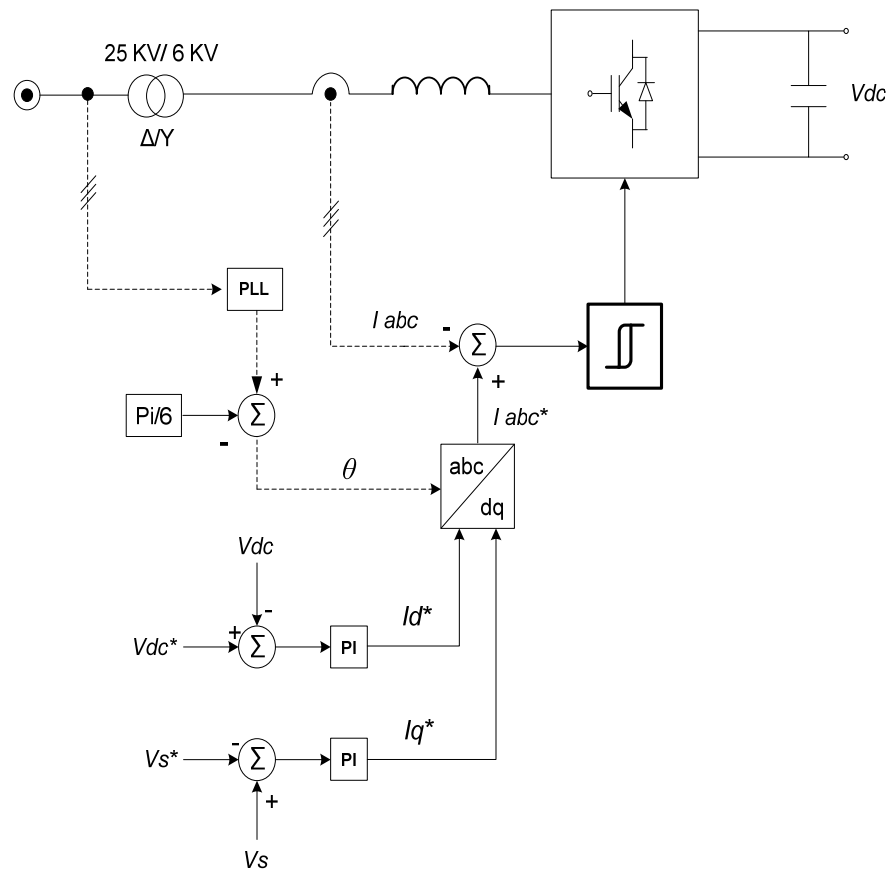


Fig. 5.10. Control algorithm of VSC

The proposed SMES with an auxiliary PLL controller is shown in Fig. 5.10. HCC is comparing the 3-phase line currents (I_{ABC}) with the reference currents (I_{ABC}^*) which is dictated by the I_D^* and I_Q^* references. The values of I_D^* and I_Q^* are generated through the conventional PI controllers based on the error values of V_{DC} and V_S . The value of I_D^* and I_Q^* is converted through the Park's transformation ($dq0-abc$) to produce the reference current (I_{ABC}^*). The Park's transformation has been much explained in detail in Chapter 3.

The proposed control system described in Fig. 5.10 can be explained through the fundamental concept of $d-q$ frame method as below:

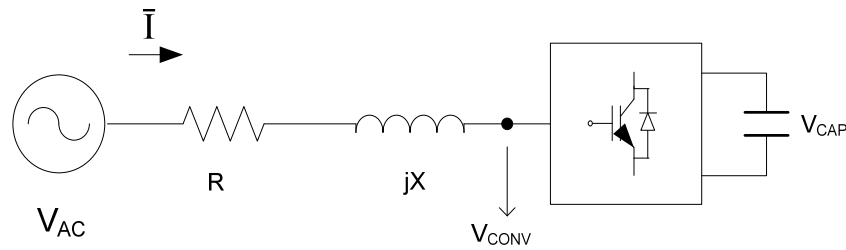


Fig. 5.11. Single line equivalent circuit of VSC

Let Fig. 5.11 as a simplified single line equivalent circuit of VSC where V_{AC} and V_{CONV} are the *rms* value of AC line voltage and output voltage of the converter. R and X are the representative of the resistance and reactance leakage respectively and \bar{I} is the phasor current. I_D and I_Q are attributed to the real and the imaginary components of \bar{I} respectively.

By splitting into its $d-q$ components, it can be obtained:

$$\bar{I} = \frac{V_{AC} - (V_D + jV_Q)}{R + jX} \quad (5.9)$$

Since, $\bar{I} = I_D + jI_Q$,

$$I_D + jI_Q = \frac{V_{AC} - (V_D + jV_Q)}{R + jX} \cdot \frac{(R - jX)}{(R - jX)}$$

$$= \frac{[R(V_{AC} - V_D) - V_Q X] - j[R V_Q + V_{AC} X - V_D X]}{R^2 + X^2}$$

$$I_D = \frac{1}{R^2 + X^2} [R(V_{AC} - V_D) - V_Q X] \quad (5.10)$$

$$I_Q = -\frac{1}{R^2 + X^2} [R(V_Q - V_{AC} X) - V_D X] \quad (5.11)$$

If R is very small, it can be obtained:

$$I_D \propto V_Q \text{ and } I_Q \propto V_D$$

Since, $P = \text{Real}(V_{AC} \bar{I}^*) = V_{AC} I_D$

$$Q = \text{Imaginary}(V_{AC} \bar{I}^*) = V_{AC} I_Q$$

Thus, it can be concluded that:

$$P \propto I_D \text{ and } Q \propto I_Q$$

$$P \propto V_Q \text{ and } Q \propto V_D$$

Therefore, active and reactive power from the VSC can be controlled in such away with their corresponding proportional d - q axis currents and d - q axis voltages. Applying conventional PWM signal switching method will require that both the d - q axis references frame of current and voltage have to be simultaneously employed with the traditional PI controllers, thus it will be inevitable to apply at least four PIs controllers in such control system as introduced in Refs [9, 10]. Tuning the optimal parameters of four PIs, however, will consume massive times to gain the best transient response as well as the stability of the overall system. In this thesis however, only d - q axis currents are proportionally used for hysteresis current controller as shown in Fig. 5.10 which will only use two PIs controller, this configuration moreover will be much simpler and more time efficient.

5.3. Fuzzy Logic Control (FLC)

For accurate control of highly nonlinear systems with time varying parameters, an intelligent or a hybrid intelligent technique must be considered. One of the well-known and widely accepted intelligent techniques during the last decades is the fuzzy logic controller which was proposed by Lotfy Zadeh in 1965 [32].

There are some benefits of using fuzzy controllers compare with the conventional controllers as expressed below [32]:

1. Compared to conventional PID controllers, FLCs are more robust since they can cover a much wider range of operating conditions than PID can, and can operate with noise and disturbance of different nature.
2. Developing a FLC is cheaper than developing a model-based or other controller to do the same thing.
3. Since it is easier to understand and modify their rules, FLCs are customizable which not only use a human operator's strategy but also are expressed in natural linguistic terms.
4. It is attractive because easy to learn how FLC operate and how to design and apply them to a concrete application.

The common step of designing a FLC can be described in the following steps [32]:

1. Determine the inputs and what is the value of output that should be achieved
2. Define the condition interface- fix the way in which observations of the process are expressed as fuzzy sets.
3. Design the rule base to determine which rules are to be applied under which conditions. This is usually easier if design is in table model. This can be said to be the part of the inference engine.
4. Design the computational unit- supply algorithms to perform fuzzy computations. Those will generally lead to fuzzy output.

5. Determine rules according to which fuzzy control statements can be transformed into crisp control actions. This is also part of the defuzzification process of the fuzzy output.

In fuzzy logic there are four the most common membership functions as can be illustrated in Fig. 5.12 below:

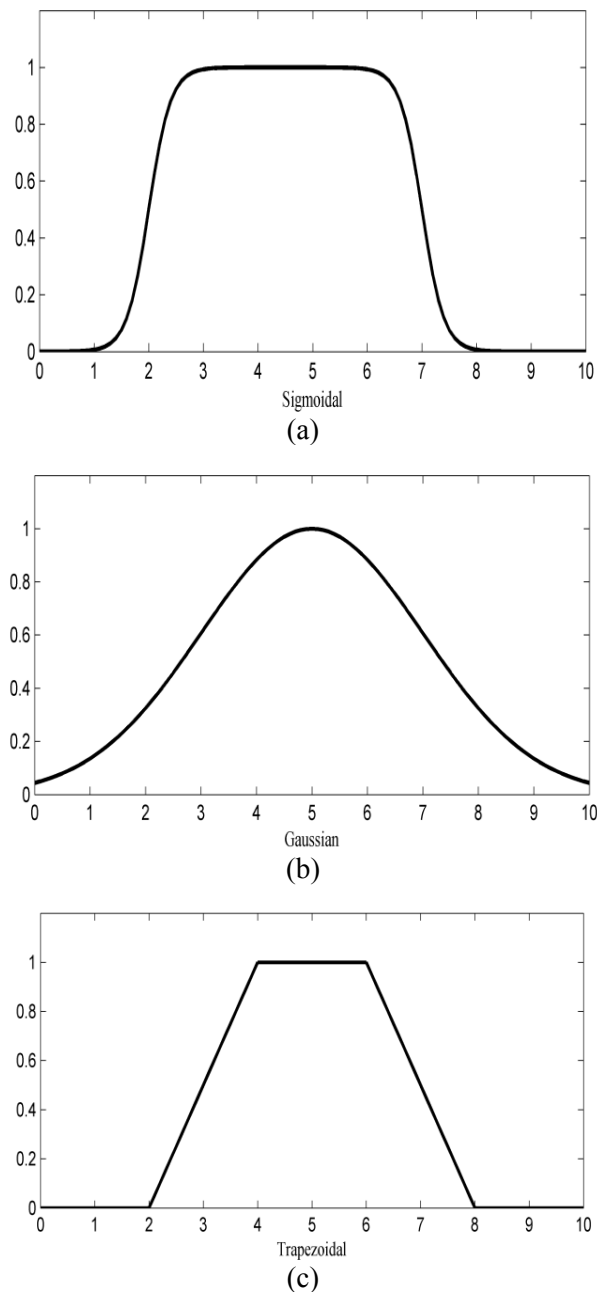


Fig 5.12. Membership function type of fuzzy logic; (a) Zigmoidal, (b) Gaussian, and (c) Trapezoidal (continued on next page)

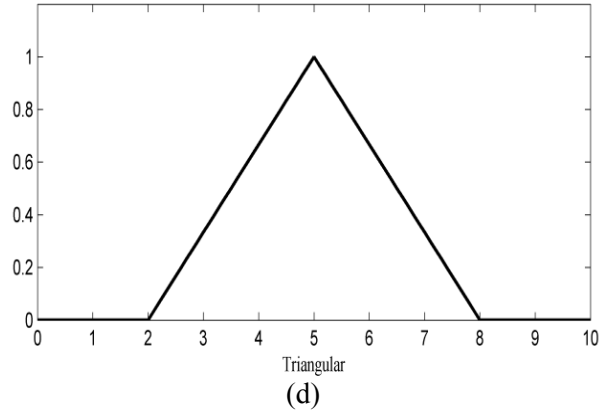


Fig 5.12. Membership function type of Fuzzy logic; (d) Triangular Sigmoid curve (Fig. 5.12(a)) can be obtained from Eq. 5.12

$$f(x: a, c) = \frac{1}{1 + e^{-a(x-c)}} \quad (5.12)$$

Gaussian curve (Fig. 5.12(b)) can be obtained Eq. 5.13

$$f(x: \sigma, c) = e^{-\frac{(x-c)^2}{2\sigma^2}} \quad (5.13)$$

Trapezoidal curve (Fig. 5.12(c)) can be obtained Eqs. 5.14 and 5.15

$$f(x, a, b, c, d) = \left\{ \begin{array}{ll} 0, & x \leq a \\ \frac{x-a}{b-a}, & a \leq x \leq b \\ 1, & b \leq x \leq c \\ \frac{d-x}{d-c}, & c \leq x \leq d \\ 0, & d \leq x \end{array} \right\} \quad (5.14)$$

Or more compactly, by:

$$f(x; a, b, c, d) = \max \left[\min \left[\frac{x-a}{b-a}, 1, \frac{d-x}{d-c} \right], 0 \right] \quad (5.15)$$

Triangular curve (Fig. 5.12(d)) can be obtained Eqs. 5.16 and 5.17

$$f(x; a, b, c) = \begin{cases} 0, & x \leq a \\ \frac{x-a}{b-a}, & a \leq x \leq b \\ \frac{c-x}{c-b}, & b \leq x \leq c \\ 0, & d \leq x \end{cases} \quad (5.16)$$

Or simplify, by:

$$f(x; a, b, c) = \max \left[\min \left[\frac{x-a}{b-a}, \frac{c-x}{c-b} \right], 0 \right] \quad (5.17)$$

Triangular or trapezoidal (piecewise linear) and sigmoidal functions have proved to be more popular with fuzzy logic practitioners rather than higher order based functions such as quadratic, cubic, etc. [32].

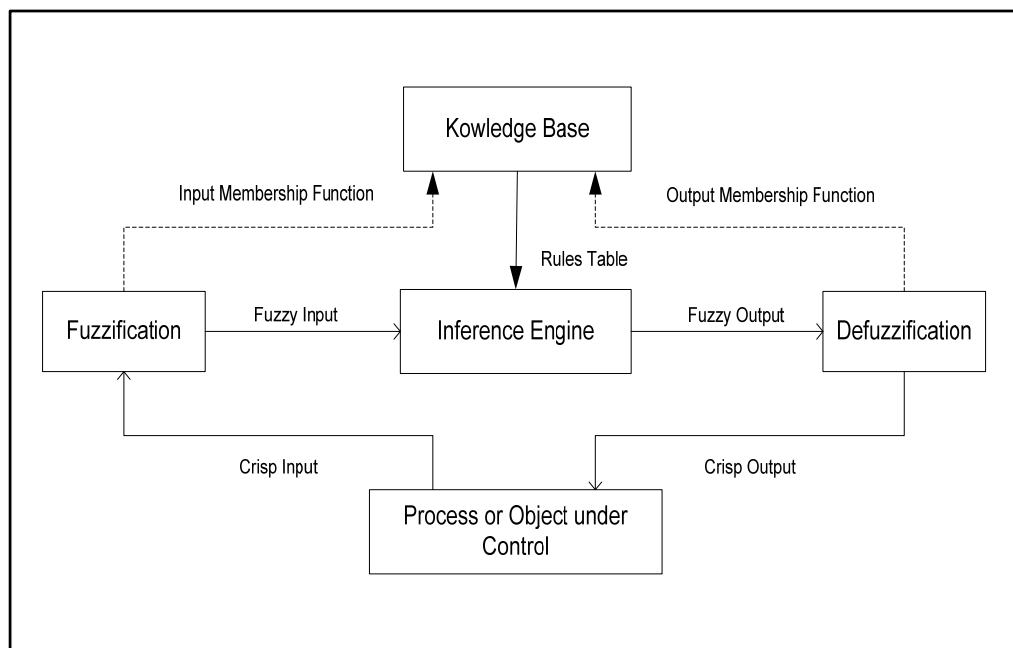


Fig. 5.13. Typical structure of a FLC

In this study, to control the power transfer between SMES coil and the AC system, a DC-DC chopper is used and fuzzy logic is selected to control its duty cycle (D) as shown in Fig. 5.14. The FLC is developed according to the fuzzy inference flowchart depicted in Fig. 5.13 which is a process of formulating the mapping from a given input to the designated output. Input variables for the model are the real power generated by the DFIG and SMES coil current.

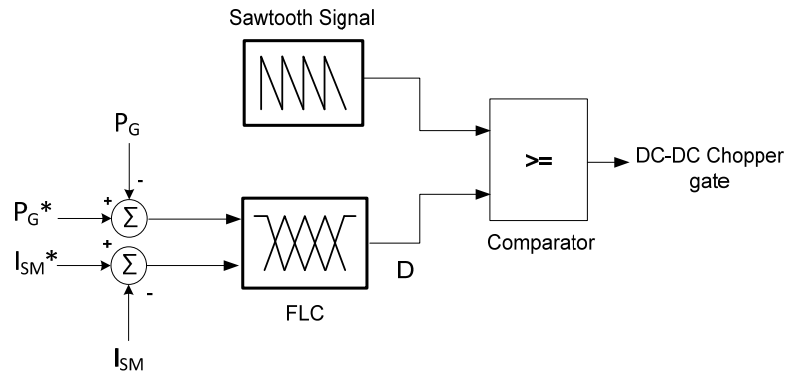


Fig. 5.14. Control algorithm of DC-DC chopper

The output of FLC is D for class D DC-DC chopper that is shown in Fig. 5.15(a). The V-I operational range for the SMES coil is shown in Fig 5.15(b). The duty cycle determines the direction and magnitude of power exchange between the SMES coil and the AC system as presented in Table 5.1.

Table 5.1. Rules of duty cycle

Duty Cycle (D)	SMES Coil Action
$D = 0.5$	Standby Condition
$0 \leq D < 0.5$	Discharging Condition
$0.5 < D \leq 1$	Charging Condition

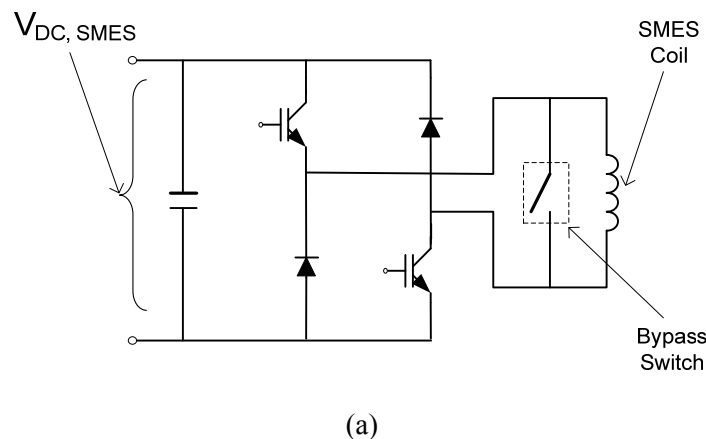
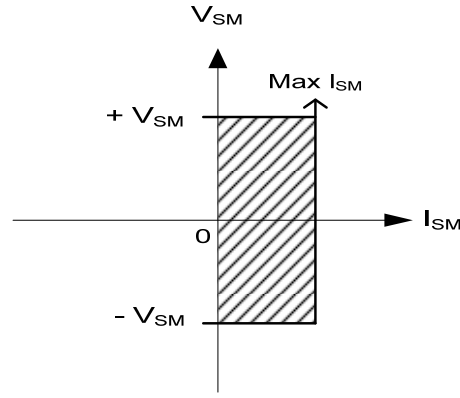


Fig. 5.15. (a) Class D DC-DC chopper topology with a SMES coil
(continued on next page)



(b)

Fig. 5.15. (b) Operation range of SMES coil

If the D is equal to 0.5, no action will be taken by the coil and the system is under normal operating condition. In this condition, a bypass switch that is installed across the SMES coil (shown in Fig. 5.15(a)) will be closed to avoid the draining process of SMES energy during normal condition. The bypass switch is controlled in such a way it will be closed if D is equal to 0.5 otherwise it will be opened. This technique has been introduced in some studies in the literature [2, 9]. When the grid power is reduced, D will be reduced accordingly to be in the range of 0 to 0.5 and the stored energy in the SMES coil will be transferred to the ac system. Charging process of the SMES coil takes place when D is in the range of 0.5 to 1.0.

The relation between V_{SMES} and $V_{DC,SMES}$ can be written as [2]:

$$V_{SMES} = (1 - 2D)V_{DC,SMES} \quad (5.18)$$

where:

V_{SMES} is the average voltage across the SMES coil (V)

D is duty cycle

$V_{DC,SMES}$ is the average voltage across the DC link capacitor (V)

The model is built using the graphical user interface tool provided by MATLAB. Each input was fuzzified into five sets of gaussmf type membership function (MF). The Gaussian curve is a function of a vector, x , and depends on parameters σ and c as given by:

$$f(x, \sigma, c) = e^{-(x-c)^2/2\sigma^2} \quad (5.19)$$

where:

σ is variable that determine the centre of the peak

c is the width of the bell curve, respectively

The corresponding membership functions for all the input variables (P_G and I_{SMES}) and output variables (D) are presented in Chapter 6.

5.4. Summary

In this chapter, the most common configurations of SMES are discussed. The advantages of VSC based SMES over CSC based SMES is presented. The new control scheme of SMES using the HCC and FLC is described. Explanation of the two-level hysteresis comparator theory is provided and the detail concept of using HCC in controlling VSC is also demonstrated. The selection of HCC in this study is based on its advantages, including simplicity, insensitivity to load parameters variations, fast dynamic response and inherent maximum current limiting characteristics. To allow optimal transfer/absorption of some degree of power to/from SMES, FLC is selected. FLC has some advantages; particularly, that it can cover a much wider range of operating conditions than a PID controller can, and can also operate with the noise and disturbance of a different nature. Moreover, since it is easier to understand and modify its rules, a fuzzy logic controller is customizable, which not only uses a human operator's strategy but is also expressed in natural linguistic terms. Finally, developing a FLC is cheaper than developing a model-based or other controller to do the same thing.

A diagram of the full control concept of SMES with HCC and FLC is also provided, such as the use of Park's transformation and PLL. The reason for using Park's transformation was explained in detail in Chapter 3, since it is also widely used in the model of DFIG. PLL basic concepts are introduced in this chapter to replenish the whole explanation of the proposed controller in this study. However, the corresponding membership functions of both inputs and outputs of FLC are included in Chapter 6, for the case of voltage sag/swell and short load variation.

5.5. References

- [1] A. Abu-Siada and S. Islam, "Application of SMES Unit in Improving the Performance of an AC/DC Power System", *IEEE Transactions on Sustainable Energy*, vol. 2, pp. 109-121. 2011
- [2] I. D. Hassan, R. M. Bucci, and K. T. Swe, "400 MW SMES Power Conditioning System Development and Simulation", *IEEE Transactions on Power Electronics*, vol. 8, pp. 237-249. 1993
- [3] T. Ackermann, "Wind Power in Power System", West Sussex: John Wiley and Sons Ltd. 2005
- [4] A. R. Kim, S. Hyo-Ryong, K. Gyeong-Hun, P. Minwon, Y. In-Keun, Y. Otsuki, J. Tamura, K. Seok-Ho, S. Kideok, and S. Ki-Chul, "Operating Characteristic Analysis of HTS SMES for Frequency Stabilization of Dispersed Power Generation System", *IEEE Transactions on Applied Superconductivity*, vol. 20, pp. 1334-1338. 2010
- [5] J. Hee-Yeol, A. R. Kim, K. Jae-Ho, P. Minwon, Y. In-Keun, K. Seok-Ho, S. Kideok, K. Hae-Jong, S. Ki-Chul, T. Asao, and J. Tamura, "A Study on the Operating Characteristics of SMES for the Dispersed Power Generation System", *IEEE Transactions on Applied Superconductivity*, vol. 19, pp. 2028-2031. 2009
- [6] S. Jing, T. Yuejin, X. Yajun, R. Li, and L. Jingdong, "SMES Based Excitation System for Doubly-Fed Induction Generator in Wind Power Application", *IEEE Transactions on Applied Superconductivity*, vol. 21, pp. 1105-1108. 2011
- [7] M. G. Molina and P. E. Mercado, "Power Flow Stabilization and Control of Microgrid with Wind Generation by Superconducting Magnetic Energy Storage", *IEEE Transactions on Power Electronics*, vol. 26, pp. 910-922. 2011
- [8] A. M. Shiddiq-Yunus, M. A. S. Masoum, and A. A. Siada, "Application of SMES to Enhance the Dynamic Performance of DFIG During Voltage Sag and Swell", *IEEE Transactions on Applied Superconductivity*. 2012 (In Press)
- [9] M. H. Ali, P. Minwon, Y. In-Keun, T. Murata, and J. Tamura, "Improvement of Wind-Generator Stability by Fuzzy-Logic-Controlled SMES", *IEEE Transactions on Industry Applications*, vol. 45, pp. 1045-1051. 2009
- [10] M. H. Ali, W. Bin, and R. A. Dougal, "An Overview of SMES Applications in Power and Energy Systems", *IEEE Transactions on Sustainable Energy*, vol. 1, pp. 38-47. 2010
- [11] P. Ching-Tsai and C. Ting-Yu, "An improved hysteresis current controller for reducing switching frequency", *IEEE Transactions on Power Electronics*, vol. 9, pp. 97-104. 1994
- [12] D. Xu, J. Gu, H. Liu, and M. Gong, "Improved hysteresis current control for active power filter," in *International Symposium on Industrial Electronics, 2003. IEEE*, vol. 2, pp. 836-840. 2003
- [13] Q. Yu and D. Shanshan, "A Novel Adaptive Hysteresis Band Current Control Using A DSP for A Power Factor Corrected On-Line UPS", in *23rd International Conference on Industrial Electronics, Control and Instrumentation, 1999*, vol.1, pp. 208-212. 1997
- [14] G. Vazquez, P. Rodriguez, R. Ordóñez, T. Kerekes, and R. Teodorescu, "Adaptive Hysteresis Band Current Control for Transformerless Single-Phase PV Inverters", in *35th Annual Conference of IEEE Industrial Electronics, 2009. IECON '09*, pp. 173-177. 2009

- [15] T. A. Lipo, "Recent Progress in The Development in Solid-State AC Motor Drives", *IEEE Transactions on Power Electronic*, vol. 3, pp. 105-117. 1988
- [16] P. C. Sen, "Electric Motor Drives and Control - Past, Present and Future", in *14 Annual Conference of Industrial Electronics Society, 1988. IECON '88*, pp. 534-544. 1988
- [17] B. K. Bose, "Recent Advances in Power Electronics", *IEEE Transactions on Power Electronics*, vol. 7, pp. 2-16. 1992
- [18] D. M. Brod and D. W. Novotny, "Current Control of VSI-PWM Inverters", *IEEE Transactions on Industry Applications*, vol. IA-21, pp. 562-570. 1985
- [19] C. Tae-Won and C. Meong-Kyu, "Development of Adaptive Hysteresis Band Current Control Strategy of PWM Inverter with Constant Switching Frequency", in *Applied Power Electronics Conference and Exposition, 1996*, vol.1, pp. 194-199. 1996
- [20] J. Holtz, "Pulsewidth Modulation-A Survey", in *Power Electronics Specialists Conference, 1992*, vol.1, pp. 11-18. 1992
- [21] J. Holtz and E. Bube, "Field-Oriented Asynchronous Pulse-Width Modulation For High-Performance AC Machine Drives Operating At Low Switching Frequency", *IEEE Transactions on Industry Applications*, vol. 27, pp. 574-581. 1991
- [22] S. Fukuda, H. Hasegawa, and Y. Iwaji, "PWM Technique for Inverter With Sinusoidal Output Current", in *Power Electronics Specialists Conference, 1988*, vol.1, pp. 35-41. 1988
- [23] M. P. Kazmierkowski and W. Sulkowski, "A Novel Vector Control Scheme for Transistor PWM Inverter-Fed Induction Motor Drive", *IEEE Transactions on Industrial Electronics*, vol. 38, pp. 41-47. 1991
- [24] M. Marchesoni, M. Mazzucchelli, and S. Tenconi, "A Non Conventional Power Converter for Plasma Stabilization", in *Power Electronics Specialists Conference, 1988*, vol.1, pp. 122-129. 1988
- [25] M. Marchesoni, "High-Performance Current Control Techniques for Application to Multilevel High-Power Voltage Source Inverters", *IEEE Transactions on Power Electronics*, vol. 7, pp. 189-204. 1992
- [26] J. Li and D. Wang, "Study and Simulation of a Novel Hysteresis Current Control Strategy," in *Second International Conference on Intelligent Computation Technology and Automation, 2009*, pp. 306-309. 2009
- [27] K. Bong-Hwan, K. Tae-Woo, and Y. Jang-Hyoun, "A Novel SVM-Based Hysteresis Current Controller", *IEEE Transactions on Power Electronics*, vol. 13, pp. 297-307. 1998
- [28] M. Milosevic. "Hysteresis Current Control in Three-Phase Voltage Source Inverter", http://www.eeh.ee.ethz.ch/uploads/tx_ethpublications/milosevic_hysteresis.pdf, accessed: 19 February, 2011
- [29] M. Mohseni and S. Islam, "A Novel Current Controller for Three-Phase Voltage-Source Inverters", in *35th Annual Conference of IEEE Industrial Electronics, 2009*, pp. 76-81. 2009
- [30] L. Malesani and P. Tenti, "A Novel Hysteresis Control Method for Current-Controlled Voltage-Source PWM Inverters with Constant Modulation Frequency", *IEEE Transactions on Industry Applications*, vol. 26, pp. 88-92. 1990

- [31] <http://www.hep.ph.ic.ac.uk/~hallg/Instrumentation/Lectures/Phasesensitivedetection.pdf>, accessed: 11 June, 2012
- [32] L. Reznik, "Fuzzy Controllers", Oxford ; Boston: Newnes. 1997
- [33] P. Ching-Tsai and C. Ting-Yu, "An Improved Hysteresis Current Controller for Reducing Switching Frequency", *IEEE Transaction on Power Electronic*, vol. 9, pp. 97-104. 1994

“Every reasonable effort has been made to acknowledge the owners of copyright material. I would be pleased to hear from any copyright owner who has been omitted or incorrectly acknowledged.”

Chapter 6

Application of SMES Unit on the Power System with Doubly Fed Induction Generator (DFIG)

6.1. Introduction

Although superconductivity was discovered in 1911, no reports on the superconductor's potential to become an energy storage option for power system applications were introduced until the 1970s [1]. Since the successful commission tests of the Bonneville Power Administration (BPA), which managed to install a 30-MJ SMES unit for system stabilizer at Tacoma, Washington in 1983 [2] (although the unit was retired in 1984), the SMES has become ever more attractive to researchers who wish to study the extension of its application on various purposes in the power system. Notably, after the shaft damage incident at the Mohave Power Station in 1970 and 1971 [3], which was caused by the sub-synchronous resonance (SSR) phenomena as a result of employing a series capacitor compensator (SCC), researchers began to explore appropriate techniques to dampen the effect of SCC on the transmission lines [4]. SMES has been proven as one of the promising solutions to mitigate the adverse impact of SSR as discussed in [5, 6].

Power imbalance is a serious problem in any power system. In many references such as [7-20], the SMES unit is successfully demonstrated its capability as a power leveller or a power conditioner to reduce power imbalances between the generator and the load side with various control and load applications. The experimental and test studies of SMES applications on power system have been also reported in many Refs. [2, 21-25].

Although studies have lavished attention on the application of SMES on AC power systems, they have largely overlooked SMES application on DC power systems. A few SMES unit applications on high voltage DC (HVDC) have been introduced, such as those in [26-29]. The recent increase in electric vehicle (EV) production and utilization has presented a critical challenge for power utility systems since its revival in 1990 after EV almost became extinct in the 1930s [30]. After developers succeed to reduce the size and weight of batteries while still maintaining their high energy capacities, EVs became noticeably more popular, and a large number have been produced in a few countries. Therefore, EVs stations are in demand in a number of locations around the world. A few stations have been implemented in some countries, such as the US and some European countries. With the recent interest and high appetite for the innovative smart grid technologies, it is expected that plug-in electric vehicles (PEVs) and PEV charging stations will soon populate the residential and distribution networks as has been studied in many literatures such as in Refs [31, 32]. The overloading during charging of a large number of PEVs will burden the smart grid. One possible response that governments can make is to enforce charging schedules. However, such PEV charge coordination could greatly inconvenience the end consumers (PEV owners), so storage energy devices such as SMES units, might present a desirable alternative. The application of SMES units in conjunction with renewable energy resources along with PEVs has been addressed in Ref [33]. In [33] coordinated control method of a SMES and V2G (Vehicle to Grid) operation has been proposed to balance the grid under both steady and transient states. A combination of SMES, fuel cells with liquid hydrogen vehicle stations and renewable energy is introduced in Ref [34]. In addition, an advanced superconducting power conditioning system (ASPCS) has just been introduced, which consists of a 5-MW class renewable energy resource, a 1.0-MW class hybrid storage system, a commercial utility grid and an LH₂ station for vehicles. By using a Kalman filter, the adequate sharing among the storage devices can be achieved to control the fluctuating power.

Besides the various SMES applications discussed above, some studies have discussed others SMES utilizations in the area of power systems. In [35-37], the SMES unit was used to fulfil spinning reserve requirements. When the power generating system must go out of service, the spinning reserve of some unloaded

generating system must be kept intact (due to service task when fault occur or for routine check up schedule, some generating systems must be unloaded, normally the connected loads will be connected to back up generating systems). Due to its large capacity, the SMES can handle the spinning reserve condition, and studies have claimed that under these circumstances, SMES is more cost effective than other methods of maintaining spinning reserve. In [35], the authors mentioned that the SMES unit is applicable for automatic generation control (AGC). A SMES unit can serve as a controlling function in an AGC system that ensures minimal error in the area control. In the same study, the authors also mentioned that the SMES unit might be able to function as a reactive volt-ampere (VAR) controller as well as a power factor correction devise, so the SMES unit will be able to improve the stability and the carrying capacity of a transmission line. Additionally, a SMES unit could provide enough power to start a generating unit without connecting to the grid. This is useful for grid restoration when area failures have occurred. The other possible application of a SMES unit that this study mentions is working as bulk energy management. Because a SMES unit is capable of storing large quantities of energy, it can act as storage transfer point for bulk quantities of energy. Consequently, a SMES unit could potentially reduce the cost of electricity.

In general, a SMES unit and its associated converter equipment have been shown to be effective in providing voltage support that will consequently improve the power transfer limitation of the transmission line [38]. A few of the SMES unit's functions are discussed in Ref [38], including its capability to improve dynamic voltage stability during the loss of generation or during heavy load condition on the power system, to improve power quality, to backup the power supply when the main supply is lost and to reduces the power angle difference across a circuit breaker. Therefore, the reclosing of a circuit breaker at momentary fault clearance can be performed faster if a SMES unit is connected to the power system. Additionally, when the power system loses its main generating system, power frequency will drop significantly and continue to decline until the generation system and the load balanced is restored. Since a SMES unit is capable of injecting active and reactive power simultaneously in a rapid way into the system, it is an effective method to offset or to reduce under-frequency load shedding because it reduces the mismatch between the load and supply capability of the system disturbance. The other possible

task of a SMES unit mentioned in this reference is its application on tie-line control. When power is scheduled between utility control areas, it is vital that the actual net power closely matches the scheduled power. Unfortunately, when generators are ramped up in one control area and ramped down in the receiving control area in order to send power, the system load can change, causing an error in the actual power delivered. This area control error (ACE) is an inefficient use of generation. With the appropriate controls, a SMES unit can effectively supply power to virtually eliminate this error and assure that generation is proficiently used and that power schedules are met.

A SMES unit is also very attractive for military applications, such as an electromagnetic launcher [39]. An electromagnetic launcher requires a very high power pulse source to run the railgun. A railgun can launch projectiles at velocities higher than 2000 m/s, and the high power density of a SMES unit would be able to support this military application system.

In short, SMES have numerous advantages, including their ultra high efficiency, their high power capacity and their long life cycle that makes them suitable for applications that require constant cycling as well as a continuous mode of operation [3]. Moreover, the SMES unit is applicable to most power system utilities, so it is not pleonastic to say that SMES is one of the most promising candidates for renewable systems. The application of the SMES unit to renewable energy systems is discussed in detail in Chapter 4.

As mentioned in Chapter 1, variable speed WECSs were introduced to overcome the shortcomings of the fixed speed WECS, However, particularly for DFIG based WECS, power quality distortions such as voltage sag and swell at the grid side may introduce detrimental problems to the DFIG's performance that could lead to their disconnection from the power grid. Moreover, disconnection of a WECS would be overwhelmingly costly if it contributes a large portion of power to the grid. To avoid such circumstances, a SMES unit is employed in this chapter to improve the DFIG's performance during the occurrence of voltage sag and swell at the grid side. As aforementioned, since the successful installation of the 30-MJ SMES unit at Bonneville Power Company in 1982, although it was dismantled after the test in 1984 [2], SMES has persuaded many researchers to study its potential applications in

power system [27, 40, 41]. Many papers in the literature have investigated the application of SMES to WECS. However, most of these studies have only focused on the engagement of the SMES unit to smooth the output power of the fixed speed WECS during wind speed fluctuations in order to avoid system instability problems [42-49]. However, no information available yet regarding test and experiment results of SMES application on wind turbine system. As described in previous chapters, most of SMES studies are proposing ideal concept for improving wind energy system performance.

This chapter presents a new application of the SMES unit to improve the performance of wind turbines that are equipped with DFIG during voltage sags and voltage swells at the grid side. A new control system for the SMES unit based on HCC in conjunction with FLC is proposed and implemented. In this chapter, application of SMES on the short term load variation and its application during converter faults in the DFIG's converters such as misfire and fire-through are also investigated and discussed. Simulink/Matlab software is used to simulate the wind turbine, the model under study, and the SMES unit (shown in appendix C-1). Results are analysed to highlight the improved dynamic performance of WECS in conjunction with a SMES unit [50].

6.2. Fault Ride Through of Spain's Grid Code

In the earlier stages of their operation, WECSs were allowed to be disconnected from the power grid to protect them from possible damages. After the rapid injection of WECS into the existing network over the last few decades, the TSOs require WECS to stay connected in a certain level of fault to continue to support the grid. This new requirement has been compiled in the new grid code. However, most of grid code provide only low voltage ride through (LVRT) in their code without any restriction information regarding the high voltage ride through (HVRT), which might lead instability in the PCC [51]. The FRT or so called voltage ride though (VRT) of some international grid codes can be classified in two; first is called LVRT and second is HVRT. The LVRT of some international codes can be obtained from Refs [52, 53]. Fig. 6.1 shows the FRT of Spain's grid code that is used to comply with the conditions of the system under study. The FRT of Spain is selected for the analysis of this thesis because it has established codes for both LVRT and HVRT.

Since voltage sag is a common power quality problem in power systems, most studies have focused on the performance of WECS during voltage sag [54-65]. Although it occurs less frequently, voltage swell may also lead to the disconnection of WECS from the grid, but the HVRT capability of DFIG has not been given much attention in the literature. Only a few studies highlighted this issue, such as [66, 67].

In Fig. 6.1, the fault ride through of Spain’s grid code is divided into three main blocks. The “A” block represents the HVRT of Spain’s grid code. The maximum allowable high voltage in the vicinity of the point of PCC is 130%, and this swell can only last for duration of 0.5s from the instant of fault occurrence.

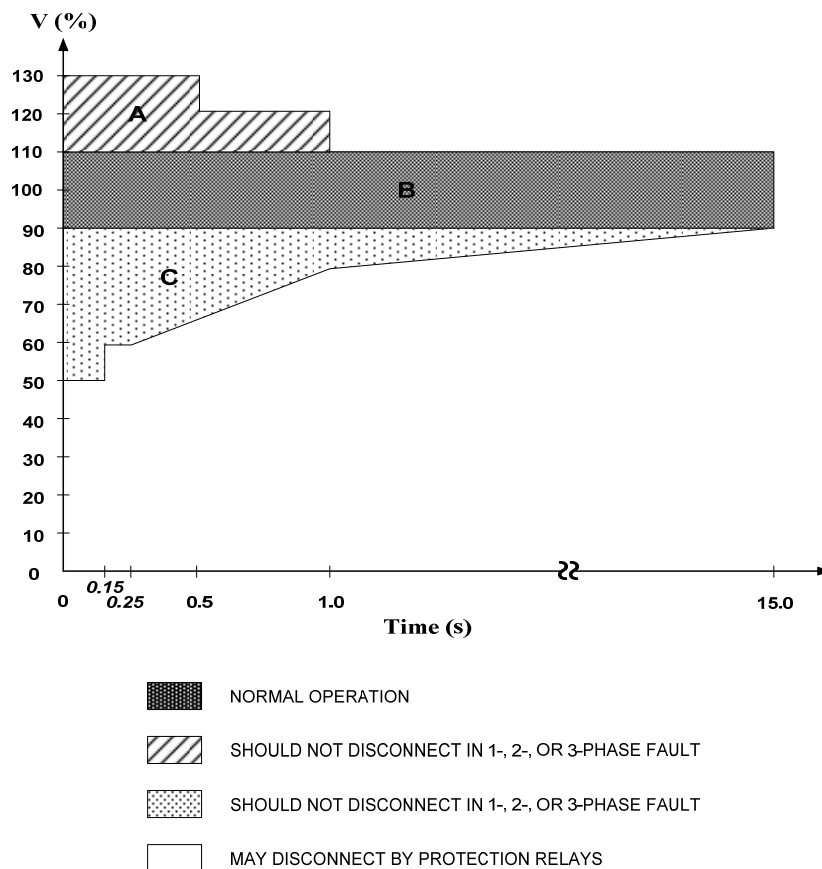


Fig. 6.1. Fault ride through of Spain’s grid code [53]

After that, the maximum voltage must reduce to no greater than 120% for the next 0.5s in order for the WECS not to disconnect. All high voltage profiles above the “A” block will lead to the disconnection of WECS from the system. The normal condition of this grid code lies on the “B” block. All voltage profiles within this

block range (90% to 110%) are classified as normal conditions. LVRT appears in the “C” block. The minimum voltage drop allowed in this grid code is 50%, which can last for only 0.15s from the instant of fault occurrence and then must increase to 60% for 0.1 s for the WECS not to disconnect. The low voltage restriction then ramps up to 80% at 1.0s and reaches the normal condition at 15s after the instant of fault occurrence. Similar to the HVRT, any voltage level at the PCC below the levels constrained by the “C” block will lead to the disconnection of WECS from the system.

6.3. Application of SMES Unit on DFIG During Grid Disturbances

6.3.1. System Under Study

The system under study is shown in Fig. 6.2. It consists of six-1.5 MW DFIG connected to the AC grid at PCC via Y/Δ step up transformer. The grid is represented by an ideal 3-phase voltage source of constant frequency and is connected to the wind turbines via 30 km transmission line. The reactive power produced by the wind turbine is regulated at 0 MVAR at normal operating conditions. For an average wind speed of 15 m/s which is used in this study, the turbine output power is 1.0 pu and the generator speed is 1.0 pu. SMES Unit is connected to the 25 kV bus and is assumed to be fully charged at its maximum capacity of 1.0 MJ. The overall simulated system parameters can be found in Appendixes B-1 to B-6 and the detail information of the DFIG model can be found in Refs. [68, 69]. The time step in all simulations are 5 μs to achieve accuracy of maximum 2700 Hz switching frequency.

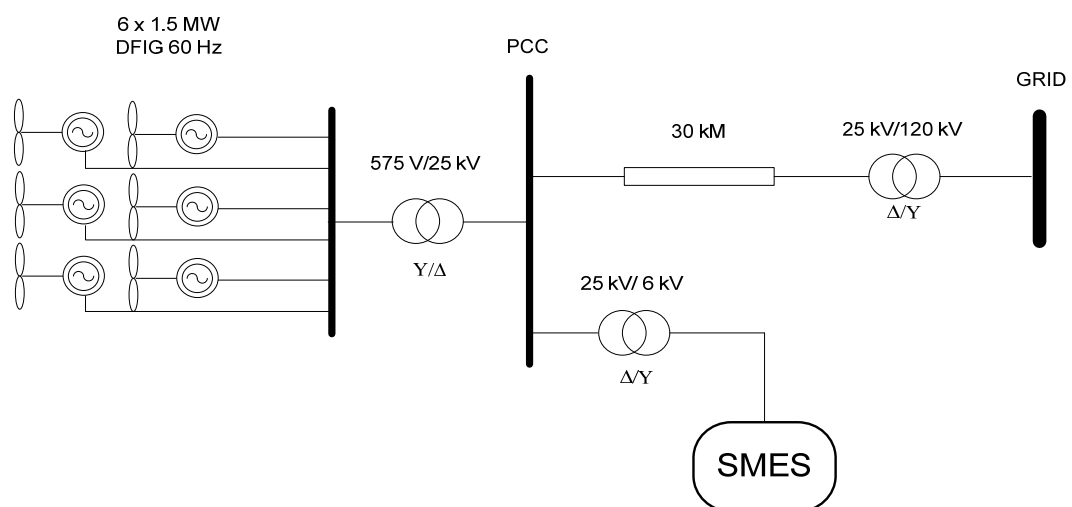


Fig. 6.2. System under study

The details of the SMES configuration and its control algorithms are presented in Chapter 5. Therefore, only the newly defined designated membership functions of the FLC are presented in this chapter.

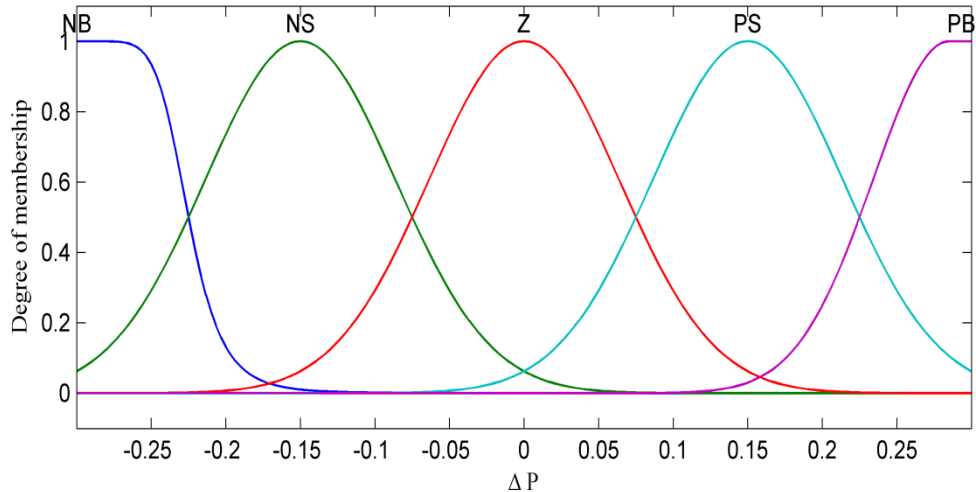
In this case, the corresponding membership functions for the input variables P_G and I_{SMES} are shown in Fig. 6.3 and Fig. 6.4, respectively. The membership functions for the output variable (duty cycle) are considered on the scale 0 to 1.0 as shown in Fig. 6.5.

Centre-of-gravity which is widely used in fuzzy models is used for defuzzification process where the desired output z_0 is calculated as [70]:

$$z_0 = \frac{\int z \cdot \mu_c(z) dz}{\int \mu_c(z) dz} \quad (6.1)$$

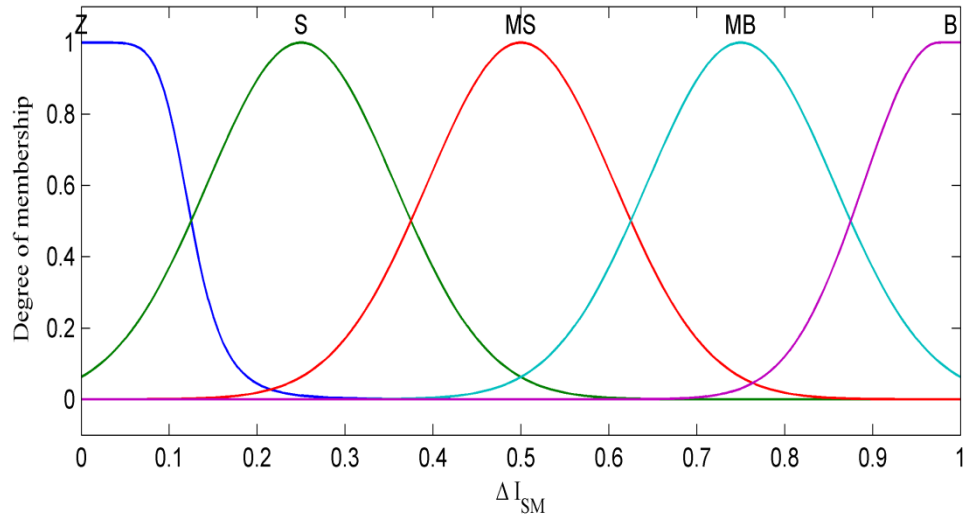
where:

$\mu_c(z)$ is the membership function of the output.



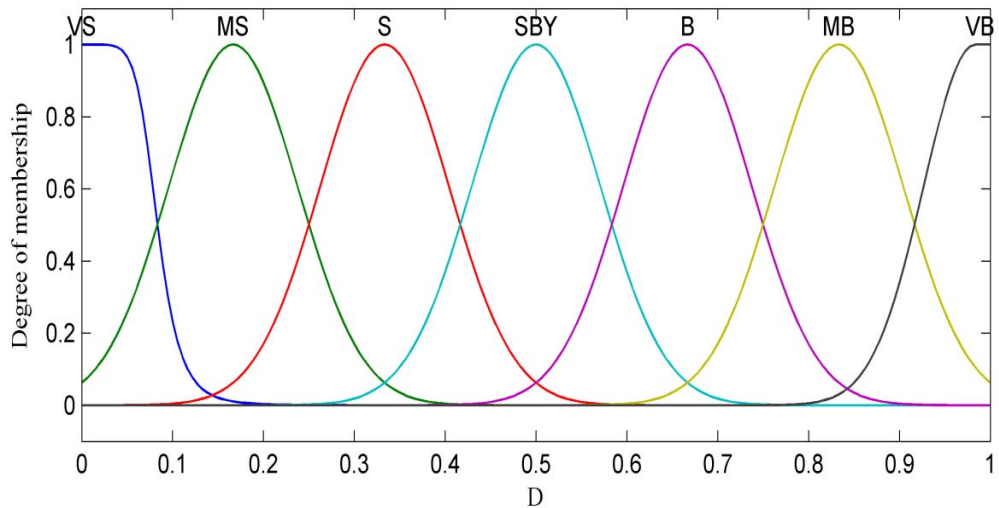
NB=Negative Big, NS= Negative Small, Z= Zero, PS=Positive Small, PB=Positive Big

Fig. 6.3. Memberships function for the input variable P_G (pu)



Z=Zero, S= Small, MS=Medium Small, MB= Medium Big, B= Big

Fig. 6.4. Memberships function for the input variable I_{SMES} (pu)



VS=Very Small, MS= Medium Small S=Small, SBY= Stand-By, B=Big, MB=Medium Big VB=Very Big

Fig. 6.5. Memberships function for the output variable D (duty cycle)

The variation range in SMES current and DFIG output power, as well as the corresponding duty cycle are used to develop a set of fuzzy logic rules in the form of (IF-AND-THEN) statements to relate the input variables to the output. The duty cycle for any set of input variable (P_G and I_{SMES}) can also be evaluated from the surface graph shown in Fig. 6.6.

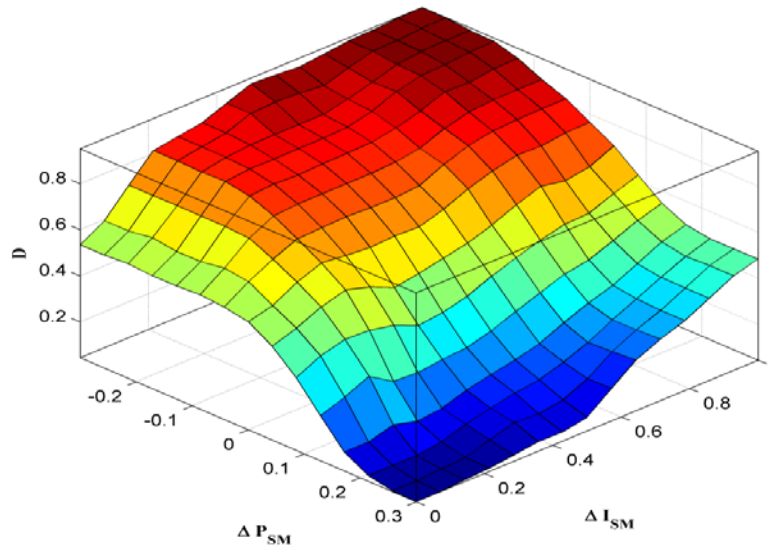


Fig. 6.6. Surface graph-duty cycle

6.3.2. Voltage Sag

Power quality issue is the common consideration for new construction or connection of power generation system including WECS installation and their connection to the existing power system. In this paper, voltage sag (dip) and swell at the grid side will be simulated as the compliance of the fault ride through capability of WECS equipped with DFIG. Voltage sag is a decrease to between 0.1 and 0.9 pu in *r-m-s* voltage or current at the power frequency for durations of 0.5 cycles to 1.0 minute. Voltage sags are usually associated with system faults but can also be caused by switching of heavy loads or starting of large motors [71, 72].

A voltage sag depth of 0.5 pu lasting for 0.05 s is applied at $t=2.0$ s at the grid side of the system under study (Fig. 6.2). Without the SMES unit, the real power produced by the DFIG will drop to 0.6 pu and it reaches maximum overshooting of 40% during the clearance of the fault as shown in Fig 6.7(a). As can be seen in Fig 6.7(a), with the SMES unit connected to the system, DFIG output power will drop to only 0.875 pu. Fig. 6.7(b) implies that with the connection of the SMES unit and during the event of voltage sag the reactive power support by the DFIG is reduced and the steady state condition is reached faster compared with the system without SMES. The voltage at the PCC is shown in Fig. 6.7(c), where without SMES, voltage will drop to 0.6 pu. However, by connecting the SMES unit, voltage drop at the PCC will be reduced to only 0.8 pu which will lead to a voltage drop at the generator

terminal to a level of 0.8 pu that is referenced as a safety margin by the wind turbine manufacturers [73].

The DFIG power drop causes the generator speed to be accelerated to compensate for the power imbalance. As can be observed in Fig. 6.7(d), the generator speed will accelerate and oscillate without the SMES unit; however, with the SMES connected to the system, the power drop is reduced, the settling time of the generator speed is substantially reduced and the overshooting level is significantly decreased. Another effect of the voltage sag on the DFIG's behavior is on the voltage across the DFIG DC link capacitor that is shown in Fig. 6.7(e). The voltage overshoot across the DC link capacitor during fault clearance is slightly reduced with the SMES unit connected to the system.

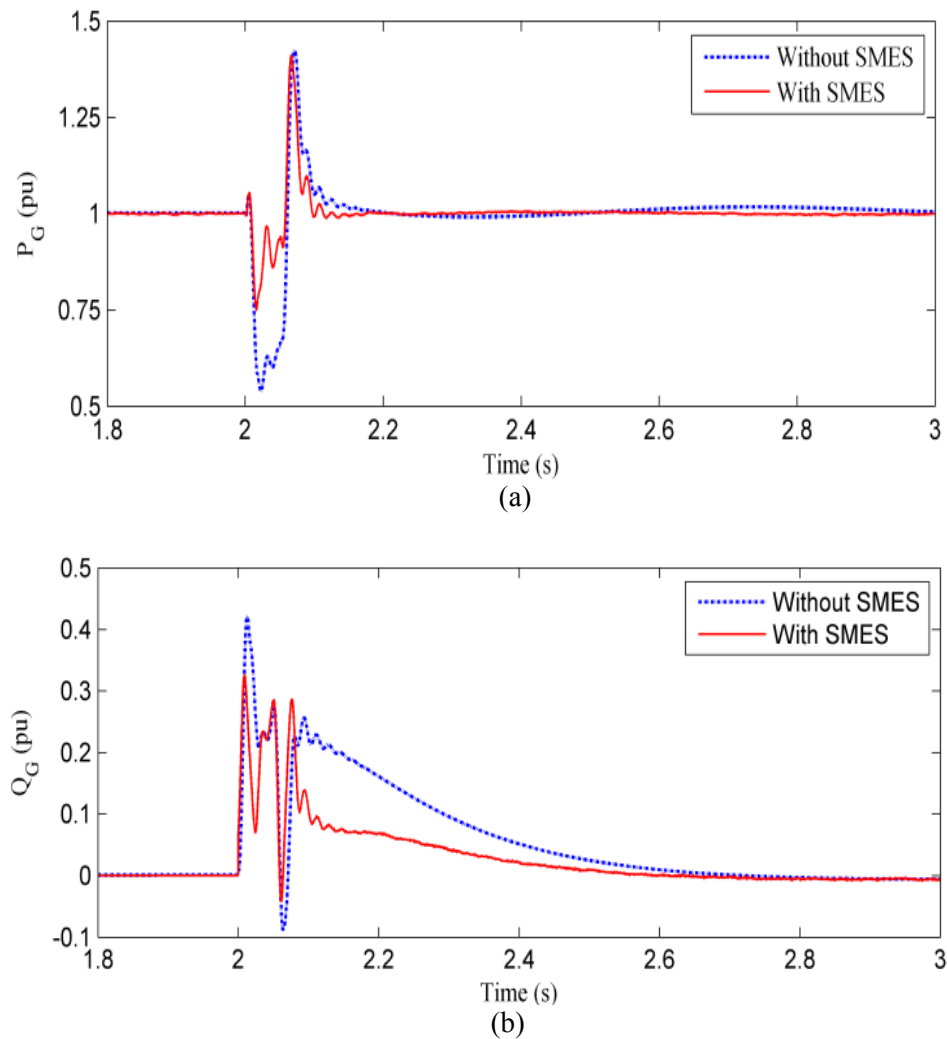


Fig. 6.7. DFIG responses during voltage sag without/with a SMES unit; (a) Active power and (b) Reactive power (continued on next page)

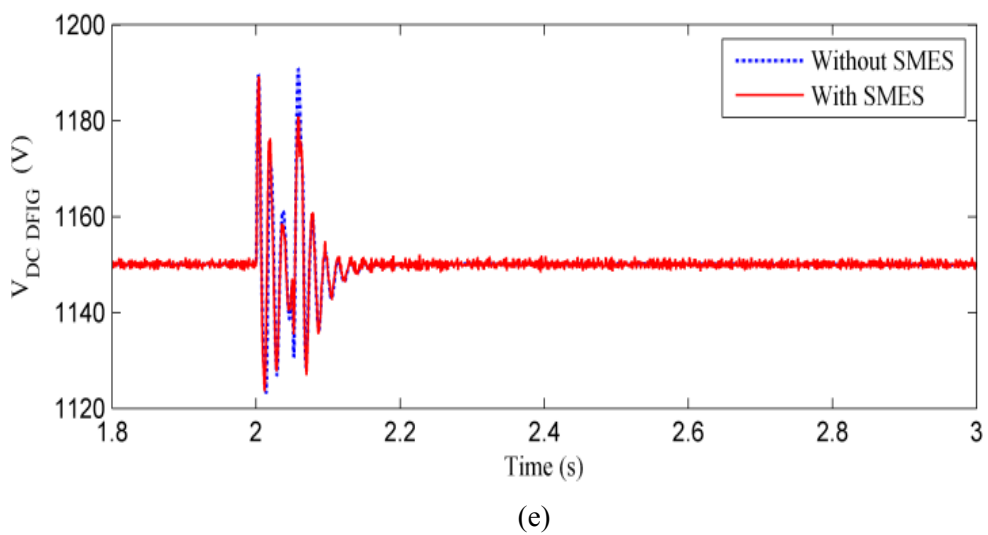
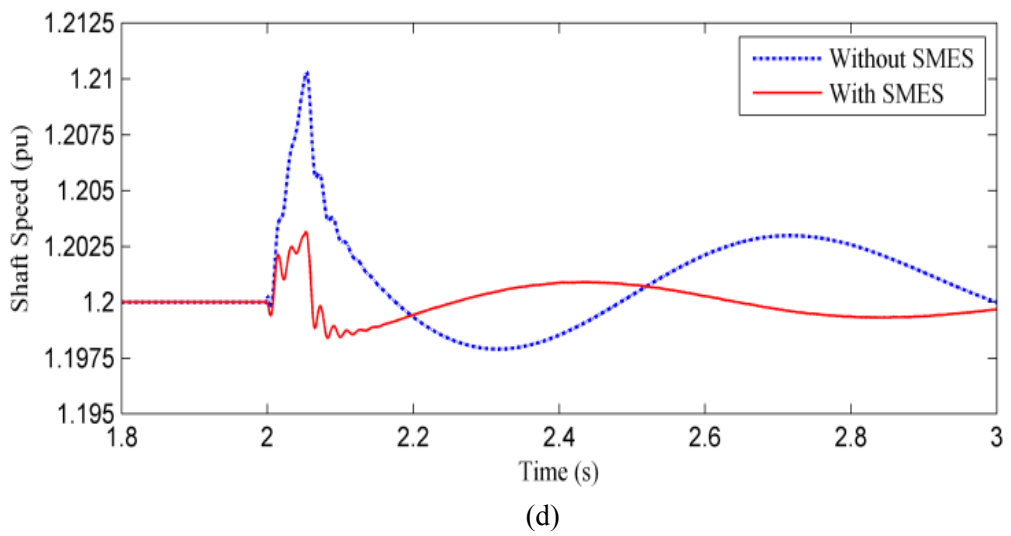
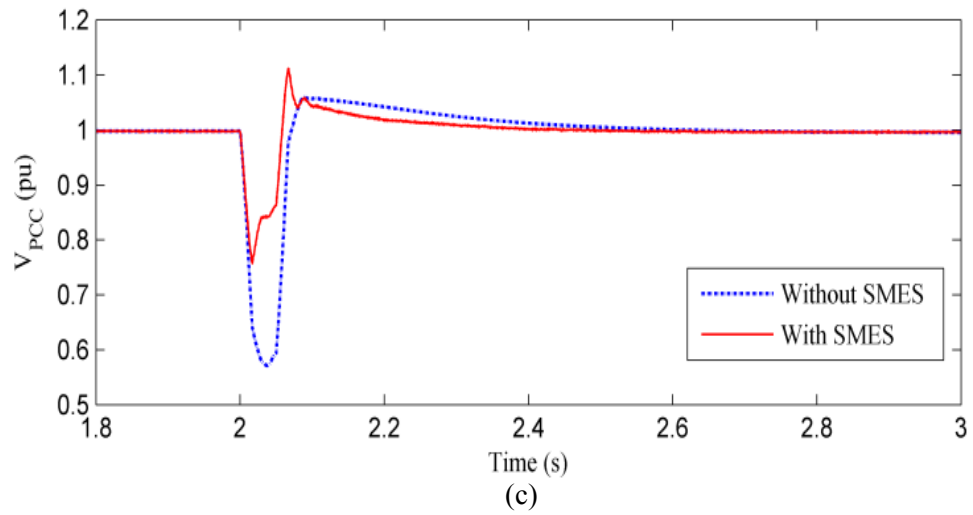


Fig. 6.7. DFIG responses during voltage sag without/with a SMES unit; (c) PCC voltage, (d) Shaft speed, and (e) Voltage at DC link of DFIG

6.3.3. Voltage Swell

A swell is defined as an increase in *r-m-s* voltage or current at the power frequency for durations from 0.5 cycles to 1.0 minute. Typical magnitudes are between 1.1 and 1.8 pu. As with dips, swells are usually associated with system fault conditions, but they are much less common than voltage dips. A swell can occur due to a single line-to-ground fault on the system resulting in a temporary voltage rise on the un-faulted phases. Swells can also be caused by switching off a large load or switching on a large capacitor bank [71, 72].

In this simulation, a voltage swell is applied by increasing the voltage level at the grid side to 1.5 pu. The voltage swell is assumed to start at $t=2.0$ s and lasts for 0.05 s. In this event, DFIG generated power will increase upon the swell occurrence and will be reduced when it is cleared as shown in Fig. 6.8 (a).

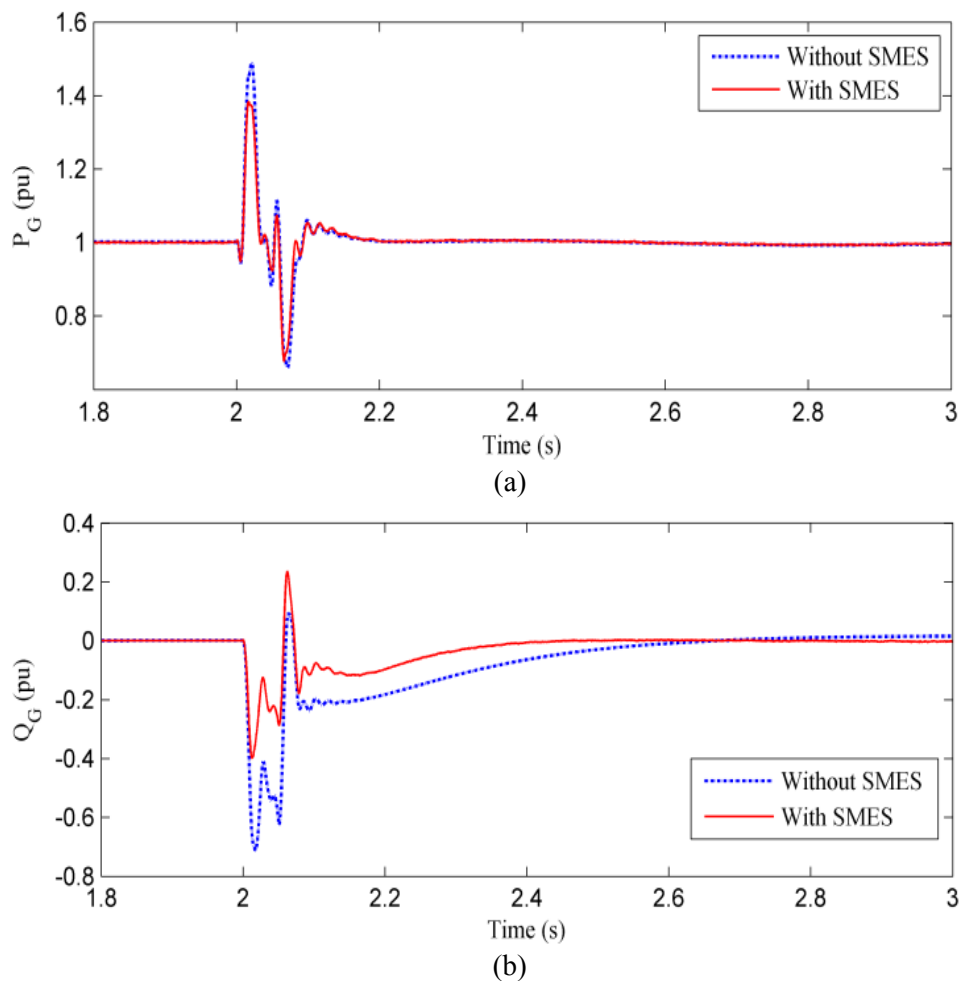


Fig. 6.8. DFIG responses during voltage swell without/with a SMES unit; (a) Active power and (b) Reactive power (continued on next page)

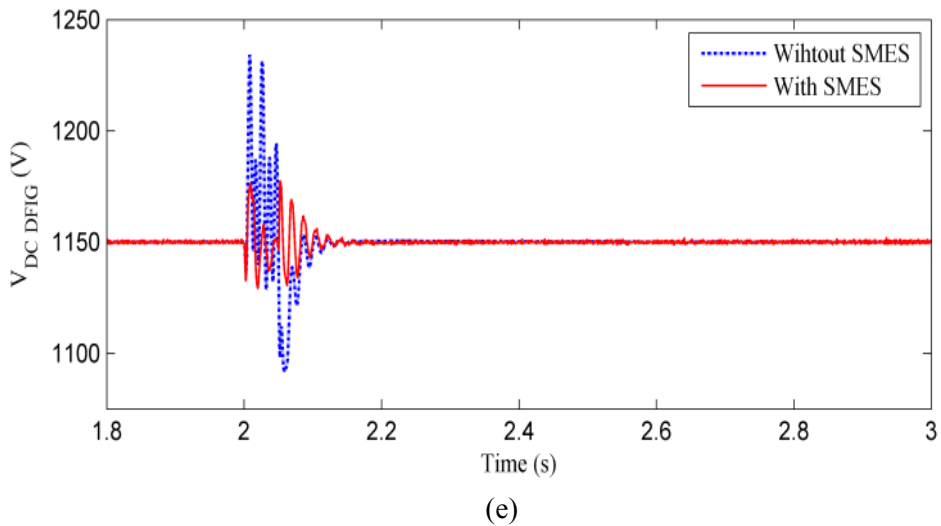
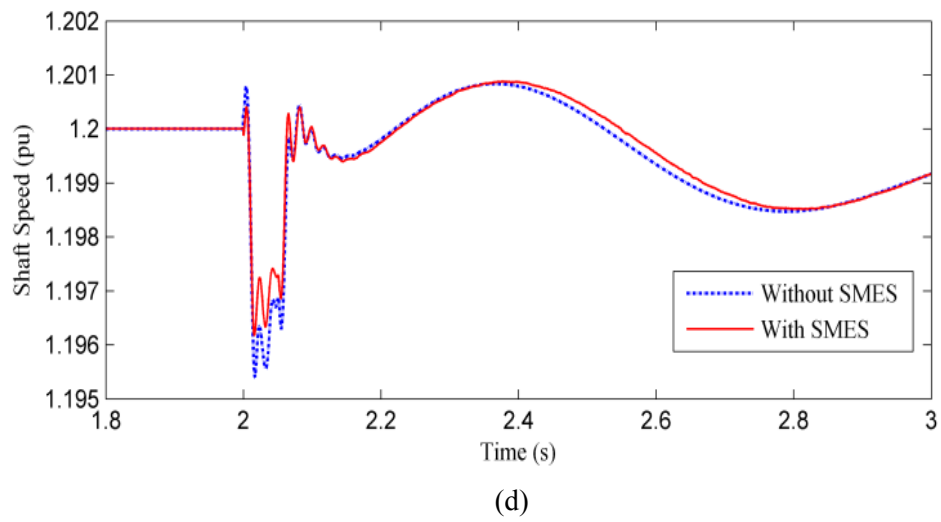
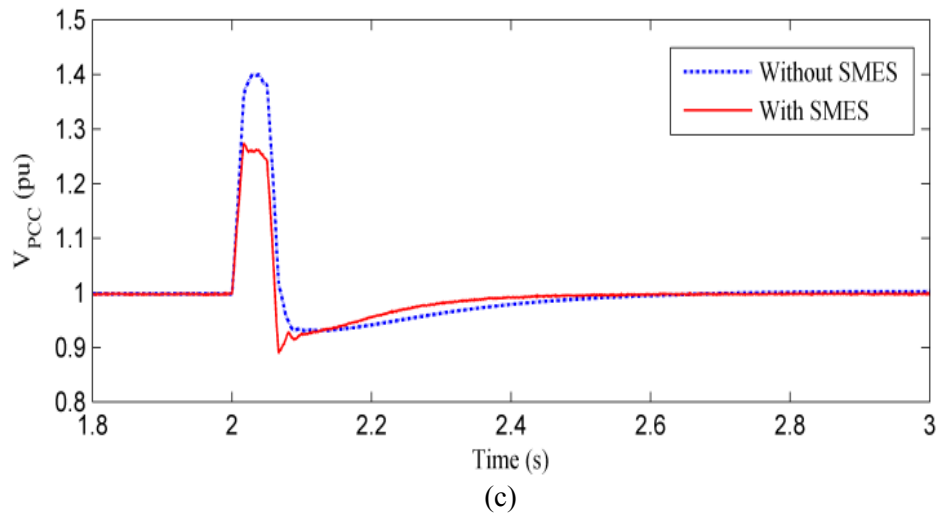


Fig. 6.8. DFIG responses during voltage swell without/with a SMES unit; (c) PCC voltage (d) Shaft speed, and (e) Voltage at DC link of DFIG

The maximum power overshoot is slightly reduced with the SMES unit connected to the system. To compensate for the voltage rise, DFIG will absorb the surplus reactive power as shown in Fig. 6.8(b). The amount of reactive power absorbed by the DFIG is lesser with SMES connected to the PCC since the voltage profile at the PCC is rectified to a level below 1.3 pu with the connection of the SMES unit while this voltage will remain above 1.3 pu without SMES connected to the PCC (Fig 6.8(c)). Without the connection of the SMES unit, the voltage at the PCC does not comply with the HVRT of Spain and Australia grid codes [53, 74] which will lead to the disconnection of the DFIG from the system. The shaft speed (shown in Fig. 6.8(d)) is slightly improved with the connection of SMES unit to the system. Without the connection of the SMES unit, the voltage across the DFIG DC link capacitor will experience significant oscillations and overshooting level upon voltage swell incidence as can be shown in Fig. 6.8(e). In some occasions, this may lead to the blocking of the converters [73]. As shown in Fig. 6.8(e), voltage oscillations as well as voltage overshooting level are significantly reduced by connecting SMES unit to the system.

6.3.4. SMES Responses During Voltage Sag and Swell

The current I_{SMES} passing through the superconducting inductor is unidirectional; however, the voltage V_{SMES} across the inductor terminals can be varied in a wide range between positive and negative values through the control of the duty cycle of the DC-DC chopper (D), thus reversibility as well as magnitude control of power flow is achieved continuously and smoothly through the control of the duty cycle. There are three operation modes of SMES unit:

- (i) **Standby mode** when D is equal to 0.5, the voltage across the SMES coil is equal to zero and the SMES coil current is held constant at its rated value (2.0 kA for the SMES unit under study), consequently, there will be no energy transferred between SMES unit and the AC system and maximum energy (1.0 MJ for the SMES unit under study) is stored within the superconductor coil. The voltage across the DC link capacitor of the SMES configuration ($V_{DC,SMES}$) is maintained at constant level of 10 kV during this mode of operation. This mode will take place during normal operating condition of the WECS and is shown in Fig. 6.9 prior and after the occurrence of the fault.

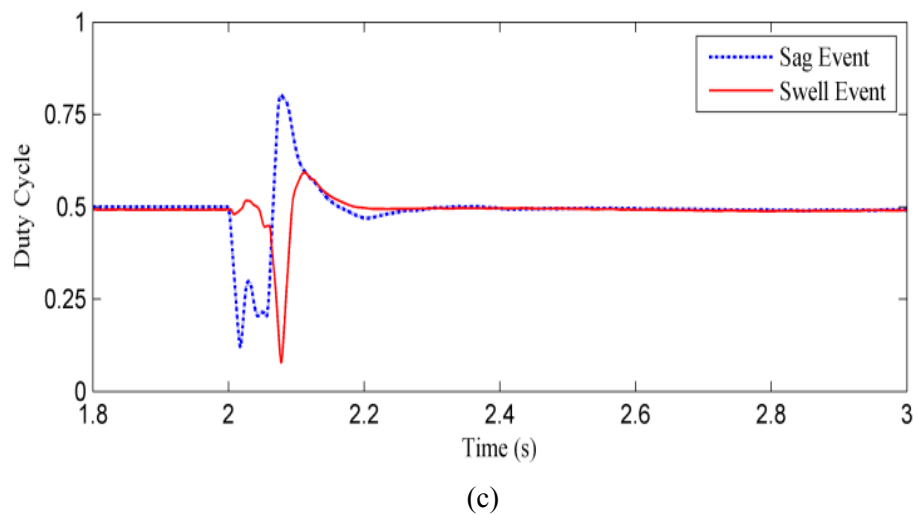
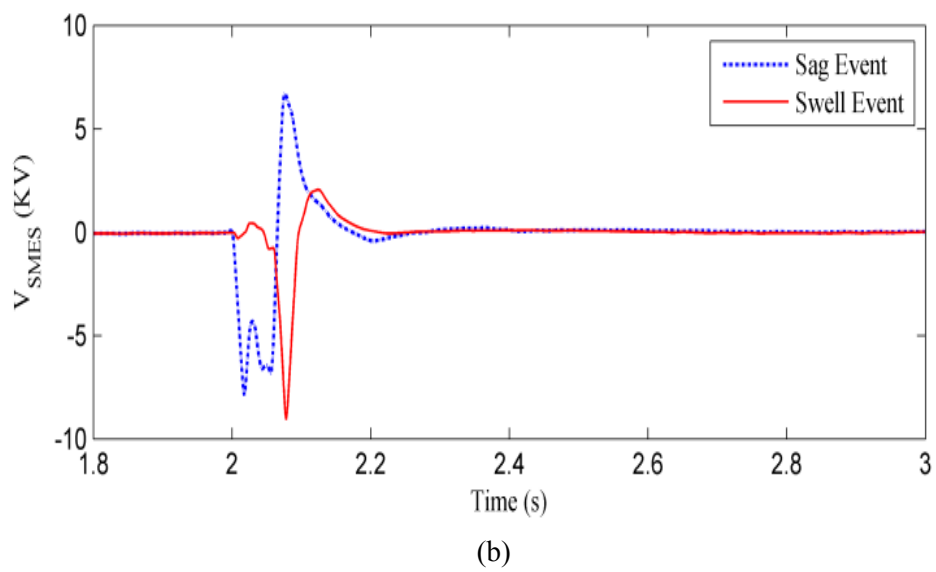
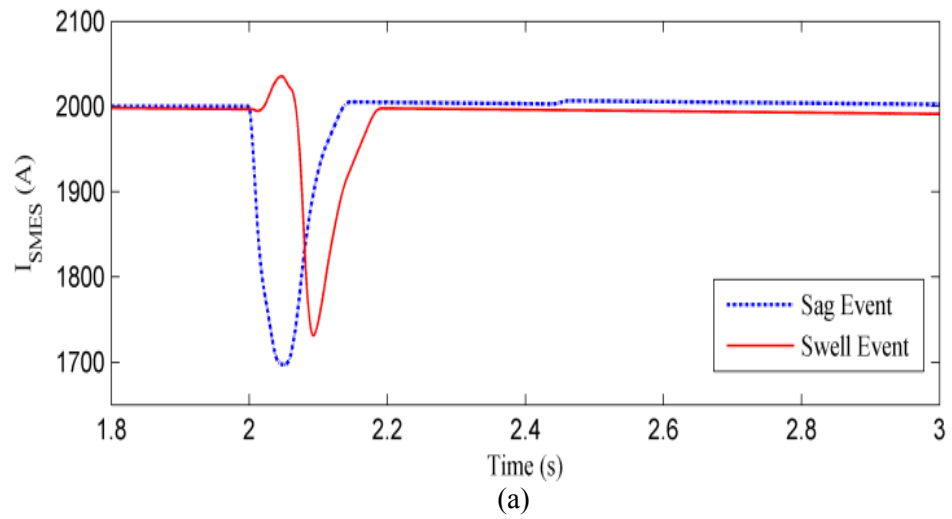


Fig. 6.9. SMES transient responses during voltage sag and swell including; (a) Current (b) Voltage, and (c) Duty cycle (continued on next page)

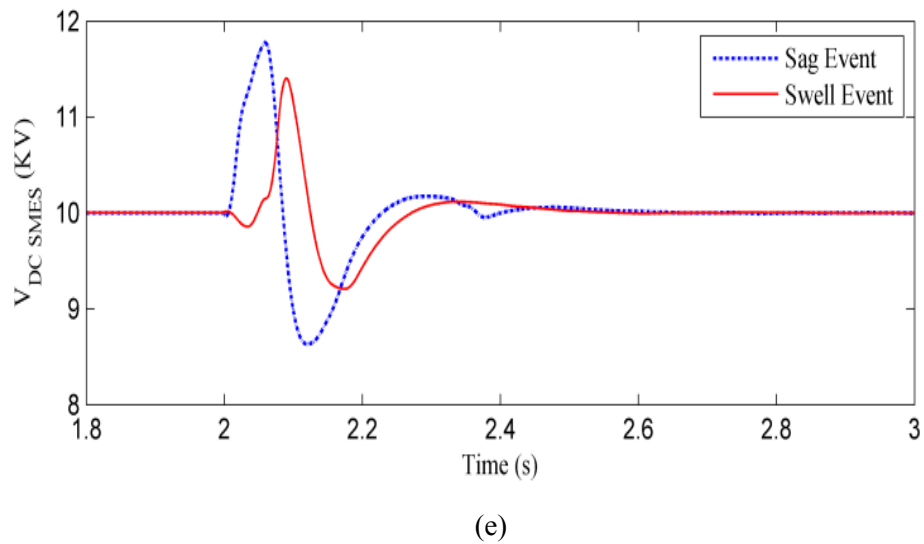
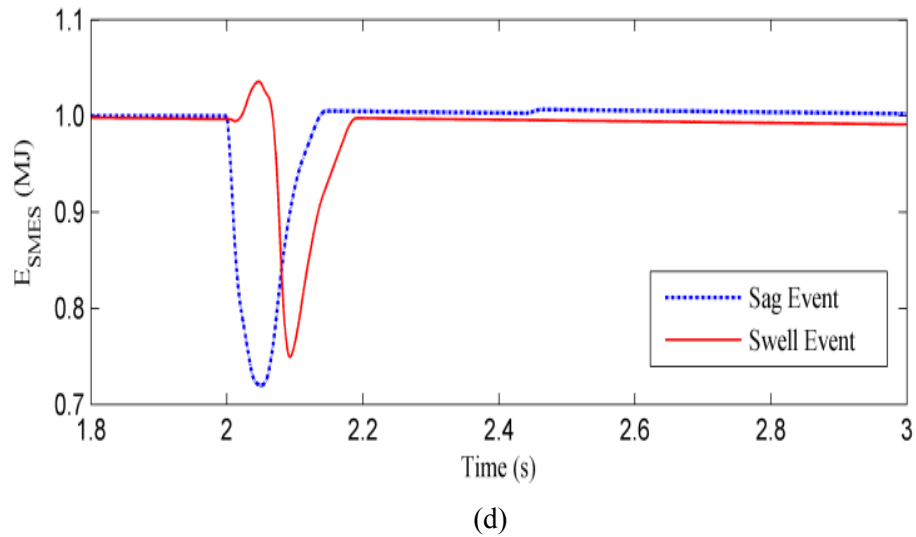


Fig. 6.9. SMES transient responses during voltage sag and swell including; (d) Stored energy and (e) Voltage at DC link of SMES

- (ii) ***Discharging mode*** will take place when voltage sag disturbance occurs at the grid side. In this case, the value of D lies in the range of 0 to 0.5. When voltage sag occurs at $t = 2.0\text{s}$, the SMES coil current decreases giving a negative slope (di/dt) and consequently the voltage across the coil is turning negative. The magnitude of the voltage across the SMES coil is controlled by the level of the duty cycle as well as the voltage across the SMES DC link capacitor as given in (5.21) in Chapter 5. The energy stored in the coil is being delivered to the AC system during this mode and the coil will be recharged at $t = 2.05\text{ s}$, exactly at the time when the fault is cleared according to the rules of the designated FLC for P_G and I_{SMES} . During discharging mode, the rate of coil current change

is decided by the level of the duty cycle. It is observed that the SMES voltage V_{SMES} responds rapidly and the transfer of SMES energy is done immediately upon the occurrence of voltage sag at $t= 2.0s$. This mode of operation is shown by the dashed plots in Fig. 6.9 during the period $t= 2 s$ to $t= 2.2 s$.

- (iii) **Charging mode** will take place when voltage swell disturbance occurs at the grid side. In this case the value of D lies in the range of 0.5 to 1.0. When voltage swell occurs at $t=2.0s$, the SMES coil current increases giving a positive slope (di/dt) and consequently the voltage across the coil is turning positive. The energy is transferred from the system to the SMES coil till the maximum coil energy capacity designated by the fuzzy rules is reached (1.03 MJ in the system under study to allow for power modulation during voltage swell disturbance) after which the voltage across the SMES coil decreases and returns back to zero level when the maximum current in the SMES coil is reached. This mode of operation is shown by the solid plots in Fig. 6.9 during the period $t= 2.0s$ to $t= 2.2s$.

The following general observations can be concluded:

- It can be observed that the SMES coil current in both voltage sag and voltage swell events has a similar trend to the coil stored energy and their levels at any time are mathematically correlated by the relation given in (4.5) in Chapter 4.
- In both voltage sag and voltage swell events, voltage across the SMES coil will be maintained at zero level once the maximum current in the SMES coil is reached. Once a system with SMES unit has regained post fault stability, the SMES coil is not preferred to be kept on continuously to avoid the draining process of SMES energy during normal operating conditions. Furthermore, turning it off can reduce the generator shaft speed oscillations to some extent. It also reduces the operating expenses of the SMES unit. This is achieved by short circuiting the SMES coil through a bypass switch shown in Fig. 5.13(a) in Chapter 5.
- In both voltage sag and voltage swell events, it is observed that the voltage across the DC link capacitor of the SMES configuration ($V_{DC,SMES}$) oscillates in opposite manner to V_{SMES} and its level at any time is related to the level of

V_{SMES} . The level of V_{SMES} at any time is correlated to the level of $V_{DC,SMES}$ and the duty cycle value by the relation given in (5.21) in Chapter 5.

- The maximum voltage overshoot in $V_{DC,SMES}$ shown in Fig. 6.9(d) is still remaining within a safety margin of 1.25 pu of the nominal value [73] which is corresponding to 12 kV in the studied case. It is also noted that the voltage across the SMES coil and the duty cycle have the same trend during disturbance event. This aligns well with the results presented in [20].

6.3.5. SMES Capacity

The capacity of SMES unit depends on its application and charging/discharging duration. Very high energy rating has excellent impact on damping oscillations rapidly but the cost of the unit will be too high due to large current in the coil. Meanwhile, if the energy rating is too low, the output of the SMES unit will be limited during disturbances and it will not be very effective in controlling system oscillations quickly. The first SMES unit rated 30 MJ with a rated coil current of 5 kA was installed in Bonneville power administration, Tacoma in 1982 [75]. A SMES coil energy E_{SMES} of a value less than 0.15 pu of the generator rated power will be adequate in safeguarding against momentary power interruption [27, 41]. In the system under study, the DFIG rated power is 9 MW and the rated energy of the SMES coil is designed to be 1.0 MJ. As the SMES coil inductance is chosen to be 0.5 H, the inductor nominal current is 2.0 kA. To make the SMES coil effective in voltage swell events, the rated inductor current is set at a level higher than the nominal coil current [76]. In the system under study, the rated coil current was chosen to be 2.03 kA. This will allow the SMES coil to absorb maximum energy up to 1.03 MJ during voltage swell event.

6.3.6. Voltage Sag Compliance with FRT of Spain

In this study, voltage sag is applied at the grid side of the system under study shown in Fig. 6.2. In such way causing voltage drop at the PCC about 0.65 pu. The fault is assumed to start at 0.5 s and cleared at 0.58 s. Fig. 6.10 shows the $r-m-s$ voltage at the PCC bus without and with the connection of the SMES unit. As shown in Fig. 6.10, without SMES unit connected to the PCC bus, DFIG should be disconnected from

the system as the voltage at the PCC across the lowest voltage level requirement of the LVRT of Spain grid code. However with SMES unit connected to the PCC bus, the voltage profile at the PCC bus is improved and the voltage sag for DFIG is reduced to a level within the safe margin of the LVRT of Spain grid code as can be seen in Fig. 6.10 (approximately drop only 0.2 pu). Therefore DFIG connection can be maintained during fault when the SMES unit is connected to the system.

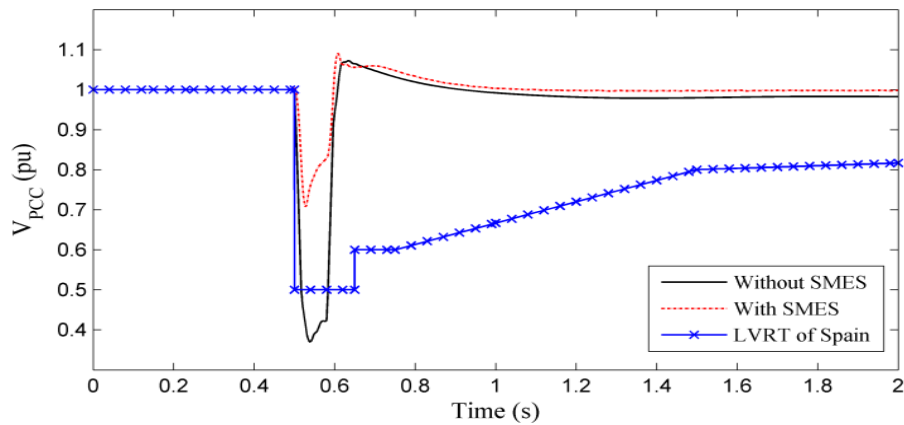
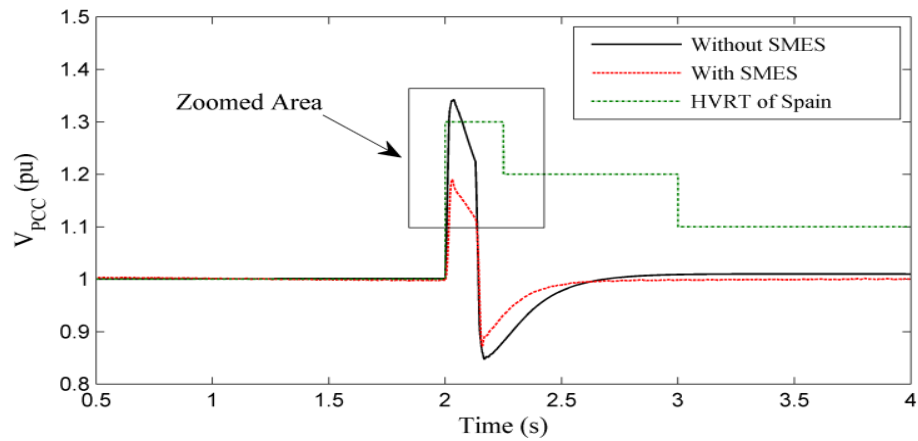


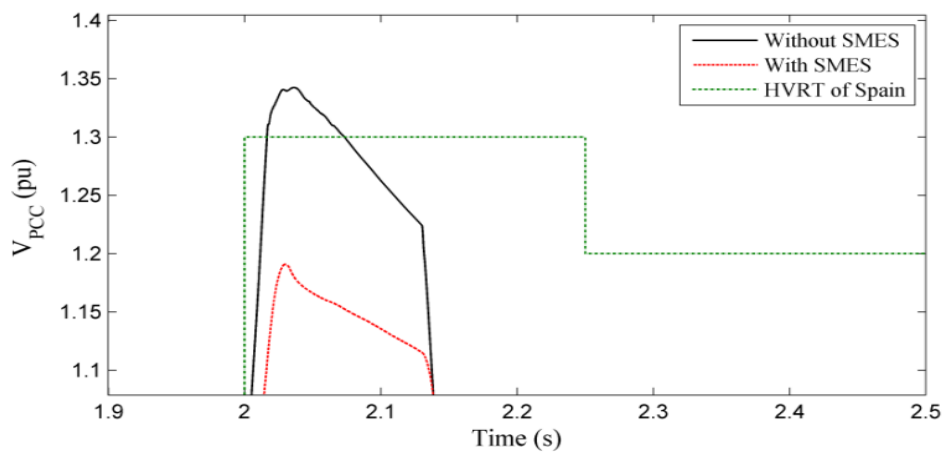
Fig. 6.10. Voltage profile at PCC where the DFIG based WECS is connected

6.3.7. Voltage Swell Compliance with FRT of Spain

Voltage swell of 1.4 pu is applied at the grid side and is assumed to start at 2.0s and cleared out at 2.13s. As can be seen from Fig. 6.11(a) and the zoomed area shown in Fig. 6.11(b), without SMES, voltage at the PCC bus will increase to 1.35 pu. By applying the HVRT of Spain grid code, the WECS equipped with DFIG have to be disconnected from the grid in this case. However, when SMES unit is connected to the PCC, the high voltage level at the PCC will be reduced below the maximum voltage level of HVRT of Spain grid code. Therefore, disconnection can be avoided by connecting SMES to the PCC bus. When the fault is cleared at 2.13 s, the voltage at the PCC will be reduced to 0.85 pu when the SMES unit is not connected to the system, however, while with the SMES unit, this level is increased to 0.9 pu as can be seen in Fig. 6.11(a).



(a)



(b)

Fig. 6.11. Voltage response at PCC during swell event; (a) Voltage response at the PCC and (b) Zoomed area of voltage response at the PCC

6.4. Application of SMES to Improve the Dynamic Performance of DFIG

6.4.1. Small Disturbance

The load frequency control issue occurs as a result of sudden and small load perturbation which creates an instantaneous mismatch between real power supply and demand. This problem can be controlled by the governor action in conventional thermal power plants. The load frequency control problem is attributed to the fact that the inertia of the rotating parts is the only storage capacity in a conventional power system where the additional power demand can be met through the kinetic energy of the generator rotor. This will limit the degree to which frequency variation can be minimized by appropriate governor control. The problem is more serious in case of WECS based on DFIG in which the inertia is much lower than their power

rating. Solving this problem by attaching a flywheel to the rotor shaft to increase its inertia will significantly increase the torsional stress on the shaft during dynamic oscillation. Since the wind turbine generated power depends on wind speed which cannot be controlled, the wind turbine can only be down-regulated to match the reduce power demand by applying additional controllers [77]. However, when loads are increased above the rated power output of the generated power, in particular when wind speed is low, the power imbalance will take place causing the load frequency control problem. The case of such situation had occurred for example, on the European outage on November, 2006, caused the tripping of 4892 MW of wind-origin power in Western Europe exacerbating the imbalance between demand and supply in this area [78]. Adding a SMES unit which has a very fast time response to the load bus can improve the system overall performance during such conditions [34].

The system under study is slightly modified from the previous study as shown in Fig. 6.12. For study of the dynamic system, a local load is added at the PCC. Fig. 6.13 shows the load profile used in the simulation studies. It is assumed that the nominal load power is constant under normal operating condition and is fed through the power generated from the wind turbine. The load is assumed to experience a ± 0.2 pu fluctuation for a duration of 0.5s at $t= 3.0$ s and $t= 4.0$ s respectively.

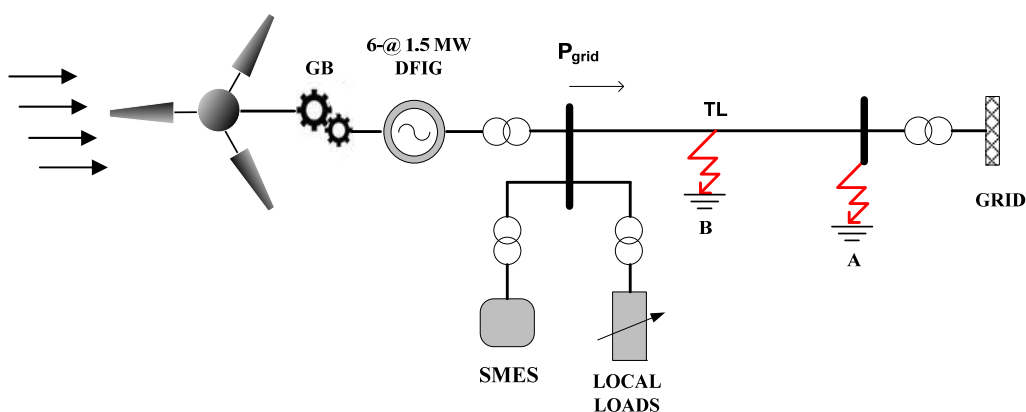


Fig. 6.12. System under study [79]

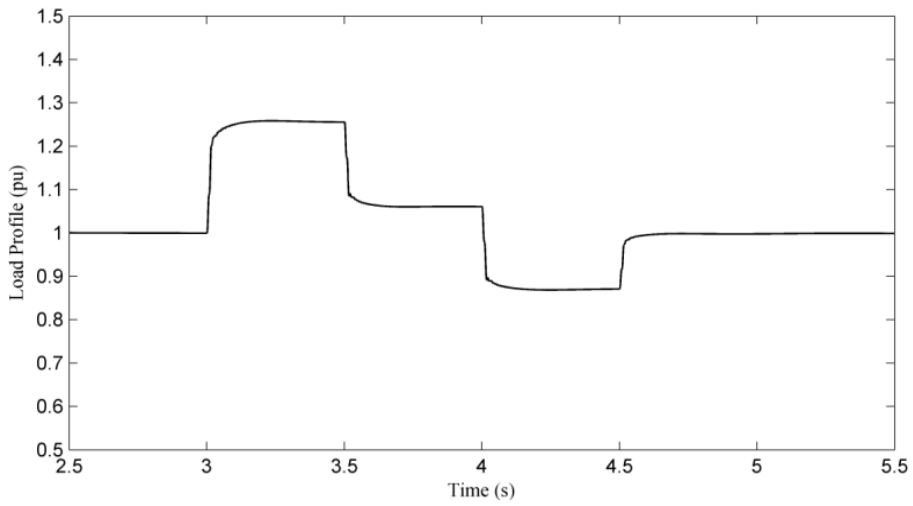
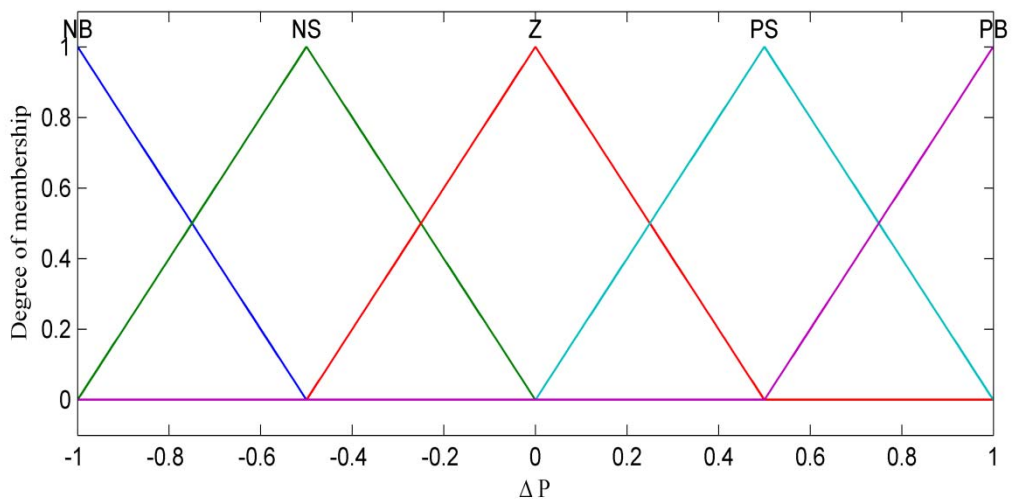


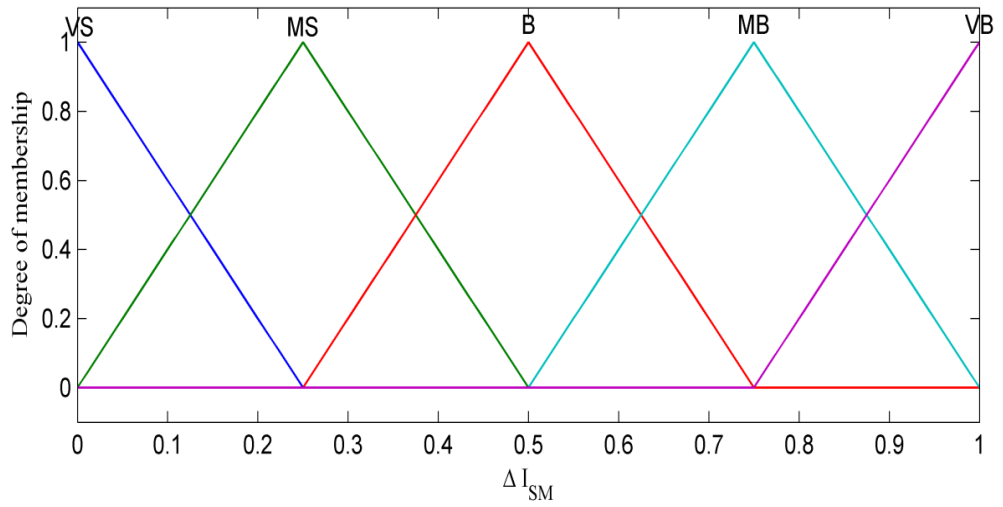
Fig. 6.13. Load profile under study

In this short load variation study, the control rules of the fuzzy set are modified as provided in Figs. 6.14 to 6.16, to gain better results of the study.



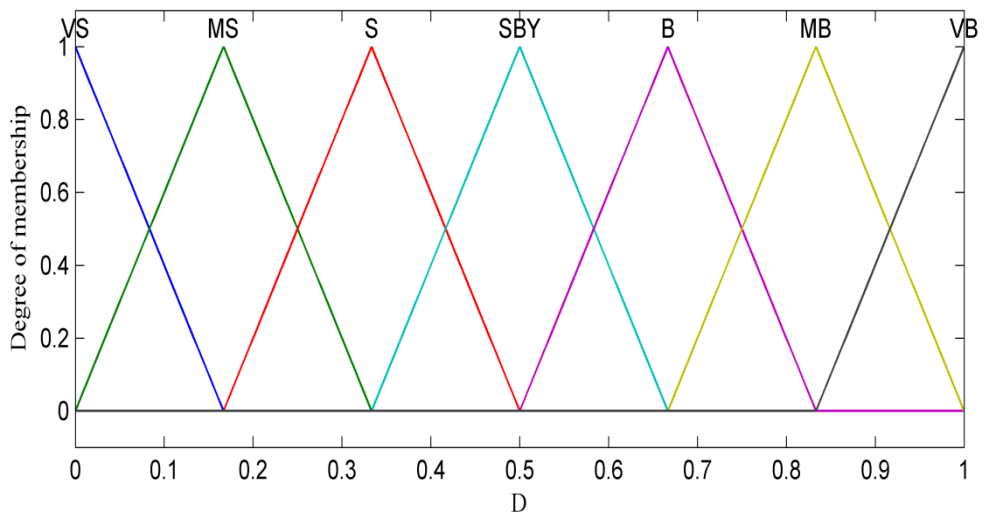
NB=Negative Big, NS=Negative Small, Z=Zero, PS=Positive Small, PB=Positive Big

Fig. 6.14. Memberships function for the input variable P_G (pu)



VS=Very Small, MS=Medium Small, B=Big, MB=Medium Big, VB=Very Big

Fig. 6.15. Memberships function for the input variable I_{SMES} (pu)



VS=Very Small, MS=Medium Small, S=Small, SBY=Stand-By, B=Big, MB=Medium Big, VB=Very Big

Fig. 6.16. Memberships function for the output variable D (duty cycle)

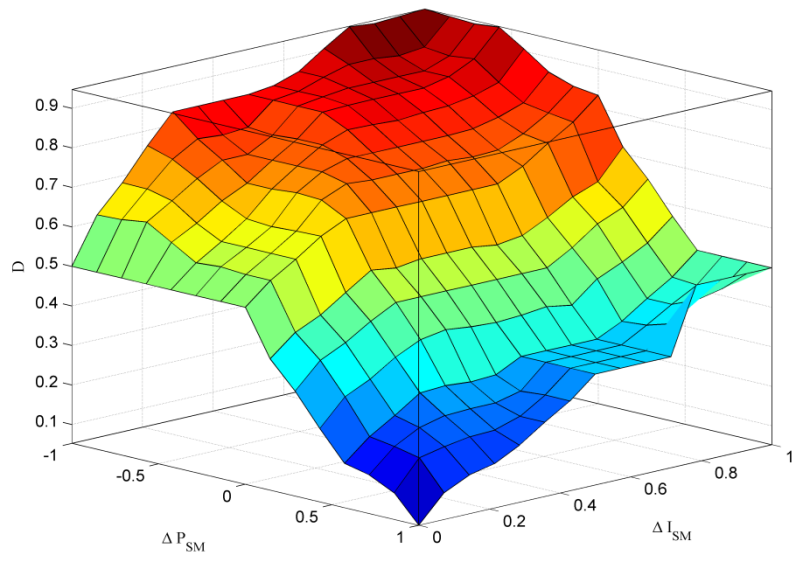
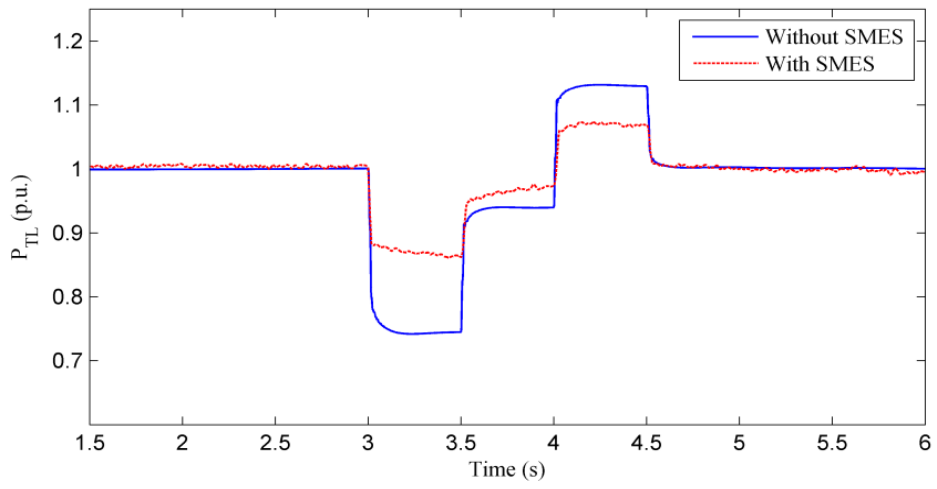
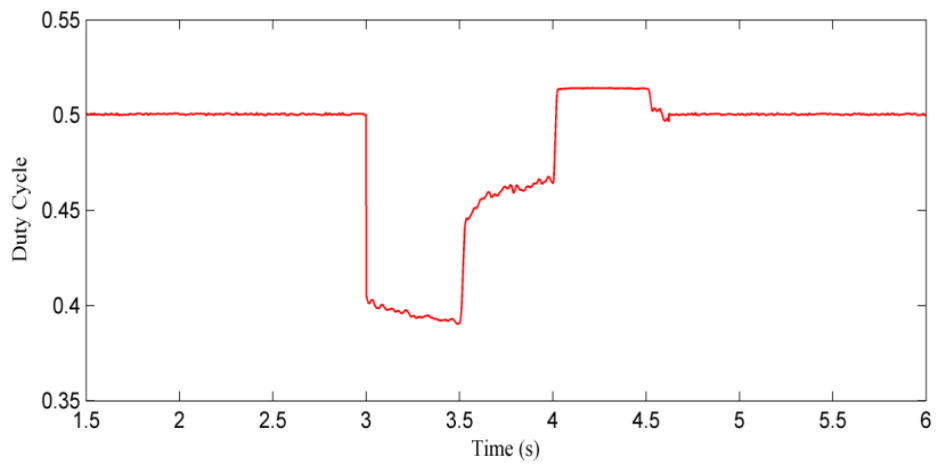


Fig. 6.17. Surface graph-duty cycle

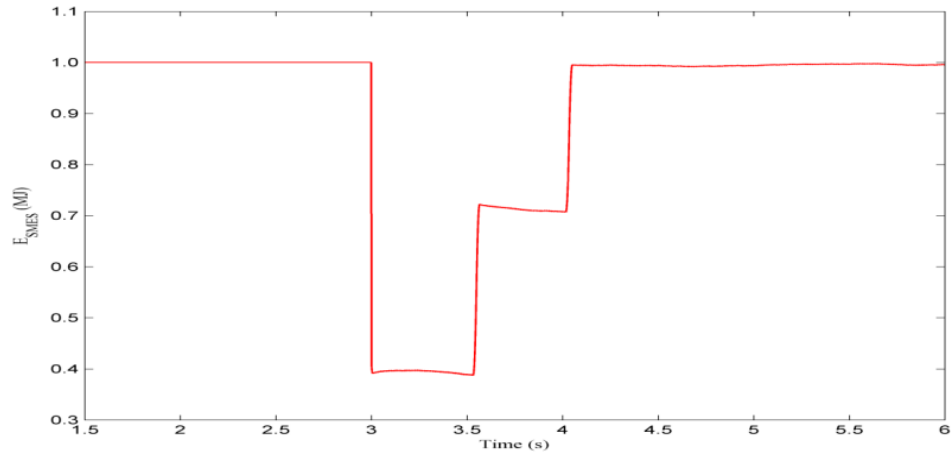


(a)



(b)

Fig. 6.18. (a) Power transfer to the grid and (b) Duty cycle response during dynamic event (continued on next page)



(c)

Fig. 6.18. (c) Stored energy of SMES during dynamic event

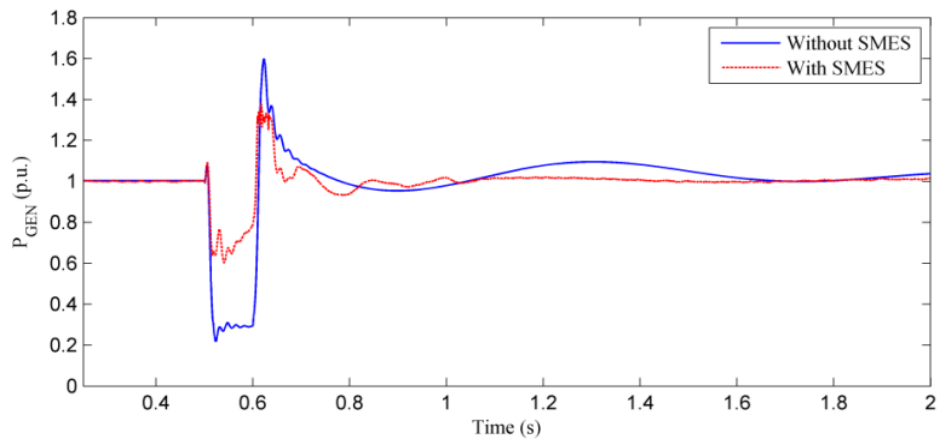
Fig. 6.18(a) shows the power transferred to the grid through the transmission line. When load power demand increases at $t= 3.0$ pu, the power transfer through the transmission line is decreasing by 30% and it increases by only 10% due to transmission power transfer capability when the load is decreased at $t= 4.0$ s. By connecting the SMES unit to the DFIG bus, the two levels can be substantially decreased to only 10% and 5% respectively. The DC-DC chopper duty cycle D is shown in Fig. 6.18(b) where at normal operating conditions, the value of D is maintained by the FLC at a level of 0.5 and the SMES coil current is held constant at its rated value, consequently, there will be no energy transferred between SMES unit and the grid as can be shown from the coil stored energy in Fig. 6.18(c) when the load increases suddenly at $t= 3.0$ s, the controller will act to decrease the value of D below 0.5 level and energy stored in the coil will be discharged to the grid to provide active power support. When the load returns to its steady state level, the coil will be partially charged but not to its full capacity. When the load is decreased at $t= 4.0$ s, the value of D will be increased due to the controller action to a level above 0.5 and the surplus power in the system will be used to fully charge the SMES coil.

6.4.2. Large Disturbance

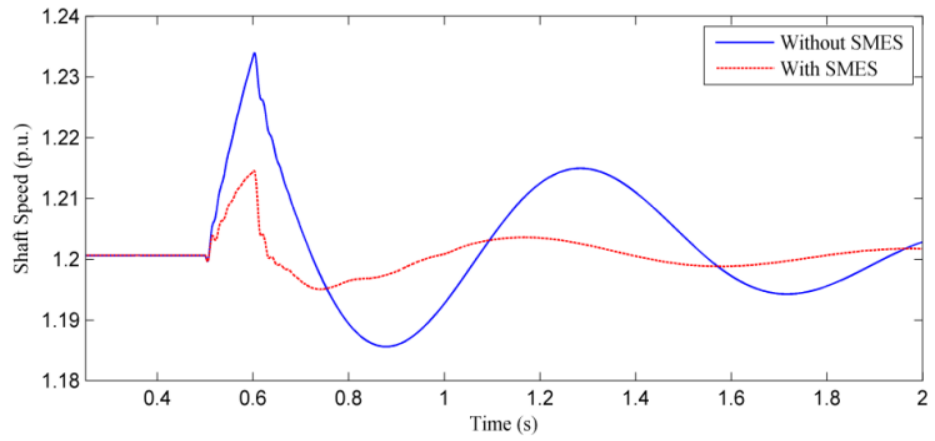
To examine the ability of the SMES unit to improve the DFIG dynamic performance during a large disturbance, a six-cycle three-phase short circuit fault is applied at $t= 0.5$ s and is assumed to last for 6 cycles. Two fault locations are

considered; case A where the short circuit fault is assumed to take place at the grid terminals (point A in Fig. 6.12) and case B where the fault is located at the middle of the transmission line (point B in Fig. 6.12).

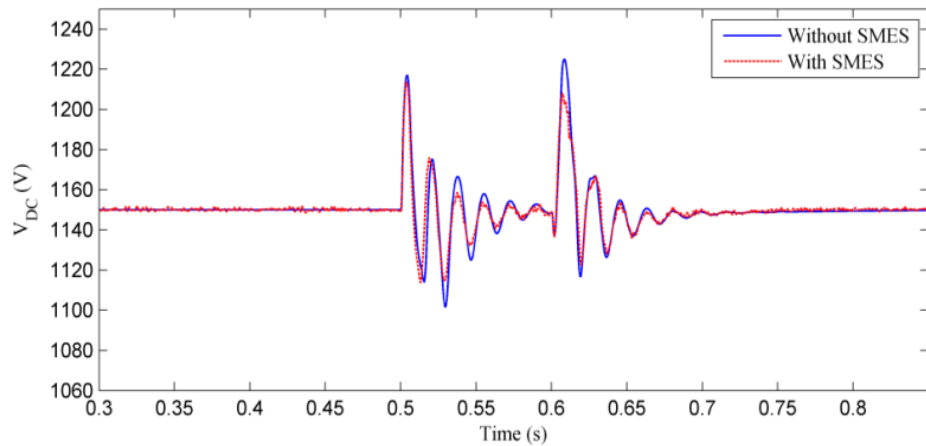
Case A: Fig. 6.19(a) shows that the active power generated by the DFIG is reduced by 75% at the instant of fault occurrence and it experiences a maximum overshooting of 60% at the instant of fault clearance. As a result of generated power reduction, the shaft speed accelerates during the fault and experiences some oscillations after fault clearance as shown in Fig. 6.19(b). The large amount of power loss will definitely influence the supply for local loads and the power transfer to the grid. If the DFIG is the main power supply to the local load, the economic loss will be significant. The voltage across the DFIG DC-link capacitor (shown in Fig. 6.19(c)) will experience significant oscillations and overshooting level through fault duration; however, its maximum overshooting remains within the safety margin of 1.2 p.u. as specified in [73]. The voltage at the point of common coupling (PCC) is reduced to a level of 0.4 p.u. during the fault. When compared to the Spain fault ride through (FRT) requirement, the voltage profile at the PCC violates the permissible lower limit as shown in Fig. 6.19(c) which calls for the disconnection of WECS from the grid. When the short circuit is cleared, the DFIG converters act to provide reactive power support to the grid to recover the voltage to its rated value [80]. By connecting the SMES unit to the DFIG bus, the proposed controller acts to change the duty cycle level and hence the energy transfer direction according to the system requirements. As shown in Fig. 6.19(e), the duty cycle is reduced below 0.5 during the fault and the entire SMES stored energy will be discharged to support the system during the fault as shown in Fig. 6.19(f). As a result, the DFIG generated power will be reduced by only 30% and its maximum overshooting and settling time are substantially reduced as shown in Fig. 6.19(a). As a result of this improvement, the acceleration and settling time of the rotor shaft speed will be significantly reduced as can be seen in Fig. 6.19(b). There is a slight improvement in the DFIG DC-link voltage (Fig. 6.18 (c)) in terms of the over shooting levels but as mentioned above, these levels are within the safety margins specified in [73]. Connecting the SMES unit to the system will bring the voltage at the PCC to the safety margin of Spain grid codes as shown in Fig. 6.19(d). In this case, the WECS connection to the grid can be maintained to support the grid during the fault duration.



(a)

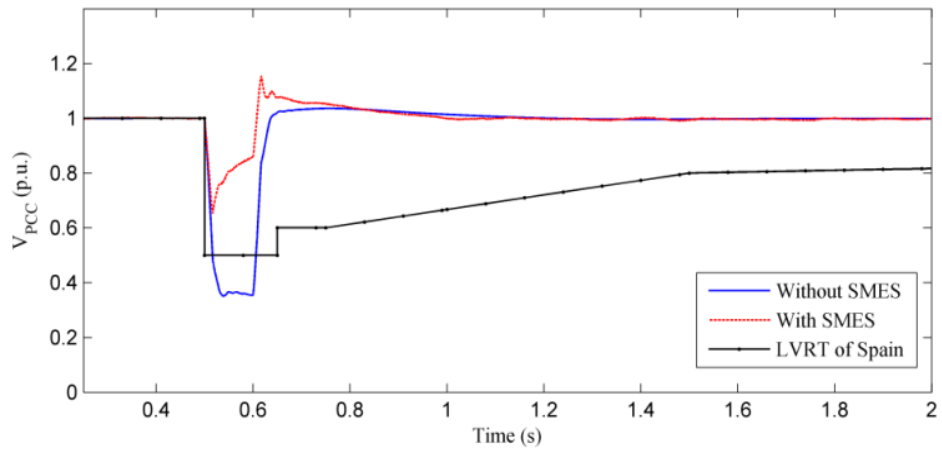


(b)

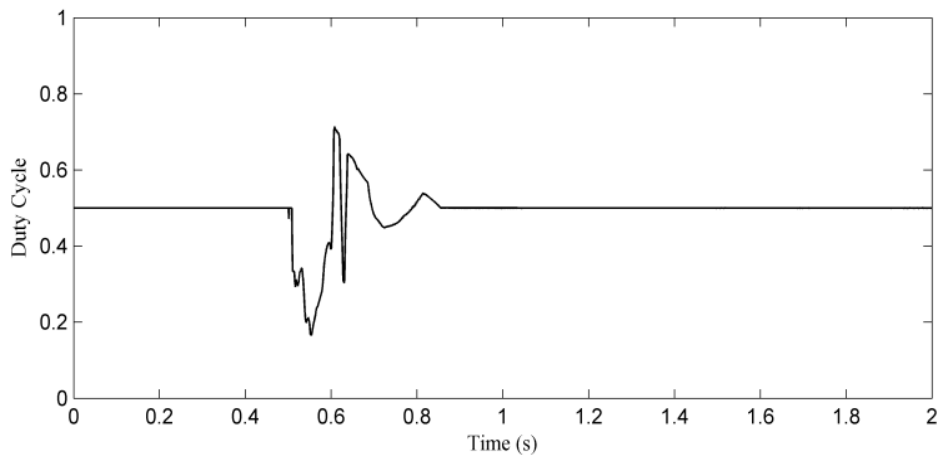


(c)

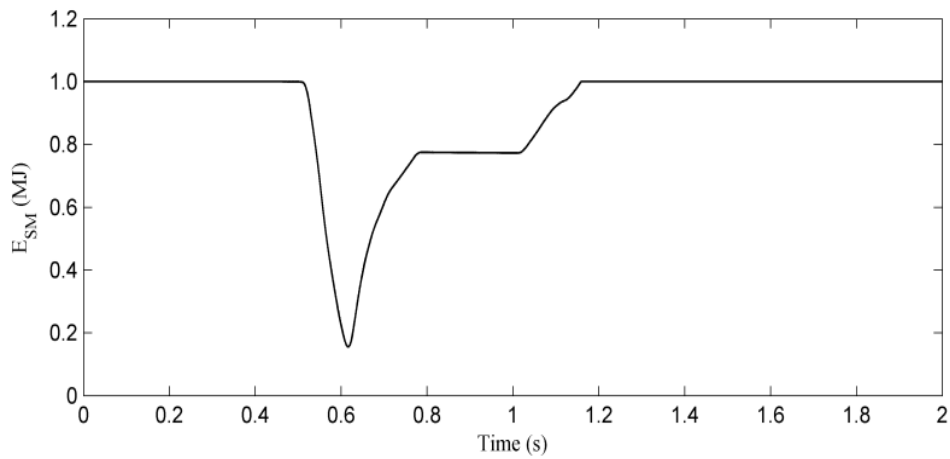
Fig. 6.19. Response of the DFIG during 3-phase short circuit fault at point A; (a) Generated power of DFIG, (b) Rotor shaft speed and (c) Voltage across DFIG DC-link (continued on next page)



(d)



(e)



(f)

Fig. 6.19. Response of the DFIG during 3-phase short circuit fault at point A; (d) Voltage profile at PCC, (e) Duty cycle response of the SMES unit, and (f) Stored energy response of the SMES unit

Case B: When 3-phase short circuit fault occurs at the middle of the transmission line, DFIG generated power drops significantly as shown in Fig. 6.20(a). The impact of this fault on the shaft speed and DC-link capacitor voltage is worse when compared to the previous case as shown in Figs. 6.20(b) and (c), respectively. Voltage level at the PCC reaches 0.1 p.u. and it violates the low voltage ride through level of Spain grid code as shown in Fig. 6.20(d). With the SMES unit connected to the PCC bus; generated power drop can be improved compared to the system without SMES unit as shown in Fig. 6.20(a). Also, shaft speed and DC link voltage shown in Figs 6.20(b) and (c) are improved with the connection of the SMES unit. With the connection of the SMES unit, the connection of the wind turbine to the grid during such fault can be maintained as shown in Fig. 6.20(d), where the voltage drop at the PCC is brought to a safety margin of the Spain's FRT. The trend of duty cycle and energy stored within superconductor coil is similar to case A however; they are slightly larger than those in case A as shown in Figs. 6.20(e) and (f).

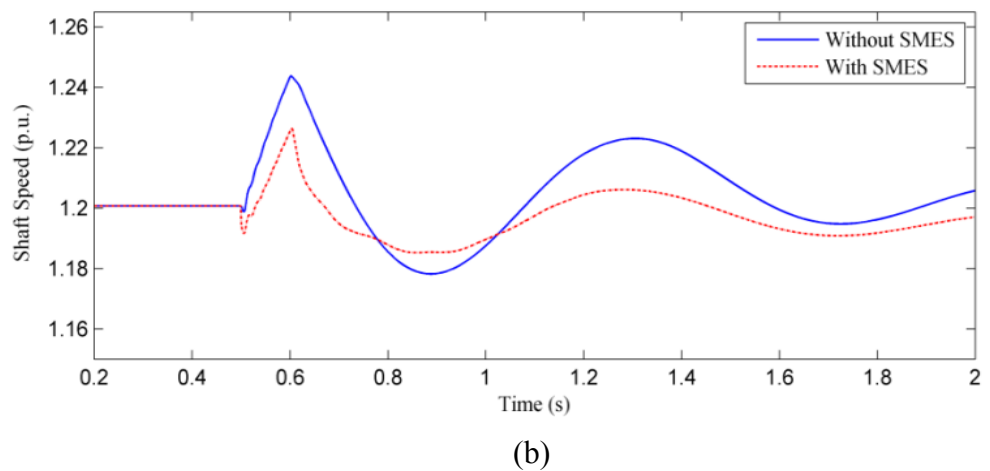
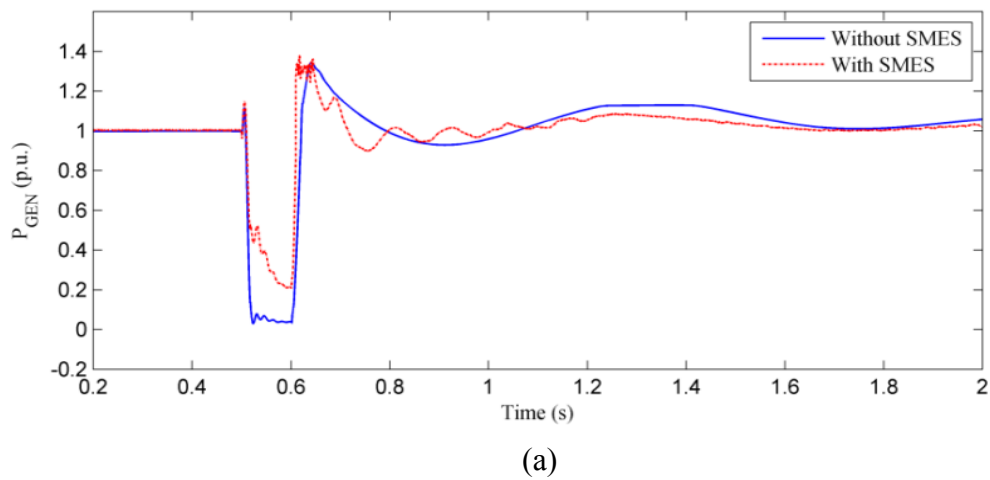
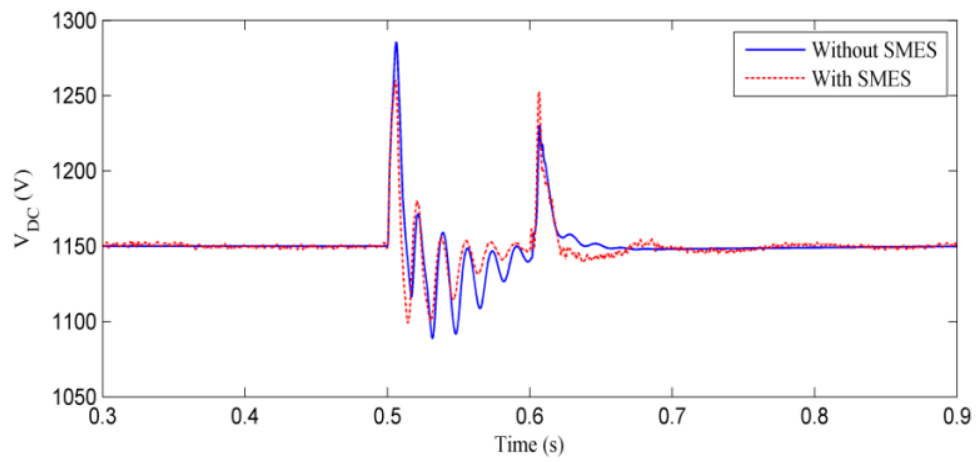
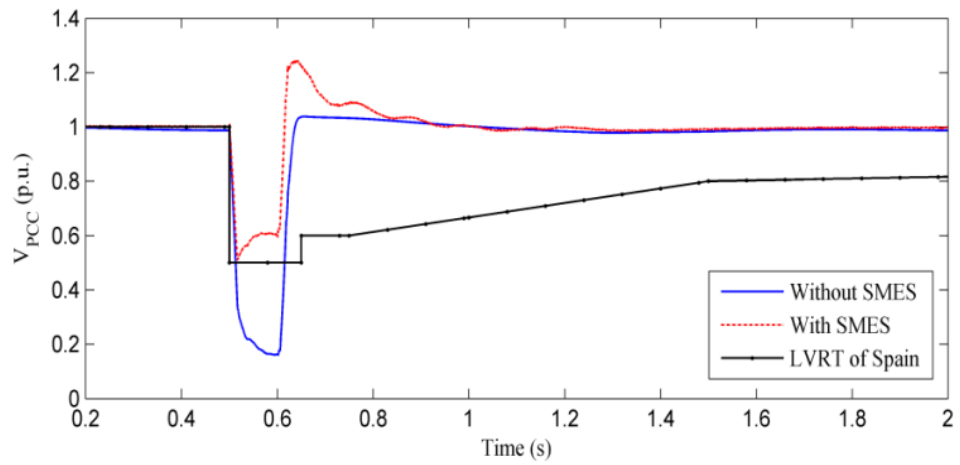


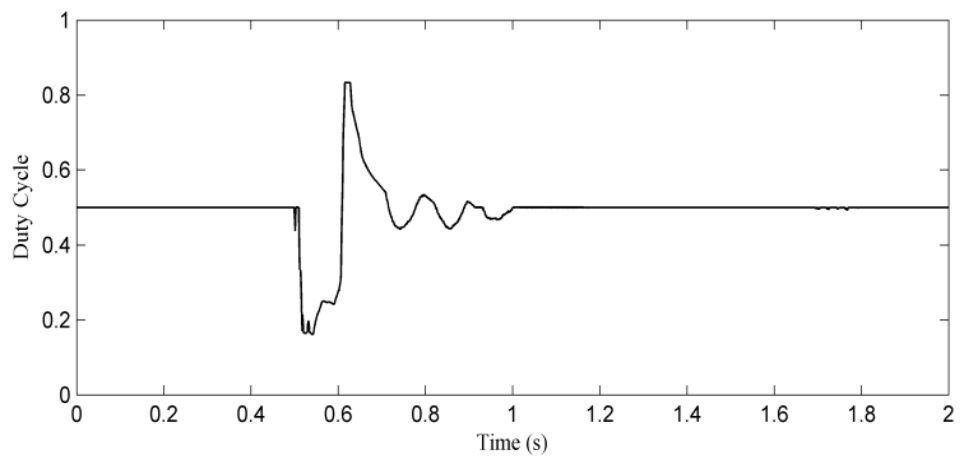
Fig. 6.20. Response of the DFIG during 3-phase short circuit fault at point B; (a) Generated power of DFIG and (b) Rotor shaft speed (continued on next page)



(c)



(d)



(e)

Fig. 6.20. Response of the DFIG during 3-phase short circuit fault at point B; (c) Voltage across DFIG DC-link, (d) Voltage profile at PCC, and (e) Duty cycle response of the SMES unit (continued on next page)

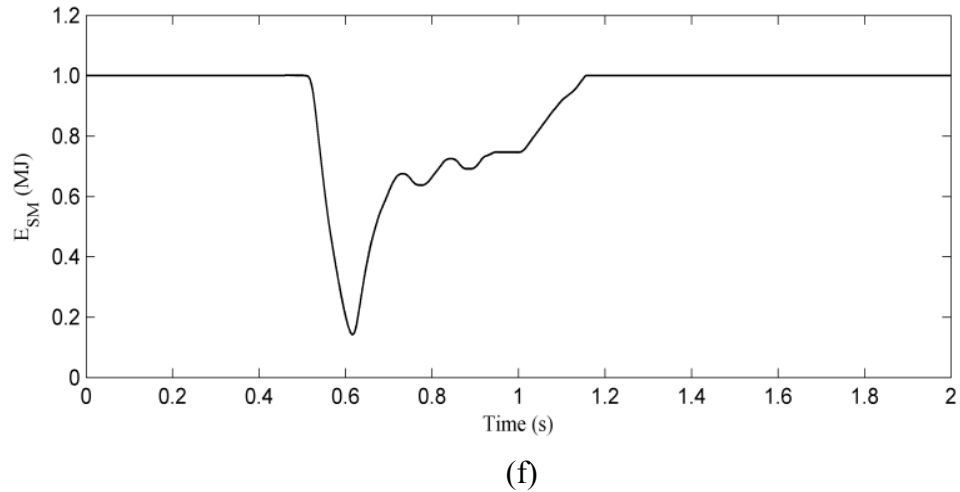


Fig. 6.20. Response of the DFIG during 3-phase short circuit fault at point B;
(f) Stored energy response of the SMES unit

6.5. Impact of SMES on DFIG Power Dispatch During Intermittent Misfire and Fire-Through Faults

6.5.1. Misfire and Fire-Through

The DFIG is interfaced to the AC network through GSC and RSC which are considered as the crux of the wind power system. The converter stations determine the ability of wind turbine to optimally operate during wind speed fluctuation and can provide reactive power support during grid disturbance events. Therefore, any faults within the converter stations will affect the overall performance of the DFIG. Due to the utilization of two converters, it is very vulnerable for the DFIG to have switching malfunctions on its converters such as misfire and fire-through. Misfire is defined as the failure to fire a valve during a scheduled conducting period and fire-through is the failure to block a valve during a scheduled non-conducting period. These faults are caused by various malfunctions in the control and firing equipment [81]. Some of these converter faults are self clearing if the causes that led to these faults are of transient nature. However they can still cause a major problem to system particularly when they occur on inverter station instead of the rectifier station [82]. When gate-misfiring occurs on IGBT based converter, it can cause catastrophic breakdown of the device, if the faults remains undetected [83]. Although switching of renewable energy can lead to power quality issue [72], with proper small step-wise control of the AC transmission line power, this variation frequency can be controlled better as discussed in Ref [84]. However, as mention in [81], the switching malfunctions are

still possible to occur. To clearly understand the system under study, the DFIG along with the SMES is re-configured in Fig. 6.21. The parameters of the DFIG used in this study can be obtained in Appendix B-7. In this thesis, control algorithm concept and all parameters of the SMES unit are the same with the case of grid sag and swell which is available in Chapter 5. Most of literature has been dedicated to DFIG performance during various grid disturbances such as voltage sag [54-56, 59, 60, 85, 86]. Although, there are few studies in the literatures about the effect of converter faults on the overall performance of HVDC system [27, 87, 88] and misfiring detection on PWM inverter [89], there is no attention given to the performance of the DFIG during misfire and fire-through faults. In this study, both misfire and fire-through are applied to the IGBT-1 in the RSC and GSC of Fig. 6.22.

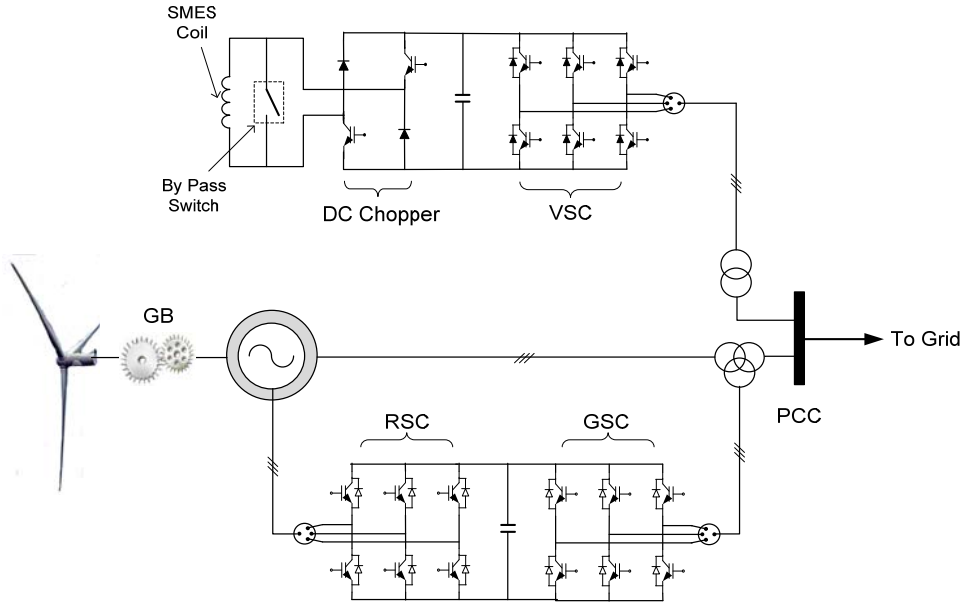


Fig. 6.21. System under study for DFIG-SMES with misfire and fire-through [90]

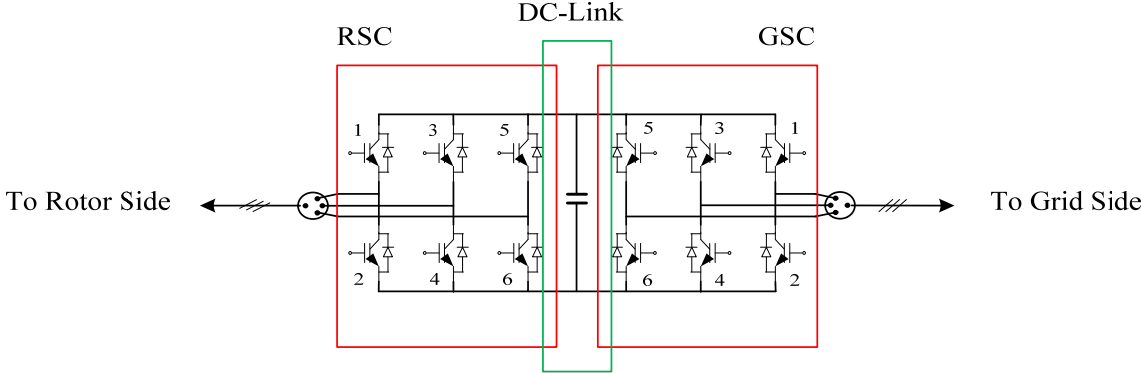
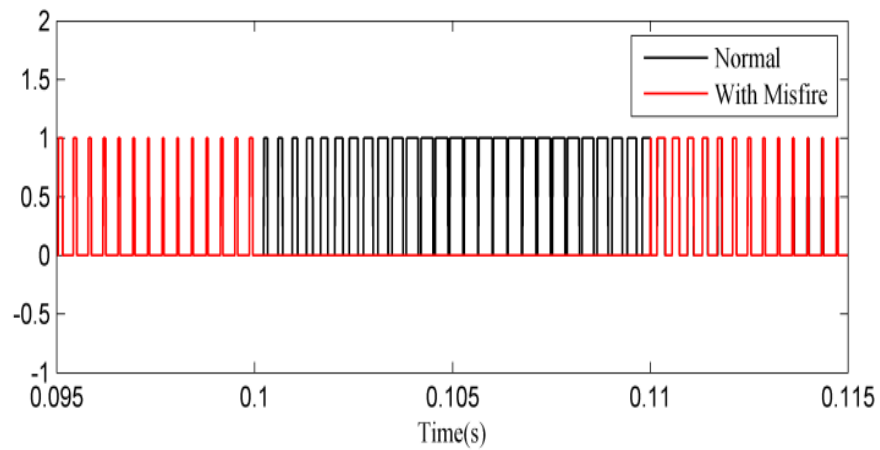
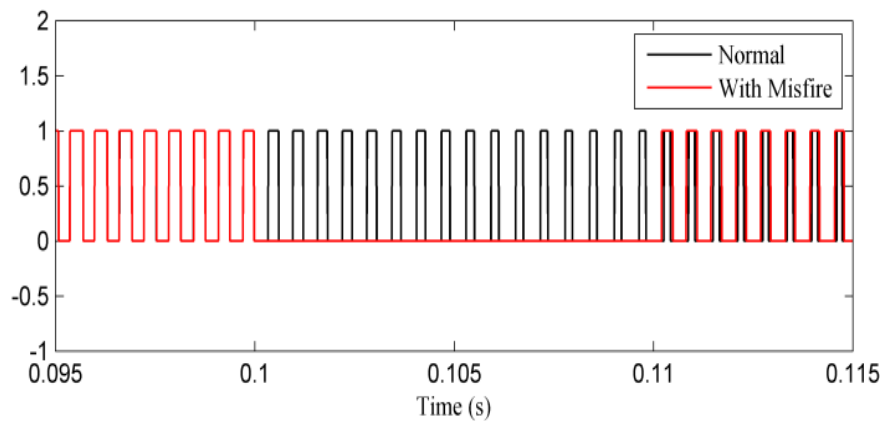


Fig. 6.22. Converters configuration of the DFIG [91]

The example of misfire and fire-through in DFIG's converters is demonstrated in Figs. 6.23 and 6.24 respectively [91]. The faults are assumed to start at 0.1 s and lasts for 10 ms as shown in the IGBT-1 pulse signals for GSC and RSC of the DFIG. In the case of misfire the generated signals from PWM for both GSC and RSC are failed to fire the IGBT-1 valve in its scheduled conducting period as shown in Figs. 6.23(a) and (b). For fire-through case, shown in Figs. 6.24(a) and (b), the generated switching signals from PWM are failed to block its valve during a scheduled non-conducting period.



(a)



(b)

Fig. 6.23. Simulation of misfire fault in IGBT-1; (a) GSC signal and (b) RSC signal [91]

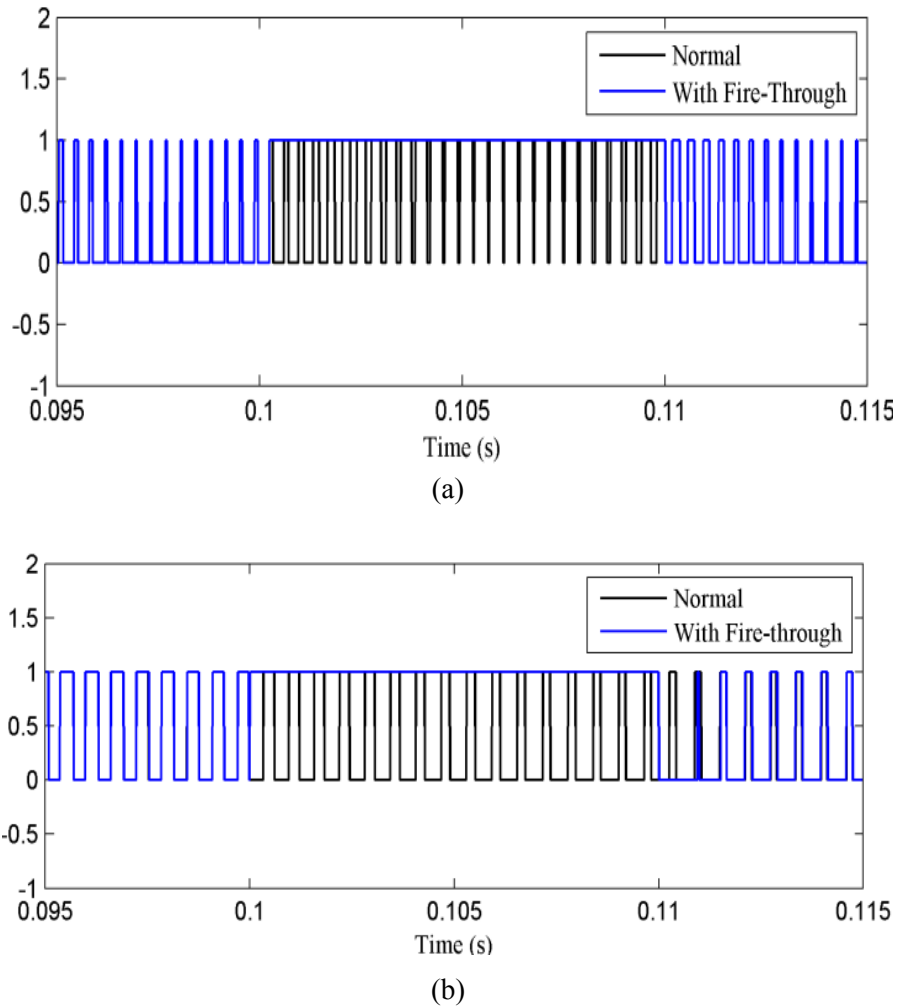


Fig. 6.24. Simulation of Fire-through fault in IGBT-1; (a) GSC signal and (b) RSC signal [91]

6.5.2. Misfire on GSC and RSC

In this study, intermittent misfire and fire-through are simulated in both GSC and RSC of the DFIG based WECS. In all studied cases, the fault is assumed to occur on switch-1 (as shown in Fig. 6.22) at $t= 0.50s$ and self-healed at $t= 0.55s$.

When a misfire is applied to the GSC, the generated power (P), shaft speed and the voltage at PCC (V_{PCC}) are not significantly influenced, this is attributed to the fact that GSC has no direct connection with the DFIG's rotor and hence its influence on its dynamic performance will be trivial. This is evidenced by the slight oscillations that the above parameters will experience during fault period as shown in Fig. 6.25.

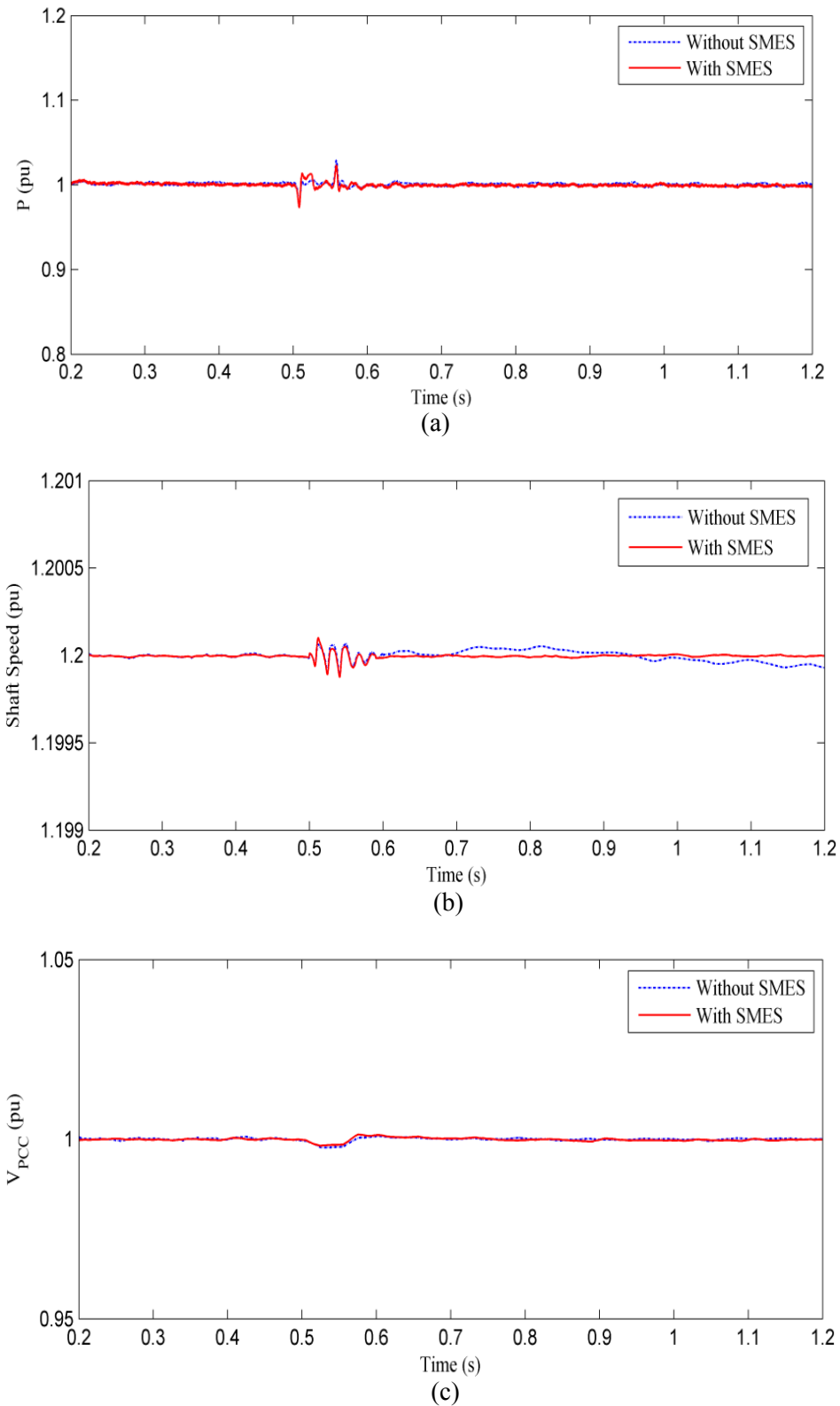


Fig. 6.25. Effect of GSC misfire on DFIG dynamic responses with and without SMES coils; (a) Power and (b) Shaft speed (c) Voltage at PCC

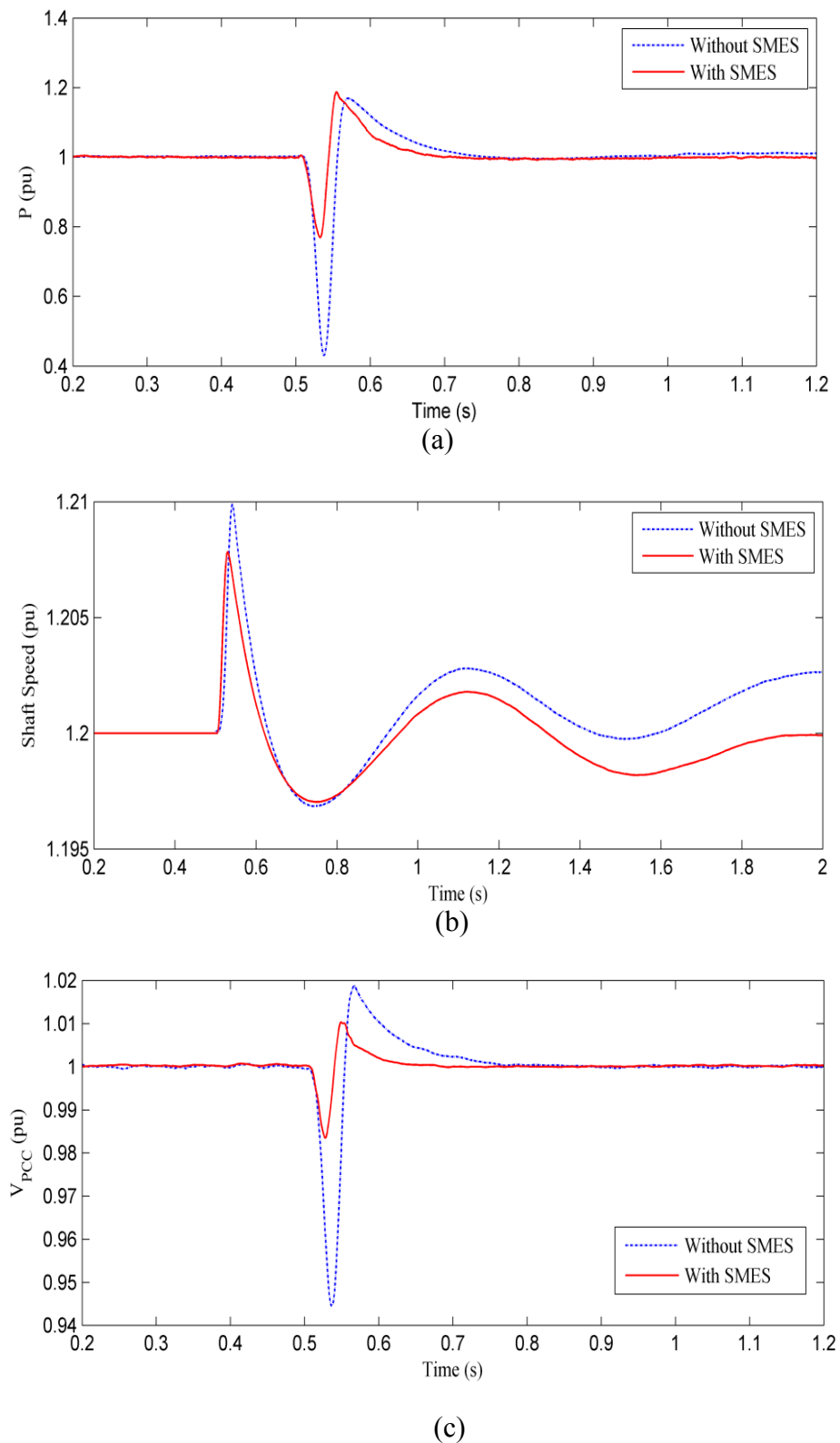


Fig. 6.26. Effect of RSC misfire on DFIG dynamic responses with and without SMES unit; (a) Power, (b) Shaft speed, and (c) Voltage at PCC

The SMES unit when connected to the system will slightly reduce the oscillations and the settling time however, its contribution is not significant as all variables are within safe margins.

When misfire is applied to RSC, the DFIG generated power is reduced dramatically by 60% as shown in Fig. 6.26(a), shaft speed exhibits maximum overshooting at the instant of fault occurrence and it does not settle down to the original level of 1.2 pu as shown in Fig. 6.26(b), and the voltage at the PCC is reduced by 6% (Fig. 6.26(c)). SMES unit can modulate both active and reactive power and support the system during the fault. Thus by connecting SMES unit to the system, the generated power reduction will be only 20% as shown in Fig. 6.26(a). The overshooting in shaft speed is reduced and the settling time is substantially decreased as shown in Fig. 6.26(b). The voltage at the PCC is significantly improved during the fault and after fault clearance as can be shown in Fig. 6.26(c).

6.5.3. Fire-Through on GSC and RSC

Fig. 6.27 shows the dynamic response of the studied system when fire-through is applied to the GSC. As shown in this figure, without SMES the dispatched power will be dropped to 0.1 pu and it takes 0.2s to settle down to the original level after fault clearance. SMES unit will slightly improve the power and correct it to 0.25 pu during the fault and it reduces the settling time. Fig. 6.27(b) shows that with SMES unit, shaft speed oscillation is reduced and settling time is substantially decreased after the clearance of the fault, thus it will reach steady condition faster than the system without SMES. Furthermore, the voltage at PCC is also improved from 0.6 pu during fault and without the connection of the SMES unit to 0.8 pu when SMES is connected to the system as shown in Fig. 6.27(c).

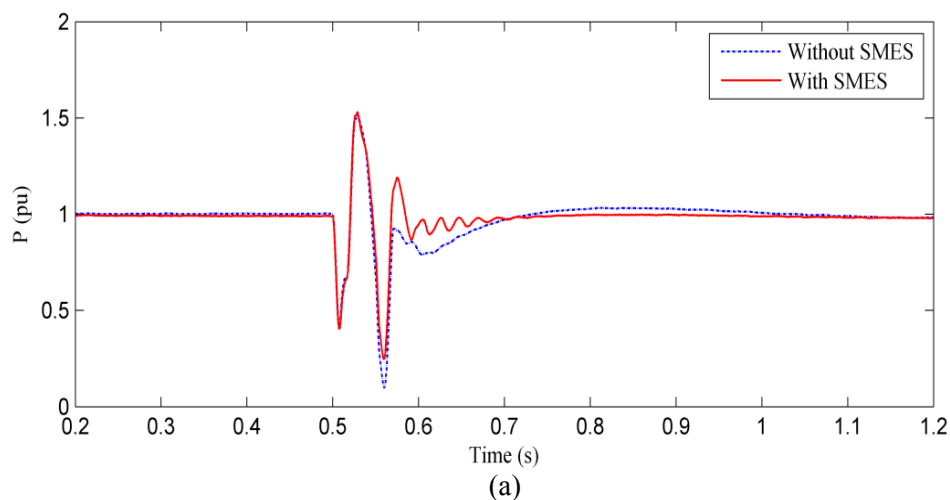
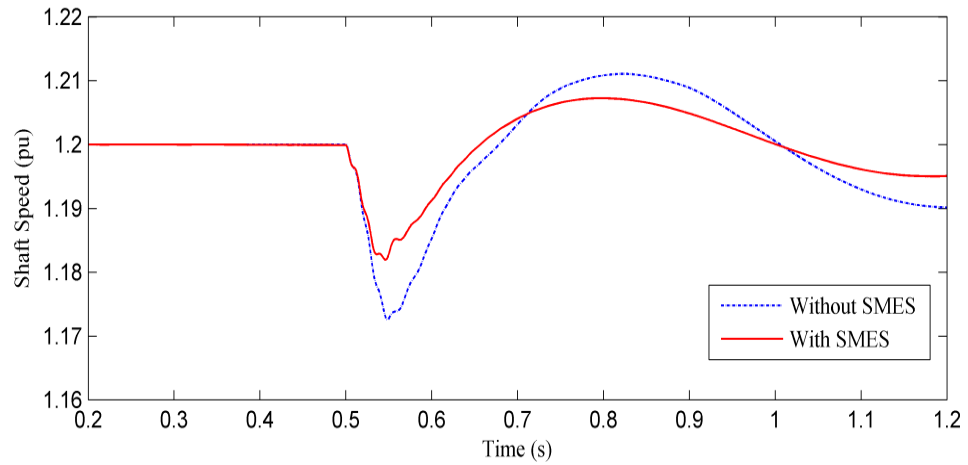
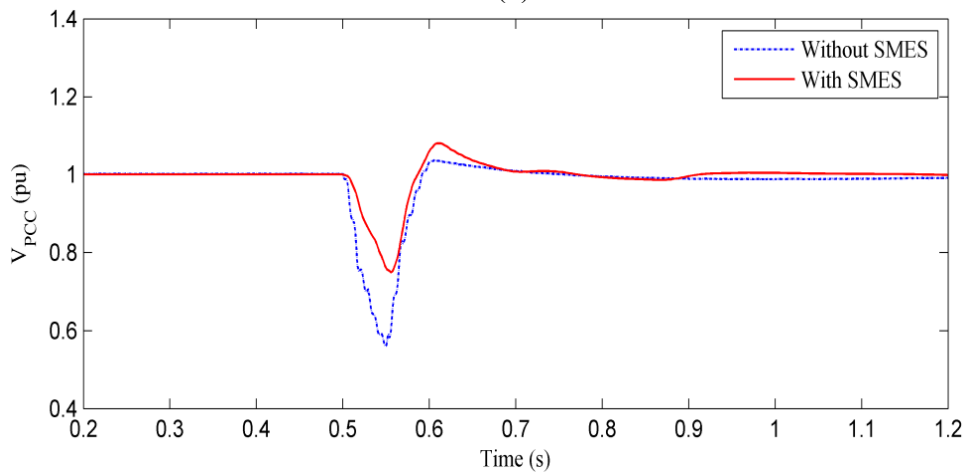


Fig. 6.27. Effect of fire-through at GSC on DFIG's responses with and without SMES unit;
(a) Power (continued on next page)

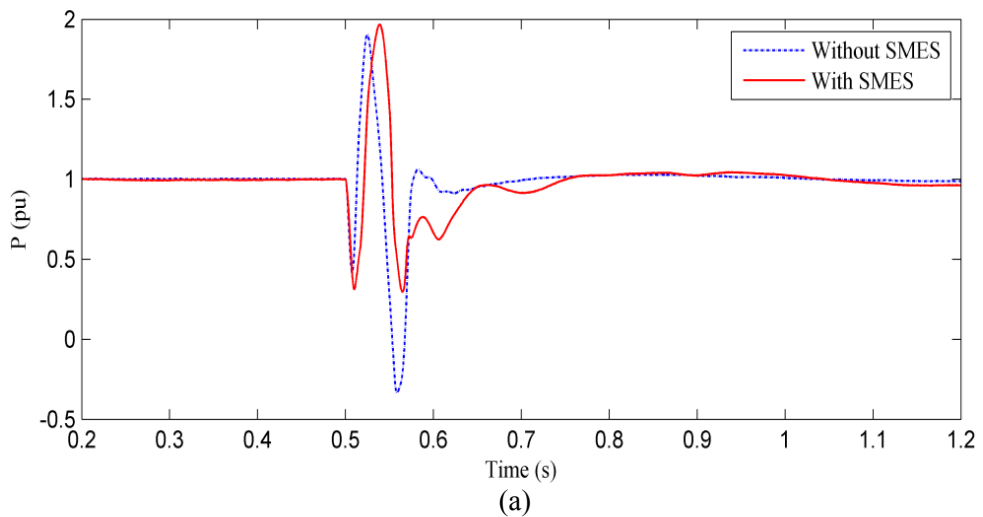


(b)



(c)

Fig. 6.27. Effect of fire-through at GSC on DFIG's responses with and without SMES unit; (b) Shaft speed, (c) Electromagnetic torque and (d) Voltage at PCC



(a)

Fig. 6.28. Effect of fire-through at RSC on DFIG's responses with and without SMES coil; (a) Power (Continued to next page)

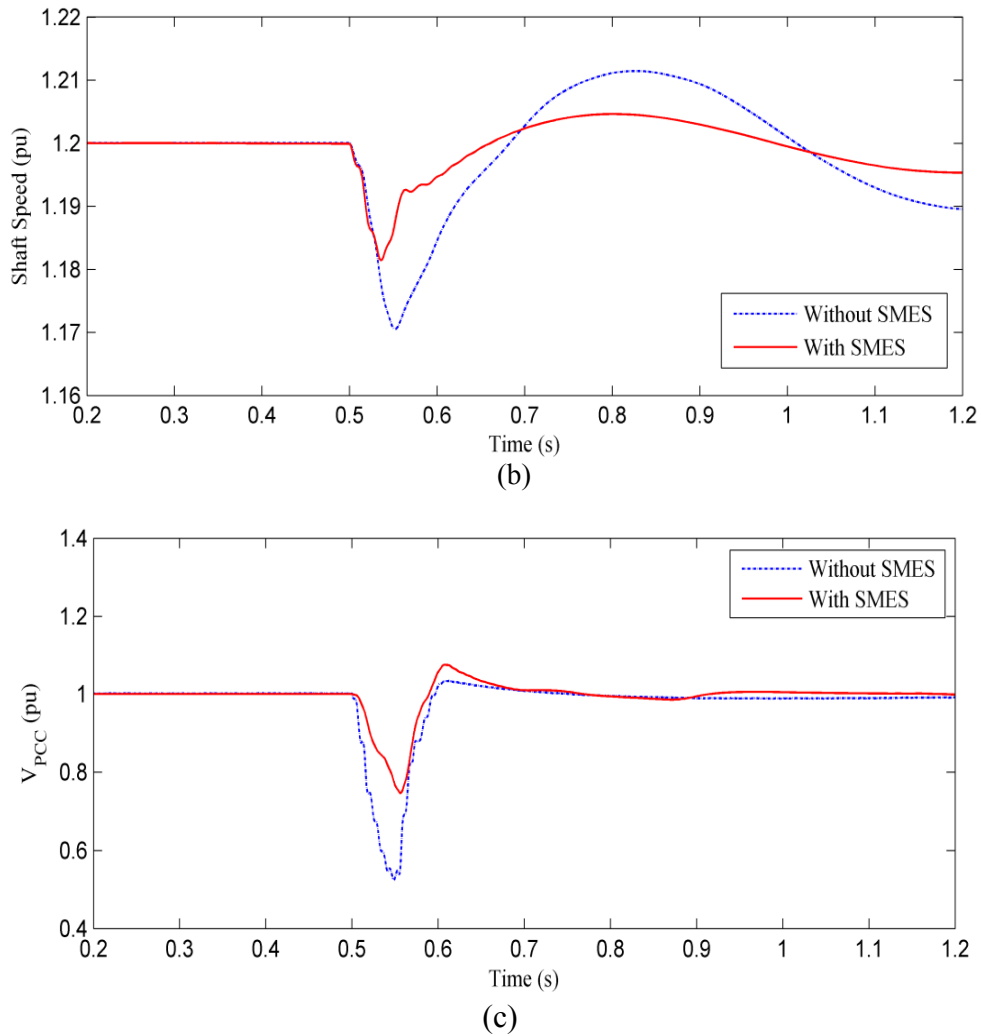


Fig. 6.28. Effect of fire-through at RSC on DFIG's responses with and without SMES coil; (b) Shaft speed and (c) Voltage at PCC

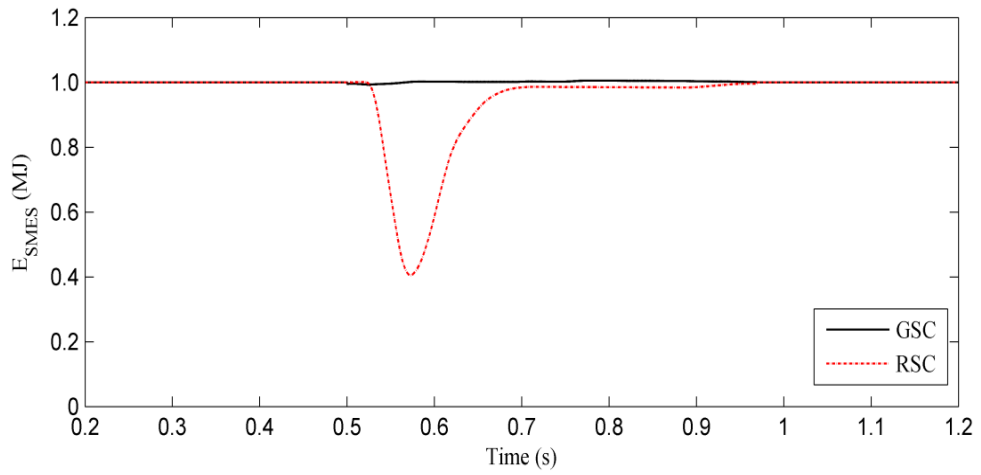
Compared to other cases, fire-through when occurs within RSC is the worse case. Without SMES unit connected to the system, generated power will oscillate and drops to negative level where the machine absorbs power from the grid and acts as a motor as shown in Fig. 6.28(a). In this condition, protection devices such as crowbar will be activated to isolate the WTG and to protect the converter stations against excessive current. However, with the SMES unit connected to the system, the drop in generated power is modulated to 0.25 pu as shown in Fig. 6.28(a), Both shaft speed and V_{PCC} are also significantly improved by the connection of the SMES unit as shown in Figs. 6.28(b) and (c) respectively.

6.5.4. SMES Behaviours

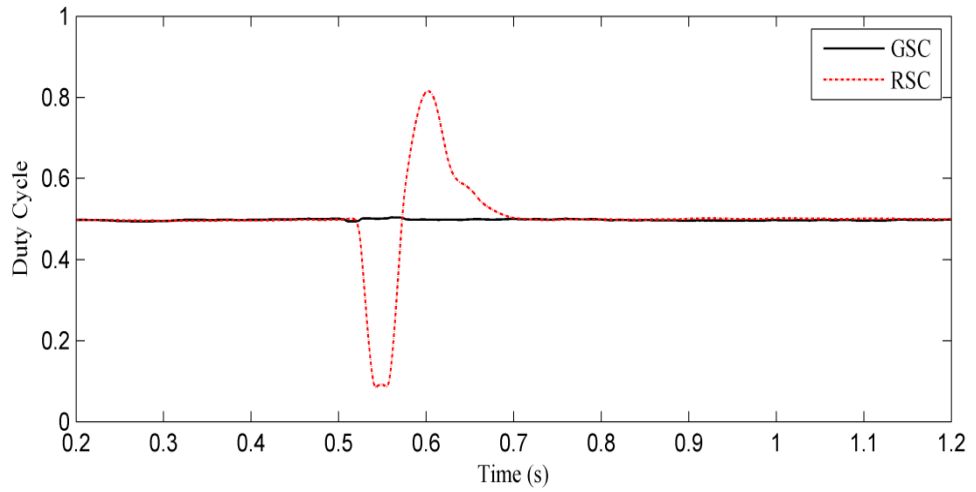
The SMES coil behaviours during misfire and fire-through events are shown in Figs. 6.29 and 6.28, respectively. Fig. 6.29(a) shows that the stored energy within the SMES coil is discharged to the grid during the event of misfire within the RSC. The insignificant impact of the misfire within GSC will not trigger the SMES controller and the coil stored energy is maintained during the fault as shown in Fig. 6.29(a). The behaviour of coil stored energy during misfire within GSC and RSC can be examined through the duty cycle response and the voltage across the SMES coil as shown in Figs. 6.29 (b) and (c), respectively where the duty cycle is maintained at 0.5 level (standby condition) and the voltage across the coil is maintained at zero level by short circuiting the SMES coil using the bypass switches shown in Fig. 5.13(a) in Chapter 5. The duty cycle drops to a level below 0.5 (discharge condition) when misfire occurs within the RSC. The bypass switches will open to allow for energy transfer and the voltage across the coil becomes negative.

When the misfire within RSC is cleared, coil energy recovery takes place by controlling the duty cycle to be in a level higher than 0.5 (charging condition) until maximum energy stored is retained after which the duty cycle drops back to 0.5 level again to maintain the voltage across the coil at zero level.

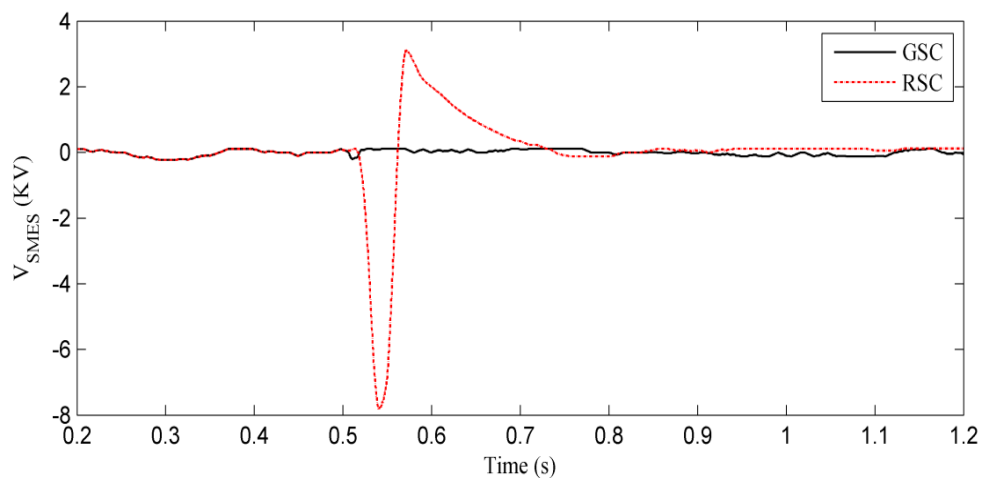
The SMES coil behaviour when fire-through occurs within GSC and RSC is similar to its behaviour for misfire within RSC shown in Fig. 6.30. However, more energy discharge is demanded from the coil in case of fire-through as shown in Fig. 6.30(a). Also, oscillations in the duty cycle response and the voltage across the SMES coil are noticeable during and after the fault clearance as shown in Figs. 6.30(b) and (c). Fig. 6.30 shows that the SMES coil discharges more energy to the system during fire-through within RSC than the case when fire-through takes place within GSC. This is attributed to the severity of RSC fire-through when compared to the same fault within GSC as elaborated in Section 6.5.3.



(a)



(b)



(c)

Fig. 6.29. SMES behaviours during misfire fault; (a) Energy, (b) Duty cycle, and (c) Voltage across the SMES coil

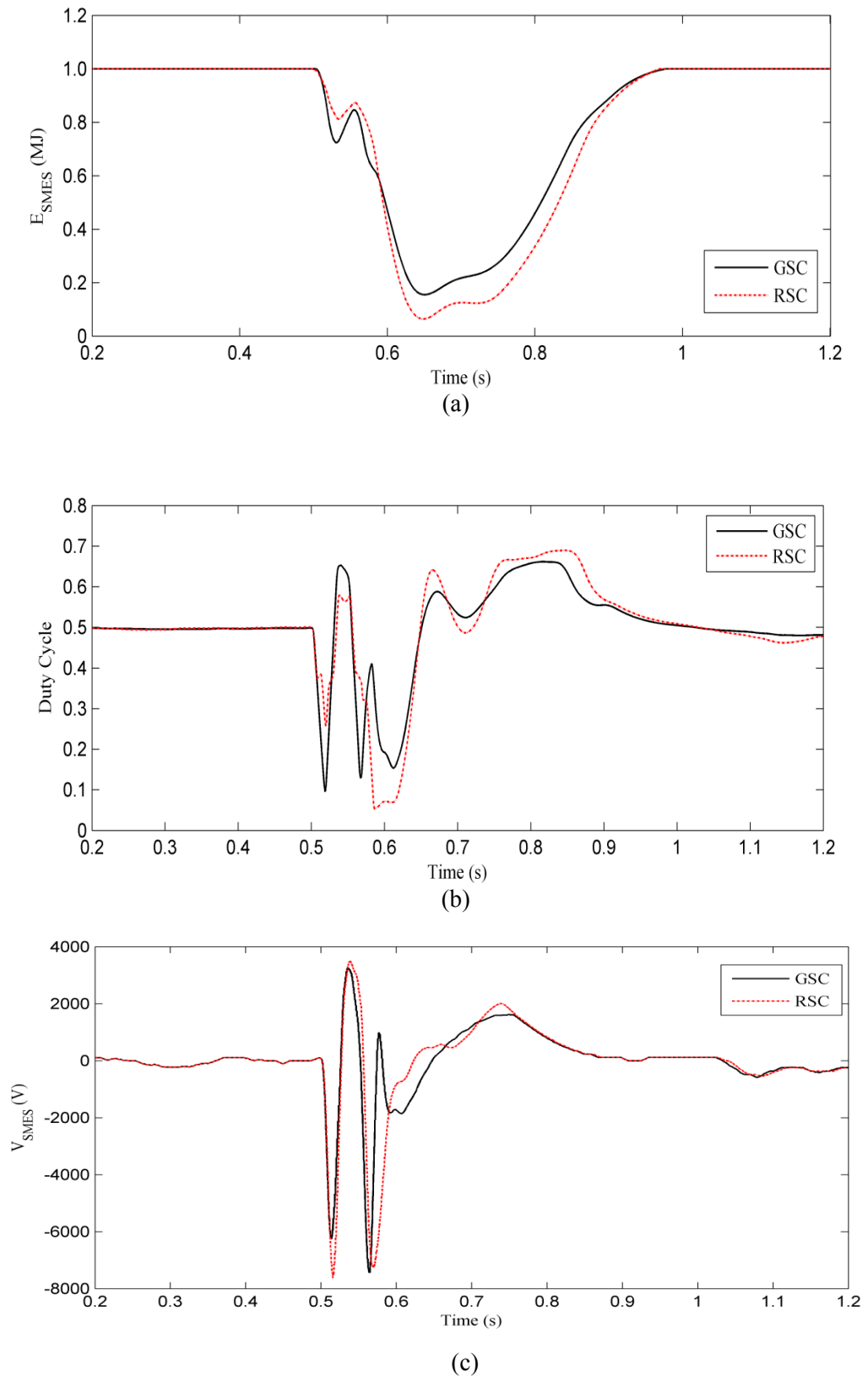


Fig. 6.30. SMES behaviours during fire-through fault; (a) Energy, (b) Duty cycle, and (c) Voltage across the SMES coil

6.6. Summary

Most of literature has studied the ability of the DFIG's control system to meet the grid requirements. This strategy however, is suitable only for new connections of WECS to the grid. When existing WECS must comply with new grid requirements, it is much more effective to introduce FACTS devices such as SMES. In this case, SMES are more cost effective in since there will be no need to dismantle and re-connect the WECS.

Although voltage swells are rarely encountered at the grid side, they may still cause disconnection of WECS from the grid if the WECS complies with some recent international grid codes such as Spain's grid code. For this reason, this chapter has also included voltage swell events in addition to the voltage sags.

The significance of the present study was introduced in the discussion that appears earlier in this chapter. This chapter also presented a novel SMES control scheme and applied it on DFIG system subjected to voltage sag and swell conditions.

Another novelty that is discussed in this thesis is the section of converter faults, such as misfire and fire-through on both GSC and the RSC of DFIG. Although these converter faults scarcely occur, they could cause catastrophic damage on both the converters and the machine of the DFIG, especially when they occur at RSC. Therefore, as a part of this research, these faults were simulated and discussed to investigate their impact on the overall performance of the DFIG. Furthermore, SMES coil is employed to mitigate the severe impact of these faults on DFIG's performance. The results indicate that misfire has little impact compared to the fire-through fault. The worst case is the fire-through fault when it occurs at RSC. Therefore, more energy was transferred to the DFIG system in the case of fire-through, while only very little energy was transferred during the misfire case, as this fault will not cause the investigated-DFIG's parameters being violated from the designated safety margin of the system.

6.7. References

- [1] R. Boom and H. Peterson, "Superconductive energy storage for power systems", *IEEE Transactions on Magnetics*, vol. 8, pp. 701-703. 1972
- [2] H. J. Boenig and J. F. Hauer, "Commissioning Tests of The Bonneville Power Administration 30 MJ Superconducting Magnetic Energy Storage Unit", *IEEE Transactions on Power Apparatus and Systems*, vol. PAS-104, pp. 302-312. 1985
- [3] A. Akhil, S. Swaminathan, and R. K. Sen, "Cost Analysis of Energy Storage Systems for Electric Utility Applications", California. 1997
- [4] W. Li, "Damping of Torsional Oscillations Using Excitation Control of Synchronous Generator: The IEEE Second Benchmark Model Investigation", *IEEE Transactions on Energy Conversion*, vol. 6, pp. 47-54. 1991
- [5] J. B. X. Devotta, M. G. Rabbani, and S. Elangovan, "Application of Superconducting Magnetic Energy Storage Unit for Damping of Subsynchronous Oscillations in Power Systems", *Energy Conversion and Management*, vol. 40, pp. 23-37. 1999
- [6] M. G. Rabbani, J. B. X. Devotta, and S. Elangovan, "Multi-Mode Wide Range Subsynchronous Resonance Stabilization Using Superconducting Magnetic Energy Storage Unit", *International Journal of Electrical Power and Energy Systems*, vol. 21, pp. 45-53. 1999
- [7] T. Ishikawa, S. Akita, S. Taniguchi, S. Kohso, and T. Tanaka, "Power System Stabilization by SMES Using Current-Fed PWM Power Conditioner", in *Power Electronics Specialists Conference, 1988. PESC '88*, vol.1, pp. 334-341. 1988
- [8] A. R. Kim, K. Gyeong-Hun, K. Jae-Ho, M. H. Ali, P. Minwon, Y. In-Keun, K. Hae-Jong, K. Seok-Ho, and S. Ki-Chul, "Operational Characteristic of the High Quality Power Conditioner with SMES", *IEEE Transactions on Applied Superconductivity*, vol. 18, pp. 705-708. 2008
- [9] A. Moghadasi, S. M. Torabi, and M. Salehifar, "Performance Evaluation of Unified Power Quality Conditioner with SMES", in *First Power Quality Conference (PQC), 2010*, pp. 1-6. 2010
- [10] A. Moghadasi, S. M. Torabi, and M. Salehifar, "Combined Operation of the Unified Power Quality Conditioner with SFCL and SMES", in *First Power Quality Conference (PQC), 2010*, pp. 1-7. 2010
- [11] D. Casadei, G. Grandi, U. Reggiani, G. Serra, and A. Tani, "Behavior of a Power Conditioner for Micro-SMES Systems Under Unbalanced Supply Voltages and Unbalanced Loads", in *Proceedings of the IEEE International Symposium on Industrial Electronics, 1999*, vol.2, pp. 539-544. 1999
- [12] T. Ise, "Studies on Power Conditioning System for SMES in ITER", *IEEE Transactions on Applied Superconductivity*, vol. 11, pp. 1896-1899. 2001
- [13] M. V. Aware and D. Sutanto, "Improved Controller for Power Conditioner Using High-Temperature Superconducting Magnetic Energy Storage (HTS-SMES)", *IEEE Transactions on Applied Superconductivity*, vol. 13, pp. 38-47. 2003
- [14] S. Funabiki, T. Yorioka, and T. Fujii, "An Experiment of Fuzzy Control for Leveling Load Power Fluctuations Using An SMES Simulator", in *Thirty-Third IAS Annual Meeting Industry Applications Conference, 1998*, vol.2, pp. 1269-1274. 1998

- [15] S. Funabiki, H. Nakano, and T. Tanaka, "A Fuzzy-Based Control Strategy for Levelling Electric Power Fluctuations in Railroad Substations", in *4th IEEE International Conference on Power Electronics and Drive Systems, 2001*, vol.2, pp. 796-800. 2001
- [16] E. S. M. Ahmed, "DSP Based Robust Fuzzy Logic Controller for Firing Scheme for Smes Power Conditioning System", in *International Conference on Electrical, Electronic and Computer Engineering, 2004*, pp. 367-372. 2004
- [17] L. Hui, M. Steurer, and D. Cartes, "Investigations on a 5-level VSI-Chopper for A Superconductive Magnetic Energy Storage (SMES) Power Conditioning System", in *The 29th Annual Conference of the IEEE Industrial Electronics Society, 2003*, vol.1, pp. 531-537. 2003
- [18] N. Celanovic, D. H. Lee, D. Peng, D. Borojevic, and F. C. Lee, "Control Design of Three-Level Voltage Source Inverter for SMES Power Conditioning System", in *30th Annual IEEE Power Electronics Specialists Conference, 1999*, vol.2, pp. 613-618. 1999
- [19] L. Hui, D. Cartes, M. Steurer, and T. Haibin, "Control Design of STATCOM with Superconductive Magnetic Energy Storage", *IEEE Transactions on Applied Superconductivity*, vol. 15, pp. 1883-1886. 2005
- [20] I. D. Hassan, R. M. Bucci, and K. T. Swe, "400 MW SMES Power Conditioning System Development and Simulation", *IEEE Transactions on Power Electronics*, vol. 8, pp. 237-249. 1993
- [21] J.D. Rogers, R.I. Schermer, B.L. Miller, J.F. Hauer, "30-MJ Superconducting Magnetic Energy Storage System for Electric Utility Transmission Stabilization", *IEEE Proceeding*, Vol. 71. pp. 1099 – 1107. 1983
- [22] H. Salbert, D. Krischel, A. Hobl, M. Schillo, N. Ulacha, A. Tronnm, W. Roesgca, "2 MJ SMES for an Uninterruptible Power Supply", *IEEE Transactions on Applied Superconductivity*, vol. 10, pp. 777-779. 2000
- [23] R. Kreutz, H. Salbert, D. Krischel, A. Hobl, C. Radermacher, N. Blacha, P. Behrens, and K. Dütsch, "Design of a 150 kJ High- T_c SMES (HSMES) for a 20 kVA Uninterruptible Power Supply System", *IEEE Transactions on Applied Superconductivity*, vol. 10, pp. 1860-1862. 2003
- [24] T. Mito, A. Kawagoe, H. Chikaraishi, R. Maekawa, T. Hemmi, K. Okumura, R. Abe, T. Baba, H. Ogawa, M. Yokota, Y. Morita, K. Yamauchi, M. Iwakuma, A. Kuge, A. Nakamura, and F. Sumiyoshi, "Development of 1 MJ Conduction-Cooled LTS Pulse Coil for UPS-SMES", *IEEE Transactions on Applied Superconductivity*, vol. 17, pp. 1973-1976. 2007
- [25] L. Ottonello, G. Canepa, P. Albertelli, E. Picco, A. Florio, G. Masciarelli, S. Rossi, L. Martini, C. Pincella, A. Mariscotti, E. Torello, A. Martinolli, and M. Mariani, "The Largest Italian SMES", *IEEE Transactions on Applied Superconductivity*, vol. 16, pp. 602-607. 2006
- [26] A. Abu-Siada and S. Islam, "Superconducting Magnetic Energy Storage Unit, an Efficient Energy Technology for Power Systems", in *12th International Middle-East Power System Conference, 2008*, pp. 447-452. 2008
- [27] A. Abu-Siada and S. Islam, "Application of SMES Unit in Improving the Performance of an AC/DC Power System", *IEEE Transactions on Sustainable Energy*, vol. 2, pp. 109-121. 2011
- [28] S. Nomura, N. Tanaka, K. Tsuboi, H. Tsutsui, S. Tsuji-Iio, and R. Shimada, "Design Considerations for SMES Systems Applied to HVDC Links", in *13th European Conference on Power Electronics and Applications, 2009*, pp. 1-10. 2009

- [29] S. Ganapathy and S. Velusami, "MOEA Based Design of Decentralized Controllers for LFC of Interconnected Power Systems with Nonlinearities, AC-DC Parallel Tie-Lines and SMES Units", *Energy Conversion and Management*, vol. 51, pp. 873-880. 2010
- [30] M. Bellis, "History of Electric Vehicle", <http://inventors.about.com/od/cstartinventions/a/History-Of-Electric-Vehicles.htm>, accessed: 17 February, 2012
- [31] S. Deilami, A. S. Masoum, P. S. Moses, and M. A. S. Masoum, "Real-Time Coordination of Plug-In Electric Vehicle Charging in Smart Grids to Minimize Power Losses and Improve Voltage Profile", *IEEE Transactions on Smart Grid*, vol. 2, pp. 456-467. 2011
- [32] A. S. Masoum, S. Deilami, P. S. Moses, M. A. S. Masoum, and A. Abu-Siada, "Smart Load Management of Plug-In Electric Vehicles in Distribution and Residential Networks with Charging Stations for Peak Shaving and Loss Minimisation Considering Voltage Regulation", *Generation, Transmission & Distribution, IET*, vol. 5, pp. 877-888. 2011
- [33] S. Gao, K. T. Chau, C. Liu, D. Wu, and J. Li, "SMES Control for Power Grid Integrating Renewable Generation and Electric Vehicles", *IEEE Transactions on Applied Superconductivity*, vol. 22, pp. 5701804. 2012
- [34] T. Hamajima, H. Amata, T. Iwasaki, N. Atomura, M. Tsuda, D. Miyagi, T. Shintomi, Y. Makida, T. Takao, K. Munakata, and M. Kajiwara, "Application of SMES and Fuel Cell System Combined with Liquid Hydrogen Vehicle Station to Renewable Energy Control", *IEEE Transactions on Applied Superconductivity*, vol. PP, pp. 1-1. 2011
- [35] P. D. Baumann, "Energy Conservation and Environmental Benefits that May Be Realized from Superconducting Magnetic Energy Storage", *IEEE Transactions on Energy Conversion*, vol. 7, pp. 253-259. 1992
- [36] C. S. Hsu and W. J. Lee, "Superconducting Magnetic Energy Storage for Power System Applications", *IEEE Transactions on Industry Applications*, vol. 29, pp. 990-996. 1993
- [37] X. D. Xue, K. W. E. Cheng, and D. Sutanto, "Power System Applications of Superconducting Magnetic Energy Storage Systems", in *Fourtieth IAS Annual Meeting Industry Applications Conference, 2005*, vol. 2, pp. 1524-1529. 2005
- [38] W. V. Torre and S. Eckroad, "Improving Power Delivery through the Application of Superconducting Magnetic Energy Storage (SMES)", in *Power Engineering Society Winter Meeting, 2001. IEEE*, vol. 1, pp. 81-87. 2001
- [39] A. Badel, P. Tixador, M. Amiet, and V. Brommer, "SMES to Supply an Electromagnetic Launcher", *IEEE Transactions on Applied Superconductivity*, vol. PP, pp. 1-1. 2011
- [40] M. H. Ali, W. Bin, and R. A. Dougal, "An Overview of SMES Applications in Power and Energy Systems", *IEEE Transactions on Sustainable Energy*, vol. 1, pp. 38-47. 2010
- [41] A. Abu-Siada, "Application of Superconducting Magnetic Energy Storage Units to Improve Power System Performance (PhD Thesis)," in *Electrical and Computer Engineering*, Perth: Curtin University of Technology. 2004
- [42] J. Hee-Yeol, A. R. Kim, K. Jae-Ho, P. Minwon, Y. In-Keun, K. Seok-Ho, S. Kideok, K. Hae-Jong, S. Ki-Chul, T. Asao, and J. Tamura, "A Study on the Operating Characteristics of SMES for the Dispersed Power Generation System", *IEEE Transactions on Applied Superconductivity*, vol. 19, pp. 2028-2031. 2009

- [43] S. S. Chen, L. Wang, W. J. Lee, and Z. Chen, "Power flow Control and Damping Enhancement of A Large Wind Farm Using A Superconducting Magnetic Energy Storage Unit", *Renewable Power Generation, IET*, vol. 3, pp. 23-38. 2009
- [44] M. H. Ali, P. Minwon, Y. In-Keun, T. Murata, and J. Tamura, "Improvement of Wind-Generator Stability by Fuzzy-Logic-Controlled SMES", *IEEE Transactions on Industry Applications*, vol. 45, pp. 1045-1051. 2009
- [45] F. Zhou, G. Joos, C. Abbey, L. Jiao, and B. T. Ooi, "Use of Large Capacity SMES to Improve the Power Quality and Stability of Wind Farms", in *Power Engineering Society General Meeting IEEE, 2004*, vol.2, pp. 2025-2030. 2004
- [46] M. R. I. Sheikh, S. M. Muyeen, R. Takahashi, T. Murata, and J. Tamura, "Minimization of Fluctuations of Output Power and Terminal Voltage of Wind Generator by Using STATCOM/SMES", in *PowerTech, 2009 IEEE Bucharest*, pp. 1-6. 2009
- [47] T. Asao, R. Takahashi, T. Murata, J. Tamura, M. Kubo, A. Kuwayama, and T. Matsumoto, "Smoothing control of Wind Power Generator Output by Superconducting Magnetic Energy Storage System", in *International Conference on Electrical Machines and Systems, 2007*, pp. 302-307. 2007
- [48] J. Hee-yeol, P. Dae-Jin, S. Hyo-Ryong, P. Minwon, and Y. In-Keun, "Power Quality Enhancement of Grid-Connected Wind Power Generation System by SMES", in *Power Systems Conference and Exposition, 2009*, pp. 1-6. 2009
- [49] J. M. Miller, J. C. K. Yeung, Y. Q. Ma, and G. Sartorelli, "Ultracapacitors Improve SWECS Low Wind Speed Energy Recovery. Ultracapacitor and Battery for Low Wind Energy Harvesting", in *Power Electronics and Machines in Wind Applications, 2009*, pp. 1-6. 2009
- [50] A. M. Shiddiq-Yunus, M. A. S. Masoum, and A. A. Siada, "Application of SMES to Enhance the Dynamic Performance of DFIG During Voltage Sag and Swell", *IEEE Transactions on Applied Superconductivity*. 2012 (In Press)
- [51] A. M. Shiddiq-Yunus, A. A. Siada, and M. A. S. Masoum, "Application of SMES Unit to Improve the Voltage Profile of The System with DFIG during Grid Dip and Swell", *International Journal of Advances in Engineering & Technology (IJAET)*, vol. 1, pp. 1-13. 2011
- [52] M. Tsili and S. Papathanassiou, "A Review of Grid Code Technical Requirements for Wind Farms", *Renewable Power Generation, IET*, vol. 3, pp. 308-332. 2009
- [53] M. Altin, O. Goksu, R. Teodorescu, P. Rodriguez, B. B. Jensen, and L. Helle, "Overview of Recent Grid Codes for Wind Power Integration", in *12th International Conference on Optimization of Electrical and Electronic Equipment*, pp. 1152-1160. 2010
- [54] R. K. Behera and G. Wenzhong, "Low Voltage Ride-Through and Performance Improvement of a Grid Connected DFIG System", in *International Conference on Power Systems, 2009*, pp. 1-6. 2009
- [55] S. Hu and H. Xu, "Experimental Research on LVRT Capability of DFIG WECS during Grid Voltage Sags", in *Power and Energy Engineering Conference*, pp. 1-4. 2010
- [56] K. Lima, A. Luna, E. H. Watanabe, and P. Rodriguez, "Control strategy for the Rotor Side Converter of A DFIG-WT Under Balanced Voltage Sag", in *Power Electronics Conference, 2009*, pp. 842-847. 2009

- [57] L. Trilla, O. Gomis-Bellmunt, A. Junyent-Ferre, M. Mata, J. Sanchez, and A. Sudria-Andreu, "Modeling and validation of DFIG 3 MW Wind Turbine Using Field Test Data of Balanced and Unbalanced Voltage Sags", *IEEE Transactions on Sustainable Energy*, vol. PP, pp. 1-1. 2011
- [58] Y. Xiangwu, G. Venkataramanan, P. S. Flannery, and W. Yang, "Evaluation the Effect Of Voltage Sags due to Grid Balance and Unbalance Faults on DFIG Wind Turbines", in *International Conference on Sustainable Power Generation and Supply, 2009*, pp. 1-10. 2009
- [59] Y. Xiangwu, G. Venkataramanan, P. S. Flannery, W. Yang, D. Qing, and Z. Bo, "Voltage-Sag Tolerance of DFIG Wind Turbine With a Series Grid Side Passive-Impedance Network", *IEEE Transactions on Energy Conversion*, vol. 25, pp. 1048-1056. 2010
- [60] W. Yulong, L. Jianlin, H. Shuju, and X. Honghua, "Analysis on DFIG Wind Power System Low-Voltage Ride-Through", in *International Joint Conference on Artificial Intelligence, 2009*, pp. 676-679. 2009
- [61] M. Mohseni, M. A. S. Masoum, and S. Islam, "Emergency Control of DFIG-Based Wind Turbines to Meet New European Grid Code Requirements", in *Innovative Smart Grid Technologies (ISGT)*, pp. 1-6, 2011
- [62] J. Zhang, J. Wang, Y. Mo, and F. Xin, "Study of Torque Characteristics of DFIG During the Voltage Sag", in *International Conference on Materials for Renewable Energy & Environment (ICMREE), 2011*, pp. 592-595. 2011
- [63] Y. Xiangwu, G. Venkataramanan, P. S. Flannery, and W. Yang, "Evaluation the Effect of Voltage Sags due to Grid Balance And Unbalance Faults On DFIG Wind Turbines", in *International Conference on Sustainable Power Generation and Supply, 2009*, pp. 1-10. 2009
- [64] S. Hu and H. Xu, "Experimental Research on LVRT Capability of DFIG WECS during Grid Voltage Sags", in *Conference of Power and Energy Engineering*, pp. 1-4. 2010
- [65] Y. Xiangwu, G. Venkataramanan, P. S. Flannery, W. Yang, D. Qing, and Z. Bo, "Voltage-Sag Tolerance of DFIG Wind Turbine With a Series Grid Side Passive-Impedance Network", *IEEE Transactions on Energy Conversion*, vol. 25, pp. 1048-1056. 2010
- [66] C. Feltes, S. Engelhardt, J. Kretschmann, J. Fortmann, F. Koch, and I. Erlich, "High Voltage Ride-Through of DFIG-Based Wind Turbines", in *Power and Energy Society General Meeting - Conversion and Delivery of Electrical Energy in the 21st Century, 2008*, pp. 1-8. 2008
- [67] M. Mohseni, M. A. S. Masoum, and S. M. Islam, "Low and High Voltage Ride-Through of DFIG Wind Turbines Using Hybrid Current Controlled Converters", *Electric Power Systems Research*, vol. 81, pp. 1456-1465. 2011
- [68] N. W. Miller, J. J. Sanchez-Gasca, W. W. Price, and R. W. Delmerico, "Dynamic Modelling of GE 1.5 and 3.6 MW Wind Turbine Generators for Stability Simulations" in *Power Engineering Society General Meeting 2003*, pp.1977-1983. 2003
- [69] www.mathworks.com
- [70] H. Li and M. M. Gupta, "Fuzzy Logic and Inteligent System", Massachusetts: Kluwer Academic Publisher. 1995
- [71] A. N. S. (ANSI), "IEEE Recommended Practice for Monitoring Electric Power Quality". 1995
- [72] E. F. Fuchs and M. A. S. Masoum, "Power Quality in Power Systems and Electrical Machines", Elsevier. 2008

- [73] V. Ahkmatov, "Analysis of Dynamic Behaviour of Power Systems with Large Amount of Wind Power," <http://www.dtu.dk/upload/centre/cet/projekter/99-05/05-va-thesis.pdf>, accessed: 25 February, 2011
- [74] www.aemo.com.au, accessed: 31 December, 2011
- [75] J. Rogers, H. Boenig, R. Schermer, and J. Hauer, "Operation of the 30 MJ Superconducting Magnetic Energy Storage System in the Bonneville Power Administration Electrical Grid", *IEEE Transactions on Magnetics*, vol. 21, pp. 752-755. 1985
- [76] M. G. Rabbani, J. B. X. Devotta, and S. Elangovan, "Application of Simultaneous Active and Reactive Power Modulation of SMES Unit under Unequal Alpha-Mode for Power System Stabilization", *IEEE Transactions on Power Systems*, vol. 14, pp. 547-552. 1999
- [77] T. Ackermann, "Wind Power in Power System", West Sussex: John Wiley and Sons, Ltd. 2005
- [78] "Final Report System Disturbances on 4 November 2006", https://www.entsoe.eu/fileadmin/user_upload/_library/publications/ce/otherreports/Final-Report-20070130.pdf, accessed: 22 February, 2011
- [79] A. M. Shiddiq Yunus, A. Abu Siada, M. A. S. Masoum, "Improving Dynamic Performance of Wind Energy Conversion System using Fuzzy-Based Hysteresis Current Controlled SMES", *Power Electronics, IET*. 2012 (In Press).
- [80] P. Boussean, P. Gautier, E. Garzulino, I. Juston, and R. Belhomme, "Grid Impact of Different Technologies of Wind Turbine Generator Systems", EDF Electricite de France, Clamart Cedex. 2003
- [81] J. Arrillaga, "High Voltage Direct Current Transmission", London: Peter Peregrinus, Ltd. 1983
- [82] K. R. Padiyar, "HVDC Power Transmission Systems", New Delhi: John Wiley & Sons. 1990
- [83] L. Bin and S. Sharma, "A Survey Of IGBT Fault Diagnostic Methods for Three-Phase Power Inverters", in *International Conference on Condition Monitoring and Diagnosis, 2008*, pp. 756-763. 2008
- [84] W. L. Fuchs and E. F. Fuchs, "Frequency Variations of Power System Due to Switching of Renewable Energy Sources", in *International Conference on Renewable Energies and Power Quality (ICREPQ'12)*, Santiago de Compostela, Spain, p.6. 2012
- [85] A. M. Shiddiq-Yunus, A. Abu-Siada, and M. A. S. Masoum, "Improvement of LVRT Capability of Variable Speed Wind Turbine Generators Using SMES Unit", in *Innovative Smart Grid Technologies (ISGT) Asia, IEEE PES*, Perth, Western Australia. 2011
- [86] L. Trilla, O. Gomis-Bellmunt, A. Junyent-Ferre, M. Mata, J. Sanchez, and A. Sudria-Andreu, "Modeling and Validation of DFIG 3 MW Wind Turbine Using Field Test Data of Balanced And Unbalanced Voltage Sags", *IEEE Transactions on Sustainable Energy*, vol. PP, pp. 1-1. 2011
- [87] S. O. Faried and A. M. El-Serafi, "Effect of HVDC converter Station Faults on Turbine-Generator Shaft Torsional Torques", *IEEE Transactions on Power Systems*, vol. 12, pp. 875-881. 1997
- [88] H. A. Darwish, A. M. I. Taalab, and M. A. Rahman, "Performance of HVDC Converter Protection during Internal Faults", in *Power Engineering Society General Meeting, 2006*, pp. 7. 2006

- [89] H. B. A. Sethom and M. A. Ghedamsi, "Intermittent Misfiring Default Detection and Localisation on a PWM Inverter Using Wavelet Decomposition", *Journal of Electrical System*, vol. 4, pp. 222-234. 2008
- [90] A. M. Shiddiq-Yunus, A. A. Siada, and M. A. S. Masoum, "Impact of SMES on DFIG Power Dispatch During Intermittent Misfire and Fire-through Faults", *IEEE Transactions on Applied Superconductivity*. (Submitted in 2012 and under second revision)
- [91] A. M. S. Yunus, A. Abu-Siada, and M. A. S. Masoum, "Impact of Converter Station Faults on Dynamic Performance of Wind Turbines with Doubly Fed Induction Generators", *Sustainable Energy, IET*. (Submitted in 2011)

“Every reasonable effort has been made to acknowledge the owners of copyright material. I would be pleased to hear from any copyright owner who has been omitted or incorrectly acknowledged.”

Chapter 7

Conclusion and Future Works

7.1. Summary of the Work

Chapter 2 presents comprehensive information of WECS, including the importance of renewable energy, the basic theory underlying WECS and the recent technological developments of WECS. This chapter also provides the market share information of the WECS types for the year 2004. The general information of fixed speed, limited variable speed WECS, DFIG and Type D (full converter WECS) are also presented along with their basic designs and configurations.

The aim of Chapter 3 is to discuss comprehensively the entire systems, models and simulations of the DFIG in detail. The models and simulations of the system under study were conducted with Simulink/MATLAB.

Chapter 4 provides a literature review on the studies that examine storage device technology for renewable energy systems such as batteries, ultracapacitors, SMES, flywheels, and then analyses and discusses these studies. Their fundamental principles of operation and recent applications for renewable energy, as well as their advantages and their disadvantages are included. The final part of Chapter 4 draws comparisons in terms of efficiency, lifetime, energy capacity and estimated cost in comprehensive graphs and tables for easy comparison.

The focus of Chapter 5 is the inclusive explanation of the SMES configuration based on the VSC with a DC chopper. This configuration was chosen due to the fact that VSC with a DC chopper is 173% more economical in its number of switching devices compared to the equivalent CSC. Moreover, the VSC technology has a better self-commutating capability, and injects lower harmonic currents into the AC grid than a comparable CSC. In this configuration, utilization of IGBTs is more beneficial than GTOs since the switching frequency of an IGBT lies in the range of 2-20 kHz, whereas GTO's switching frequency cannot exceed 1.0 kHz. HCC is used for VSC in this study because of its simplicity, insensitivity to load parameter variations, fast dynamic response and inherent maximum current limiting characteristic. Meanwhile, fuzzy logic is more suitable for systems that are highly nonlinear and involve parameters that change or drift in time. Therefore, input parameters of the DC-DC chopper are fuzzified to obtain better responses. These control schemes were discussed comprehensively in Chapter 5.

In Chapter 6, the key points of this PhD research for the safe operation of WECS subjected to voltage sag and swell disturbances are analysed and discussed in detail, and the significances and contributions are explicitly described. The dynamic responses of a DFIG connected to SMES during short load variations are also presented in the chapter. Furthermore, detailed studies and simulations are presented to investigate the impacts of misfire and fire-through faults in both the GSC and the RSC on the performance of DFIG. Finally, a SMES unit is applied along with the presence of these converters' faults and proved that the DFIG's dispatch power is significantly improved, particularly in the case of the fire-through fault.

7.2. List of Contributions of Thesis

1. This thesis has proposed a new control algorithm along with a new application of the SMES unit with the aim of improving the dynamic and transient responses of the wind turbine generators equipped with DFIG during voltage sag/swell events, short load variations, and converter internal faults. The results of the simulation show that the SMES unit is very effective in improving the dynamic performance of wind turbines equipped with DFIG during voltage sag and voltage swell at the grid side.

2. The SMES configuration along with the control scheme is also effective in DFIG's application to improve the dynamic performance of DFIG with small (short load variation) and large disturbances (short circuit on transmission line). It is shown that the SMES is capable of providing energy to the grid during a short load variation condition. Thus, this short load variation study justifies the installation of SMES with multi-purposes.
3. The impact of misfire and fire-through when they take place within the GSC and RSC of the DFIG are investigated. While a simulation study shows that misfire has less impact on the DFIG dynamic performance, the fire-through fault presents a severe impact on the DFIG dynamic performance, and will lead to the disconnection of the wind turbine and converters to avoid any damages, especially when it takes place within the RSC.
4. With the proposed HCC and FLC schemes for the control of SMES unit, the power dispatch of DFIG has been improved in the event of misfire and fire-through in the DFIG converters. This control configuration is relatively simple, easy to implement, improves the power dispatch of DFIG in the event of converter internal faults, and prevents the disconnection of the WECS in case of voltage sag and voltage swell events.
5. The SMES unit is still a costly piece of equipment, however due to the rapid development of high temperature superconducting materials, its applications in WECS is expected to become more viable in the near future.

7.3. Future Works

There remain many topics that can be targeted in future in conjunction with this research. For example, although, Type D WECS is less popular than DFIG, its applications comprised about 20% of the total installations in 2004 [1], which is approximately 9.52 GW of the total installations worldwide [2]. Therefore, study of Type D WECS in conjunction with grid disturbances is an important issue that can be targeted for future work. The SMES unit can be considered as an optional compensation device candidate.

The application of the SMES unit on DG systems may also be investigated, since the distributed SMES (D-SMES) has been broadly applied in many countries nowadays [3, 4].

Enhanced control systems may also be developed to improve the robustness of the SMES's configuration. The use of IGCT in SMES converters may also be an option in the future, since IGCT has more capacity output than IGBT [5]. This future work, however, will carry an even stronger validity if studies conduct successful hardware tests, since most software nowadays has no IGCT block available in their library.

The SMES's ability to improve power quality during flicker events can also be studied further. As the simulations results of this thesis have demonstrated the effectiveness of SMES units in improving the performance of WECS in the events of voltage sag and swell, it should also be possible to use them for mitigating the impact of flicker on the system's voltage profile.

The installation of a distributed wind energy conversion systems at several nodes of a large interconnection network might increase the system's overall instability. Connecting SMES units, however, can further improve the stability of the system. To pursue this concept, researchers must study optimal placement of SMES units in order to learn how to depress their ratings, which would then suppresses the cost. This could be another future project for SMES unit systems. The study of weak bus identification is important, particularly when some DGs are included in the large interconnecting systems; these studies are sometimes called bus ranking studies. The study of bus ranking can be extended to the condition of unbalanced loading and/or network conditions as presented in [6]. The injection of one or more SMES units might reduce the number or level of some weak-buses. Therefore, researchers should conduct proper studies on SMES unit placement and learn how to improve the voltage stability and increase the maximum loading factor, as well.

Study of SMES unit in conjunction with other FACTS devices is also attractive. That is instead of connecting a large scale SMES unit; a combination of a relatively small SMES unit and a few FACTS devices (such as UPFC, VSC, STATCOM, etc.)

might be more cost effective. However, pre-intensive studies on control and coordination management within these devices as well as cost study need to be initiated.

7.4. References

- [1] H. Polinder, D.-J. Bang, H. Li, and Z. Cheng, "Concept Report on Generator Topologies, Mechanical and Electromagnetic Optimization", Project UpWind. 2007
- [2] <http://upload.wikimedia.org/wikipedia/commons/6/64/GlobalWindPowerCumulativeCapacity.png>, accessed: 13 March, 2012
- [3] http://www.ornl.gov/sci/oetd/news/american_transmission.htm, accessed: 7 May, 2012
- [4] R. Baxter, "Energy Storage: A Nano Technical Guide, Oklahoma", PenWell Corporation. 2006
- [5] S. Heier, "Grid Integration of Wind Energy Conversion Systems", Chichester: John Wiley and Sons, Ltd. 2006
- [6] P. Juanuwattanakul and M. A. S. Masoum, "Voltage Stability Enhancement for Unbalanced Multiphase Distribution Networks," in *Power and Energy Society General Meeting, 2011 IEEE*, pp. 1-6. 2011

“Every reasonable effort has been made to acknowledge the owners of copyright material. I would be pleased to hear from any copyright owner who has been omitted or incorrectly acknowledged.”

APPENDIX

Appendix A-1

Table A-1. Approximation of power curves

WECS	c_1	c_2	c_3	c_4	c_5	c_6	c_7	c_8	c_9
Heier (1998)	0.5	116	0.4	0	-	5	21	0.08	0.035
Constant Speed WECS	0.44	125	0	0	0	6.94	16.5	0	-0.002
Variable Speed WECS	0.73	151	0.58	0.002	2.14	13.2	18.4	-0.02	-0.003

Appendix B-1

Table B-1. Drive train parameters of the simulated DFIG

Drive Train Parameters	Value
Wind Turbine Inertia Constant, H (s)	4.32
Shaft Spring Constant (p.u. of Mechanical Torque/Rad)	80.27
Shaft Mutual Damping(p.u. of Mechanical Torque/pu dw)	1.5
Turbine Initial Speed (p.u.)	1.2
Initial Output Torque (p.u.)	0.8

Appendix B-2

Table B-2. Converter parameters of the simulated DFIG

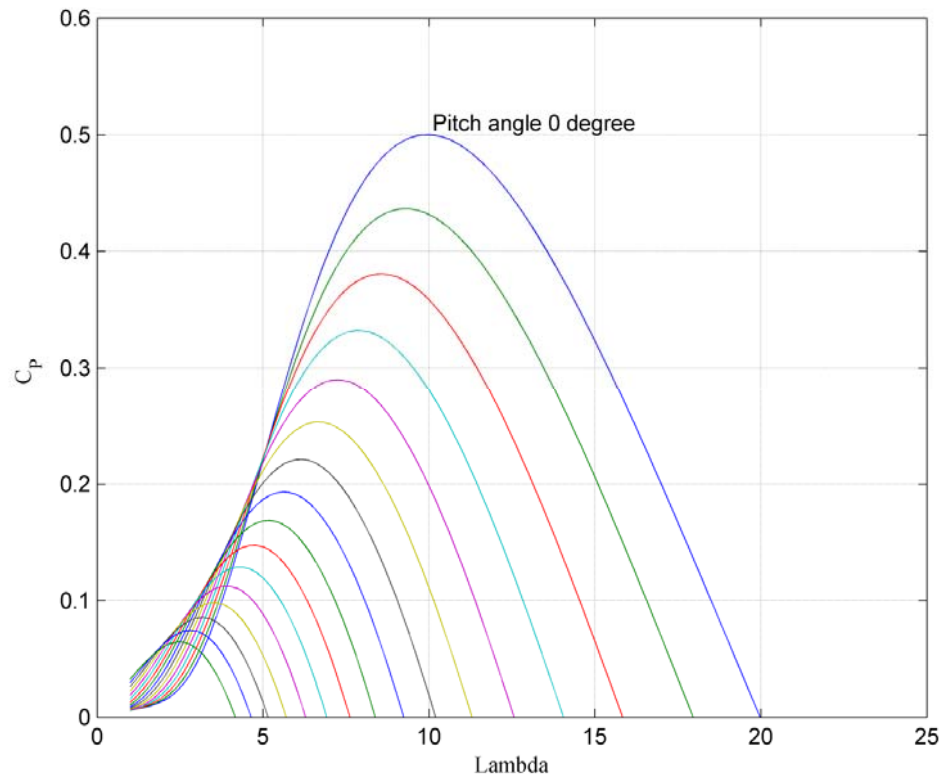
Converters Parameters	Value
Grid Side Coupling Inductor, (L,R) (p.u.)	[0.3 0.003]
Nominal DC bus Voltage (V)	1150
DC Bus Capacitor (F)	10000e-6
Line Filter Capacitor, (Q=50) (VAr)	120e3
Grid Side Coupling Inductor, (L,R) (p.u.)	[0.3 0.003]

Appendix B-3

Table B-3. Generator parameters of the simulated DFIG

Generator Parameters	Value
Number of pair poles, p	3
Mutual Inductance, L_m (p.u.)	2.9
Stator Leakage Inductance, $L_{\sigma s}$ (p.u.)	0.18
Rotor Leakage Inductance, $L_{\sigma r}$ (p.u.)	0.16
Stator Resistance, R_s (p.u.)	0.023
Rotor Resistance, R_r (p.u.)	0.016
Moment of Inertia (s)	0.685

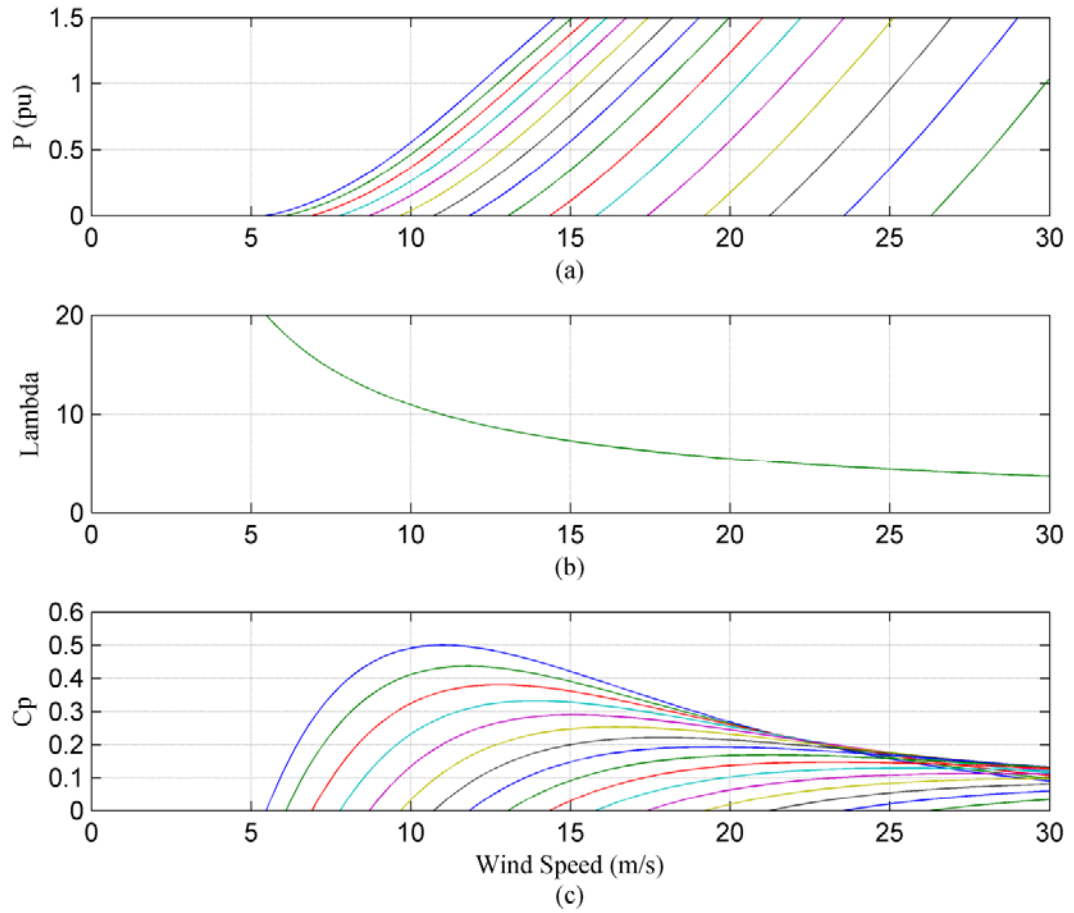
Appendix B-4



Note: Wind turbine C_p characteristic (pitch angle increases by step of 2 deg)

Fig. B-4. Typical C_p - λ (λ) characteristic of simulated wind turbine

Appendix B-5



(Note: Wind turbine characteristics ($w = 1.2$ pu, pitch angle increases by step of 2 deg.)

Fig. B-5. Turbine characteristic of simulated DFIG; (a) Power vs. wind speed, (b) λ (*lambda*) vs. wind speed and (c) C_p vs. wind speed

Appendix B-6

Table B-6a. Parameters of the DFIG

Parameters	Value
Rated Power	9 MW (6 x @1.5 MW)
Stator Voltage	575 V
Frequency	60 Hz
R_S	0.023 pu
R_R	0.016 pu
V_{DC}	1150 V

Table B-6b. Parameters of the transmission line

Parameters	Value
R_1, R_0 (Ω/km)	0.1153, 0.413
L_1, L_0 (H/km)	1.05×10^{-3} , 3.32×10^{-3}
C_1, C_0 (F/km)	11.33×10^{-9} , 5.01×10^{-9}

Table B-6c. Parameters of the proposed SMES unit

Parameters	Value
Rated Energy	1.0 MJ
L_{SMES}	0.5 H
I_{SMES}	2000 A

Appendix B-7

Table B-7a. Parameters of the DFIG

Parameters	Value
Rated Power	3 MW
Stator Voltage	575 V
Frequency	60 Hz
R_S	0.023 pu
R_R	0.016 pu
V_{DC}	1150 V

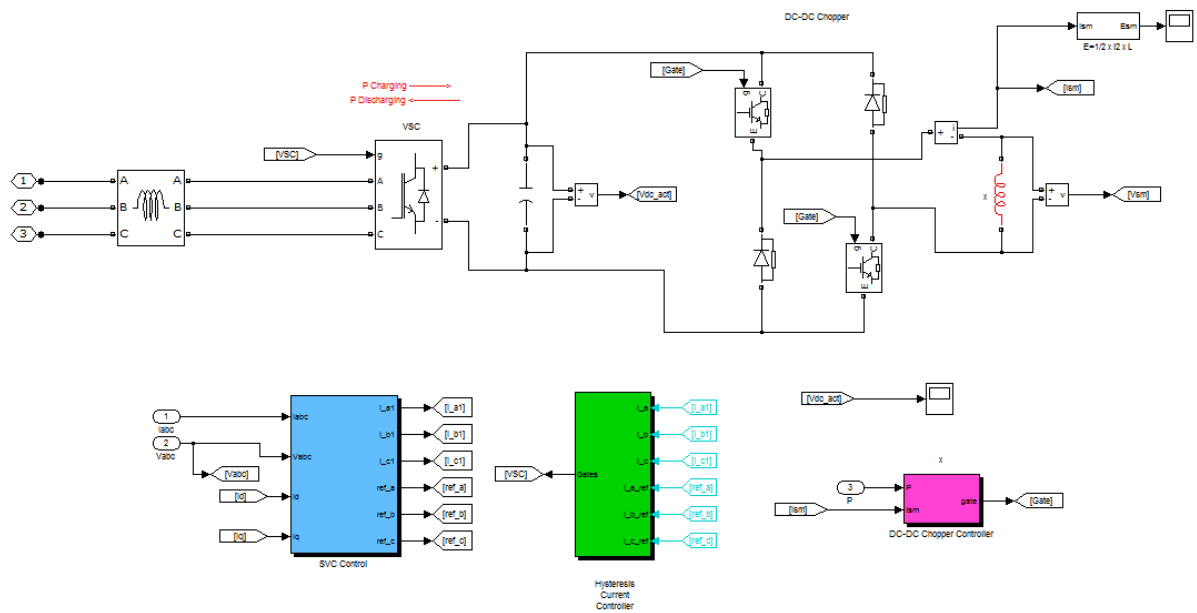
Table B-7b. Parameters of the transmission line

Parameters	Value
R_1, R_0 (Ω/km)	0.1153, 0.413
L_1, L_0 (H/km)	1.05×10^{-3} , 3.32×10^{-3}
C_1, C_0 (F/km)	11.33×10^{-9} , 5.01×10^{-9}

Table B-7c. Parameters of the proposed SMES unit

Parameters	Value
Rated Energy	1.0 MJ
L_{SMES}	0.5 H
I_{SMES}	2000 A

Appendix C-1



(a)

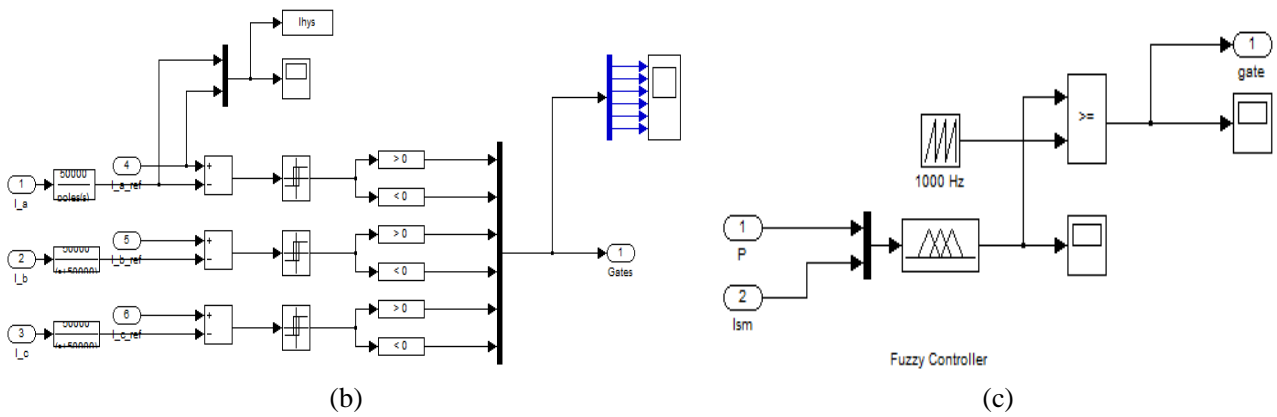


Fig. C-1. (a) Block Diagram of simulated SMES configuration, (b) Hysteresis current controller, and (c) Fuzzy logic controller

Biography



A. M. Shiddiq Yunus was born in Makassar, Sulawesi Selatan, Indonesia on August 4th, 1978. He obtained his B.Sc. degree in Electrical Engineering from Hasanuddin University, Makassar, Indonesia in May 2000 (awarded with the highest student GPA achievement) and his M. Eng. Sc. in Electrical Engineering Department from Queensland University of Technology (QUT), Brisbane, Queensland, Australia in 2006. In October 2008, he started his PhD study at Electrical and Computer Engineering Department, Curtin University, Perth, Western Australia. From January 2001 he joined with Mechanical Engineering Department, Conversion Energy Study Program, State Polytechnic of Ujung Pandang, Makassar, Indonesia, until now as a lecturer. He is also member of assessor institution of Indonesia in electrical engineering since 2007. His special fields of interest included superconducting magnetic energy storage (SMES), renewable energies and smart grid. At the moment, Shiddiq has published 4 journal papers and 11 conference papers.